Deep-Sea Research II 56 (2009) 675

Contents lists available at ScienceDirect

Deep-Sea Research II

journal homepage: www.elsevier.com/locate/dsr2

Editorial

Multi-disciplinary forays into the southern Tyrrhenian Sea, western Mediterranean—CIESM/SUB cruises 1 and 2

Introduction

As evidenced by core records taken from different areas of the basin, the Mediterranean Sea experienced in the past 100,000 years several rapid modifications of hydrographic conditions in response to climatic anomalies, driving in turn ecological events of various scales. As we know from recent studies, today's Mediterranean circulation is still characterised by much variability, both interannual and seasonal, with strong mesoscale patterns. In particular, we now understand how atmospheric anomalies, amplified in winter, are able to change circulation patterns for several years, particularly in the eastern Mediterranean, by triggering the formation of dense water.

The relation between the eastern and western basins is driven by complex dynamical systems that are not well understood. Through its geographic position at the interface with the eastern Basin, the Tyrrhenian Sea is most interesting in this respect, as it is assumed to play a crucial role as "transformer" of eastern water masses and physical processes. Indeed a number of studies have documented recent increases in salinity and temperature in the deep Tyrrhenian Sea, often suggesting that this evolution is linked to the Eastern Mediterranean Climatic Transient. Yet the degree to which western Mediterranean processes are affected by inflows from the eastern basin, rather than by Atlantic influences, is a matter of open debate.

To explore the dynamics of this poorly known, deep maritime region, CIESM (the Mediterranean Science Commission) renewed its historic tradition, initiated in the 1920s, of international oceanographic campaigns. In the summer and winter 2005, we invited some 40 scientists from different countries (Italy, France, Greece, Morocco, Tunisia) to take part in two research cruises aimed at investigating the entire water column in key areas of the southern Tyrrhenian Sea. The gracious disposal by two Italian agencies, CoNISMa and CNR, of the *Universitatis* and *Urania* research vessels, made all this possible.

To begin understand how physical, geological and geochemical processes are related to biodiversity patterns from the sea surface to the sea bottom, a multi-disciplinary approach was necessary. The survey included geomorphologists, who carried out high-resolution mapping of a very complex seabed where deep-sea basins are joined by networks of canyons and separated by seamounts. Physicists, planktonologists, geochemists, benthos zoologists and deep-sea microbiologists joined forces to decipher the main fluxes of matter and energy—from hydrodynamics to microbiological production—in the area targeted for study.

The most striking results of these cruises are presented in the collection of 10 articles, carefully reviewed by international specialists, that follow. A preliminary conclusion, stemming from this volume, is that collected data on nutrient dynamics, on plankton size distribution and on the hydrological structure of the water column all attest of the impact of the Eastern Mediterranean Transient in this critical area of the western basin. The coming decades will determine whether this pattern cascades further into the western basin and how it will be reflected in the macro-biota.

The microbiota, for its part, is very well covered in this special issue, with no less than five papers that range from the diversity and distribution of Bacteria and Archaea to viral production.

In the Tyrrhenian Sea, as elsewhere, bacteria and viruses are major players in the coupling between the bathy-pelagic realms via biogeochemical cycles. Further, this region harbours deep-sea niches of unusual complexity, distributed within the arc-shape southern Apennines–Calabrian arc-Sicilian Maghrebides area. Our campaigns took advantage of this major opportunity to investigate newly described metabolic pathways, typical of the deep sea, which appear to play a fundamental—yet underestimated—role in supporting marine productivity (e.g., autotrophic and ammonia-oxidizing Crenarchaeal assemblages). Finally the reader will learn about new molecular tools, developed here, that allow direct search for genes of possible ecological importance (e.g., *luxA* genes, responsible for bioluminescence) in the deep sea.

Future microbiological research in the deep Tyrrhenian Sea will need to explore the temporal and spatial environmental gradients constraining microbial diversity—determining whether genetic groups have specific biogeographic distributions—and to broaden the search for genetic markers.

Frederic Briand, Laura Giuliano
Co-Editors of this Special Issue
E-mail address: fbriand@ciesm.org (F. Briand)

Available online 5 November 2008

0967-0645/$ - see front matter © 2008 Published by Elsevier Ltd.
doi:10.1016/j.dsr2.2008.10.004

Deep-Sea Research II 56 (2009) 676–686

Contents lists available at ScienceDirect

Deep-Sea Research II

journal homepage: www.elsevier.com/locate/dsr2

Nutrient and pigment distributions in the southern Tyrrhenian Sea during mid-summer and late fall 2005

M. Ribera d'Alcalà *, C. Brunet, F. Conversano, F. Corato, R. Lavezza

Laboratorio di Oceanografia Biologica, Stazione Zoologica "A. Dohrn", Villa Comunale, 80121 Naples, Italy

ARTICLE INFO

Article history:
Accepted 16 July 2008
Available online 25 November 2008

Keywords:
Nutrients
Mediterranean
Tyrrhenian
Eastern Mediterranean Transient or EMT
Pigments

ABSTRACT

Nutrient, dissolved oxygen and pigment distributions measured in two cruises conducted during mid-summer and late fall 2005 in the southern Tyrrhenian Sea were analyzed to address specific questions on the biogeochemical dynamics of the region in the context of Mediterranean biogeochemistry. The sampled area was characterized by a homogeneous spatial distribution of most properties, including the relative abundance in chemotaxonomic pigment groups in both seasons. The only evident structure was a persistent anticyclonic eddy, which did not play a relevant role in differentiating phytoplankton communities at least during these two seasons. An interesting feature was the presence of a summer deep nitracline, well below the pycnocline, which is likely the result of an already depleted Modified Atlantic Water reaching the area. This implies less effective refueling of nutrients in the mixed layer and, possibly, a low primary production rate. Oxygen and nutrient concentrations in the subsurface layer supported the view of the area being oligotrophic. In deeper layers, there was no specific feature that suggested that the significant double diffusive processes occurring in the region played a role in the vertical distributions of nutrients; on the other, the temporal trend in the nutrient pool showed the impact of the Eastern Mediterranean Transient on the basin.

1. Introduction

Nutrients dynamics in the ocean is tightly coupled with the food web, particularly in plankton communities, with abiotic forcing imposing gross biological constraints. In the Mediterranean Sea nutrient concentrations display peculiar patterns in the distributions (pronounced E–W and often N–S gradients; e.g., Kress and Herut, 2001; Ribera d'Alcalà et al., 2003), anomalous elemental ratios in the deep pools (Bethoux et al., 1992; Ribera d'Alcalà et al., 2003; Krom et al., 2004), increasing trends with time (Bethoux et al., 2002), all of which reflect the main forcings of the basin and its biogeochemical dynamics. Previous studies have either focused on bulk properties and budgets (Bethoux et al., 1992; Ribera d'Alcalà et al., 2003; Krom et al., 2004) or on the analysis of the externals sources (Herut et al., 2002; Migon et al., 1989; Kouvarakis et al., 2001 and references therein). In contrast to the large-scale surveys conducted in the Eastern Basin over the last two decades, the information on nutrient distributions in the Western Mediterranean is mostly regional and basically absent for a large part of the Tyrrhenian Sea (Astraldi et al., 2002).

The Tyrrhenian Sea plays a crucial role in the physical processes of the basin, mostly as water-mass transformer (e.g., Gasparini et al., 2005). A branch of the surface water of Atlantic origin is modified within the basin to ultimately feed, through the Strait of Corsica, the Liguro-Provencal current in the northern boundary of the Mediterranean Sea (Astraldi and Gasparini, 1992). On the other hand, all the intermediate waters flowing from the east through the Straits of Sicily enter the Tyrrhenian Sea, due to constraints imposed by the shallow banks at the Sicily Channel (Fig. 1), generating complex circulation patterns. The resultant mixing processes are not yet fully characterized, but ultimately lead to the formation of two branches that feed the intermediate layers of the Ligurian basin to the north through the Corsica Channel and of the Algero-Provencal basin to the west through the Sardinia Channel.

The impact of the physical processes on the biogeochemical dynamics of the southern Tyrrhenian is poorly known. Little attention has been paid so far to the vertical distribution in the upper layer and its seasonal variation, e.g., the position of the nutricline (but see Kress and Herut, 2001; Marty et al., 2002; Souvermezoglou et al., 1999).

Likewise for the seasonal cycle, there is no evidence of a late winter–early spring bloom as in other areas of Northern Mediterranean Sea, although slight increases in chlorophyll *a* (Chl *a*) concentrations are seen during fall and early winter (see the analysis by D'Ortenzio, 2003 based on Ocean Color data).

* Corresponding author.
E-mail address: maurizio@szn.it (M. Ribera d'Alcalà).

0967-0645/$ - see front matter © 2008 Elsevier Ltd. All rights reserved.
doi:10.1016/j.dsr2.2008.07.028

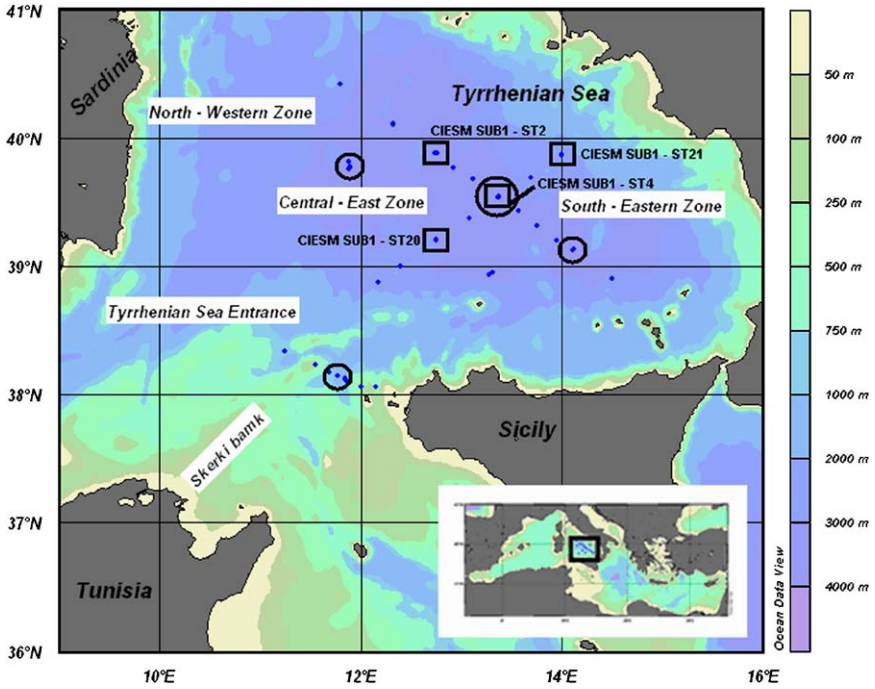

Fig. 1. Map of southern Tyrrhenian Sea with station locations (the circles indicate the different zones). Tyrrhenian Sea Entrance (Mater 1—September 1996; Mater 2—January 1997; Mater 3—October 1997; Mater 4—April 1998; Mater 6—May 1999; Ciesm_Sub1—July 2005)–North-Western Zone (Mater 3—October 1997; Mater 6—May 1999; Massflux—October 2001; Ciesm_Sub1—July 2005; Ciesm_Sub2—December 2005)–Central-East Zone (Ciesm_Sub1—July 2005; Ciesm_Sub2—December 2005; Vector_TM2—February 2007)–South-Eastern Zone (Ciesm_Sub1—July 2005; Ciesm_Sub2—December 2005).

This cycle is consistent with the results of the analysis conducted by D'Ortenzio et al. (2005) on the time course of the mixed-layer depth, which in the central and southern Tyrrhenian Sea, while displaying horizontal heterogeneities, never exceeds 110 m.

A peculiar feature is seen in the deep layer of the southern Tyrrhenian Sea (especially in the 700–2500-m interval) where vertical profiles display, over a large area, a stepped structure in hydrographic properties, mostly caused by double diffusivity (Zodiatis and Gasparini, 1996). This disappears along the borders of the basin, where, according to Zodiatis and Gasparini (1996), advection dominates over the vertical diffusivity. The impact of such horizontal heterogeneity on the vertical transport of nutrients has not yet been examined.

Within the frame of CIESM-SUB effort we have addressed three questions.

- Whether horizontal gradients in nutrient concentrations are correlated with the spatial differences of the mixed-layer depth or in the deep layers and along a latitudinal gradient. Further, is there any biological signature associated with them?
- What is a typical nutrient vertical profile in the southern Tyrrhenian Sea area, to what extent it differs from the typical profiles of the Eastern Mediterranean (quite deep and gradual nutricline), and Western Mediterranean (quite shallow and sharp nutricline), and what is its seasonal cycle in terms of phytoplankton response. In other words, to what extent is the nutrient vertical distribution linked to seasonal patterns suggested by satellite observations?
- Are the property redistributions caused by the Eastern Mediterranean Transient (see Roether et al., 2007 for an updated review) detectable in temporal variations of nutrient distributions?

This contribution gives a first account of our analysis.

2. Materials and methods

Cruise rationale and tracks have already been described elsewhere in this issue. In Fig. 1, we show station locations where physical parameters, nutrient, dissolved oxygen and photosynthetic pigments concentrations were measured. In addition we show the location of stations sampled on other cruises that we utilized to better resolve time variability and to improve spatial coverage (MATER 1—September 96, MATER 2—January 97, MATER 3—October 97, MATER 4—April 98, MATER 6—May 99, MASSFLUX—October 01, CIESM-SUB1—July 05, CIESM-SUB2—December 05, VECTOR-TM2—February 07). At each station a vertical profile of temperature, salinity and dissolved oxygen was obtained by a Neil Brown CTD MK3C (WOCE) (MATER Cruises and MASSFLUX) or by a SeaBird CTD SBE 911plus (CIESM-SUB1, SUB2, VECTOR-TM2) mounted on a General Oceanics Rosette equipped with 24 L bottles for collection of discrete water samples.

Samples for determining nutrient concentrations were collected in 20-mL polyethylene vials. During cruises MATER 1 and 3 the analyses were performed on board the ship just after the cast. In all the other cases the samples were quickly frozen and stored at $-20\,^{\circ}C$. The concentrations were determined within a few weeks after the end of each cruise using a hybrid Brän-Luebbe-Technicon AutoAnalyzer following classical methods (Grasshoff, 1976) with slight modifications. In brief, flow rates of reagents were reduced and their concentrations changed to obtain the same quantity of reagents in the mixed flow though reducing the dilution of the sample and, thus increasing the sensitivity by a factor of two.

All nutrient concentrations were determined using running standards for each batch (in general two or three stations) calibrated versus Ocean Scientific standards. All samples were analyzed twice and MASSFLUX samples were analyzed in parallel at two different laboratories with an overall interlab root-squared difference of 10% for concentrations higher than 4 $\mu mol\,dm^{-3}$ in

nitrate. All the analyses were carried out with the same setup of equipment.

In addition to the oxygen profile derived from the probe mounted on the CTD, parallel determination of oxygen concentration was carried out on all the bottle samples using the Winkler method (Carpenter, 1965) with an automatic endpoint detection burette Metrohm 716 DNS Titrino.

For photosynthetic pigments 2 L samples were filtered onto Whatman GF/F glass fiber filters and immediately stored in liquid nitrogen for later pigment analysis. High-performance liquid chromatography (HPLC) analyses were performed within two weeks of collection according to the protocol described in Dimier et al. (2007). Briefly, pigment filters were extracted in 5 mL 100% methanol and 500 μL of 1 mol L^{-1} ammonium acetate was added to the 1-mL pigment extract for five minutes before the analysis in a Hewlett Packard series 1100 HPLC (Hewlett-Packard, Wilmington, NC, USA). A 3-μm C_8 BDS column (ThermoHypersil, Runcorn, UK) was used and the mobile phase was composed of a two-solvent mixture: A, methanol, aqueous ammonium acetate (70:30), and B, methanol. Pigments were detected at 440 nm and for each pigment the absorption spectrum between 400 and 700 nm was done using a photodiode array detector (model DAD series 1100, Hewlett Packard). Chlorophyll and derivatives also were analyzed by fluorometry (series 1100 fluorometer, Hewlett Packard), using a 410-nm excitation wavelength and a 665-nm emission wavelength, and quantified using standards from the V.K.I. (Water Quality Institute, Horsholm, Denmark).

3. Results

As discussed by Budillon et al. (2008) the Tyrrhenian Sea is a three-layer system. The top layer (0–200 m) is occupied by the so-called Modified Atlantic Water (MAW), whose original core is the water entering at Gibraltar from the Atlantic Ocean. The intermediate layer (200–700 m) is occupied by a mixture of intermediate waters, which especially before the 1990s (Gasparini et al., 2005), were dominantly the Levantine Intermediate Water (LIW). The deep layer, on the other hand, is occupied by two dense water masses, the Tyrrhenian Deep Water (TDW) and the Western Mediterranean Deep Water (WMDW) with the latter being denser and the former being a modification of the WMDW after mixing with the LIW within the basin. Within this general framework nutrient and pigment distributions were analyzed along four different lines.

3.1. Horizontal dimension

Due to the sampling design, nutrient signatures in the upper layer can be better visualized along the two main sections (NW–SE and SW–NE) visited during the cruises. In July a strong anticyclonic eddy occupied the NW part of the NW–SE section (Budillon et al., 2008) whereas isopycnals were quite flat along the transversal SW–NE section. In December the same eddy was still the most relevant structure in the area. As analyzed in depth by Budillon et al. (2008) the eddy was a lens of Winter Intermediate Layer that did not outcrop to the surface.

In Fig. 2, we report nitrate distributions along the two sections during the two cruises. Panels 2A and B clearly evidence the anticyclonic eddy, with panel 2B also highlighting a slight doming in the central-southern part of the NW–SE transect. The density distribution (not shown) does not support the feature as doming, whereas salinity shows lower values in the same area. Along the sections in the transversal direction the nitrate distribution does not display relevant gradients. Only toward the south-western station along the Sicily-Sardinia transect is there, in July, an uplift of the nitrate isoline (panel 2C). Silicates and phosphates (not shown) display similar patterns with a more pronounced uplift of phosphate isoline toward the SW station in July. Overall, the surface layer was everywhere depleted in all nutrients down the 60-m isobath ($NO_3 < 0.5$ μmol dm^{-3}, $SiO_2 < 1.1$ μmol dm^{-3}, $PO_4 < 0.05$ μmol dm^{-3}) in both periods. This also implies that the MAW, which occupied the same depth interval (in July the core salinity minimum was located at 30 m), is basically depleted of nutrients in summer. The late fall salinity distribution was more complex (Budillon et al., 2008) and vertical mixing redistributed the low-salinity water over the upper part of the water column (150–200 m). Therefore it is not possible to discriminate between advective transport and local vertical processes in determining the nutrient profile. However, as mentioned above, the putative layer of the MAW was still nutrient-depleted.

Besides the anticyclonic structure observed in July, active in the upper 500 m, and a higher nutrient concentrations in the SW stations paralleling the higher concentrations in the upper layer, the nitrate concentration in the 200–700-m depth interval ranged from 5.5 to 6.7 μmol dm^{-3}. The LIW core in the area could be traced either as salinity maximum or as the isopycnal 29.05. Mapped on the former the nitrate concentrations showed a slight diminishing trend towards the area interior (Fig. 3). Silicate and phosphate showed similar patterns with the former ranging from 5.5 to 6.2 μmol dm^{-3} and the latter ranging from 0.20 to 0.24 μmol dm^{-3} (not shown).

In deep layers, we mapped nutrient concentrations on three depth horizons, 1000, 2000 and 3000 m. The first two are within the depth interval of the stepped structure, whereas the third encompasses the WMDW and the TDW. The region where the density vertical profiles evidence a stepped structure is roughly that overlying the deepest part of the basin (Fig. 1). Therefore all the stations of the NW–SE transect, with the exception of the two extremes, showed a stepped structure between 800–900 and 2500 m, whereas only in the two center stations of the SW–NE transect the density profile were stepped in the deep layer (see Fig. 5A for characteristic profiles).

At both the 1000- and 2000-m horizons the differences were minimal with slight increase of salinity 0.01–0.02 units toward NE and a corresponding decrease in nutrient concentrations of 0.3–0.5 μmol dm^{-3} for nitrate and silicates (Fig. 5B). At 3000 m (only the interior of the region reaches that depth) there was no pattern in the property distributions, with minimal horizontal differences and a concentration around 8.1 μmol dm^{-3} for nitrates 0.31 μmol dm^{-3} for the phosphates and 9.3 μmol dm^{-3} for the silicates.

To complement the extensive analysis conducted on phytoplankton and microbial biomass and activities by Decembrini et al. (2008) we analyzed at selected stations the photosynthetic pigment composition of phytoplankton to determine any horizontal differences in group composition. It is worth repeating that HPLC pigment data are particularly informative for low-chlorophyll areas, as in our case, where a relevant part of the community is composed of picoplankton (see Decembrini et al., 2008), which cannot be determined by traditional microscopic techniques. HPLC pigment analysis is therefore one of the most suitable techniques to estimate and discriminate the presence of these small species, as *Prochlorococcus*, *Synechococcus* and picoeukayotes. Moreover, pigment data have been shown to be good candidates to track different water masses (for instance, Casotti et al., 2000; Brunet et al., 2003).

As mentioned above, the most prominent structure in the area during the summer cruise was the anticyclone in the NW–SE transect. Indeed, that area did not display strong pigment signatures that can be related to the presence of the gyre, with little difference in the biomarker chemotaxonomic pigments, and

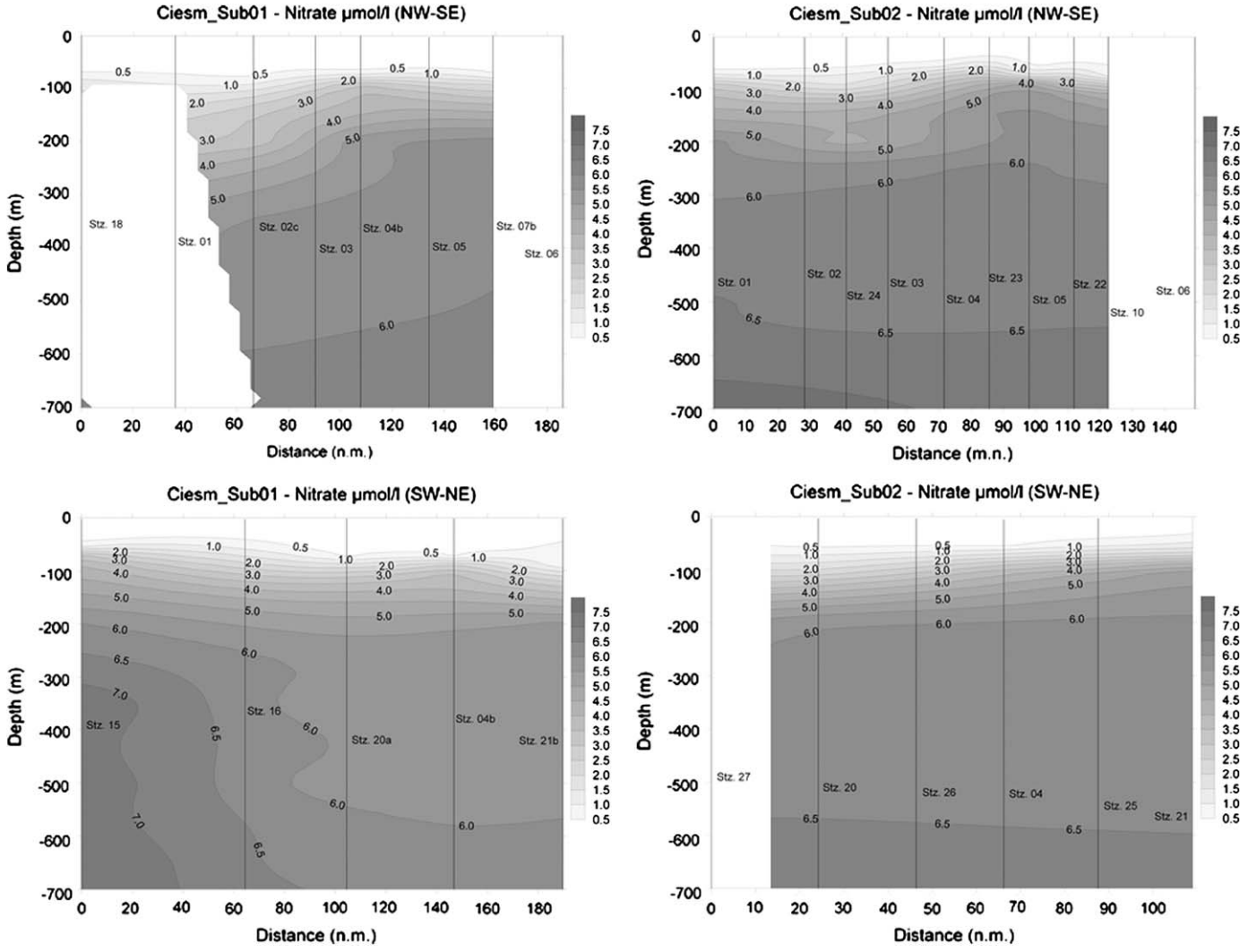

Fig. 2. Nitrate distributions along the NW–SE transect (upper panels) and the SW–NE transect (lower panels) during the two cruises (panels (top left) and (bottom left) summer, panels (top right) and (bottom right) late fall).

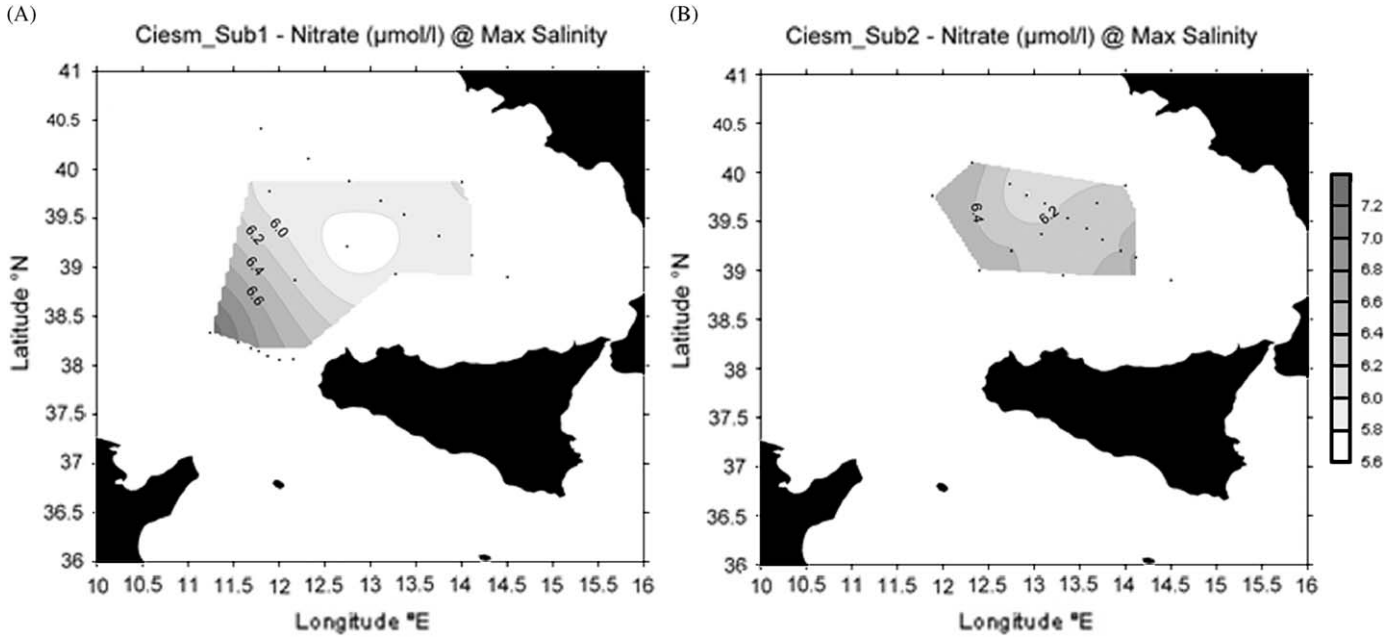

Fig. 3. Nitrate distribution at the 29.05 isopycnal.

Table 1
Pigment characteristics (mean and standard deviations) of the station 2 ($n = 3$ and $n = 2$, for the surface and DCM layers, respectively) with respect to the other stations in July ($n = 15$ and $n = 9$, for the surface and DCM layers, respectively)..

	Chl*a* ($\mu g\,L^{-1}$)	dvchl*a* vs. Chl*a*	19Bf/Chl*a*	Fuco/Chl*a*	19Hf/Chl*a*	Zeax/Chl*a*	Chl*b*/Chl*a*	Dt/(Dt+Dd)	Dd/Chl*a*	Dt/Chl*a*	Bcar/Chl*a*
Station 2											
Surface	0.023	0.024	0.13	0.07	0.40	0.20	0.24	0.22	0.262	0.067	0.084
DCM	0.12	0.33	0.30	0.07	0.54	0.20	0.97	0.10	0.050	0.006	0.149
Other stations											
Surface	0.035	0.033	0.10	0.068	0.33	0.23	0.22	0.25	0.181	0.051	0.091
	(0.008)	(0.01)	(0.02)	(0.02)	(0.04)	(0.04)	(0.11)	(0.060)	(0.054)	(0.025)	(0.019)
DCM	0.36	0.18	0.24	0.23	0.35	0.06	0.65	0.054	0.040	0.004	0.108
	(0.15)	(0.10)	(0.09)	(0.08)	(0.21)	(0.04)	(0.33)	(0.020)	(0.019)	(0.004)	(0.034)

Fuco: fucoxanthin (diatoms), 19Bf: 19′butanoyloxfucoxanthin (pelagophytes), 19Hf: 19′hexanoyloxfucoxanthin (prymnesiophytes), zeax: zeaxanthin (cyanophytes), Chl*b*: chlorophyll *b* (green algae), Dt: diatoxanthin, Dd: diadinoxanthin, Bcar: Bcarotene.

no specific horizontal pattern, which could suggest a significant difference in the community structure. Very briefly, Chl*a* biomass was lower than in the other stations of the area (Table 1), and the divinylchlorophyll *a* (dvchl*a*) vs. Chl*a* ratio in the surface layer also lower than at the other stations, while 19′butanoyloxyfucoxanthin (19Bf) and 19′hexanoyloxyfucoxanthin (19Hf) vs. Chl*a* were slightly higher. Unfortunately, due to the low number of data (between 2 and 3), the statistical significance of these differences could not be tested.

In the deep chlorophyll maximum layer, dvchl*a* and Chl*b* vs. Chl*a* were higher while fucoxanthin vs. Chl*a* was lower than in the other stations. The main features revealed at the site concerned the photodependent pigments, Dt/(Dd+Dt), Dd/Chl*a*, Dt/Chl*a*, or βcarotene/Chl*a* ratios (Table 1) that were higher in the DCM than those of the other stations.

In summary, despite the presence of some mesoscale activity, the southern Tyrrhenian proper, i.e. the region overlying the deepest part of the basin, did not show any relevant spatial patterns in either nutrient or pigment distribution during either the summer or in late fall.

3.2. The vertical distribution

A better appreciation of the vertical distribution of nutrients (e.g., nitrate) in the upper layer can be seen in Fig. 4. For the sites at Tyrrhenian Sea entrance and in the NW area, the data cover an interval of 10 years. At all sites during all the sampling events the nitracline starts below 75 m. The slope is not sharp and a concentration of around 6 $\mu mol\,dm^{-3}$ is reached at 200 m, which is the upper boundary of the intermediate layer. The concentration at 120 m never exceeds 3.5 $\mu mol\,dm^{-3}$, being around 2 $\mu mol\,dm^{-3}$ in the mid-1990s (MATER 1 and 3 cruises).

Oxygen profiles, spanning until February 2007 for the central site (Fig. 6) clearly evidence the absence of any exchange with atmosphere below 20 m in summer and below 65 m in late fall-winter.

The correspondent vertical distribution of phytoplankton groups in the upper layer is as follows. In July, the surface chl*a* value, as determined by HPLC, was 0.035 $\mu g\,L^{-1}$ while in the DCM layer the average value was 0.20 $\mu g\,L^{-1}$. During winter, no significant difference was revealed between the 1–50-m depth layer and the 60–100-m depth layer (0.061 and 0.051 $\mu g\,L^{-1}$).

The distribution of pigments was mainly driven by the vertical gradient of environmental conditions in summer, in relation with the strong thermal stratification and therefore with heterogeneity of the physico-chemical properties of the water column. Indeed, all the chemotaxonomic biomarker pigments were correlated to temperature, density and nitrate concentrations ($p<0.01$) from the surface to 100 m, probably revealing that nitrate was the main limiting factor for algal growth. Only the 19′hexanoyloxyfucoxanthin (19Hf) and zeaxanthin (Zeax) did not present significant correlation ($p>0.05$) with the environmental parameters. The latter traces the cyanophyte abundance, which are often present in the surface layer with the species *Synechococcus* sp. The former revealed the presence of prymnesiophytes with lower biomass in surface than in the DCM, even though not all prymnesiophytes contained 19Hf. Indeed, the $chlc_3$ pigment—another biomarker of prymnesiophytes—presented the same trend as the other pigments, revealing that the non-containing 19Hf-prymnesiophytes followed a vertical gradient.

During winter, the distribution of pigments was less exclusively dependent on the vertical gradient of the environmental parameters (e.g., temperature, nutrient concentrations, salinity). Indeed, few pigments were significantly correlated to environmental parameters, revealing a little effect of nutrient concentration on the algal distribution.

The proportion of photoprotective pigments was significantly higher in July than in December, as revealed by the diadinoxanthin (Dd) vs Chl*a* ratio (Fig. 7). The vertical gradient was much more accentuated in summer than in winter, due to the increase of Dd values in the surface layer in summer, while the deeper layer values were rather similar between the two seasons.

In the surface layer, the diatoxanthin (Dt) pigment, which corresponds to the quick-reacting photoprotective xanthophyll, contributed at 20% and 10% to the xanthophyll-cycling pigments (sum of diatoxanthin and diadinoxanthin), in summer (Table 1) and in winter, respectively.

The grazing indicator (phaeophorbides *a* vs chl*a*) was generally low (Table 2), in relation to the investigated seasons where the biological activity was low (Decembrini et al., 2008). The grazing activity was higher in winter than in summer in the surface layer, in agreement with the higher primary production (Decembrini et al., 2008), even though the abundance of copepods was lower (G. Gorski, pers. comm.). In the DCM, phaeophorbides *a* vs Chl*a* values were 2 times higher with respect to the surface layer, in relationship with the higher algal biomass.

The average divinyl-Chl*a* concentration (biomarker of *Prochlorococcus*) was the same between the two cruises (~0.011 $\mu g\,L^{-1}$), thus contributing to the 10 and 20% of total chl*a* biomass over the water column in July and December, respectively. The great difference between the two seasons appeared in the surface layer and could be due to the huge decrease (~by 3 to 5 times) in dvchla per cell of *Prochlorococcus* in response to the high irradiance level in summer (e.g., Brunet et al., 2006, 2007). Fig. 8 well illustrates this feature with the two different significant regressions ($p<0.01$) found between the concentrations of dvchla and zeaxanthin, corresponding to the surface layer

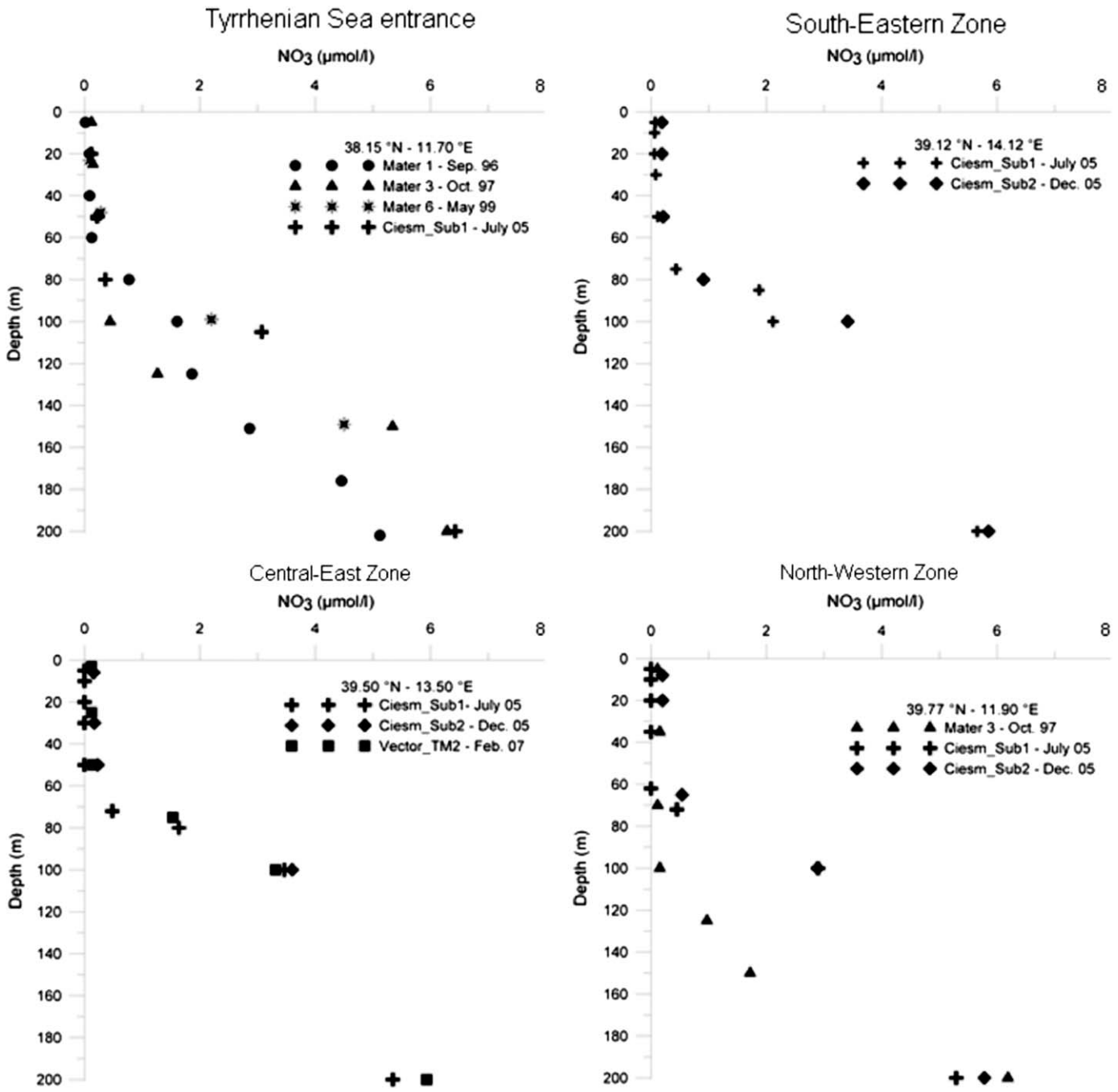

Fig. 4. Nitrate profiles for the upper layer at four sites in the southern Tyrrhenian Sea. The four sites are those marked in Fig. 1 with circles. The sampling times and correspondent cruises are reported in the inset.

(0 to 50 m depth) and the DCM (50–100 m), respectively. The dvchla content was higher in the deeper layer than in the surface layer, corresponding to the two surface and deeper layer ecotypes, as already discussed by many authors (see Brunet et al., 2006 and references therein). The season, summer or winter, did not affect these regressions since data from the two cruises were included into the graph and only the deeper layer drove the variability.

3.3. The anticyclonic eddy

An in-depth analysis of the structure and dynamics of the eddy is reported by Budillon et al. (2008). They state that the eddy was very stable during the 5-month interval between the cruises and that is was mostly filled with Winter Intermediate Water coming from the northwestern Basin. They also showed that oxygen distribution was homogeneous down to 300 m. The nutrient distribution displays a similar pattern of internal homogeneity, with a nitrate concentration being less than 3.5 μmol dm^{-3} at 200 m opposed to the 5 μmol dm^{-3} in the station outside the eddy. Interestingly there is no significant difference in nutrient concentrations within the eddy between the two cruises.

On the other hand the typical vertical motions linked to mesoscale activity (Strass et al., 2002) could be detected at a station SE of the eddy sampled during the late fall cruise. For that station the data of the concentrations of dvchl*a* and zeaxanthin for the entire water column fit into the surface-layer regression

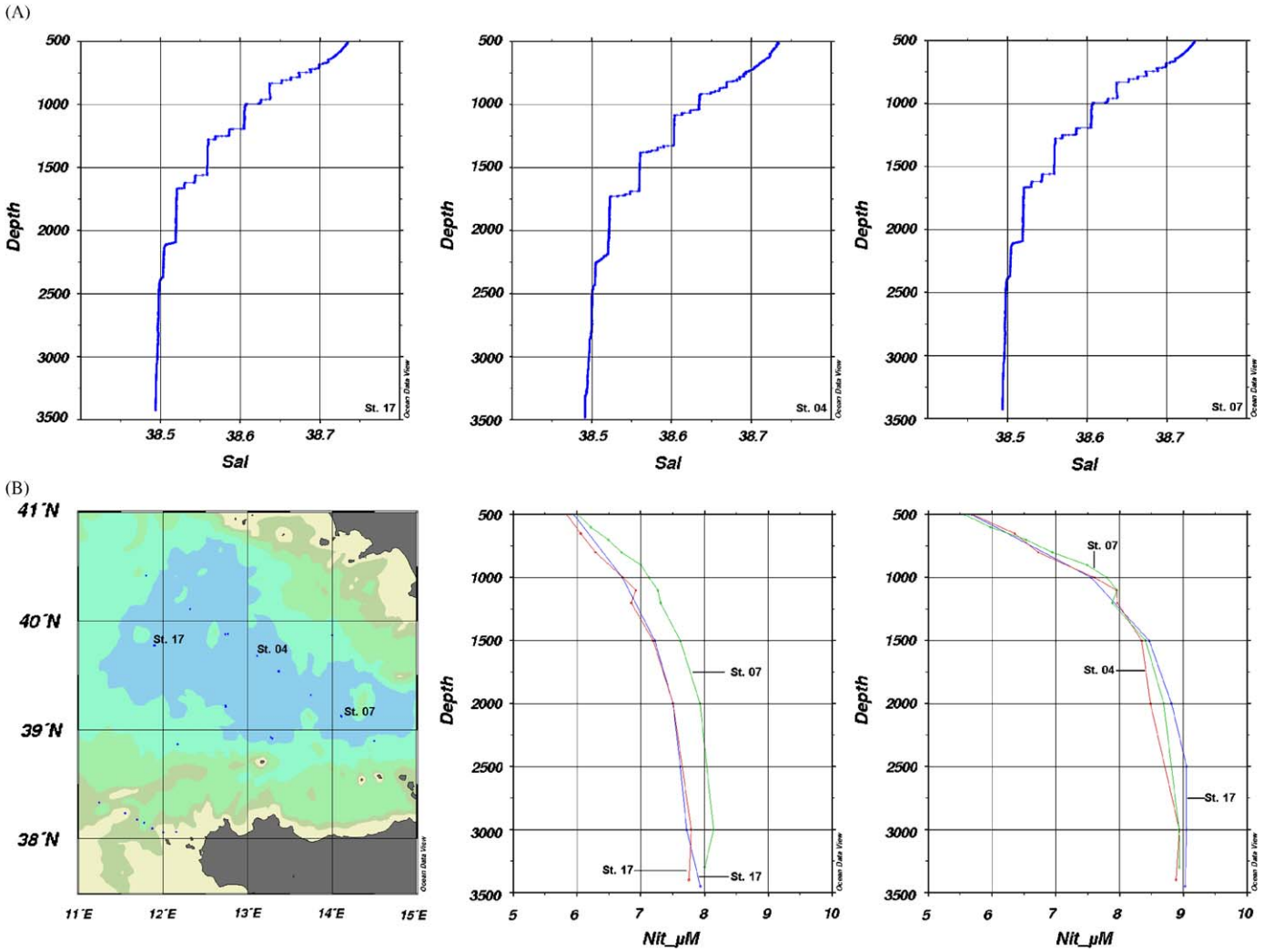

Fig. 5. Salinity profiles in stepped structures in different stations (A) and vertical distributions of nitrate and silicate in the same stations (B) from 500 m to bottom.

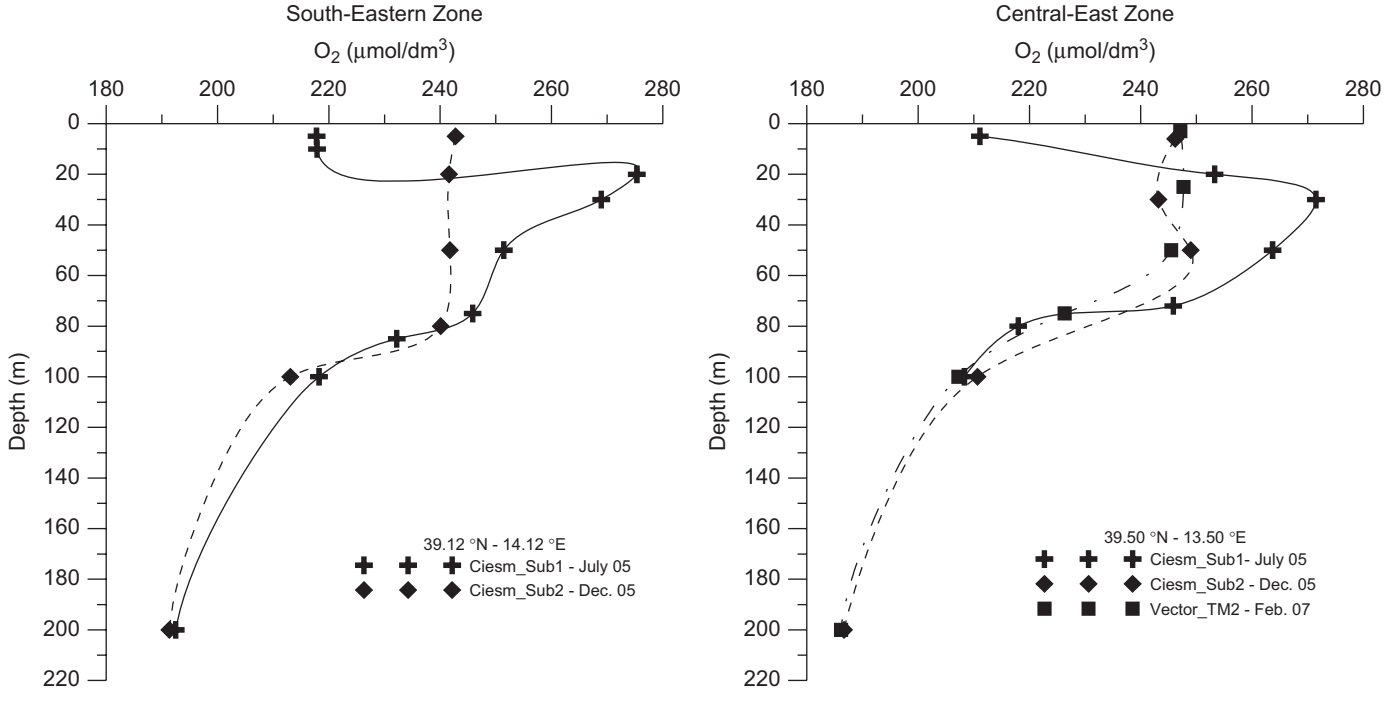

Fig. 6. Dissolved oxygen profiles for two of the sites shown in Fig. 1.

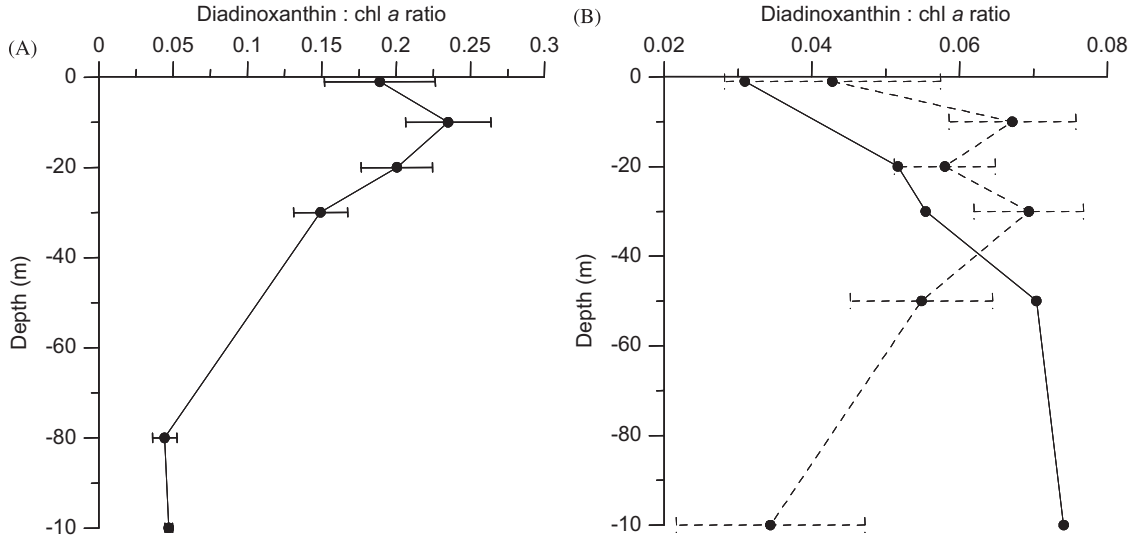

Fig. 7. Distribution of the diadinoxanthin: chl*a* ratio along the first 100-m depth of the water column: (A) mean profile during the CIESM 1 cruise (July 2005) and (B) mean profile of the stations 20 and 21 (dashed line) and profile of the station 4 during the CIESM 2 cruise (December 2005).

Table 2
Pigment characteristics (mean and standard deviations) of the water masses in July ($n = 18$ and 12, for the surface and DCM layers, respectively) and December 2005 ($n = 9$ and 6, for the surface and DCM layers, respectively)..

	chl*a* ($\mu g\,L^{-1}$)	dvchla vs. chl*a*	19Bf/chl*a*	Fuco/chl*a*	19Hf/ch*a*	Zeax/chl*a*	Chl*b*/chl*a*	PrD/chl*a*
July								
Surface	0.035	0.028	0.120	0.064	0.370	0.220	0.200	0.024
	(0.009)	(0.042)	(0.025)	(0.041)	(0.045)	(0.050)	(0.120)	(0.012)
DCM	0.200	0.270	0.260	0.170	0.450	0.130	0.810	0.070
	(0.008)	(0.012)	(0.070)	(0.010)	(0.050)	(0.060)	(0.190)	(0.040)
December								
Surface	0.061	0.150	0.180	0.048	0.360	0.200	0.340	0.050
	(0.009)	(0.009)	(0.030)	(0.002)	(0.050)	(0.010)	(0.140)	(0.014)
DCM	0.051	0.310	0.260	0.063	0.410	0.160	1.010	0.080
	(0.019)	(0.090)	(0.070)	(0.010)	(0.050)	(0.050)	(0.200)	(0.040)

dvchl*a*: divinylchlophyll *a*, Fuco: fucoxanthin (diatoms), 19Bf: 19′butanoyloxyfucoxanthin (pelagophytes), 19Hf: 19′hexanoyloxyfucoxanthin (prymnesiophytes), Zeax: zeaxanthin (cyanophytes), Chl*b*: chlorophyll *b* (green algae), PrD: sum of phaeophorbides a (grazing indicator).

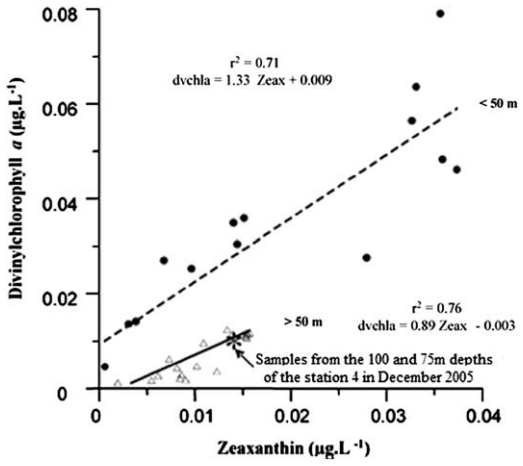

Fig. 8. Relationships between the concentrations ($\mu g\,L^{-1}$) in dvchla (biomaker of *Prochlorococcus*) and zeaxanthin (biomaker of *Prochlorococcus* and *Synechococus*). The two linear regressions correspond to the two data sets of the surface layer (0–50-m depth) and below 50-m depth, respectively. Black dots indicate values from July 2005 and the empty triangles indicate samples from December 2005. It can be noticed that the samples of at 100 and 75 m (*) of the station 4 in December 2005 belong to the "surface-layer data set".

(Fig. 8). This means that the ecotype of *Prochlorococcus* present in the deeper layer at that station was the surface ecotype, as opposed to the data from the same depths (75 and 100 m) at all the other stations. This could be interpreted as the deepening of the surface layer at this station due mesoscale activity. This is further supported by the profile of diadinoxathin:chl*a* ratio (Fig. 6B, continuous line), which showed that at the same station the Dd/Chl*a* increased in the layer above 50 m, suggesting an origin from high light level (surface layer) for the water mass occupying that layer.

Below 200 m the nutrient concentrations increase progressively, with the typical slower pace for silicates, reaching 6.2–6.3 $\mu mol\,dm^{-3}$ in the LIW core (between 400 and 500 m) and 8.1–8.2 $\mu mol\,dm^{-3}$ in the layer of the WMDW (Fig. 9).

3.4. The possible impact of the Eastern Mediterranean Transient (EMT)

The profiles reported in Fig. 9 span over a 10-year period. Besides the already highlighted smoother slope in the nutricline in the upper layer, the differences in nutrient concentrations are not large between the post EMT phase (mid-1980s) and

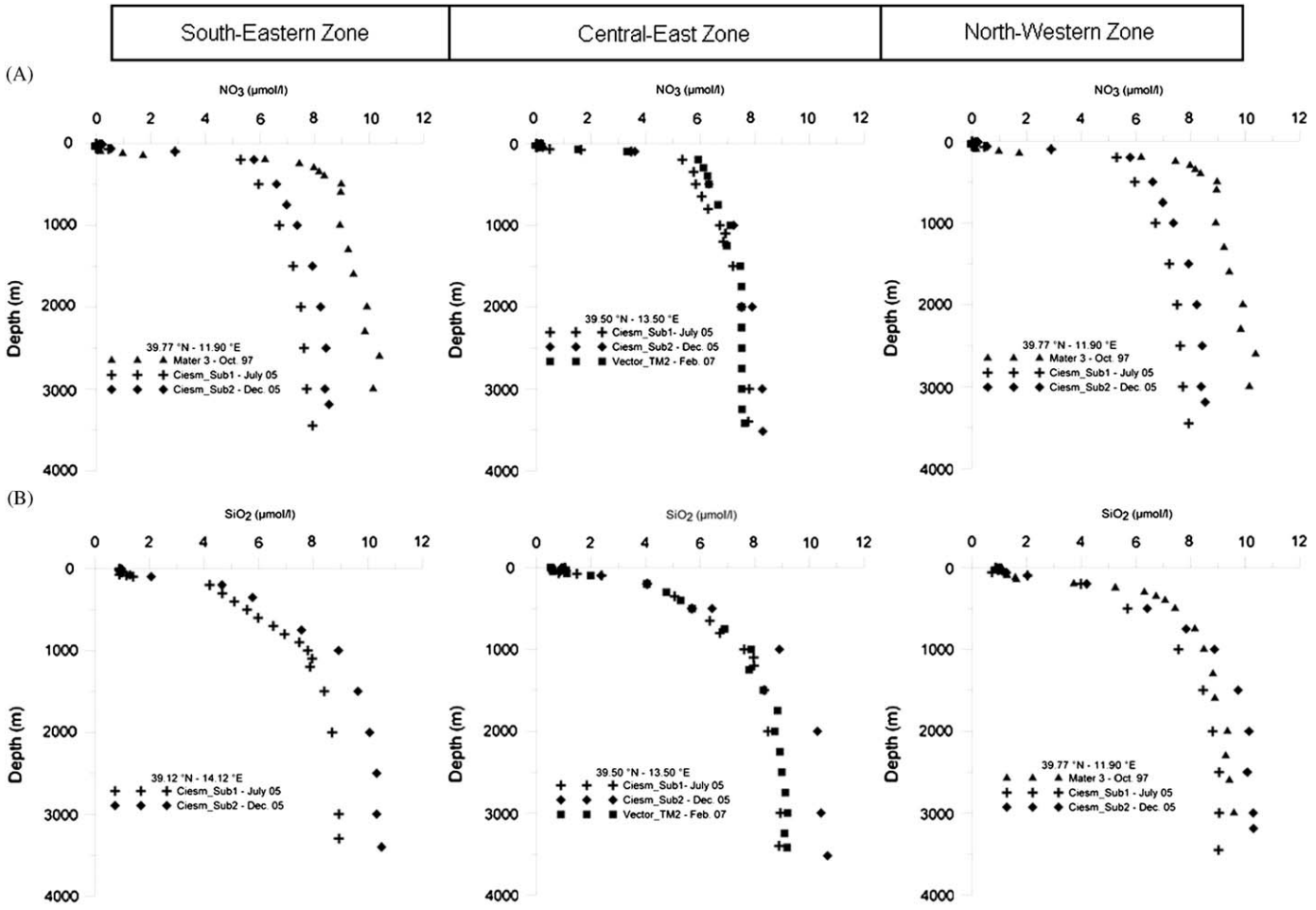

Fig. 9. Nitrate (A) and silicate (B) vertical profiles for different sites in the southern Tyrrhenian Sea. The sampling times and correspondent cruises are shown in the inset.

2006–2007, years of the last observations reported in this short note. To better highlight possible differences and filter the inter-sample variance, we computed the depth integrated average over the intermediate (200–600 m), transitional (600–1200 m), and deep (1200-m bottom) layers, at the SE entrance of the basin and at a deep central site (Fig. 9). Unfortunately, the observations are very few and scattered in space and time; therefore the plots are based on a reduced number of points.

The dominant pattern is of an increase in nitrate concentration in the intermediate and transitional waters entering the basin during the years 1996–1998 (from 5.7 to 7 µmol dm^{-3}), which becomes stable afterwards (but note the large gap in observations). On the other hand, in the basin interior there is decrease in concentration, especially in the deep layer.

4. Discussion and conclusions

The highly multidisciplinary scope of the two CIESM-SUB surveys was aimed at providing the first direct information on the biogeochemical features of the Southern Tyrrhenian Sea both in the water column and at the sea bottom. Before those surveys such information was very scanty and no information at all was available in the open literature.

An intriguing question relates to the seasonal cycle in the area, because of the opposite patterns observed in the southeastern and northwestern Mediterranean (D'Ortenzio, 2003). The data collected showed that the vertical structure of the water column, while having a different density profile, displays a similar depth for the start of nitracline. In both summer and late fall the depth at which nitrate concentration detaches from the background level is always located in the same narrow depth interval. This suggests that the mixing produced after the inversion of buoyancy fluxes in fall, which is typical of mid-latitudes, does not penetrate below 70–80 m. Because this is the same depth of the nutricline during summer, not too much nutrient enrichment has to be expected in fall. Interestingly the same profile was kept until the following February, i.e. in mid-winter. It is not possible to ascertain whether 2007 was an anomalous year in terms of mixed-layer dynamics, but such a shallow mixed layer is definitely anomalous, especially if compared with climatological data (e.g., D'Ortenzio et al., 2005).

The similarity among the two seasons also was confirmed by the absence of relevant changes in the composition of the algal pigments and, therefore, in the community structure. Even though some of the environmental conditions were different (namely light and temperature) the pigment community composition was stable. This means that the reduced light in winter or the reduced nutrients in summer has a similar impact on community composition in the surface layer, at least for what can be derived from pigment spectra. Only in the DCM, the biomass concentration differs, being more abundant in summer than in winter, where synergistic effects of low light preventing any photoinhibition, but with a longer photoperiod, and nutrient availability

favor the persistence of the peak in biomass mainly composed of pelagophytes and green algae, which are very well adapted to this peculiar environment (e.g., Brunet et al., 2006, 2007 and references therein).

While the depth of the autumnal nitracline (75 m) is consistent with a typical seasonal cycle for such latitudes, it is anomalous that the nitracline is at same depth in summer, especially considering that the pycnocline is much shallower. We speculate that the reason for such a distribution resides in the dynamics of MAW. It is likely that MAW reaches the area already depleted in nutrients in the upper layer, because east of the Alboran gyre the water is already nutrient-poor, which are further stripped on the way to the southern Tyrrhenian. The only mechanisms to refuel the upper layer during late spring–summer are the upward diffusion provoked by the horizontal shear with the intermediate water, the mesoscale activity and the atmospheric deposition. Neither of those seems to be sufficiently intense after the entrance in the basin to be able to markedly refuel the upper layer. Overall the phytoplankton biomass value was in fact very low ($0.058\,\mu g$ chl$a\,L^{-1}\pm0.025$, $0.094\,\mu g$ chl$a\,L^{-1}\pm0.120$, respectively, in December and July 2005) and matched the low nitrogen concentrations.

As a matter of fact, the comparison of nitrogen and oxygen in the intermediate layer over the whole area did not show statistically significant differences. We interpret this as the result of a low export production over the more than five months interval between the cruises. This is further confirmed by the very low changes observed in the anticyclonic eddy. According to Budillon et al. (2008) the exchange between the eddy and the surrounding water was negligible. Therefore, the oxygen consumption over the 5-month interval can be taken as a proxy of the export from the surface. The consumption was around 4 mmol m^{-3} over approximately 150 m. This corresponds to about 30 mg $C\,m^{-2}\,d^{-1}$ of primary production exported to the subsurface layer, which is not at all a large number.

Systems that do not host large seasonal blooms and produce small export production are not necessarily ineffective in transferring the production to higher trophic levels (Pauly and Christensen, 1995). In other words the relative oligotrophy of the area, at least from the point of the standing stock of phytoplankton biomass, does not exclude that the basin may support a reasonable stock of higher predators, but this needs further investigation. This might be mainly based on the microbial loop, as could be suggested by the high presence of picoplankton as for instance the cyanophytes (*Prochlorococcus* and *Synechococcus*) revealed by the pigment analysis during this study in agreement with other studies from the Strait of Sicily (Brunet et al., 2006, 2007).

The whole region displays a homogeneous distribution of nutrient and phytoplankton biomass, with the exception of the SW area. Budillon et al. (2008) infer from the persistence of the eddy that the advective field was quite weak and, correspondingly, also the mesoscale should have not been very energetic. As opposed to other systems, e.g., the Gulf of Naples (Casotti et al., 2000), the biological tracers of hydrological/hydrodynamical features do not indicate any significant patchiness, even within the MAW.

It was mentioned above that the vertical distribution of nutrients in the Mediterranean Sea displays an evident E–W trend with a progressive shoaling of the nitracline and an increase in the absolute values of the subsurface waters. In the Southern Tyrrhenian the profile is more of eastern type, with a nitrate concentration of $6\,\mu mol\,dm^{-3}$ only below 200 m. This is definitely different from the profile of the northwestern Mediterranean as reported for the Dyfamed site where the $6\,\mu mol\,dm^{-3}$ isoline is often detected at 100 m (Marty et al., 2002) and for other areas of the Algero-provencal basin where the same isoline is also located between 100 and 130 m (G. Civitarese, pers. comm.). This is also consistent with a seasonal cycle basically deprived of a spring bloom.

Two additional questions were raised at the start of this analysis.

The first was whether the double diffusion acting in the deepest part of the basin does in fact affect the vertical distribution of nutrients. Even considering that the detectable differences in nutrient concentrations do not allow for resolving the differences to the same resolution as for T, S and density anomaly, the vertical profiles do not show signatures reflecting processes linked to double diffusion, neither there are spatial differences (within the stepped structure region or outside it) which allow for classifying the areas as diverse. Our explanation is that, below 1000 m the nutrient concentrations are nearly uniform in the Western Mediterranean and therefore the double diffusion does not affect them, at least in the limit of the resolution of our measurements.

The final issue was related to the impact of the EMT. It is important to note that we lack coverage for most of the period (1987–1997) when the impact of the EMT produced striking changes in the water-mass properties of the Straits of Sicily and the southern Tyrrhenian Sea (Gasparini et al., 2005). We only have the repetitive sampling during Mater (2006–2008) and the most recent one. 1996 was already in a decaying phase of the EMT, but its modifications were still exported in the western basin. Years 1996–1998, according to Gasparini et al. (2005), were characterized by denser water crossing the Straits of Sicily which was progressively saltier. This corresponded to the transition from the import of the denser, nutrient-rich, sub-intermediate water of the Eastern Mediterranean to a mixture with a larger fraction of Cretan Intermediate Water. The nutrient concentrations at the basin entrance showed a corresponding decrease, as expected, to reach the present stable values. The pattern in the central site of the Southeastern Mediterranean is also qualitatively consistent with this scenario but, unfortunately, it is not possible to verify its quantitative consistency.

In brief, the denser intermediate water flowing in the Tyrrhenian spreads down to deeper isopycnals, thus exporting more salt in the deep layer (Gasparini et al., 2005) but, because of the lower concentration of nutrients as compared to the values in the deep water, diluting their nutrient content. We interpret the decrease shown in Fig. 10 as a dilution effect. Gasparini and colleagues estimated an average input of intermediate water in the deep layer of approximately 0.3 Sv over the 1900–2000 interval, all flowing in the deep Tyrrhenian Sea whose volume was assumed to be $2\times10^{14}\,m^3$. The change in concentration is consistent with those numbers if one assumes that the previous deep concentration was around $10\,\mu mol\,dm^{-3}$ and the observed change was of $2\,\mu mol\,dm^{-3}$ (Fig. 11). With the fluxes estimated by Gasparini et al. (2005) the source water should have had a nitrate concentration of $5.8\,\mu mol\,dm^{-3}$, which is in the range of the concentrations of water exiting the Sicily Channel. We speculate also that the denser intermediate water reduced the nitrogen renewal of the subsurface layer in the Tyrrhenian Sea, possibly reducing the export production and the nitrogen normally exported at depth. In other words, a larger fraction of the nitrogen reaching the deep layers o f the basin was pre-formed nitrogen (i.e. nitrogen already present in the source water as nitrate) than exported nitrogen (nitrate derived from the re-mineralization of particulate organic nitrogen sinking from the surface). A robust test of this hypothesis could be performed by a modelling study and an intensive analysis of remote-sensed imageries, which is part of an ongoing study.

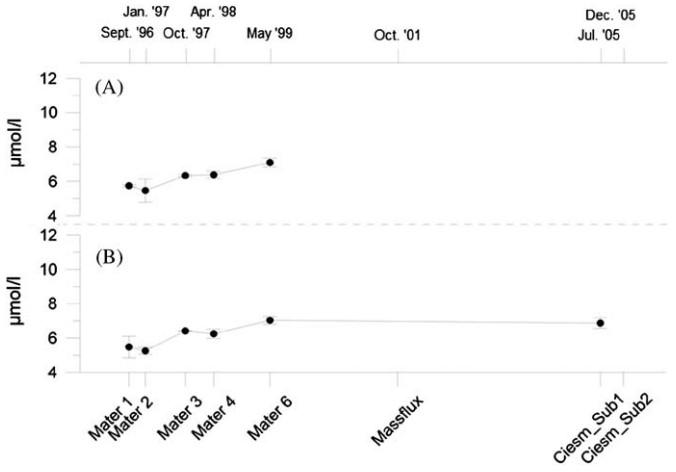

Fig. 10. Time trends of depth-integrated nitrate concentrations from 1996 through 2006 for the 200–600 m (A) and 600–1200 (B) depth intervals at the entrance of southern Tyrrhenian site.

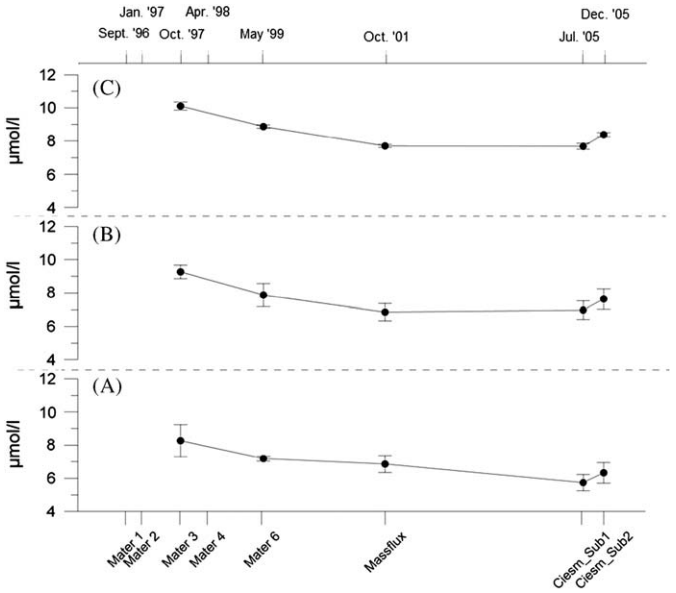

Fig. 11. Time trends of depth-integrated nitrate concentrations from 1996 through 2006 for the 200–600 m (A) and 600–2000 m (B) and 2000-m bottom (C) depth intervals at the NW site.

Acknowledgements

This paper falls also in the aims of the program VECTOR (VulnErabilità delle Coste e degli ecosistemi marini italiani ai cambiamenti climaTici e loro ruolO nei cicli del caRbonio mediterraneo) which supported part of the sampling in Tyrrhenian sea.

References

Astraldi, M., Conversano, F., Civitarese, G., Gasparini, G.P., Ribera d'Alcalà, M., Vetrano, A., 2002. Water mass properties and chemical signatures in the central Mediterranean region. Journal of Marine Systems 33–34, 155–177.

Astraldi, M., Gasparini, G.P., 1992. The seasonal characteristics of the circulation in the north Mediterranean basin and their relationship with the atmospheric–climatic conditions. Journal of Geophysical Research 97, 9531–9540.

Bethoux, J.P., Morin, P., Medec, C., Gentili, B., 1992. Phosphorus and nitrogen behavior in the Mediterranean Sea. Deep-Sea Research I 39, 1641–1654.

Bethoux, J.P., Morin, P., Ruiz-Pino, D., 2002. Temporal trends in nutrient ratios: chemical evidence of Mediterranean ecosystem changes driven by human activity. Deep-Sea Research II 49, 2007–2016.

Brunet, C., Casotti, R., Aronne, B., Vantrepotte, V., 2003. Measured photophysiological parameters used as tools to estimate vertical water movements in the coastal Mediterranean. Journal of Plankton Research 25 (11), 1413–1425.

Brunet, C., Casotti, R., Vantrepotte, V., Corato, F., Conversano, F., 2006. Picophytoplankton diversity and photophysiology in the Strait of Sicily (Mediterranean Sea) in summer. I. Mesoscale variations. Aquatic Microbial Ecology 44, 127–141.

Brunet, C., Casotti, R., Vantrepotte, V., Conversano, F., 2007. Vertical variability and diel dynamics of picophytoplankton in the Strait of Sicily (Mediterranean Sea) in summer. Marine Ecology Progress Series 346, 15–26.

Budillon, G., Gasparini, G.P., Schroeder, K., 2008. Persistence of an eddy signature in the central Tyrrhenian Basin Deep-Sea Research II, this issue [doi:10.1016/j.dsr2.2008.07.027].

Carpenter, J.H., 1965. The accuracy of the Winkler method for the dissolved oxygen analysis. Limnology and Oceanography 10, 135–140.

Casotti, R., Brunet, C., Aronne, B., Ribera d'Alcalà, M., 2000. Mesoscale features of phytoplankton and planktonic bacteria in a coastal area as induced by external water masses. Marine Ecology Progress Series 195, 15–27.

D'Ortenzio, F., 2003. Space and time occurrence of algal blooms in the Mediterranean: their significance for the trophic regime of the basin. Ph.D. Thesis, Open University of London, UK, 298pp.

D'Ortenzio, F., Iudicone D., de Boyer Montegut, C., Testor, P., Antoine, D., Marullo, S., Santoleri, R., Madec, G., 2005. Seasonal variability of the mixed layer depth in the Mediterranean Sea as derived from in situ profiles. Geophysical Research Letters 32, doi:10.1029/2005gl022463.

Decembrini, F., Caroppo, C., Azzaro, M., 2008. Size structure and production of phytoplankton community and carbon pathways channelling in the Southern Tyrrhenian Sea (Western Mediterranean). Deep-Sea Research II, this issue [doi:10.1016/j.dsr2.2008.07.022].

Dimier, C., Corato, F., Tramontano, F., Brunet, C., 2007. Photoprotection and xanthophyll cycle activity in three diatoms. Journal of Phycology 43 (5), 937–947.

Gasparini, G.P., Ortona, A., Budillon, G., Astraldi, M., Sansone, E., 2005. The effect of the Eastern Mediterranean Transient on the hydrographic characteristics in the Strait of Sicily and in the Tyrrhenian Sea. Deep-Sea Research I 52, 915–935.

Grasshoff, K., 1976. Methods of seawater analysis. New York, 317pp.

Herut, B., Collier, R., Krom, M.D., 2002. The role of dust in supplying nitrogen and phosphorus to the South East Mediterranean. Limnology and Oceanography 47, 870–878.

Kouvarakis, G., Mihalopoulos, N., Tselepides, A., Stavrakakis, S., 2001. On the importance of atmospheric inputs of inorganic nitrogen species on the productivity of the eastern Mediterranean Sea. Global Biogeochemical Cycles 15, 805–817.

Kress, N., Herut, B., 2001. Spatial and seasonal evolution of dissolved oxygen and nutrients in the Southern Levantine Basin (Eastern Mediterranean Sea): Chemical characterisation of the water masses and inferences on the N:P ratios. Deep-Sea Research I 48, 2347–2372.

Krom, M.D., Herut, B., Mantoura, R.F.C., 2004. Nutrient budget for the Eastern Mediterranean: implications for phosphorus limitation. Limnology and Oceanography 49, 1582–1592.

Marty, J.C., Chiaverini, J., Pizay, M.D., Avril, B., 2002. Seasonal and interannual dynamics of nutrients and phytoplankton pigments in the western Mediterranean Sea at the DYFAMED time-series station (1991–1999). Deep-Sea Research II 49, 1965–1985.

Migon, C., Copin-Montegut, L., Elegant, L., Morelli, J., 1989. Atmospheric input of nutrients to the costal Mediterranean area: biogeochemical implications. Oceanologica Acta 12, 87–191.

Pauly, D., Christensen, V., 1995. Primary production required to sustain global fisheries. Nature 374, 255–257.

Ribera d'Alcalà, M., Civitarese, G., Conversano, F., Lavezza, R., 2003. Nutrient ratios and fluxes hint at overlooked processes in the Mediterranean Sea, Journal of Geophysical Research 108 (C9), doi:10.1029/2002JC001650.

Roether, W., Klein, B., Manca, B.B., Theocharis, A., Kioroglou, S., 2007. Transient Eastern Mediterranean deep waters in response to the massive dense-water output of the Aegean Sea in the 1990s. Progress in Oceanography 74, 540–571.

Souvermezoglou, E., Krasakopoulou, E., Pavlidou, A., 1999. Temporal variability in oxygen and nutrient concentrations in the southern Aegean Sea and the Straits of the Cretan Arc. Progress in Oceanography 44, 573–600.

Strass, V.H., Naveira Garabato, A.C., Pollard, R.T., Fischera, H.I., Hensea, I., Allen, J.T., Read, J.F., Leach, H., Smetacek, V., 2002. Mesoscale frontal dynamics: shaping the environment of primary production in the Antarctic Circumpolar Current. Deep-Sea Research II 49, 3735–3769.

Zodiatis, G., Gasparini, G.P., 1996. Thermohaline staircase formations in the Tyrrhenian Sea. Deep-Sea Research I 43, 655–678.

Deep-Sea Research II 56 (2009) 687–699

Contents lists available at ScienceDirect

Deep-Sea Research II

journal homepage: www.elsevier.com/locate/dsr2

Size structure and production of phytoplankton community and carbon pathways channelling in the Southern Tyrrhenian Sea (Western Mediterranean)

Franco Decembrini [a,*], Carmela Caroppo [b], Maurizio Azzaro [a]

[a] CNR-IAMC, Istituto Sperimentale Talassografico, Spianata S. Raineri 86, 98122 Messina, Italy
[b] CNR-IAMC, Istituto Sperimentale Talassografico, Via Roma 3, 74100 Taranto, Italy

ARTICLE INFO

Article history:
Accepted 7 July 2008
Available online 5 November 2008

Keywords:
Primary production
Size-fractionated phytoplankton
Chlorophyll *a*
Carbon pathways
Tyrrhenian Sea

ABSTRACT

In the frame of a multidisciplinary international joint effort, supported by CIESM, phytoplankton composition, distribution and activity in summer and late autumn in the Southern Tyrrhenian Sea were investigated. The main aim of the study was to obtain a preliminary characterization of the autotrophic community structure of a poorly investigated and complex basin during two contrasting seasonal conditions (stratification vs homogeneity). On both occasions the phytoplankton biomass, as chlorophyll *a*, was low in the euphotic layer of water column (8.9 mg m^{-2} in July and 10.7 mg m^{-2} in December), with a clear dominance of the pico-phytoplanktonic component (64% and 76%, respectively), and a pronounced summer Deep Chlorophyll Maximum. Interestingly, primary production was higher in December (429 mg C m^{-2} d^{-1}) than July (273 mg C m^{-2} d^{-1}), again with a major contribution of pico-class in both seasons (90% and 52% in late autumn and summer, respectively). The dominant contribution of small size classes to the total photosynthetic efficiency and their fast carbon turnover time within the community hint at a preferential carbon pathway through the small-sized components of the food web that contrasts with the traditional views of the Tyrrhenian Sea as a typical component of the temperate Western Mediterranean Sea.

1. Introduction

The size structure of the phytoplankton community is the most relevant ecological property that controls the flow through the marine food web. In open waters two extreme trophic pathways are described: the "herbivorous" food web based on the presence of large phytoplankton, herbivorous zooplankton and fishes, and the "microbial" loop composed by autotrophic and heterotrophic microbes (<2.0 μm) and protozoa. The shift between the "herbivorous" and "microbial" food webs determines the ecosystems ability to export or recycle biogenic carbon (Legendre and Le Fèvre, 1989; Legendre and Rassoulzadegan, 1996). Between these two food webs the environmental trophic continuum includes "multivorous" and "microbial" pathways (Legendre and Rassoulzadegan, 1995). In the first one the herbivorous and microbial trophic patterns both play significant simultaneous roles, while the microbial food web includes the microbial loop and nano-phytoplankton (Rassoulzadegan, 1993). Each of these food webs expresses different ecological and biogeochemical significances linked to the biogenic carbon flux.

In the oligotrophic systems, as well as the open waters of the Mediterranean Sea (MS), the phytoplankton communities are dominated by the presence of small-sized cells. A complex microbial food web favours the recycling of a significant fraction of organic carbon (DOC) within the upper layer (Chisholm et al., 1988). This food web based on the pico- and nano-phytoplankton is persistent in terms of biomass and production, and these small-sized cells can be considered as a background component of the autotrophic community (Magazzù and Decembrini, 1995; Cermeño et al., 2006). In some areas or periods (divergence zones or short spring-blooms) the injection of nitrate in the euphotic zone by hydrodynamic forcing (such as winter mixing, upwelling or cyclonic gyres) stimulates high carbon production. In these cases the community is dominated by large phytoplankters (diatoms and nanoflagellates) and characterized by high export of fixed carbon (POC) to upper trophic levels through a short food chain (Eppley and Peterson, 1979).

Phytoplankton size structure depends on physical and biological factors that ultimately are influenced by local and mesoscale hydrodynamics of the system (Riegman et al., 1993) such as eddies and unstable fronts (Rodriguez et al., 2001). Particularly relevant factors are the water-column stability that controls large-sized

* Corresponding author. Tel.: +39 90669003; fax: +39 90669007.
E-mail addresses: franco.decembrini@iamc.cnr.it (F. Decembrini), carmela.caroppo@iamc.cnr.it (C. Caroppo), maurizio.azzaro@iamc.cnr.it (M. Azzaro).

0967-0645/$ - see front matter © 2008 Elsevier Ltd. All rights reserved.
doi:10.1016/j.dsr2.2008.07.022

cells losses by passive sinking or accumulation and the selective zooplankton grazing (Irwin et al., 2006).

Although a great deal of effort has been given to primary production study in the MS (Vidussi et al., 2000, 2001; Marty and Chiavérini, 2002; Marty et al., 2002; Moutin and Raimbault, 2002), less is known at basin scale for the Tyrrhenian Sea. This basin acts as the interface in the exchanges with the eastern MS, and both the Eastern Mediterranean Transient (EMT) and climate oscillations influence the complex dynamics of biological fluxes that occur in time and space. The Tyrrhenian Sea has a surface wider than 203,000 km^2 and its central-southern zone is characterized by an abyssal plain ($>$3000 m depth). The hydrographical structure identifies an upper layer of a relatively fresh water of Atlantic origin (Modified Atlantic Water, MAW) in the uppermost 200 m. An underlying layer (200–700 m) is occupied by the Levantine Intermediate Water (LIW), and the Western Mediterranean Deep Water (WMDW) characterizes the water column from 700 m to seabed (Hopkins, 1988; Astraldi and Gasparini, 1994; Sparnocchia et al., 1999). The surface layer, the subject of this study, is characterized by wide seasonal variability of the hydrographic forcings that induce a wind-driven mixing in winter and strong stratification in summer. These two conditions drive the seasonal trophic regimes, with oligo-mesotrophy mainly in spring and oligotrophy in summer (Claustre et al., 1989; Morel and Andrè, 1991).

This work evaluates the contribution of different phytoplankton size-classes and species community structure to the carbon synthesis process in the Southern Tyrrhenian Sea open waters. The main questions addressed in this study concern how efficiently the carbon is assimilated in the two contrasting hydrographical conditions and what are the prevailing pathways of biogenic carbon channelled by primary producers.

2. Materials and methods

2.1. Sampling and hydrographical characteristics

The study was performed in the open waters of the Southern Tyrrhenian Sea (Fig. 1) during two CIESM cruises carried out, respectively, in summer on board the R/V *Universitatis* (21–30 July 2005) and in late autumn on board the R/V *Urania* (13–22 December 2005). Hydrographical profiling and biological sampling were conducted at several fixed stations (9 in July and 17 in December) located along two main NW–SE and NE–SW transects.

Temperature, conductivity (salinity) and dissolved oxygen were recorded by a SeaBird Electronics SBE-911plus CTD profiler equipped with a Turner fluorometer (mod. Aquatracka) for chlorophyll *a* profiling. At each station five samplings were carried out using a Rosette sampler with 24 10-L Niskin bottles based on surface, oxygen maximum, thermohaline structures, the deep chlorophyll maximum (DCM) when present, and base of euphotic zone (0.1%E_0^+).

Surface (E_0^+) and underwater scalar irradiance of photosynthetically available radiation (PAR: 400–700 nm) were measured with a PNF-300 profiler (Biospherical Instruments, USA). To calculate the irradiance penetration, an exponential model based on the relative available light recorded in the water column ($PAR_{water}/PAR_{surface}$%) was adopted.

2.2. Photosynthetic pigments and primary production

Chlorophyll *a* (chl*a*) and phaeophytin (phaeo) concentrations were measured fluorometrically (Yentsch and Menzel, 1963). Water samples (1.5–2.0 L) were sequentially filtered on polycarbonate filters (10.0 and 2.0 μm) and then through a Whatman GF/F glass-fibre filter to separate three size classes: micro- ($\geqslant$10.0 μm), nano- ($\leqslant$2.0 and $<$10.0 μm), and pico-phytoplankton ($\leqslant$0.2 and $<$2.0 μm). Filters were stored in aluminium foil at −20 °C until the laboratory analysis. chl*a* and phaeo were extracted in a 90% acetone solution, at 4 °C for 24 h in the dark, and measured with a spectrofluorometer (mod. Varian Cary Eclipse) before and after acidification. Excitation and emission wavelengths (429 and 669 nm) were selected after standardization with a solution of chl*a* extracted from *Anacistys nidulans* (by Sigma Co). The chl*a* and phaeo concentrations were calculated according to Lorenzen (1967). The conversion of chl*a* in carbon was evaluated assuming that chl*a* was on average the 1.5% of the phytoplankton biomass (Morán et al., 2001).

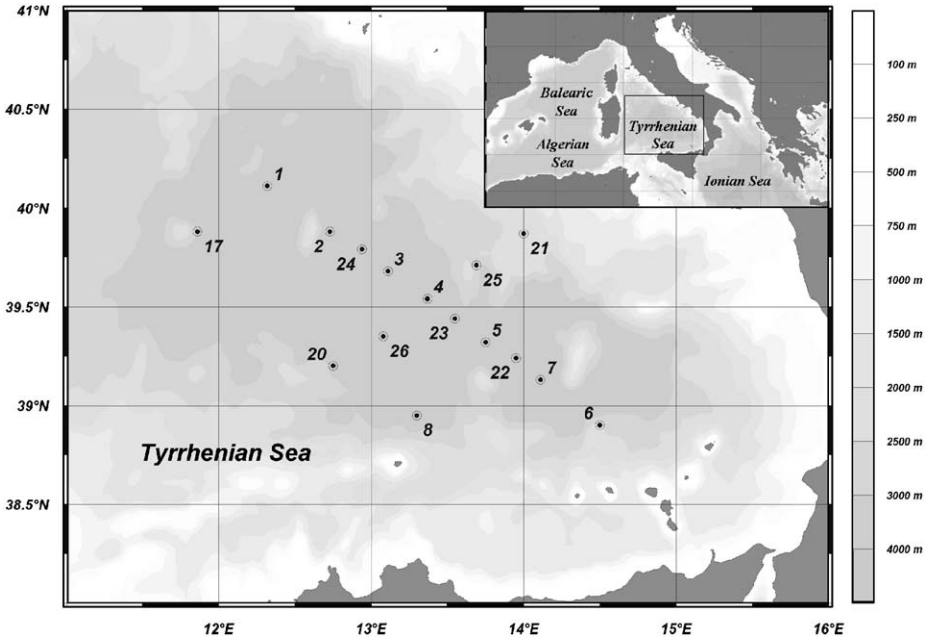

Fig. 1. Study area and location of the sampling stations in the open waters of Southern Tyrrhenian Sea during the two cruises.

Primary production (PP) of the three phytoplankton size classes was assessed with the standard ^{14}C label technique (Steeman-Nielsen, 1952). Two samples from each optical depth (taken at seven stations in July and five in December) were placed into light and dark 450-mL polycarbonate bottles and added with 1 mL of a sodium bicarbonate solution ($10\,\mu Ci\,mL^{-1}$). Samples were incubated in a continuous seawater flow "on deck" incubator equipped with a set of neutral density plastic screens, in order to reproduce the irradiance intensities (% E_0^+) at the depth from the samples were collected. After four hours of light exposure samples were sequentially filtered as already described for chl*a*. Filters were transferred into 20-mL vials with 10 mL of "Ultima Gold" scintillation cocktail and radioactivity was assessed on a liquid scintillation counter (Perkin Elmer LS1440). Readings of samples were performed until the statistical significance of dpm was reached. Alkalinity and pH were measured on board using the potentiometric method and the available total carbon dioxide calculated by UNESCO (1983) algorithm.

The mean chl*a* and PP values and the derived photosynthetic parameters along the water column were computed at the optical depths of sampling (% E_0^+). Integrated chlorophyll *a (Ichla) and primary production (IPP) were calculated with trapezoidal method in the 0–100 m layer. Daily production was obtained assuming a photoperiod of 12 h in July and 10 h in December.*

Physiological state of size-classed phytoplankton community was determined by using three *in situ* photosynthetic parameters. Specific production P_b ($mg\,C\,(mg\,chl a)^{-1}\,h^{-1}$) indicates the synthesis of organic carbon per biomass unit. The photosynthetic efficiency *PE* ($mg\,C\,(mg\,chl a)^{-1}\,h^{-1}\,[\mu E\,m^{-2}\,s^{-1}]^{-1}$), obtained by P_b normalization with irradiance at each sampling depth, is the capacity to convert light energy into organic carbon. The turnover time T_T (in days, after conversion of chl*a* in carbon) provides the time needed to synthesize the phytoplankton carbon biomass.

Prevailing carbon pathways sustained by photosynthetic producers were determined by combining the ecological ratios between the size fractions and the total concentrations of phaeo ($phaeo_F/phaeo_T$) and PP (PP_F/PP_T). The ranges of these ratios associated with specific food webs have been already established (Legendre and Rassoulzadegan, 1996; Mousseau et al., 2001) and validated in open and coastal waters (Mousseau et al., 2001; Cermeño et al., 2006).

2.3. Phytoplankton direct counts

Pico-phytoplanktonic abundance samples (50 mL) were preserved with formaldehyde (2%) and stored at 4 °C in the dark. The epifluorescence direct count to estimate pico-phytoplankton (Maugeri et al., 1990) was applied by using an Zeiss AXIOPLAN 2 *imaging* microscope. Carbon stock was calculated multiplying the abundances in cells by $250\,fg\,C\,cell^{-1}$ currently adopted in marine studies when *Synechococcus* spp. prevail (Partensky et al., 1999).

Large-phytoplankton samples were examined with an Labovert FS Leitz (equipped with phase contrast) inverted microscope following the standard method (Utermöhl, 1958). Species identification was done as reported in Caroppo (2000), and a distinction between photosynthetic and non-photosynthetic phytoflagellates species was made (Chrétiennot-Dinet, 1990; Larsen and Sournia, 1991). For large phytoplankton (45 taxa, 98% of total cell numbers) cell volumes were calculated by assigning to cells one or more geometrical bodies, and applying standard formulae. Carbon content was calculated using the relationship reported by Strathmann (1967) and Verity et al. (1992). Shannon diversity index (H') was calculated for all the identified species.

3. Results

3.1. Water-column structure and light climate

Vertical CTD profiles of temperature, salinity, dissolved oxygen, chl*a* derived from fluorescence data and underwater irradiance at station 4 in the two contrasting hydrographical conditions are displayed in Fig. 2 together with nitrate concentration samplings. The surface zone occupied by the Modified Atlantic Water (MAW) showed different physico-chemical and biological characteristics. In July a well-defined thermocline layer between 20 and 40 m divided the warmer uppermost waters (maximum of 28 °C) from the deeper and colder ones (14.0 °C). Due to summer evaporation, salinity was higher (38.1) at the surface than the top of thermocline stratification (37.9), and progressively it increased with depth (38.6 at 200 m). Oxygen over-saturation (114%) was reached at 35 m depth whereas a gradual under-saturation (82%) progressed downwards. In December the thermo-haline structure, due to the beginning of convective-mixing processes, exhibited a homogeneous layer (0–70 m) with temperature of 16.0 °C, salinity of 38.2, and dissolved oxygen close to the saturation level (98%). This upper layer was slightly warmer, saltier and less under-saturated than the underlying one. Nitrate concentration showed similar vertical patterns in the two samplings: lower values (close to 0.2 μM) in the 0–60 m layer and an abrupt increase in the underlying zone.

The incident mean PAR (E_0^+) values ranged between $2352\pm293\,\mu E\,m^{-2}\,s^{-1}$ in July and $1912\pm144\,\mu E\,m^{-2}\,s^{-1}$ in December. Different optical characteristics of water column can be evidenced by the 1% E_0^+ depths (Table 1) that varied in the range 67–77 m in July (mean 71 ± 4 m) and 45–62 m in December (51 ± 6 m).

3.2. Size-fractioned phytoplankton biomass

Total chl*a* concentration in the 0–100-m layer showed low and similar mean values between $0.09\pm0.09\,mg\,m^{-3}$ ($n=37$) in July and $0.08\pm0.04\,mg\,m^{-3}$ ($n=77$) in December and distinct vertical distributions (Fig. 3). The particularly high standard deviation in summer depends on a greater contribution of vertical phytoplanktonic patchiness.

The vertical patterns of biomass describe two different conditions linked to hydrographical regimes. In July a well-defined 26-m-thick DCM layer was seen at 78 ± 6 m depth in correspondence of very low light intensities (~0.1% E_0^+). The mean chl*a* concentration reached the maximum of $0.25\,mg\,m^{-3}$ at DCM, while towards the surface the values decreased by one order of magnitude ($0.02\,mg\,m^{-3}$) and downwards the euphotic layer they were lower than $0.1\,mg\,m^{-3}$. On average, the mean chl*a* was higher than 50% with respect to phaeo along the water column, with the maximum above the DCM (>70%) and the minimum (<40%) in the deeper euphotic zone. In December the chl*a* distribution was homogeneous (~$0.1\,mg\,m^{-3}$) in the upper layer (0–60 m) and decreased ($0.02\,mg\,m^{-3}$) downwards. The mean chl*a* was generally lower (<50%) than phaeo.

Different size classes contributions to the total chl*a* were observed in the two samplings (Fig. 3), characterized by an increasing dominance of pico-phytoplankton from summer (64 ± 16%) to late autumn (76 ± 10%). A constant contribution to total chl*a* is given by the nano-fraction (17 ± 7%); whereas a statistically different role (ANOVA: $F=11.1$, $p=0.01$) is played by the large fraction (micro-) accounting 19% in July especially at the DCM and 7% in December. Significant correlations between fractions and total chl*a* were found in both July (micro-: 0.92, $p<0.01$; nano-: 0.40, $p<0.05$; pico-: 0.93, $p<0.01$; $n=30$) and

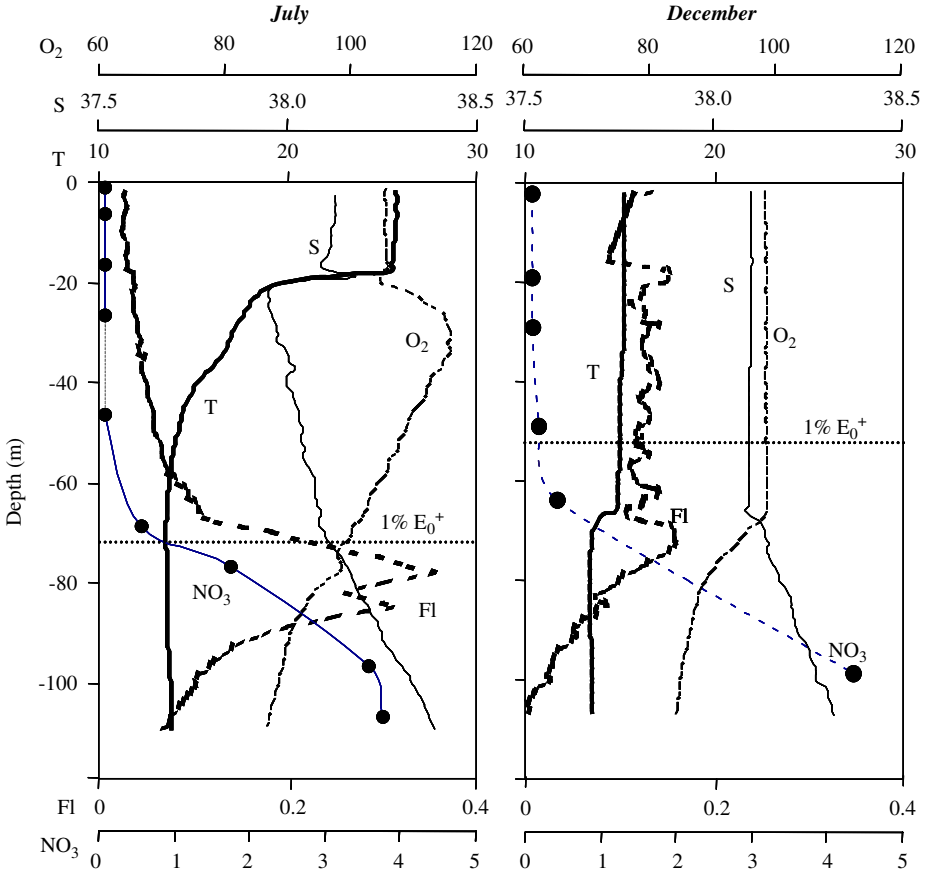

Fig. 2. CTD vertical profiles of temperature (T in °C), salinity (S), dissolved oxygen (O_2% saturation), chl*a* by fluorescence (mg m^{-3}), depth of 1% of E_0^+ PAR and nitrate concentration (μM L^{-1}) of station 4 in July and December.

December (micro-: 0.74, $p<0.01$; nano-: 0.60, $p<0.05$; pico-: 0.95, $p<0.01$; $n=20$).

Integrated chl*a* concentrations (0–100 m layer) showed low values from 8.9 ± 4.7 mg m^{-2} in July to 10.7 ± 2.4 mg m^{-2} in December (Table 1). The dissimilar phytoplanktonic patchiness in the two conditions can be evidenced by the variation range of chl*a* that is wider in summer (13.4) than in late autumn (8.8).

3.3. Size-fractionated primary production

The mean phytoplankton PP ranged between 0.25 ± 0.08 mg C m^{-3} h^{-1} ($n=30$) in July and 0.65 ± 0.25 mg C m^{-3} h^{-1} ($n=20$) in December, and showed a statistically significant difference ($F=15.9$; $p=0.01$) between the two seasons.

Different vertical patterns of mean PP were observed during the contrasting conditions (Fig. 4). In July homogeneous PP rates close to 0.30 mg C m^{-3} h^{-1} were found at 0–62 m, decreasing downwards to a minimum of 0.16 mg C m^{-3} h^{-1}. In December the mean PP showed a vertical pattern characterized by two peaks: maximum of 1.23 mg C m^{-3} h^{-1} at the surface and a secondary maximum at 60 m (0.81 mg C m^{-3} h^{-1}) associated with an irradiance of 0.5% E_0^+. The minimum PP rate (0.05 mg C m^{-3} h^{-1}) was observed at 78 m with a low irradiance of 0.1% E_0^+.

The size fractions contribution to total PP rates was different in the two conditions (Fig. 4). In July the mean contribution to total PP showed a predominance of pico- and micro-classes (47 ± 16% and 37 ± 17%) with respect to nano- (16 ± 12%). In December pico-fraction was the dominant size class, accounting for 75 ± 28% of total PP, whereas both nano- and micro-phytoplankton decreased to 5 ± 7% and 20 ± 24% of total PP, respectively. The high contribution of micro-fraction at 78 m of depth is associated with very low total PP. The size fractions contributions to total PP rates were significantly different between the samplings (ANOVA: pico-$F=23.7$, $p=0.01$; nano-$F=4.7$, $p=0.05$; micro-$F=15.8$, $p=0.01$). As expected the size fractions also were correlated with the total PP in both seasons (July: pico-$r=0.90$, $p<0.01$; nano-$r=0.47$, $p<0.05$; micro-$r=0.77$, $p<0.01$; $n=30$ and December: pico-$r=0.99$, $p<0.01$; nano-$r=0.44$, $p<0.05$; micro-$r=0.55$, $p<0.01$; $n=20$). Integrated daily primary production (IPP) showed a mean value of 273 ± 201 mg C m^{-2} d^{-1} in July ($n=7$) and 429 ± 145 mg C m^{-2} d^{-1} in December ($n=5$).

3.4. Characteristics of size-fractionated photosynthetic indexes

The mean specific production (P_b) was similar between the two conditions, with 3.1 ± 0.7 mg C (mg chl*a*)$^{-1}$ h^{-1} in July and 3.7 ± 0.9 mg C (mg chl*a*)$^{-1}$ h^{-1} in December (Fig. 5). Summer vertical distribution of P_b showed a downwards decreasing trend of one order of magnitude (6.3–0.7 mg C (mg chl*a*)$^{-1}$ h^{-1}) opposite to the increasing trend of chl*a*. In late autumn P_b displayed the same vertical patterns of PP due to the homogeneous chl*a* distribution. High surface P_b value of 5.4 mg C (mg chl*a*)$^{-1}$ h^{-1} and a maximum of 6.2 mg C (mg chl*a*)$^{-1}$ h^{-1} at 60 m depth were observed. These contrasting P_b vertical distribution also can be evidenced by the opposite correlation between chl*a* vs PP (July: $r=-042$, $p<0.05$, $n=30$ and December: $r=48$, $p<0.05$, $n=20$). Different size class contribution to total P_b during the samplings showed a general summer prevalence of micro-fraction (53 ± 12%) and, in particular, micro- (42 ± 10%) and nano- (39 ± 6%) in correspondence of the PP maximum. In late autumn a higher P_b

Table 1
Depth of 1% E_0^+ penetration and deep chlorophyll maximum (DCM); mean and integrated chlorophyll *a* (chl*a*—I chl*a*) and primary production (PP—I PP) observed in the Southern Tyrrhenian Sea during July and December.

Cruise	Station (*n*)	1% E_0^+ (m)	DCM (m)	chl *a*				Ichl *a*				PP				I PP			
				Total ($mg\,m^{-3}$)	Micro (%)	Nano (%)	Pico (%)	Total ($mg\,m^{-3}$)	Micro (%)	Nano (%)	Pico (%)	Total ($mg\,C\,m^{-3}\,h^{-1}$)	Micro (%)	Nano (%)	Pico (%)	Total ($mg\,C\,m^{-2}\,d^{-1}$)	Micro (%)	Nano (%)	Pico (%)
July	2	73	76	0.06	9	28	63	6.0	6	29	65	0.71	27	14	59	707	27	12	61
	3																		
	4	67	85	0.15	24	26	50	17.5	35	22	44	0.26	25	24	51	271	25	24	51
	7	70	86	0.16	29	9	62	14.0	40	9	51	0.15	27	18	55	155	24	20	56
	8	70	88	0.05	13	32	55	5.9	12	30	58	0.15	34	9	57	140	34	10	57
	17	76	71	0.09	17	18	65	10.0	22	13	65	0.32	43	9	48	298	38	10	53
	19	77	85	0.08	22	21	56	8.7	31	24	45								
	20	67	88	0.05	10	15	75	4.1	12	14	74	0.23	59	18	23	203	61	15	23
	21	70	88	0.05	8	16	77	5.1	9	11	81	0.16	41	20	40	141	41	20	39
December	1	48		0.08	4	19	76	11.7	4	12	84	0.56	32	3	65	441	8	1	91
	2			0.05	4	21	75	11.1	2	10	87								
	3	47		0.06	7	19	74	7.6	5	10	85								
	4	56		0.07	9	15	76	8.6	13	11	76	0.61	19	4	77	482	6	4	90
	5			0.06	13	17	70	8.6	7	9	84								
	6			0.05	13	23	64	16.0	4	6	90								
	7	62		0.07	7	13	80	13.0	7	7	86	0.39	32	7	61	225	15	4	82
	8	50		0.09	7	11	82	7.5	4	18	78	0.94	5	2	93	620	4	2	94
	17	45		0.06	5	16	79	8.4	5	19	76								
	19	49		0.10	8	20	72	12.6	5	10	85	0.76	11	9	80	378	6	4	89
	20			0.08	6	17	77	10.2	8	8	84								
	21			0.09	7	14	79	8.7	3	12	85								
	23			0.04	12	14	74	11.4	5	11	84								
	24			0.06	5	16	80	14.1	4	10	86								
	25			0.09	7	17	77	10.1	6	11	83								
	26	49		0.09	6	18	76	11.3	6	8	86								
	27			0.07	5	15	80	10.7	6	15	79								

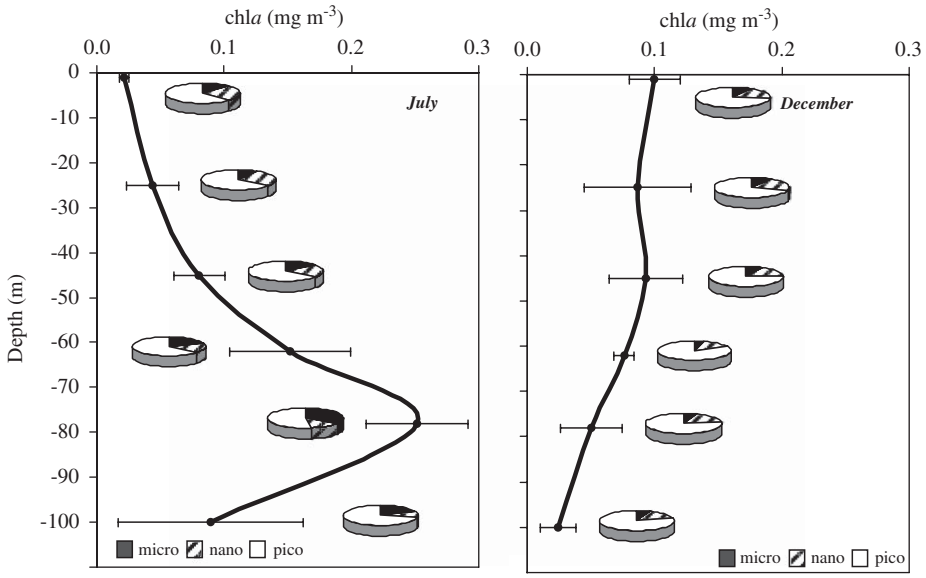

Fig. 3. Vertical distribution of chlorophyll *a* in the two sampling seasons. Averages and standard deviations (bars) on 9 (July) and 17 (December) stations are given. Pie diagrams show the mean percentage contribution of each chl*a* size class at every depth.

contribution of pico-fraction was observed at surface (34%) and at 60 m of depth (51%) in correspondence of higher PP rates.

The mean photosynthetic efficiency (*PE*) was lower in July with respect to December (0.04–0.18 ($mg\,C\,(mg\,chla)^{-1}\,h^{-1}$) [$\mu E\,m^{-2}\,s^{-1}]^{-1}$, respectively). The *PE* showed an increasing vertical pattern downwards (Fig. 6), with the maximum at 60–62 m (at ~1% E_0^+) of depth in both seasons. The contribution of size fractions to total *PE* exhibits a dominance of the micro-class in the low-productive zone (generally the upper 0–25 m layer) and a shift towards smaller fractions in the highly productive and deeper layers. Similar mean contributions of micro-, nano- and pico-fractions to total PE were found in July (43 ± 29%; 23 ± 15%; 35 ± 20%, respectively) and December (41 ± 17%; 11 ± 19%; 48 ± 14%, respectively).

The mean phytoplankton turnover time (T_T) was comparable in July (3.2 ± 5.6 d) and December (3.0 ± 3.0 d) with similar vertical

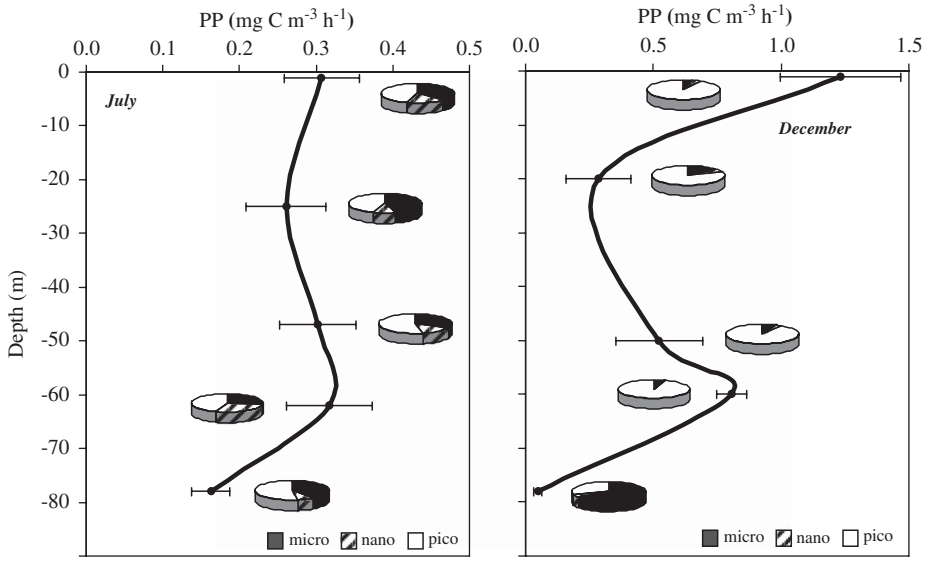

Fig. 4. Vertical distribution of primary production in the two sampling seasons. Averages and standard deviations (bars) on 7 (July) and 5 (December) stations are given. Pie diagrams show the mean percentage contribution of each PP size class at every depth.

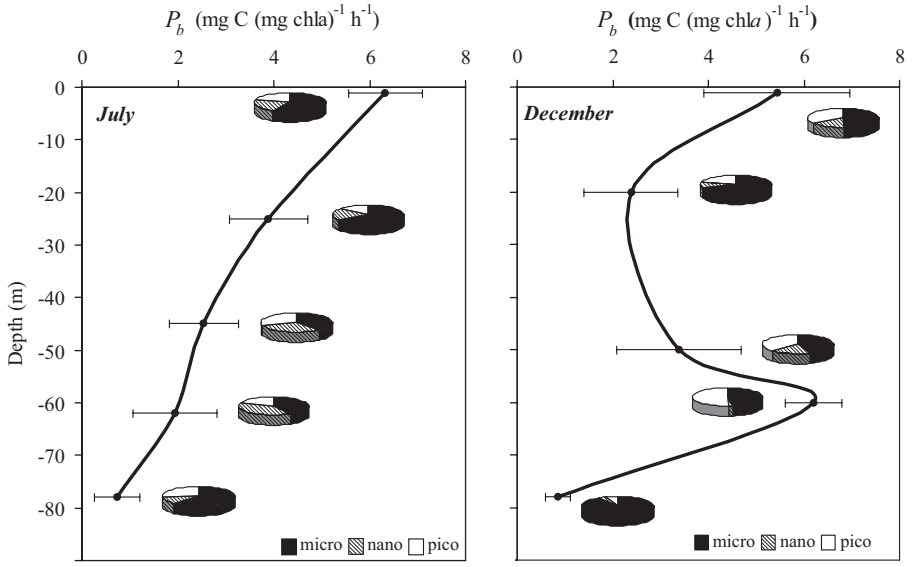

Fig. 5. Vertical distribution of specific production in the two sampling seasons. Averages and standard deviations (bars) on 7 (July) and 5 (December) stations are given. Pie diagrams show the mean percentage contribution of each P_b size class at every depth.

patterns (Table 2): a fast carbon turnover at surface (0.6 and 0.9 d, respectively) and an abrupt decrease below 60–62 m of depth (13.8 and 8.3 d, respectively). Vertically averaged T_T of each size-class fraction was different in the two samplings: similar times (3.7 ± 10.6; 4.6 ± 7.8 and 5.5 ± 12.7 d for micro-, nano- and pico-, respectively) were observed in July, whereas in December the pico-fraction showed faster carbon T_T at the high-productive layer (0.8 and 0.7 d at the surface and 60 m of depth). In late autumn again the nano-fraction exhibited slower mean T_T (9.7 ± 8.2 d) and fast turnovers for the micro-class (1.3 ± 06 d) in correspondence with low chl*a* and PP.

The ecological ratios $phaeo_F$ /$phaeo_T$ and PP_F/PP_T (Fig. 7) identify the presence of two trophic pathways corresponding to the microbial (from 0.0 to 0.2) and multivorous (from 0.2 to 0.5) food webs (Mousseau et al., 2001). The ratio between size-fractionated and total phaeo clearly showed a prevalence of the microbial (85%) on multivorous food web in July that becomes completely dominant in December. Similar indications are given by the ratio between size-fractionated and total PP, exhibiting in July a weak prevalence of the microbial food web (52%) that increases up to 82% in December when the multivorous food web is sustained only by the larger fraction ($>10\,\mu m$).

3.5. Pico- and large-phytoplankton abundances and species composition

Pico- and large-phytoplankton mean abundances and carbon contents during the two samplings are reported in Table 3. The average pico-phytoplankton abundances ranged from $10.2 \pm 2.6 \times 10^3$ cells mL^{-1} (corresponding to $2.6 \pm 2.1\,\mu g\,C\,L^{-1}$) in July to $10.7 \pm 10.1 \times 10^3$ cells mL^{-1} ($2.7 \pm 3.1\,\mu g\,C\,L^{-1}$) in December. The large-phytoplankton mean abundances were higher in July

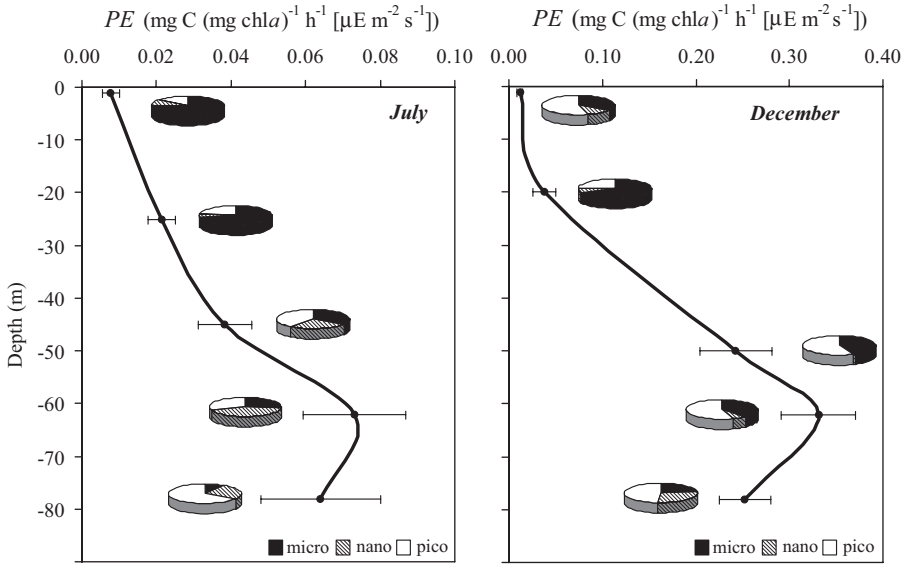

Fig. 6. Vertical distribution of photosynthetic efficiency in the two sampling seasons. Averages and standard deviations (bars) on 7 (July) and 5 (December) stations are given. Pie diagrams show the mean percentage contribution of each *PE* size class at every depth.

Table 2
Total and size-fractionated mean carbon turnover time found in the Southern Tyrrhenian Sea at the indicated sampling depths in July and December.

Depth (m)	Day			
	Total T_T	Micro	Nano	Pico
July				
−1	0.6±1.1	0.2±0.3	1.2±0.2	0.9±0.5
−25	1.4±0.3	0.3±1.1	2.4±0.3	2.6±2.5
−45	1.9±1.6	2.3±1.6	2.4±4.2	2.2±1.5
−62	4.4±3.4	5.3±3.4	3.4±7.1	15.3±26.6
−78	13.8±27.7	20.2±14.4	23.1±30.8	11.1±7.7
December				
−1	0.9±0.6	1.3±0.3	4.1±1.9	0.8±0.6
−20	3.8±2.9	1.6±0.7	4.2±3.2	3.3±3.2
−50	1.3±0.5	2.1±1.1	3.9±2.2	1.0±0.3
−60	0.9±0.3	0.9±0.3	14.6±0.4	0.7±0.2
−78	8.3±2.6	0.6±0.0	21.9±0.3	12.7±0.2

($28.5\pm16.5\times10^3$ cells L^{-1}; 2.9 ± 2.8 µg C L^{-1}) than in December ($21.3\pm7.3\times10^3$ cells L^{-1}; 1.3 ± 0.7 µg C L^{-1}).

The vertical pattern of pico-phytoplankton showed a maximum of $23.1\pm13.1\times10^3$ cells mL^{-1} (5.8 ± 3.3 µg C L^{-1}) at 62 m of depth in July (Fig. 8), while an abrupt downwards decrease in DCM ($5.3\pm4.2\times10^3$ cells mL^{-1}; 1.3 ± 1.0 µg C L^{-1}) was observed. The large-phytoplankton distribution in July was similar to that of the smaller cells, with highest mean abundances in correspondence to 62 m ($50.9\pm17.3\times10^3$ cells L^{-1}; 5.3 ± 2.0 µg C L^{-1}) and at DCM depth ($40.5\pm24.8\times10^3$ cells L^{-1}; 5.1 ± 4.2 µg C L^{-1}). In December the vertical patterns of pico-cells in the homogeneous 0–60 m layer showed a weak decrease downwards; the larger cells exhibited maximum abundance in the 0–20 m layer ($28.1\pm7.4\times10^3$ cells L^{-1}; 1.7 ± 0.4 µg C L^{-1}).

Qualitative observations of pico-phytoplankton identified orange-intensely-fluorescent round-to-rod-shaped prokaryotic cells of *Synechococcus* spp. that were dominant with respect to the rare little-red cells (range size: 0.4–0.5 µm) resembling to *Prochlorococcus* spp.. Large-phytoplankton community species composition was characterized by 114 taxa: 44 diatoms, 64 dinoflagellates, 3 coccolithophorids and 3 phytoflagellates (Table 4). In July, phytoflagellates dominated the phytoplankton community with, 52.8±28.4% abundance followed by diatoms (25.6±41.7%), whereas dinoflagellates and coccolithophorids only accounted 15.0±10.8% and 6.6±7.1%, respectively (Fig. 9). Among diatoms, the most represented were the nano-sized (e.g., *Chaetoceros* spp.) and micro-sized (e.g., *Guinardia flaccida, Leptocylindrus mediterraneus, Proboscia alata)* species. Dinoflagellates were represented by larger species such as those belonging to *Ceratium* (e.g. *C. furca, C. fusus seta*) and unarmored species <20 µm (*Heterocapsa niei* and *Prorocentrum minimum*). Phytoflagellates were mainly represented by forms of uncertain taxonomic classification (<10 µm) whereas undetermined forms (>10 µm) euglenophyceans and silicoflagellates accounted only for lower abundances, both in July and December. Phytoflagellates dominance increased in late autumn with respect to summer, reaching 75.3±28.8%, whereas the percentage of diatoms strongly decreased (8.0±6.1%). A general homogeneity for dinoflagellates (12.3±9.3%) and coccolithophorids (4.3±5.0%) between the two periods was found (Fig. 9). In December the phytoplankton community was characterized by the presence of many species already present in summer such as the diatom *Chaetoceros* spp. and the nano-sized *Thalassiosira* spp., and the dinoflagellates *Heterocapsa niei* and *Prorocentrum minimum*.

Column-averaged Shannon diversity indexes (2.24±0.59 in July and 1.63±0.58 in December) were significantly different ($p<0.02$). Highest diversity at the DCM in summer and at 60 m depth in late autumn were observed.

4. Discussion

4.1. Seasonal variability of phytoplankton biomass and production

The seasonal patterns of chl*a* and PP observed in this study showed two contrasting conditions associated with different hydrographical regimes. The low phytoplankton biomass with vertical opposite distributions in the two seasons is in agreement with the well-known Mediterranean oligotrophy (Turley et al., 2000). The primary production exhibited a significant variability, with carbon rates more than double in December with respect to July.

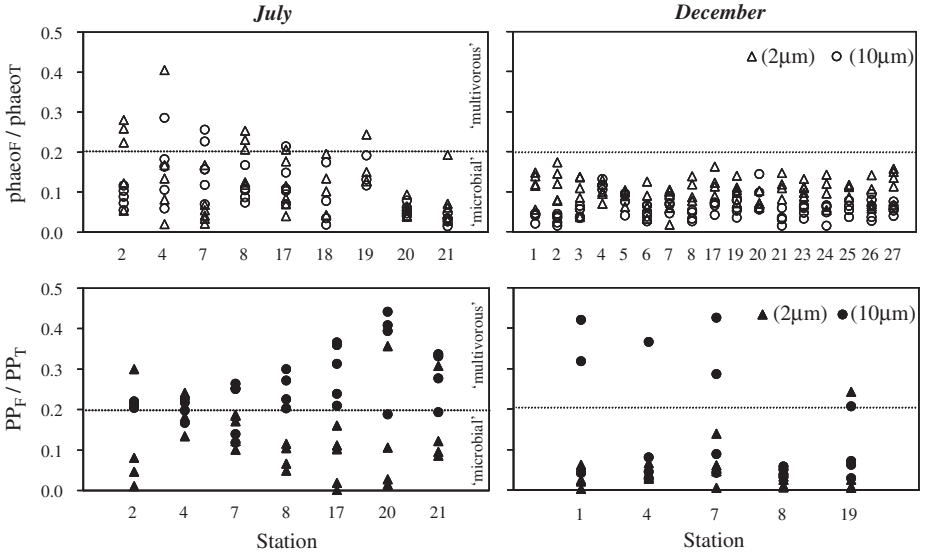

Fig. 7. Top panel: phaeophytin size-fractionated ratios-fractions ($phaeo_F$) to total ($phaeo_T$). Bottom panel: primary production (PP) ratios-fractions (PP_F) to total (PP_T). July (left) and December (right) conditions are compared.

Table 3
Carbon content ($\mu g\,C\,L^{-1}$) and cell abundance of pico-phytoplankton (cell $10^3\,mL^{-1}$) and large-phytoplankton (cell $10^3\,L^{-1}$) main groups at each station in July and December.

Station	Pico-phytoplankton			Diatoms		Dinoflagellates		Large-phytoplankton coccolithophorids		Phytoflagellates		Total		
	$10^3\,mL^{-1}$	$\mu g\,C\,L^{-1}$		$10^3\,L^{-1}$	$\mu g\,C\,L^{-1}$	$10^3\,L^{-1}$	$\mu g\,C\,L^{-1}$	$10^3\,L^{-1}$	$\mu g\,C\,L^{-1}$	$10^3\,L^{-1}$	$\mu g\,C\,L^{-1}$	$10^3\,L^{-1}$	$\mu g\,C\,L^{-1}$	
	Mean (SD)	Mean (SD)	*n*	Mean (SD)	Mean (SD)	Mean (SD)	Mean (SD)	Mean (SD)	Mean (SD)	Mean (SD)	Mean (SD)	Mean (SD)	Mean (SD)	*n*
July														
1	9.12±8.42	2.28±2.11	6											
2				0.77±0.58	0.06±0.04	3.43±2.12	0.39±0.43	1.50±1.03	0.03±0.02	9.08±2.74	0.49±0.15	14.77±2.21	0.97±0.44	5
4	7.61±3.97	1.90±0.99	5	6.64±7.51	1.25±1.59	3.21±1.51	0.74±0.48	2.08±2.87	0.04±0.06	15.68±10.13	0.85±0.55	27.60±18.43	2.88±2.54	5
6	13.48±8.91	3.37±2.23	4											
7				20.06±23.60	3.16±3.92	4.48±3.38	1.02±0.86	1.67±1.26	0.04±0.02	13.88±8.59	0.75±0.46	40.09±29.27	4.96±4.60	7
8	7.32±5.82	1.83±1.45	5	0.88±0.33	0.14±0.17	4.80±2.13	0.59±0.61	1.82±2.05	0.04±0.04	11.79±3.89	0.64±0.21	19.30±7.39	1.41±0.71	6
17	11.86±12.77	2.97±3.19	6	13.24±16.32	1.96±2.06	4.01±4.34	0.56±0.32	1.93±2.06	0.04±0.04	19.55±8.26	1.29±0.29	38.73±22.85	3.85±2.44	5
20	8.59±5.11	2.15±1.28	4	3.25±3.48	0.75±1.27	5.80±5.38	0.84±0.22	3.87±4.06	0.17±0.19	17.47±11.18	0.69±0.69	30.38±19.00	2.45±1.32	5
21	13.24±4.26	3.31±1.06	4											
December														
1	5.73±4.42	1.43±1.1	6	0.73±0.61	0.06±0.06	3.04±3.38	0.30±0.39	1.15±1.14	0.02±0.02	16.11±4.65	0.76±0.43	21.03±7.97	1.15±0.75	
4	3.12±3.03	0.78±0.76	6	2.13±1.72	0.19±0.16	2.01±0.79	0.19±0.13	1.70±1.52	0.03±0.03	20.36±5.51	1.10±0.30	26.19±8.49	1.51±0.49	3
7	4.53±4.78	1.13±1.20	6	1.28±0.39	0.28±0.30	2.70±1.48	0.41±0.36	0.11±0.16	0.00±0.00	13.64±6.29	0.75±0.35	17.72±6.58	1.44±0.71	5
8	3.55±3.69	0.89±0.92	6	2.41±1.72	0.32±0.43	2.63±1.44	0.20±0.13	1.06±0.86	0.03±0.02	15.72±9.23	0.84±0.49	21.81±11.06	1.40±0.85	5
17	25.53±28.48	6.38±7.14	5											
19				2.61±1.04	0.29±0.11	2.01±0.66	0.18±0.12	0.73±1.26	0.01±0.03	14.53±2.00	0.64±0.15	19.87±2.38	1.12±0.16	3
21	21.61±29.94	5.40±7.48	6											

Mean, standard deviation (SD) and number of samples (*n*) are displayed.

Summer conditions are characterized by a steady-state phase of the phytoplankton growth cycle as highlighted by the low PP rates and physiological state, particularly at the DCM and uppermost layers. As a consequence of water stratification the DCM layer presents (78 m depth) low irradiance (~0.5% E_0^+), relatively higher chl*a* (phaeo >50%), and minimum PP rates. These conditions are characteristic of an low-productive zone as further highlighted by the low *PE*, slow carbon T_T, low dissolved oxygen, and high nitrate concentrations. Similarly, a low-productive zone can be observed in the uppermost layer (0–40 m of depth); here the low chl*a* and PP rates are in agreement with the summer nutrient depletion (Fig. 2). In the relatively high-productive zone, located below the thermocline and above the DCM layer (40–70 m of depth), the PP increases with fast carbon T_T and the maximum of *PE* indicates a community adapted to relative low irradiance (~5% E_0^+).

Late autumn homogeneity of water column (upper 60-m-thick layer) reflects the constant and low phytoplankton biomass, whereas the PP followed a bimodal pattern of distribution with two distinguished high-productive layers. The surface PP absolute maximum exhibited high percentage of chl*a* (phaeo <50%) and fast carbon T_T. This high-productive layer, despite the nitrate depletion, seems to be sustained mainly by recycled reduced nitrogen compound (Moutin and Raimbault, 2002). The deeper relative maximum of PP located at 60 m of depth is characterized by higher *PE* (four times higher with respect to July) that indicates

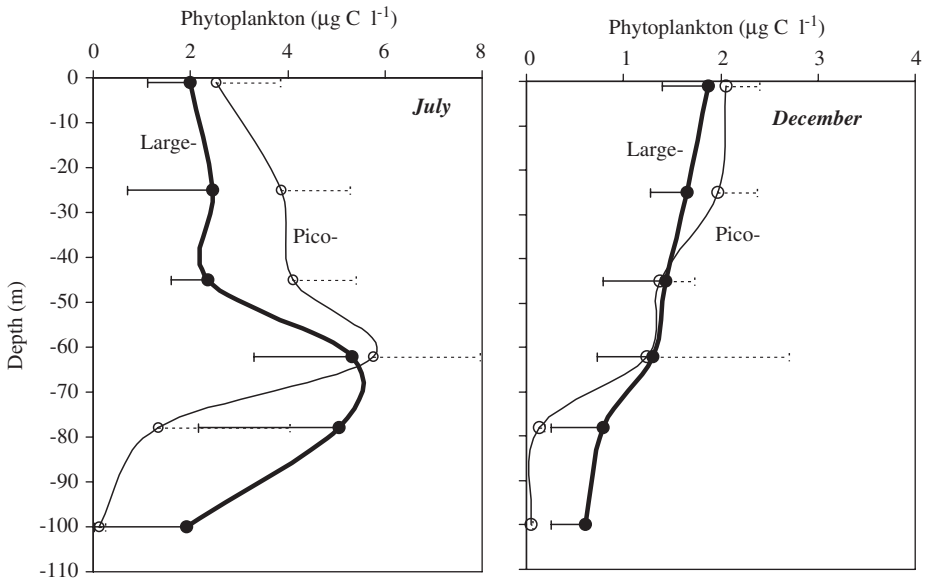

Fig. 8. Vertical distribution of carbon content (µg C L^{-1}) for pico-phytoplankton (thin line) and large-phytoplankton (thick line) in the two sampling seasons in the Southern Tyrrhenian Sea. Averages and standard deviations (bars) on 7 (July) and 5 (December) stations are given.

a well-adapted community to very low irradiance (0.5% E_0^+) and showed a fast carbon T_T similar to the surface one. The underlying low-productive layer exhibited low PP rates and chl*a* that together to low *PE* and very slow T_T characterize the base of the euphotic zone (0.1% E_0^+).

Our estimates of the phytoplankton activity are in agreement with previous findings available for the Tyrrhenian Sea and the adjacent western and eastern areas of the MS, whereas the biomass concentration differed from those reported by several authors (Table 5). Higher chl*a* values of previous studies can be due to several environmental characteristics such as phytoplankton community composition, nutrient richness, season, hydrographical water structure and dynamics, and thickness of the mixed layer. Higher spring biomass (57 mg m^{-2}) were reported for the Tyrrhenian Sea and the Algerian Current (116 mg m^{-2}) associated with particular physical conditions (Moutin and Raimbault, 2002), while low winter values were measured in the Ionian (19 mg m^{-2}) and Levantine basins (22 mg m^{-2}) (Vidussi et al., 2001).

The daily integrated PP rates (273 mg C m^{-2} d^{-1} in July and 429 mg C m^{-2} d^{-1} in December) are similar to those previously reported for the Tyrrhenian Sea (395 mg C m^{-2} d^{-1}) by Moutin and Raimbault (2002) in early summer. Our PP mean value (351 C m^{-2} d^{-1}) is similar to the average obtained in the West-to-East Mediterranean transect (Moutin and Raimbault, 2002) and to the mean calculated for the NW MS using a 7-year time series (Marty and Chiavérini, 2002).

4.2. Phytoplankton size classes distribution and species composition

Changes of phytoplankton size-fractionated structure during the two hydrographical regimes were indicated by the significant differences of pico-contribution to total PP. Generally, the pico- and nano-phytoplankton classes dominated in biomass and production, whereas the lower contribution of micro-fraction lightly increased within the low-productive zone. The relevant *PE* contributions and the faster carbon T_T of smaller fractions confirmed the main role played by these organisms in the biogenic carbon pathway. The micro- and pico-fractions characterized the phytoplankton community in July and the pico-class in December as revealed by the strong correlation vs the total chl*a* and PP.

In stratified conditions the pico-class exhibits a high contribution to total *PE* and faster carbon T_T, mainly in the relatively high-productive layer located above the DCM. In a well-mixed water column, in correspondence of higher P_b values, fast carbon T_T and strong *PE* at lower irradiance were associated with the smallest classes. Conversely, at the depths with lower P_b and slow T_T the contribution of micro-class was relatively higher. The increase of pico-contribution to total PP and chl*a* from July to December with a decrease of micro-class therefore reflects a significant change between the two seasons.

The general oligotrophy of the Tyrrhenian Sea is evidenced by low phytoplankton abundances and a community structure dominated by nano- and pico-phytoplankton (Agawin et al., 1998). In the pico-phytoplankton community the phycoerythrin-rich cyanobacteria *Synechococcus* type prevailed in pico-eukaryotic organisms as reported for the northern and central Adriatic Sea (Revelante and Gilmartin, 1995; Caroppo, 2000). The pico-phytoplankton abundance was the same order of magnitude as those reported for other MS regions (e.g. Magazzù and Decembrini, 1995; Agawin et al., 2000; Casotti et al., 2000 and 2003; Caroppo et al., 2006). The large phytoplankton abundance was comparable to those of other MS waters (Rabitti et al., 1994; Videau et al., 1994; Polat, 2002) and lower than those observed in south-western region (Mercado et al., 2005) and in coastal waters of the Tyrrhenian Sea (Ribera D'Alcalà et al., 2004). Generally, the summer species composition observed in the Southern Tyrrhenian Sea also characterized the phytoplankton community in December.

Concerning diatoms, the genera *Chaetoceros, Leptocylindrus, Nitzschia, Rhizosolenia, Skeletonema* and *Thalassiosira* distinguish the community of the eastern MS (Sachs and Repeta, 1999; Caroppo et al., 1999; Socal et al., 1999). The summer phytoplankton steady-state is supported by the maturity of the community also evidenced by the analysis of the size-fractionated physiological state. The presence of diatoms in summer is unusual for the open Tyrrhenian Sea (Innamorati, 1995) and is characteristic of coastal surface waters of the Gulf of Naples by blooms of small diatoms (Zingone et al., 1990; Ribera D'Alcalà et al., 2004). This condition is due to the coastal-pelagic coupling active in

Table 4
List of the main large-phytoplankton species found in the Tyrrhenian Sea during the samplings of July and December.

Large-phytoplankton species	July	December	Large-phytoplankton species	July	December	Large-phytoplankton species	July	December
Diatoms			Dinoflagellates			Dinoflagellates		
Amphiprora sp.	+		*Alexandrium minutum*	+		*Oxytoxum* sp.	+	+
Amphora sp.	+		*Alexandrium* sp.	+		*Phalacroma mitra*	+	
Asteromphalus sp.	+	+	*Balechina coerulea*	+	+	*Phalacroma rotundatum*	+	+
Bacteriastrum delicatulum	+	+	*Ceratium concilians*	+		*Podolampas spinifer*	+	
Chaetoceros affinis	+	+	*Ceratium extensum*		+	*Prorocentrum compressum*	+	+
Chaetoceros concavicornis	+	+	*Ceratium furca*	+		*Prorocentrum micans*	+	
Chaetoceros curvisetus	+		*Ceratium fusus seta*	+	+	*Prorocentrum minimum*	+	+
Chaetoceros decipiens	+	+	*Ceratium longipes*	+		*Prorocentrum* sp.	+	
Chaetoceros messanensis	+		*Ceratium macroceros*	+		*Pronoctiluca spinifera*	+	
Chaetoceros simplex	+	+	*Ceratium massiliense*	+		*Protoperidinium bipes*	+	
Chaetoceros teres	+		*Ceratium pentagonum*	+	+	*Protoperidinium breve*	+	
Chaetoceros sp.	+	+	*Ceratium pulchellum*	+		*Protoperidinium crassipes*	+	
Coscinodiscus sp.	+	+	*Ceratium tripos*	+	+	*Protoperidinium ovum*	+	+
Cylindrotheca closterium	+	+	*Ceratocorys horrida*	+		*Protoperidinium wiesneri*	+	
Dactyliosolen blavyanus	+		*Dinophysis caudate*	+		*Protoperidinium* sp.	+	+
Dactyliosolen fragilissimus	+		*Dinophysis fortii*	+		*Pyrocystis lunula*	+	+
Eucampia cornuta	+		*Dinophysis sacculus*	+		*Scrippsiella trochoidea*	+	+
Guinardia delicatula	+	+	*Dinophysis parvula*	+	+	*Spatulodinium pseudonoctiluca*	+	
Guinardia flaccida	+		*Diplopsalis* group	+	+	*Spiraulax kofoidii*	+	
Guinardia striata	+	+	*Glenodinium foliaceum*	+	+	*Torodinium teredo*	+	+
Haslea trompii	+		*Gonyaulax monospina*		+	*Warnowia* sp.	+	+
Haslea wawrikae	+	+	*Gonyaulax spinifera*	+		Naked dinoflagellates $<20\,\mu m$	+	+
Hemiaulus hauckii	+	+	*Gonyaulax* sp.	+	+	Naked dinoflagellates $>20\,\mu m$	+	+
Hemiaulus sinensis	+		*Gymnodinium marinum*	+	+	Thecated dinoflagellates $<20\,\mu m$	+	
Leptocylindrus danicus	+		*Gymnodinium* sp.	+	+	Thecated dinoflagellates $>20\,\mu m$	+	
Leptocylindrus mediterraneus	+	+	*Gyrodinium fusiforme*	+	+			
Leptocylindrus minutus	+		*Gyrodinium glaucum*	+	+	Coccolithophorids		
Lioloma elongatum		+	*Gyrodinium lachrymal*	+		*Emiliania huxleyi*	+	+
Lioloma pacificum	+	+	*Gyrodinium spirale*		+	*Ophiaster* sp.	+	+
Melosira nummuloides	+		*Heterocapsa niei*	+	+	*Rhabdosphaera* sp.	+	
Navicula sp.	+	+	*Heterocapsa triquetra*	+	+	Indeterminates	+	
Nitzschia bicapitata		+	*Noctiluca scintillans*	+	+			
Nitzschia longissima	+	+	*Ornithocercus magnificus*	+	+	Phytoflagellates		
Nitzschia sp.	+	+	*Ornithocercus quadratus*	+		*Dictyocha fibula*	+	+
Pleurosigma directum	+		*Ornithocercus steinii*	+		*Dictyocha octonaria*	+	+
Pleurosigma normanii	+	+	*Oxytoxum areolatum*		+	*Euglena* sp.	+	+
Pleurosigma sp.		+	*Oxytoxum longipes*	+		Phytoflagellates $<20\,\mu m$	+	+
Proboscia alata	+	+	*Oxytoxum milneri*	+	+			
Pseudo-nitzschia sp.	+	+	*Oxytoxum minutum*	+	+			
Rhizosolenia styliformis	+	+	*Oxytoxum rampi*	+				
Rhizosolenia sp.	+		*Oxytoxum reticulatum*	+				
Thalassionema bacillare	+	+	*Oxytoxum scolopax*	+	+			
Thalassionema frauenfeldii	+	+	*Oxytoxum variabilis*	+	+			
Thalassiosira sp.	+	+						

the Tyrrhenian waters (Casotti et al., 2000). In particular, summer diatoms are represented by both nano-sized (*Chaetoceros* spp.) and micro-sized species (e.g., *Thalassionema bacillare*, *T. frauenfeldii*, *Hemiaulus hauckii* and *Proboscia alata*). The vertical stratification of the water column favours the growth of small diatoms whereas turbulence favour larger ones (Peters et al., 2006). Larger species of dinoflagellates (e.g. *Ceratium* spp.) reached higher values in July as did other phytoplankton species (the diatoms *Guinardia flaccida, Leptocylindrus mediterraneus, Proboscia alata)*, a typical condition of the end phase of the succession *sensu* Margalef (1963). The highest phytoplankton abundances were detected at PP maximum, whereas at the DCM depth the micro-sized cells prevailed and were responsible for the total biomass increase. In the DCM layer a relatively diverse community composed by several diatoms and dinoflagellates species (micro-sized) co-occurred with unidentified nano-phytoflagellates. In July phytoplankton diversity reflected the highly dynamic spatial condition of both pelagic and coastal waters of the Southern Tyrrhenian Sea (Innamorati, 1995; Ribera D'Alcalà et al., 1997, 2004). The community appeared to be represented by many diatom and dinoflagellate species that were responsible for the significantly higher biodiversity detected in this period. In late autumn the phytoplankton community exhibited distinct features with respect to July concerning the dominance of undetermined nano- and pico-size classes and a low diversity index. Previous investigations carried out in the Southern Tyrrhenian Sea revealed the dominance in late autumn of the smaller fractions of phytoplankton (Casotti et al., 2000). This situation precedes proper winter conditions, characterized by late winter–spring diatoms bloom (Ribera D'Alcalà et al., 2004). The pico- and nano-phytoplankton production capacity can be explained by higher rates of nutrient uptake per unit of biomass and lower half-saturation constants due to their higher surface area to volume ratios (Hein et al., 1995). Furthermore, these small fractions were characterized by higher metabolite leakage rates, nutrient storage and irradiance interactions as expressed by higher PP, fast carbon T_T, and the higher *PE* at deeper layer.

4.3. Phytoplankton size classes and pathways of biogenic carbon

Phytoplankton community size structure is a balance of physical and biological processes and drives the carbon budget in the plankton ecosystem, sustaining specific food webs (Legendre and Le Fèvre, 1989; Legendre and Rassoulzadegan, 1996). Ecological ratios provide an additional way to assess the

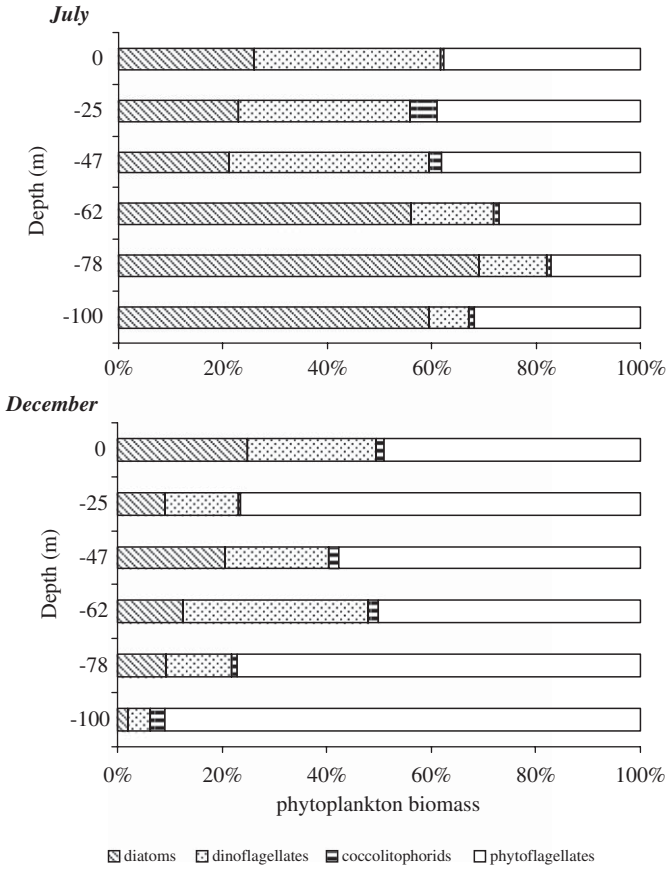

Fig. 9. Vertical distribution of the main phytoplanktonic groups percentages during July ($n = 6$ stations) and December ($n = 5$ stations) samplings in the Southern Tyrrhenian Sea.

prevailing pathways of the biogenic carbon in the planktonic food web (Mousseau et al., 2001). By combining these ratios two trophic pathways were found during the sampled conditions in the Southern Tyrrhenian Sea. The presence of multivorous and microbial food webs was consistent with the activity, physiological status and structure of phytoplankton community. The ecological ratios indicated the strong prevalence of the microbial pathway in July that is in agreement with the anomalous presence of nano-sized diatoms in summer season. The microbial food web becomes completely dominant in December as already evidenced by the high contribution of small fractions to total PP and *PE*. The weak discrepancy between the two ecological ratios in December depends on the abundance of the >10-μm fraction that channels a small percentage of the biogenic carbon towards the multivorous food web. The prevalence of the microbial food web with high PP found in the open Southern Tyrrhenian Sea in late autumn diverges from the traditional view that the pico-phytoplankton dominates the community during oligotrophic conditions.

Major consistence of the microbial food web (phaeo = 75% and PP = 52%) with respect to the multivorous food web in July has an ecological consequence that most of the photosynthetic carbon is recycled in the euphotic layer (by pico-) and that only a small amount of biogenic carbon can be exported to upper trophic levels (by nano- and micro-) or to adjacent systems (Mousseau et al., 2001). Furthermore, the dominance of microbial food web in December (phaeo = 100% and PP = 82%) and the statistically significant increase of primary production sustained by the pico-phytoplankton indicate a further decrease of biogenic carbon available for the export.

Phytoplanktonic size-fractionated carbon standing-stocks, production and channelling pathways in the two sampling conditions are summarized in a simplified scheme (Fig. 10). The different capacity of phytoplankton carbon regeneration (production/biomass ratio) is higher in July (1.3 d) than in December (0.8 d),

Table 5
Summary of phytoplankton integrated chlorophyll *a* and primary production data recently reported on different areas of the Mediterranean Sea in different seasons.

Area	Season (year)	chl *a* ($mg\,m^{-2}$)	PP ($mg\,C\,m^{-2}\,d^{-1}$)	Author
North-West MS (Dyfamed)	Spring	33	299	Vidussi et al. (2000)
		32	528	
Algerian Sea	Autumn	43	440	Morán et al. (2001)
Eastern MS	Winter	20	270	Vidussi et al. (2001)
Ionian Sea		19	250	
Aegean Sea		18	250	
Levantine Basin		22	300	
Western MS	Late spring	33	401	Moutin and Raimbalut (2002)
Tyrrhenian Sea		57	395	
Algerian Sea		116	996	
Ionian Sea		32	280	
Levantine Basin		31	189	
North-West MS (Dyfamed)	1993	28	422	Marty and Chiavérini (2002), Marty et al. (2002)
	1994	27	384	
	1995	23	425	
	1996	30	518	
	1997	27	636	
	1998	32	370	
	1999	53	236	
Tyrrhenian Sea	Summer	9	273	This study
Tyrrhenian Sea	Early autumn	11	429	This study

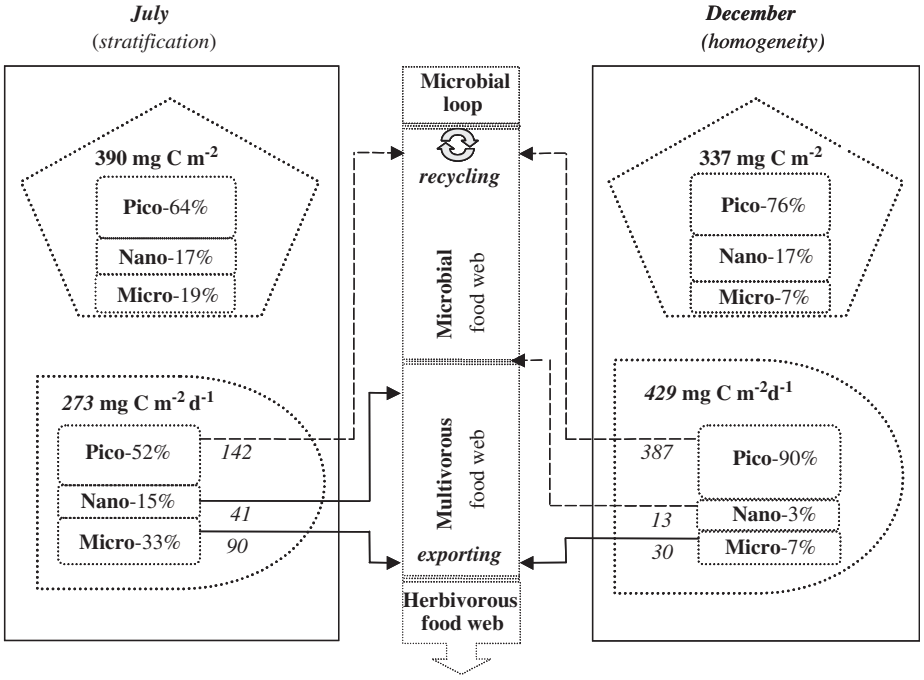

Fig. 10. Simplified scheme of phytoplankton box comparing the integrated carbon stock (top) and the daily production (bottom) found in July and December. Size classes percentage contributions are indicated. Arrows show the channelling of biogenic carbon (in italic) towards the different food webs in the continuous trophic pathway.

confirming the contrasting conditions in the trophic structure. Phytoplankton carbon stock is comparable in the two periods, whereas the total production rates in December are 1.6 times higher than in July. The biogenic carbon channelled by pico-fractionated producers towards the microbial food web ranged from 52% to 90% (July–December). In summer similar percentages of the biogenic carbon are channelled towards the recycling microbial food web (36% of the total biomass) and the exporting multivorous food web (33% i.e. 131 mg C m^{-2} d^{-1}). In late autumn only 7% of the biogenic carbon (30 mg C m^{-2} d^{-1}) is channelled by micro-fractionated producers towards the exporting multivorous food web. In this season the PP exceeds the phytoplanktonic carbon stock, indicating a net carbon transfer towards higher trophic and/or adjacent systems as supported by the positive Production/Respiration ratio of the whole microbial community (La Ferla, personal communication).

5. Conclusions

The size-fractionated phytoplanktonic biomass and primary production patterns in the open Tyrrhenian Sea showed two contrasting seasonal conditions associated with the hydrographical stratification and homogeneity regimes of the euphotic water column. In July the steady-state of phytoplankton community is characterized by low biomass and production mainly sustained by small-sized classes (pico- and nano-) associated to the pico-cells and small phytoflagellates and coccolithophorids. The evident DCM layer is composed by high micro-sized biomass represented by small diatoms and phytoflagellates with lower photosynthetic efficiencies and slow carbon turnover time. In December higher photosynthetic production with respect to July mainly in the pico-sized fraction was found, and the community was composed by pico-cells and nano-sized phytoflagellates. The physiology of this community evidenced rapid carbon turnover time and higher photosynthetic efficiencies that increased towards the base of euphotic zone, confirming the active role played by this class in the carbon production.

The photosynthetic size-classed community drives the biogenic carbon pathway along the microbial and multivorous food webs. The abundance of smallest fractions in July and their dominance in December clearly evidenced a shift of the biogenic carbon towards the microbial food web with the ecological and bio-geochemical implications linked to the dominance of processes of carbon recycling. The more active microbial food web, especially in December, receives a high amount of biogenic carbon; whereas the multivorous food web, associated with low trophism, mainly found in summer, can export little organic matter outside the euphotic system.

The dominance of small size classes in the trophic pathway during high primary production phase in December and the unusual presence of micro- and nano-sized diatoms in July differed from the well-accepted assumption of the Tyrrhenian Sea as a typical sub-basin of the temperate western Mediterranean Sea.

Acknowledgments

The authors thank Carmen Raffa and Gioacchino Ruggeri for their assistance in phytoplankton biomass and production assays and Giovanna Maimone for the pico-phytoplankton epifluorescence microscopy analysis. We are grateful to Alessandro Bergamasco and Maurizio Ribera d'Alcalà for manuscript suggestions and to the team of the Stazione Zoologica "A. Dohrn" of Naples for nutrient data. We thank the captains and crews of the R/V *Universitatis* and *Urania* for their assistance in the sampling activities.

References

Agawin, N.S.R., Duarte, C.M., Agustí, S., 1998. Growth and abundance of *Synechococcus* sp. in a Mediterranean Bay: seasonality and relationship with temperature. Marine Ecology Progress Series 170, 45–53.

Agawin, N.S.R., Duarte, C.M., Agustí, S., 2000. Response of Mediterranean *Synechococcus* growth and loss rates to experimental nutrient inputs. Marine Ecology Progress Series 206, 97–106.

Astraldi, M., Gasparini, G.P., 1994. The seasonal characteristics of the circulation in the Tyrrhenian Sea. In: La Violette, P.E. (Ed.), The Seasonal and Interannual Variability of the Western Mediterranean Sea. Coastal and Estuarine Studies, vol. 46. AGU, WA, pp. 115–134.

Caroppo, C., 2000. The contribution of picophytoplankton to community structure in a Mediterranean brackish environment. Journal of Plankton Research 22 (2), 381–397.

Caroppo, C., Fiocca, A., Sammarco, P., Magazzù, G., 1999. Seasonal variations of nutrients and phytoplankton in the coastal SW Adriatic Sea (1995–1997). Botanica Marina 42 (4), 389–400.

Caroppo, C., Turicchia, S., Margheri, M.C., 2006. Phytoplankton assemblages in coastal waters of the Northern Ionian Sea (eastern Mediterranean), with special reference to cyanobacteria. Journal of the Marine Biological Association of the United Kingdom 86, 927–937.

Casotti, R., Brunet, C., Aronne, B., Ribera d'Alcalà, M., 2000. Mesoscale features of phytoplankton and planktonic bacteria in a coastal area as induced by external water masses. Marine Ecology Progress Series 195, 15–27.

Casotti, R., Landolfi, A., Brunet, C., D'Ortenzio, F., Mangoni, O., Ribera d'Alcalà, M., 2003. Composition and dynamics of the phytoplankton of the Ionian Sea (Eastern Mediterranean). Journal of Geophysical Research 108, 1–17.

Cermeño, P., Marañon, E., Pérez, V., Serret, P., Fernandez, E., Castr, C.G., 2006. Phytoplankton size structure and primary production in a highly dynamical coastal ecosystem (Ría de Vigo, NW—Spain): seasonal and short-time scale variability. Estuarine Coastal and Shelf Science 67, 251–266.

Chisholm, S.W., Olson, R.J., Zettler, E.R., Goericke, R., Waterbury, J.B., Welschmeyer, N.A., 1988. A novel free-living prochlorophyte abundant in the oceanic euphotic zone. Nature 334, 340–344.

Chrétiennot-Dinet, M.J., 1990. Atlas du Phytoplancton Marin. Chlorarachniophycées, Chlorophycées, Chrysophycées, Cryptophycées, Euglénophycées, Eustigmatophycées, Prasinophycées, Prymnésiophycées, Rhodophycées, Tribophycées, vol. 3. Edition du C.N.R.S., Paris.

Claustre, H., Marty, J.C., Cassiani, L., 1989. Intraspecific differences in the biochemical composition of a diatoms during a spring bloom in Villefranche-sur-mer Bay, Mediterranean Sea. Journal of Experimental Marine Biology and Ecology 129, 17–32.

Eppley, R.W., Peterson, B.J., 1979. Particulate organic matter flux and planktonic new production in the deep ocean. Nature 282, 677–680.

Hein, M., Folager Pedersen, M., Sand-Jensen, K., 1995. Size dependent nitrogen uptake in micro- and macroalgae. Marine Ecology Progress Series 118, 247–253.

Hopkins, T.S., 1988. Recent observations on the intermediate and deep water circulation in the Southern Tyrrhenian Sea. Oceanologica Acta, n. SP, 41–50.

Innamorati, M., 1995. Hyperproduction of mucilages by micro and macro algae in the Tyrrhenian Sea. The Science of the Total Environment 165, 65–81.

Irwin, A., Finkel, Z.V., Schofield, O.M.E., Falkowski, P.G., 2006. Scaling-up from nutrient physiology to the size-structure of phytoplankton communities. Journal of Plankton Research 28 (5), 459–471.

Larsen, J., Sournia, A., 1991. The diversity of heterotrophic dinoflagellates. In: Larsen, J., Patterson, D.J. (Eds.), The Biology of Free-Living Heterotrophic Flagellates. Systematics Association Special, vol. 45. Clarendon Press, Oxford, pp. 313–332.

Legendre, L., Le Fèvre, J., 1989. Hydrodynamical singularities as controls of recycled versus export production in oceans. In: Berger, W.H., Smetacek, V.S., Wefer, G. (Eds.), Productivity of the Ocean: Present and Past, 44, Dahlem Workshop Reports. Life Sciences Research Report. Wiley, Chichester, England, New York, pp. 49–63.

Legendre, L., Rassoulzadegan, F., 1995. Plankton and nutrient dynamics in marine waters. Ophelia 41, 153–172.

Legendre, L., Rassoulzadegan, F., 1996. Food-web mediated export of biogenic carbon in oceans: environmental control. Marine Ecology Progressive Series 145, 179–193.

Lorenzen, C.I., 1967. Determination of chlorophyll and phaeopigments spectrophotometric equations. Limnology and Oceanography 12, 343–346.

Magazzù, G., Decembrini, F., 1995. Primary production, biomass and abundance of phototrophic picoplankton in the Mediterranean Sea. Aquatic Microbial Ecology 9, 97–104.

Margalef, R., 1963. Succession in marine populations. Advancing Frontiers of Plant Sciences 2, 137–188.

Marty, J.C., Chiavérini, J., 2002. Seasonal and interannual dynamiscs of nutrient and phytoplankton production in the nordwestern Mediterranean Sea at DYFAMED time-series stations (1991–1999). Deep Sea Research II 49, 2017–2030.

Marty, J.C., Chiavérini, J., Pizay, M.D., Avril, B., 2002. Seasonal and interannual dynamics of nutrient and phytoplankton pigments in the northwestern Mediterranean Sea at DYFAMED time-series stations (1991–1999). Deep Sea Research II 49, 1965–1985.

Maugeri, T.L., Acosta Pomar, L., Bruni, V., 1990. Picoplancton. Nova Thalassia 11, 199–205.

Mercado, J.M., Ramírez, T., Cortés, D., Sebastián, M., Vargas-Yáñez, M., 2005. Seasonal and inter-annual variability of the phytoplankton communities in an upwelling area of the Alborán Sea (SW Mediterranean Sea). Scientia Marina 69 (4), 451–465.

Morán, X.A.G., Taupier-Letage, I., Vàzquez-Domínguez, E., Ruiz, S., Arin, L., Raimbault, P., Estrada, M., 2001. Physical-biological coupling in the Algerian Basin (SW Mediterranean): influence of mesoscale instabilities in the biomass and production of phytoplankton and bacterioplankton. Deep Sea Research I 48, 405–437.

Morel, A., Andrè, J.M., 1991. Pigment distribution and primary production in the western Mediterranean as derived and modelled from Coastal Zone Colour Scanner observations. Journal of Geophysical Research 96, 12685–12698.

Mousseau, L., Klein, B., Legendre, L., Dauchez, S., Tamigneaux, E., Tremblay, E., Grant Ingram, R., 2001. Assessing trophic pathway that dominate planktonic food webs: an approach based on simple ecological ratios. Journal of Plankton Research 23 (8), 765–777.

Moutin, T., Raimbault, P., 2002. Primary production, carbon export and nutrients availability in western and eastern Mediterranean Sea in early summer 1996 (MINOS cruise). Journal of Marine Systems 33-34, 273–288.

Partensky, F., Blanchot, J., Vaulot, D., 1999. Differential distribution and ecology of Prochlorococcus and Synechococcus: a review. In: Charpy, L., Larkum, A.W.D. (Eds.), Marine Cyanobacteria. Bulletin of the Institute of Océanography, Monaco, No Special 19, pp. 431–449.

Peters, F., Arin, L., Marrasé, C., Berdalet, E., Sala, M.M., 2006. Effects of small-scale turbulence on the growth of two diatoms of different size in a phosphorus-limited medium. Journal of Marine Systems 61, 134–148.

Polat, S., 2002. Nutrients, chlorophyll *a* and phytoplankton in the Iskenderun Bay (Northeastern Mediterranean). Marine Ecology 23, 115–126.

Rabitti, S., Bianchi, F., Boldrin, A., Da Ros, L., Socal, G., Totti, C., 1994. Particulate matter and phytoplankton in the Ionian Sea. Oceanologica Acta 17, 297–307.

Rassoulzadegan, F., 1993. Protozooa pattern In the Azam–Ammerman's bacteria–phytoplankton mutualism. In: Guerrero, R.R., Pedros-Alio, C. (Eds.), Trends in Microbial Ecology. Spanish Society for Microbiology, Barcelona, pp. 435–439.

Revelante, N., Gilmartin, M., 1995. The relative increase of larger phytoplankton in a subsurface chlorophyll maximum in the Northern Adriatic Sea. Journal of Plankton Research 17, 1535–1562.

Ribera D'Alcalà, M., Modigh, M., Saggiomo, V., Civitarese, G., 1997. Nutrients in the sea. In: Gianguzza, A., Pelizzetti, E., Sammartano, S. (Eds.), Marine Chemistry. An Environmental Marine Chemistry Approach. Kluwer Academic, The Netherlands, pp. 99–114.

Ribera D'Alcalà, M., Conversano, F., Corato, F., Licandro, P., Mangoni, O., Marino, D., Mazzocchi, M.G., Modigh, M., Montresor, M., Nardella, M., Saggiomo, V., Sarno, D., Zingone, A., 2004. Seasonal patterns in plankton communities in a pluriannual time series at a coastal Mediterranean site (Gulf of Naples): an attempt to discern recurrence and trends. Scientia Marina 68 (1), 65–83.

Riegman, R., Kuipers, B.R., Noordeloos, A.A.M., White, H.J., 1993. Size differential control of phytoplankton and the structure of plankton communities. Netherlands Journal of Sea Research 31, 255–265.

Rodriguez, J., Tintoré, J., Allen, J.T., Blanco, J.M., Gomis, D., Reul, A., Ruis, J., Rodriguez, V., Echevarria, F., Jiménez-Gomez, F., 2001. Mesoscale vertical motion and the size structure of phytoplankton in the ocean. Nature 410, 360–363.

Sachs, J.P., Repeta, D.J., 1999. Oligotrophy and nitrogen fixation during eastern Mediterranean sapropel events. Science 286, 2485–2488.

Socal, G., Boldrin, A., Bianchi, F., Civitarese, G., De Lazzari, A., Rabitti, S., Totti, C., Turchetto, M., 1999. Nutrient, particulate matter and phytoplankton variability in the photic layer of the Otranto Strait. Journal of Marine Systems 20, 381–398.

Sparnocchia, S., Gasparini, G.P., Astraldi, A., Borghini, M., Pistek, P., 1999. Dynamics and mixing of the Eastern Mediterranean outflow in the Tyrrhenian Sea. Journal of Marine Systems 20, 301–317.

Steeman-Nielsen, E., 1952. The use of radioactive carbon (^{14}C) for measuring organic production in the sea. Journal Conseil International pour l'Exploration de la Mer 18, 117–140.

Strathmann, R.R., 1967. Estimating the organic carbon content of phytoplankton from cell volume or plasma volume. Limnology and Oceanography 12, 411–418.

Turley, C.M., Bianchi, M., Christaki, U., Conan, P., Harris, J.R.W., Psarra, S., Ruddy, G., Stutt, E.D., Tselepides, A., Van Wanbeke, F., 2000. Relationship between primary producers and bacteria in an oligotrophic sea—the Mediterranean and biogeochemical implications. Marine Ecology Progress Series 193, 11–18.

UNESCO, 1983. Carbon dioxide sub-group of the joint panel on the oceanographic tables and standards. UNESCO in Marine Science, 42, 18pp.

Utermöhl, H., 1958. Zur Vervollkommnung der quantitativen Phytoplankton-Methodik. Mitteilungen Internationale Vereins Theoretisch Angewiesen Limnologie 9, 1–38.

Verity, P.G., Robertson, C.Y., Tronzo, C.R., Andrews, M.G., Nelson, J.R., Sieracki, M.E., 1992. Relationships between cell volume and carbon and nitrogen content of marine photosynthetic nanoplankton. Limnology and Oceanography 37 (7), 1434–1446.

Videau, C., Sournia, A., Prieur, L., Fiala, M., 1994. Phytoplankton and primary production characteristics at selected sites in the geostrophic Almeria-Oran front system (SW Mediterranean Sea). Journal of Marine System 5, 235–250.

Vidussi, F., Marty, J.C., Chiavèrini, J., 2000. Phytoplankton pigment variations during the transition from spring bloom to oligotrophy in the northwestern Mediterranean Sea. Deep-Sea Research I 47, 423–445.

Vidussi, F., Clausure, H., Manca, B., Lucchetta, A., Marty, J.C., 2001. Phytoplankton pigment distribution in relation to upper thermocline circulation in the eastern Mediterranean Sea during winter. Journal of Geophysical Research 106 (15), 19,939–19,956.

Yentsch, C.S., Menzel, D.W., 1963. A method for the determination of phytoplankton chlorophyll and phaeophytin by fluorescence. Deep Sea Research 7, 221–231.

Zingone, A., Montresor, M., Marino, D., 1990. Summer phytoplankton physiognomy in coastal water of the Gulf of Naples. PSZNI: Marine Ecology 11, 157–172.

Deep-Sea Research II 56 (2009) 700–712

Contents lists available at ScienceDirect

Deep-Sea Research II

journal homepage: www.elsevier.com/locate/dsr2

Distribution and activity of Bacteria and Archaea in the different water masses of the Tyrrhenian Sea

Christian Tamburini [a,*], Marc Garel [a], Badr Al Ali [a], Bastien Mérigot [a], Pascal Kriwy [a], Bruno Charrière [a], Giorgio Budillon [b]

[a] Université de la Méditerranée, Centre d'Océanologie de Marseille, Laboratoire de Microbiologie, Géochimie et Ecologie Marines (LMGEM), UMR 6117 CNRS–INSU, Campus de Luminy, Case 901, 13288 Marseille, Cedex 9, France

[b] Dipartimento di Scienze per l'Ambiente (DiSAm), Facoltà di Scienze e Tecnologie, Università degli Studi di Napoli "Parthenope", Centro Direzionale-Isola C4, 80143 Napoli, Italy

ARTICLE INFO

Article history:
Accepted 7 July 2008
Available online 31 October 2008

Keywords:
Prokaryotic diversity
Mesopelagic and bathypelagic waters
Hydrostatic pressure
Organic matter degradation
Tyrrhenian Sea

ABSTRACT

This study examines the abundance of the Bacteria, Crenarchaeota and Euryarchaeota and bulk activities (phosphatase and aminopeptidase activities, heterotrophic prokaryotic production and dark CO_2 fixation) in the major water masses of the Tyrrhenian Sea (from surface to bottom: Modified Atlantic Water (MAW); Levantine Intermediate Water (LIW) and Tyrrhenian Deep Water (TDW)) in July and December 2005. Data from the catalyzed reporter deposition coupled with fluorescence *in situ* hybridization (CARD-FISH) analyses indicate that the percentage of Bacteria was always higher than the percentage of Crenarchaeota and Euryarchaeota throughout the water column. While the percentage of Euryarchaeota was relatively homogeneous (~10%) through the water column, the percentage of Crenarchaeota increased with depth (from 5% to 14% in July and from 7% to 17% in December in MAW and TDW, respectively). Regarding differences between July and December 2005, the percentage of Bacteria in the MAW was lower in July than in December (25% versus 43%, respectively) while quite constant (~40%) in the TDW. The pattern of phosphatase and aminopeptidase activity varied according to the stations considered, but both ectoenzyme activities showed higher maximum velocity rates in July than in December in the deep-sea waters. Particularly, specific activity of phosphatase in the deep-sea waters (TDW) was 7 times higher (median value) than in surface waters (MAW). Prokaryotic production, aminopeptidase and phosphatase activity measurements were always higher under *in situ* pressure conditions than after decompression. For the first time, the measurement of the dark CO_2 fixation was investigated under *in situ* pressure conditions and its decompressed counterparts. These data give new information to understanding the role of prokaryotes (Bacteria and Archaea) in biogeochemical cycles of the meso- and batypelagic waters of the oceans.

1. Introduction

Recent investigations on the role and abundance of both planktonic Archaea and Bacteria in the mesopelagic and bathypelagic waters have strongly contributed to a new perception of their biogeochemical importance into the Ocean. Using a quantitative approach such as fluorescence *in situ* hybridization (FISH) techniques, pelagic Archaea, and in particular Crenarchaeota, were observed to be nearly as abundant as Bacteria at about 1000 m depth in the subtropical Pacific Gyre (Karner et al., 2001). Several studies have confirmed this high abundance of Crenarchaeota in meso- and bathypelagic waters of the Antarctic Ocean (Church et al., 2003), the North Atlantic Ocean (Herndl et al., 2005), and the western Arctic Ocean (Kirchman et al., 2007) while Euryarchaeota are more stable throughout the water column. Hence, the importance of Archaea and especially the relative importance of Crenarchaeota group I in the cold deep waters of Ocean has been reported. Yet, there is no study reporting quantitative and relative abundance to total prokaryotes of Bacteria and Archaea through the water column in the Mediterranean Sea, much warmer and more oligotrophic than other regions previously examined, notably in the area studied here, the Tyrrhenian Sea.

Importance of a better knowledge of the quantitative and relative abundance of Bacteria and Archaea is also stressed by the fact that new findings have recently revealed unexpected roles of prokaryotes in the meso- and bathypelagic realm and have led us to revise our perception of the functioning of meso- and bathypelagic systems. In particular, recent studies have suggested that some Archaea are chemoautotrophic and capable of CO_2 fixation (Herndl et al., 2005; Ingalls et al., 2006; Wuchter et al., 2003) using ammonium or other unknown reduced compounds as

* Corresponding author.
E-mail address: christian.tamburini@univmed.fr (C. Tamburini).

0967-0645/$ - see front matter © 2008 Elsevier Ltd. All rights reserved.
doi:10.1016/j.dsr2.2008.07.021

electron donors and energy sources (Francis et al., 2005; Konneke et al., 2005). However, some oceanic Archaea are heterotrophic or mixotrophic, since a large fraction of Archaea has been shown to assimilate amino acids in the North Atlantic (Herndl et al., 2005; Teira et al., 2006) and in coastal waters of southern California (Ouverney and Fuhrman, 2000). The role of marine Archaea in assimilating other organic compounds is not clear.

The waters of the meso- and bathypelagic are probably the most understudied oceanic environments, but make up the largest volumes of the oceans. Microbial activity rates measured in the dark part of the ocean appear low relative to those described in the surface layer. However, because meso- and bathypelagic waters represent more than 80% of the volume of the global ocean, when the measured rates are integrated through the depth of each water layer, the mineralization fluxes mediated by prokaryotic populations at depths deeper than 200 m appear far from negligible (del Giorgio et al., 1997; Lefèvre et al., 1996; Tamburini et al., 2003). One of the key environmental variables that influences the life, evolution and activity of deep-sea organisms is high hydrostatic pressure. This widespread condition requires specific adaptations such as for instance, special electron transport systems (Qureshi et al., 1998; Yamada et al., 2000), regulation of outer membrane protein under high-pressure conditions (28 MPa) (Bartlett et al., 1989), specific ectoenzymes adapted to high-pressure conditions (Kato et al., 1995). For a deep-sea microbial genomics review see Lauro and Bartlett (2007). In the last three decades, several studies have proved that deep-sea planktonic microbial assemblages, in stratified conditions, are adapted to high-pressure conditions and that decompression of deep-sea samples underestimates the real level of activity both in the Ocean and in the Mediterranean Sea (see for example Bianchi and Garcin, 1993; Deming et al., 1980; Jannasch and Wirsen, 1982; Tabor and Colwell, 1976; Tabor et al., 1981; Tamburini et al., 2006; ZoBell, 1970; and the review by Tamburini, 2006), demonstrating that accurately measured deep-sea microbial activities are crucial to better estimate the real impact of deep-sea microbial activity in the carbon cycle of the ocean. The relatively warm deep waters of Mediterranean provide a good opportunity to estimate the effect of pressure on microbial activity without the additional effect of the low temperature characterizing the deep-sea waters of the global ocean.

The aims of this study are firstly to determine the distribution of prokaryotes within three distinct water masses (surface waters, mesopelagic waters and bathypelagic waters) in the Tyrrhenian Sea, and secondly to estimate prokaryotic activity (ectoenzymatic activity, heterotrophic prokaryotic production and dark fixation of CO_2) in these three water masses with their seasonal variability (summer and late autumn 2005).

2. Materials and methods

2.1. Sample collection

The CIESM-Sub cruises were the first survey of a project whose aim is to study, on the basis of a multi-disciplinary approach, the main diversity patterns of a poorly investigated area of the Mediterranean Sea, namely the Southern Tyrrhenian area. Sampling was carried out at three different depths (25, 500 and 3000 m) in the Tyrrhenian Sea (Fig. 1), during the CIESM-sub1 and CIESM-sub2 cruises in July and December 2005 on R/V *Universitatis* and R/V *Urania*, respectively.

Samples from the different depths were collected using Niskin bottles and/or high-pressure bottles (HPBs) fitted on a Sea-Bird Carousel equipped with an SBE-911plus CTD. To assess the effect of pressure on deep-sea activity, a couple of duplicates were collected using HPBs, one maintained at *in situ* pressure conditions, the other decompressed as previously described in Tamburini et al. (2003). For samples maintained at *in situ* pressure conditions, the ambient hydrostatic pressure was consistently

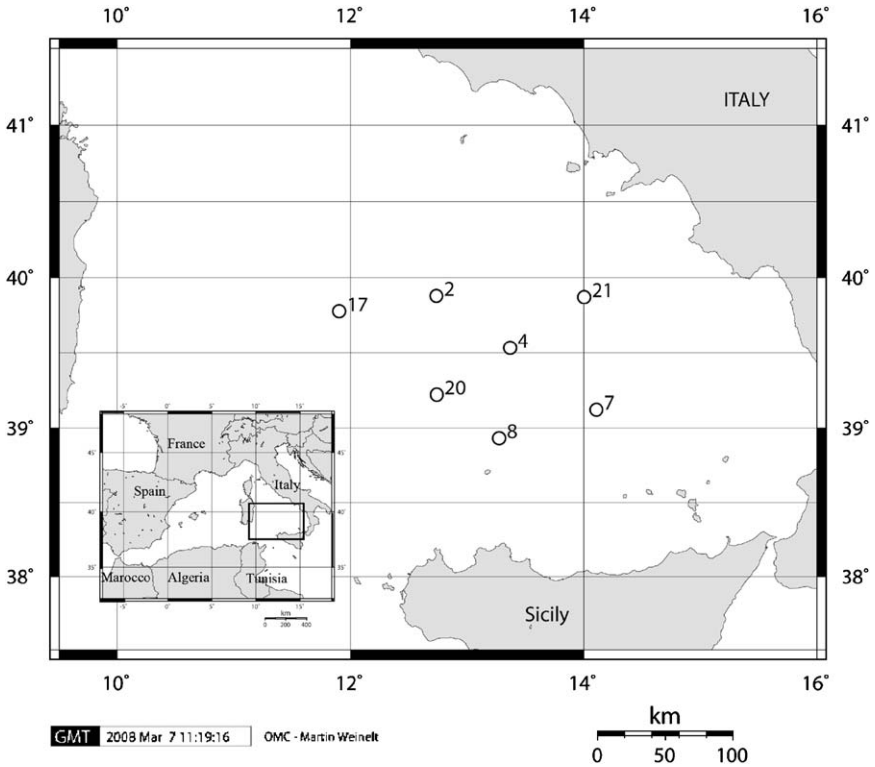

Fig. 1. Map of the sampling area during the CIESM-sub 1 and CIESM-sub 2 cruises in July and December 2005 in the Tyrrhenian Sea. Station 4 corresponds to the time-series station VECTOR. Map constructed using Only Map Creation (OMP) program (Geomar, Kiel, Germany; http://www.aquarius.geomar.de).

maintained (sampling, retrieving, incubation, transfer and subsampling) without any change of pressure.

2.2. CARD-FISH

Seawater samples devoted to further catalyzed reporter deposition coupled with fluorescence *in situ* hybridization (CARD-FISH) analysis were collected from Niskin bottles to sterilized polycarbonate bottles. Bacterioplankton were fixed with 0.2-μm filtered formaldehyde (2% final concentration), kept at room temperature for 15 min, and subsequently stored at 4 °C in the dark for around 12 h. Samples were then filtered onto 0.2-μm-pore-size polycarbonate filters supported by 0.45-μm-pore-size cellulose nitrate filters, washed twice with 0.2-μm filtered MilliQ water and air-dried. Volume of seawater filtered onto 0.2-μm pore size was 10 ml at 20 m, 40 ml at 500 m and 120 ml at 3000 m depth. Filters were stored frozen in plastic tubes at −20 °C until analysis.

Filters were embedded in low-gelling point agarose (concentration 0.1%, Sigma), dried at 37 °C for 10 min, and dehydrated with 95% ethanol. For detection of Bacteria, embedded cells were permeabilized by subsequent treatment with lysozyme (10 mg ml^{-1}, Sigma) in 0.5 M EDTA, 0.1 M Tris–HCl (pH 8.0) for 60 min at 37 °C according to Amann et al. (1995) and with achromopeptidase (60 U in 0.01 M NaCl, 0.01 M Tris–HCl, pH 8.0) for 30 min at 37 °C according Sekar et al. (2003). For detection of Archaea, embedded cells were permeabilized with proteinase K (0.2 μl ml^{-1}, Fluka) according to Teira et al. (2004). Filters were then rinsed three times with 0.2-μm filtered MilliQ water and placed in 0.01 M HCl at room temperature (to denature endogenous peroxydase). Following acid treatment, filters were washed with 0.2-μm filtered MilliQ water and dipped in 95% ethanol and air-dried. Filters were cut in sections and hybridized with a solution of 5′-horseradish peroxydase (HRP)-labeled oligonucleotide probes using a final concentration of 1 ng DNA μl^{-1}. Probes used in this work are listed in Table 1. After an amplification step with Thyramide-Alexa, the pieces of filter were mounted on slides which were examined under an Olympus BX61 microscope equipped with a 100-W Hg-lamp and appropriate filter sets for DAPI and Alexa488. The fraction of CARD-FISH-stained cells in at least 1000 DAPI-stained cells per sample was quantified. Negative control counts (hybridization with HRP-Non338) averaged 1% and were always below 5% of DAPI-stained cells.

2.3. Prokaryotic activity measurements

2.3.1. Ectoenzymatic activity

The fluorogenic substrates L-leucine-7-amino-4-methylcoumarin (Leu-MCA—Sigma Chemical Co.) and 4-methylumbelliferyl-phosphate (MUF-P) (Sigma Chemical Co.) were used to measure aminopeptidase and phosphatase activity according to Hoppe (1993) and modified as already described in Tamburini et al. (2002). For the experimental assays done under ambient pressure conditions using the HPBs (in duplicates) within deep-sea waters, substrate was added at the saturation concentration (5 μM) defined during the multi-concentration experiments (Wright and Hobbie, 1966) done on decompressed samples obtained using Niskin bottles. Several concentration kinetic curves were drawn to determine the Michaelis–Menten parameters using the multi-concentration method (Wright and Hobbie, 1966). It was observed that the saturation concentration for MUF-P and Leu-MCA was 5 μM (data not shown) as in previous study in the Ligurian Sea (Tamburini et al., 2002). Subsequently, we chose this value as the final substrate concentration to measure the maximum velocity (V_{max}), then representing potential activities.

2.3.2. Prokaryotic production

This parameter was measured over time course experiments following the protocol described in Tamburini et al. (2002). The labeled tracer was ^{3}H-leucine (Kirchman, 1993), 55 Ci $mmol^{-1}$ of specific activity (Amersham Corp.), used to give a final concentration of 20 and 10 nM in samples from the euphotic and aphotic zones, respectively. To calculate heterotrophic prokaryotic production, we used the empirical conversion factor of 1.55 ng C $pmol^{-1}$ of incorporated leucine according to Simon and Azam (1989), assuming that isotope dilution was negligible under these saturating concentrations.

2.3.3. Dark fixation of CO_2

Dark fixation of CO_2 was estimated via the incorporation of [^{14}C]bicarbonate (100 μCi; SA, 57.0 mCi $mmol^{-1}$, Amersham) in 40 ml samples in duplicate and one controlled (buffered formaldehyde addition, final concentration 2%) incubated in the dark and at *in situ* temperature for 72 h according to Herndl et al. (2005). For deep-sea samples, as for other activity measurements, experimental assays also were done under ambient pressure conditions using the HPBs (in duplicates). To calculate incorporation of [^{14}C]bicarbonate into cells, we used an *in situ* inorganic carbon concentration equal to 2.1 mM (Lefèvre comm. pers.).

2.3.4. Statistical analysis

Differences in prokaryotic abundance and ectoenzyme activity between seasons (July and December 2005) and between water masses (surface, intermediate and deep-sea waters) were, respectively, analyzed with the Mann–Whitney test and a non-parametric ANOVA (i.e., Kruskal–Wallis test).

The organization of samples in the whole study area according to both their prokaryotic abundance and activity was investigated by means of a normed principal component analysis (PCA).

All statistical analyses were performed using R software (Ihaka and Gentleman, 1996).

3. Results

3.1. Water column description

The cumulative potential temperature (θ) versus salinity (S) diagram of Fig. 2 summarizes the most important hydrographic

Table 1
16S rRNA-targeted oligonucleotide probes used in this study.

Probe	Sequence (5′–3′) of probe	Target organisms	Formamide (%)	References
Eub338	GCT GCC TCC CGT AGG AGT	Domain of Bacteria	55	Amann et al. (1990)
Cren537	TGA CCA CTT GAG GTG CTG	*Crenarchaea*	20	Teira et al. (2004)
Eury806	CAC AGC GTT TAC ACC TAG	*Euryarchaea*	20	Teira et al. (2004)
NegControl	TAG TGA CGC GCT CGA	For non-specific probe binding	55	Karner and Fuhrman (1997)

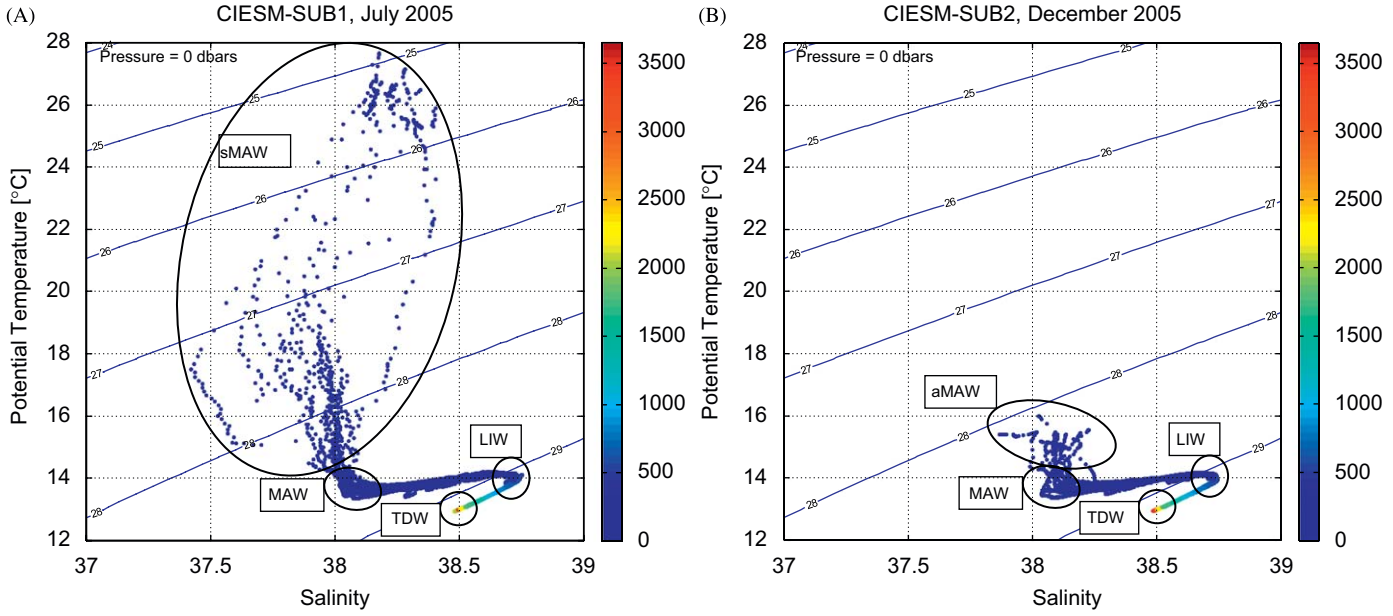

Fig. 2. Theta-S diagrams during the CIESM-SUB1cruise in July 2005 (A) and during the CIESM-SUB2 cruise in December 2005 (B). MAW: Modified Atlantic Water; sMAW: summer MAW; aMAW: autumnal MAW; LIW: Levantine Intermediate Water; TDW: Tyrrhenian Deep-sea Water.

Table 2
Summary of hydrological characteristics of the main water masses in the Tyrrhenian Sea in July and December 2005.

Season (cruise)	Water mass[a]	Depth (m)	Temperature (°C)	Salinity	Density	Oxygen (mg l^{-1})
July 2005 (CIESM-Sub1)	sMAW	0–30	$14<\theta<28$	$37.4<S<38.4$	$\sigma_t<28.6$	$4.8<O_2>5.6$
	MAW	50–70	$13<\theta<14$	$38.0<S<38.15$	$\sigma_t>28.6$	$O_2>5.6$
	LIW	300–700	$\theta\approx14$	$S>38.7$	$\sigma_t\approx29.0$	$4.3<O_2<4.5$
	TDW	Below 2500	$\theta\approx13$	$S<38.5$	$\sigma_t>29.1$	$O_2<4.3$
December 2005 (CIESM-Sub2)	aMAW	0–30	$14<\theta<16$	$37.8<S<38.25$	$\sigma_t<28.6$	$O_2\approx5.5$
	MAW	50–70	$13<\theta<14$	$38.0<S<38.15$	$\sigma_t>28.6$	$O_2\approx5.3$
	LIW	300–700	$\theta\approx14$	$S>38.7$	$\sigma_t\approx29.0$	$4.3<O_2<4.5$
	TDW	Below 2500	$\theta\approx13$	$S<38.5$	$\sigma_t>29.1$	$O_2<4.3$

[a] MAW: Modified Atlantic Water; sMAW: summer MAW ; aMAW: autumnal MAW; LIW: Levantine Intermediate Water; TDW: Tyrrhenian Deep-sea Water.

characteristics of the water column in the central Tyrrhenian Sea during the summer and late autumn seasons in 2005. In this area, the surface layer is dominated by the Modified Atlantic Water (MAW) coming from the Gibraltar Strait and flowing with the classical cyclonic pattern (Astraldi et al., 1999; Astraldi and Gasparini, 1994; Pierini and Simioli, 1998; Sparnocchia et al., 1999). In July 2005, the surface layer above the MAW (which occupies the shallowest 20 m) was modified by the summer heating (sMAW in the following) and was characterized by temperatures higher than 14 °C (with a maximum of 28 °C) and salinity ranging between 37.4 and 38.4. Instead, in December above the MAW the surface layer (aMAW) showed a smaller variability in both temperature and salinity. The samples between 300 and 700 m and below 2500 m were collected within Levantine Intermediate Water (LIW) and Tyrrhenian Deep Water (TDW), respectively. Table 2 reports a summary of hydrological characteristics of the main water masses in the sampled area in July and December 2005. For a schematic and exhaustive description of Mediterranean circulation, see Robinson et al. (2001) or Millot and Taupier-Lepage (2005). The samples taken in this study from 25, 500 and 3000 m depths were collected within the MAW, the LIW and the TDW, respectively.

3.2. Picoplankton description

3.2.1. Abundance of Bacteria and Archaea

In July 2005, prokaryotic cells abundance (as DAPI-stained cells) decreased from the surface to the deep waters, from a maximum of 570 ± 52 and $305\pm44\times10^3$ DAPI-stained-cells ml^{-1} at 25 m to a minimum of 21 ± 6 and $11\pm1\times10^3$ DAPI-stained-cells ml^{-1} at 3000 m in July and December 2005, respectively. Means of bacterial, crenarchaeal and euryarchaeal cells abundance stained by CARD-FISH in July and December 2005 are presented in Fig. 3A and B, respectively. In the Tyrrhenian Sea, Bacteria were more abundant than Crenarchaeota and Euryarchaeota. Abundances of Crenarchaeota and Euryarchaeota appeared to be roughly equivalent (Fig. 3A and B). In July, Bacteria were twice as abundant as Archaea (determined as the summed abundances of Crenarchaeota and Euryarchaeota) in surface waters (MAW). In the water column, Bacteria were quite equal in abundance to Archaea in LIW and TDW (Fig. 3A). In December, Bacteria were 3- and 2-fold more abundant than Archaea, respectively, in MAW and LIW while abundances were equal in TDW (Fig. 3B).

Regarding differences between water masses, in July 2005, Bacteria were almost 6- and 10-fold more abundant in sMAW than

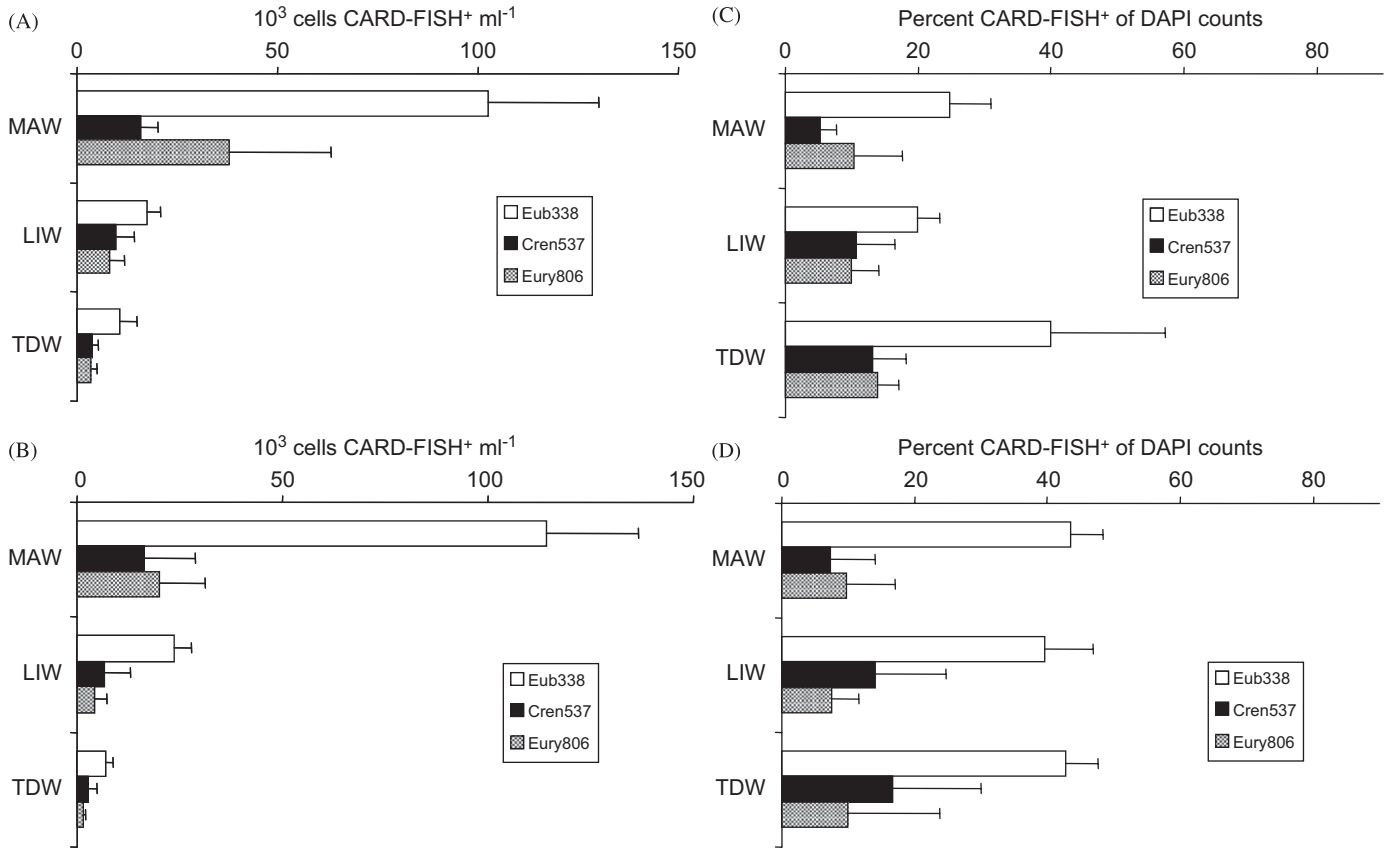

Fig. 3. Mean (±SE) of bacterial and archaeal abundance (expressed in cells ml^{-1}) in July (A) and December 2005 (B). Mean of relative bacterial and archaeal abundance (expressed as percent of total prokaryotes, DAPI-stained cells) in July (C) and December 2005 (D) detected by catalyzed reporter deposition coupled with fluorescence in situ hybridization (CARD-FISH). Eub338: Bacteria; Cren537: Crenarchaeota; Eury806: Euryarchaeota. MAW: Modified Atlantic Water; LIW: Levantine Intermediate Water; TDW: Tyrrhenian Deep-sea Water.

in LIW and in TDW, respectively (Kruskal–Wallis test; $p<0.001$). In December 2005, they were almost 5- and 17-fold more abundant in aMAW than in LIW and in TDW, respectively (Kruskal–Wallis test; $p<0.001$). In July, among Archaea, Crenarchaeota were only 1.7- and 4.3-fold more abundant in sMAW than in LIW and TDW, respectively (Kruskal–Wallis test; $p<0.01$); in December 2005, Crenarchaeota were 2.4- and 6.2-fold higher in aMAW than in LIW and TDW, respectively (Kruskal–Wallis test; $p<0.001$). In surface waters, Euryarchaeota were almost 5-fold more abundant than in LIW both in July and December 2005 and 11- and 14-fold more abundant than in TDW in July (Kruskal–Wallis test; $p<0.001$) and December 2005 (Kruskal–Wallis test; $p<0.01$), respectively.

Regarding differences among seasons, Bacteria abundance appeared similar both in July and in December 2005 in MAW (Mann–Whitney test; $p=0.53$) and TDW (Mann–Whitney test; $p=0.14$). In contrast, Bacteria abundance was slightly higher (1.5-fold) in December than in July in LIW (Mann–Whitney test; $p<0.05$). Among Archaea, while Crenarchaeota cells number was closely equivalent between July and December in the different water masses (Mann–Whitney test; $p>0.05$ in each water mass), Euryarchaeota were more abundant in July than in December 2005 only in the MAW (Mann–Whitney test; $p<0.05$).

3.2.2. *Bacteria and Archaea as a fraction of total prokaryotes*

The contribution of Bacteria and the two groups of Archaea to total prokaryotic abundance (DAPI-stained cells) for each station and each depth is presented in Table 3. As seen in the absolute numbers, percentage of Bacteria was higher than the percentage of Crenarchaeota and than the percentage of Euryarchaeota (Kruskal–Wallis test; $p<0.001$) while the percentage of Crenarchaeota and Euryarchaeota were quite similar (Fig. 3C and D). However, relative archaeal abundance (or percentage of Archaea as the sum of the percentage of Crenarchaeota and the percentage of Euryarchaeota) was roughly equivalent to the percentage of Bacteria in LIW and TDW in particular in July 2005 (Fig. 3C).

Regarding differences between water masses, contribution of Bacteria, Crenarchaeota and Euryarchaeota to total prokaryotes did not decrease with depth through the water column either in July or December 2005 in contrast to what was shown for absolute abundance. What is more, the percentage of Bacteria in deep-sea waters (TDW) of the Tyrrhenian Sea appeared, respectively, 1.6 and 2 times higher than in the surface waters (sMAW) and at 500 m depth (LIW) in July (Kruskal–Wallis test; $p<0.05$; Fig. 3C). In contrast, in December percentage of Bacteria remained constant with depth (Fig. 3D). The relative abundance of crenarchaeotal (i.e., percent of Crenarchaeota) was 2.5-fold higher in TDW than in MAW both in July and December 2005 (Kruskal–Wallis test; $p<0.05$, Fig. 3C and D). Comparison between water masses did not show significant differences for relative abundance of euryarchaeotal in either July or December 2005.

In contrast with comparison results between July and December 2005 obtained with cell abundances, percentage of Bacteria expressed significant variation according to the water masses. In MAW and LIW in the Tyrrhenian Sea, the percentage of total hybridized cells stained by CARD-FISH (i.e., sum of percentages of Bacteria, Crenarchaeota, Euryarchaeota) was 1.5-fold lower in July than in December 2005 (Mann–Whitney test; $p<0.05$ in both cases). This is essentially due to the fact that the

Table 3
Relative bacterial and archaeal abundance in the three water masses sampled at all stations.

Season (cruise)	Station	Water mass	Prokaryotes (%)							DAPI counts	
			Bact[a]	±SE	Cren	±SE	Eury	±SE	Total detected (%)[b]	10^3 cells ml^{-1}	±SE
July 2005 (CIESM-Sub1)	Station 2	sMAW	19.2	2.5	3.3	0.5	22.9	2.1	45.5	369.8	52.4
		LIW	15.4	1.6	11.8	6.6	13.4	2.4	40.6	102.2	10.8
		TDW	45.7	13.0	10.8	3.9	14.9	2.1	71.4	20.8	6.2
	Station 4 (VECTOR)	sMAW	32.8	6.2	6.2	3.1	15.2	5.4	54.2	351.2	57.1
		LIW	15.7	11.3	9.2	2.1	4.6	2.6	29.5	80.5	14.2
		TDW	70.8	11.3	20.9	4.4	15.8	2.0	107.5	25.1	4.6
	Station 7	sMAW	27.7	5.7	9.7	4.2	5.5	1.0	42.8	337.3	49.7
		LIW	21.0	5.7	14.1	2.5	13.8	3.0	49.0	91.4	11.8
		TDW	23.1	5.0	7.6	2.6	14.4	2.9	45.1	34.6	4.1
	Station 8	sMAW	26.5	7.3	3.8	0.5	15.9	7.8	46.2	439.9	66.1
		LIW	19.6	4.5	16.2	3.9	6.3	1.4	42.1	98.0	16.3
		TDW	28.5	6.7	16.6	4.8	16.2	2.9	61.4	25.1	4.3
	Station 17	sMAW	20.5	3.5	3.5	0.3	5.0	1.5	29.1	534.2	34.9
		LIW	23.5	4.1	5.3	1.4	4.6	0.1	33.5	96.9	13.2
		TDW	28.0	5.5	9.5	1.2	8.4	1.6	45.8	33.5	3.9
	Station 20	sMAW	17.9	4.3	5.0	2.1	4.5	1.4	27.4	412.5	54.5
		LIW	22.1	7.4	19.6	4.5	11.9	1.8	53.6	327.9	60.5
		TDW	31.6	5.5	11.6	0.6	12.0	1.6	55.2	269.0	60.3
	Station 21	sMAW	30.2	5.7	4.0	1.0	9.2	2.5	43.4	492.7	62.7
		LIW	21.1	5.1	3.8	0.0	11.0	2.1	35.8	77.4	8.5
		TDW	40.8	7.8	18.0	4.1	17.4	3.1	76.2	31.2	5.2
December 2005 (CIESM-Sub2)	Station 2	aMAW	44.0	11.3	12.4	3.1	14.5	1.0	70.9	305.2	43.6
		LIW	38.1	7.6	30.4	5.1	15.7	2.2	84.2	52.1	19.3
		TDW	48.2	9.5	33.5	5.9	16.9	2.1	98.6	19.6	4.1
	Station 4 (VECTOR)	aMAW	47.2	4.8	18.8	2.9	18.5	3.0	84.5	218.6	18.9
		LIW	51.4	13.6	24.3	5.5	3.0	1.4	78.7	50.5	9.0
		TDW	47.2	3.7	33.4	8.0	19.0	2.9	99.6	12.5	1.4
	Station 7	aMAW	36.9	5.2	2.8	0.4	4.8	0.1	44.5	254.5	22.1
		LIW	33.6	3.7	6.2	0.7	3.4	1.1	43.2	72.1	11.0
		TDW	37.6	5.7	6.9	1.5	4.4	0.6	48.9	16.4	1.9
	Station 17	aMAW	45.9	3.7	4.3	1.3	12.6	5.4	62.8	278.5	16.1
		LIW	45.7	2.0	12.0	2.3	16.4	0.3	74.2	50.3	6.6
		TDW	46.1	5.3	14.3	1.5	9.7	2.3	70.1	10.8	1.2
	Station 20	aMAW	38.2	3.5	2.1	0.1	3.2	0.3	43.5	227.7	33.2
		LIW	34.2	2.4	4.2	0.3	2.4	0.3	40.7	68.2	5.6
		TDW	38.9	4.8	4.6	0.5	4.6	0.2	48.2	20.3	1.7
	Station 21	aMAW	48.8	7.9	3.3	0.4	5.2	1.2	57.3	288.7	25.4
		LIW	34.8	5.1	6.9	0.9	3.8	1.0	45.5	48.8	4.0
		TDW	38.0	5.2	7.6	0.4	5.5	0.5	51.1	16.7	1.7

The negative control, which was not substracted from these data, was 2.1 ±1.9% of total prokaryotes (DAPI-positive cells).
[a] The following abbreviations are used: Bact = Bacteria, Cren = Crenarchaeota, Eury = Euryarchaeota.
[b] Total detected (%) is the sum of the percent of total prokaryotes detected as Bacteria, Crenarchaeota and Euryarchaeota calculated for each sample.

percentage of Bacteria to total prokaryotes was 1.8- and 2-fold lower in July than in December in MAW and LIW (Mann–Whitney test; $p<0.001$ in both cases) but relatively stable in TDW. In contrast to the Bacteria, percentages of Crenarchaeota and Euryarchaeota did not demonstrate significant variation between July and December 2005.

3.3. Prokaryotic activity

Aminopeptidase and phosphatase activities were measured both in July and December 2005 while heterotrophic prokaryotic production and dark CO_2 fixation were assessed only during July 2005.

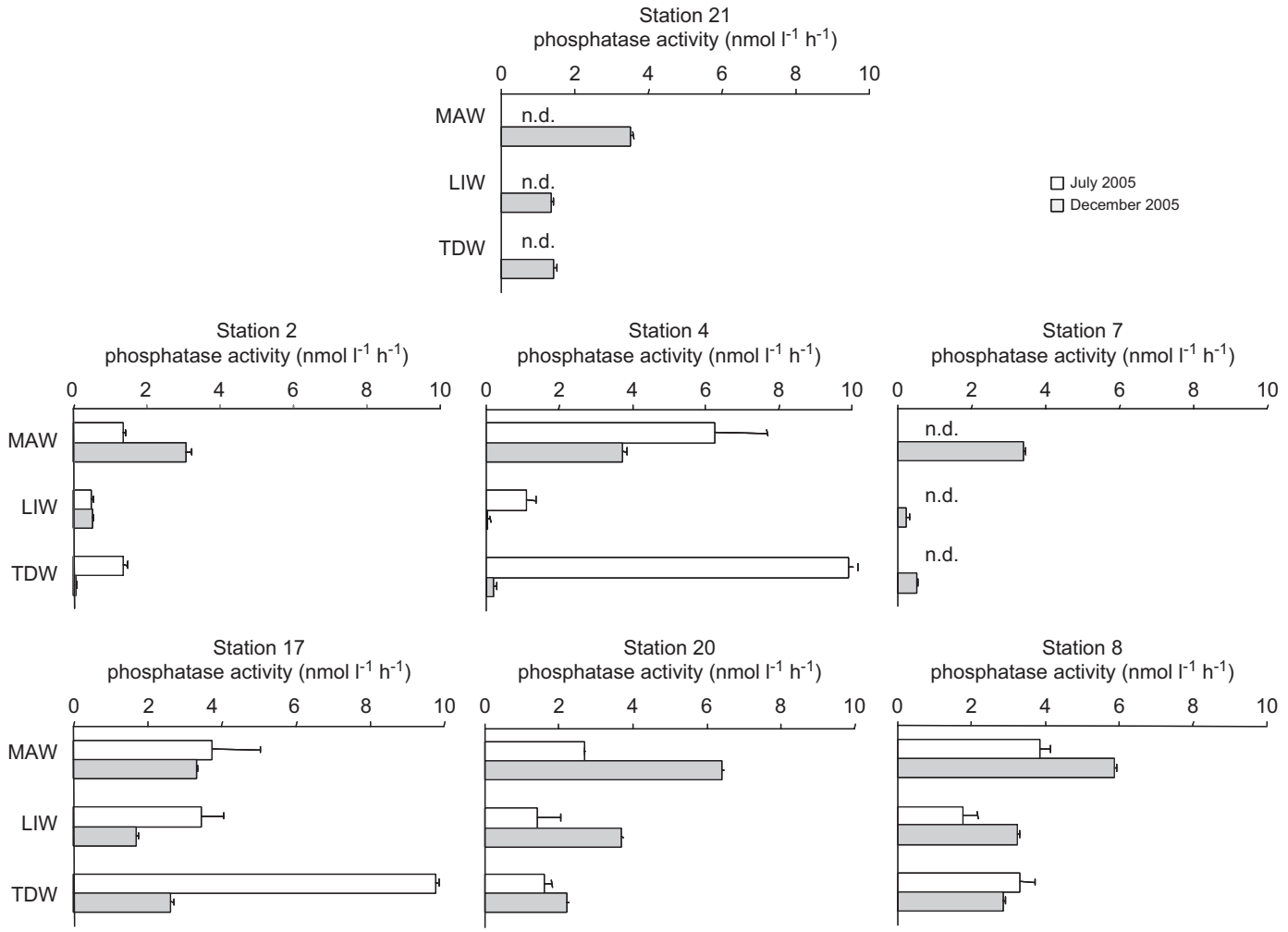

Fig. 4. Phosphatase activity in the different water masses in July and December 2005 in the Tyrrhenian Sea. MAW: Modified Atlantic Water; LIW: Levantine Intermediate Water; TDW: Tyrrhenian Deep-sea Water. n.d. = not determined.

3.3.1. *Ectoenzymatic activity*

Ectoenzymatic activity ranged between 0.5 and 9.9 nmol l^{-1} h^{-1} for phosphatase and 0.3 and 21.7 nmol l^{-1} h^{-1} for aminopeptidase activity. Patterns of phosphatase and aminopeptidase activity varied according to stations considered (Figs. 4 and 5, respectively). For example, phosphatase activity in December 2005 was remarkably stronger (around 10-fold) in surface waters than in the meso- and bathypelagic waters in the middle transect (stations 2, 4 and 7) while they were around 2-fold higher in the western transect (stations 17, 20 and 8).

Regarding differences between water masses, in July 2005, phosphatase activity was not significantly different (Kruskal–Wallis test; $p<0.05$), even if the phosphatase activity in station 17 were 2.6 times higher in TDW than in sMAW and LIW (Fig. 4). In fact, if we consider *in situ* activity measured under pressure (HP-TDW, Table 4), the phosphatase activity was higher in TDW than in MAW and LIW in July. In December 2005, phosphatase activity of surface waters (aMAW) was significantly higher (2.7- and 3.0-fold, respectively) than in LIW and TDW, respectively (Kruskal–Wallis test; $p<0.01$). Concerning aminopeptidase activity, rates were higher in MAW than in LIW both for July and December 2005 (Kruskal–Wallis test $p<0.001$ in both cases) and higher in MAW than in TDW only in July 2005 (Kruskal–Wallis test $p<0.05$).

Regarding differences between seasons, we found significant higher maximum velocity rates in July than in December in the deep-sea waters (TDW) for both phosphatase and aminopeptidase activity (Mann–Whitney test; $p<0.05$, $p<0.01$, respectively).

3.3.2. *Sample organization in the whole study area according to both prokaryotic activity and relative abundance*

When all the samples were considered in the PCA computation, it appeared that four of them affected strongly the organization of all the samples on the factorial plane due to their high ectoenzymatic activity (7 MD, 17 MJ and 17 TJ, see the legend of Fig. 6 for abbreviation meaning) or their high Bacteria abundance (4 TJ). Hence, any other trends between the remaining samples were masked by these four samples.

Consequently, in order to study more specifically the distribution of the other samples on the factorial plane, a second PCA was computed without considering these four stations. In this analysis, the two first principal components accounted for 64% of the total inertia. The first principal component (41%, Fig. 6A) was highly correlated with the phosphatase and aminopeptidase activities, and the relative abundance of Crenarchaeota and Bacteria. The second principal component (23%) was mainly explained by the relative Euryarchaeota abundance. Note that even though some correlations between these five variables appeared significant, all of them were weak (Fig. 6B). Hence, no activity was strongly linked with any particular prokaryotic abundance.

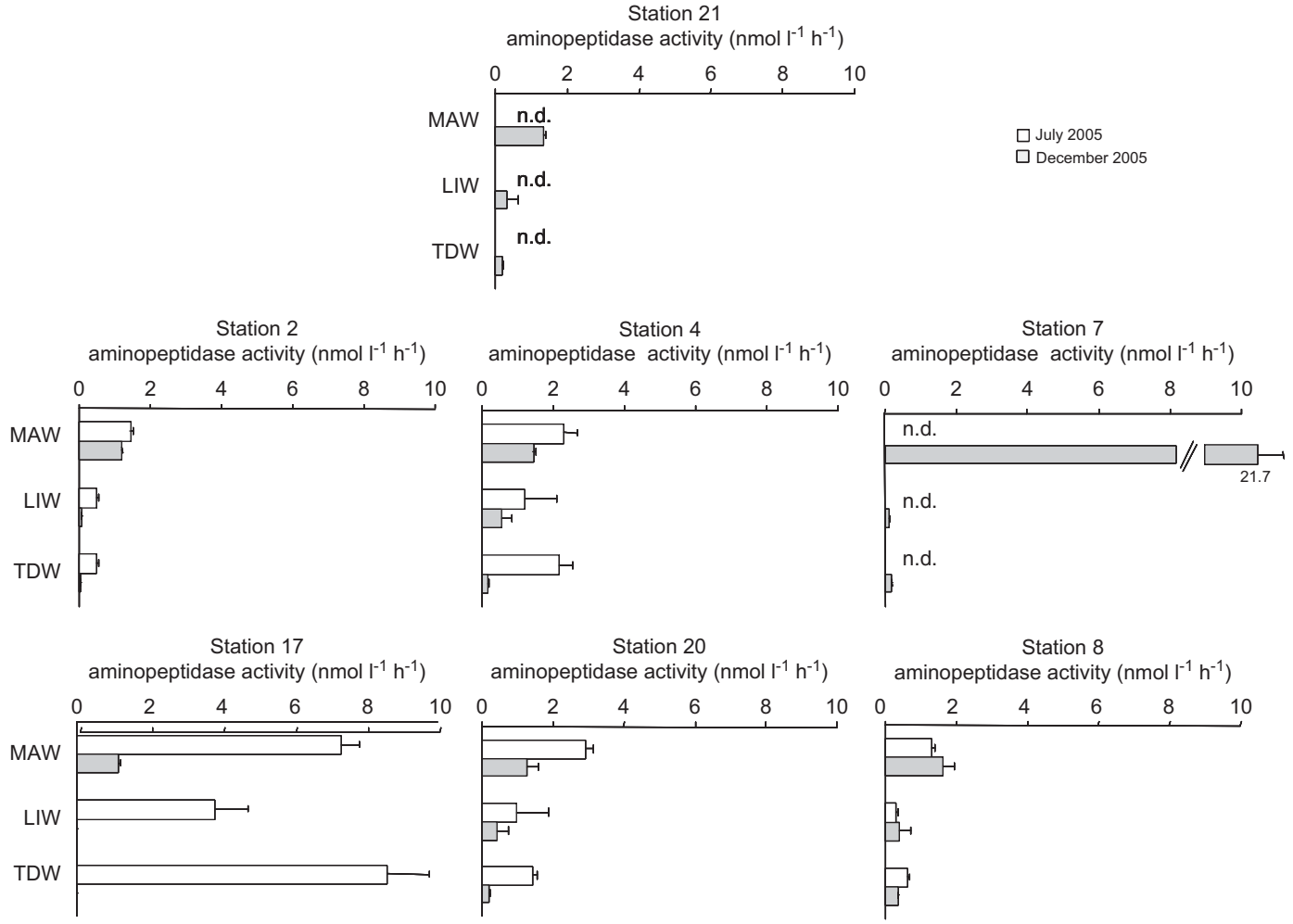

Fig. 5. Aminopeptidase activity in the different water masses in July and December 2005 in the Tyrrhenian Sea. MAW: Modified Atlantic Water; LIW: Levantine Intermediate Water; TDW: Tyrrhenian Deep-sea Water.

Table 4
Heterotrophic prokaryotic production and dark CO_2 fixation in July 2005 expressed in ng C l^{-1} h^{-1}.

Station	Water mass	Heterotrophic prokaryotic production[a] (ng C l^{-1} h^{-1})	Dark fixation of CO_2[b] (ng C l^{-1} h^{-1})
Station 2	SMAW	34.21 ± 7.68	n.d.
	LIW	0.49 ± 0.03	
	DEC-TDW[c]	0.51 ± 0.05	
	HP-TDW[d]	1.31 ± 0.01	
Station 4 (VECTOR)	DEC-TDW	0.20 ± 0.02	3.00 ± 0.37
	HP-TDW	1.71 ± 0.11	1.80 ± 0.20
Station 8	DEC-TDW	0.83 ± 0.42	7.43 ± 3.71
	HP-TDW	8.99 ± 1.14	16.92 ± 3.35
Station 17	sMAW	n.d.	0.54 ± 0.34
	LIW		3.26 ± 1.58
	DEC-TDW		22.79 ± 9.18

n.d: non-determined.

[a] To calculate heterotrophic prokaryotic production we used the empirical conversion factor of 1.55 ng C $pmol^{-1}$ of incorporated leucine according to Simon and Azam (1989).

[b] To calculate incorporation of [^{14}C]bicarbonate into cells, we used an *in situ* inorganic carbon concentration equal to 2.1 mM (Lefèvre, pers. comm.).

[c] DEC-TDW: measurements done in duplicates after decompression of deep-sea samples.

[d] HP-TDW: measurements done in duplicates maintaining *in situ* pressure conditions of deep-sea samples (see details in Section 2).

(A)

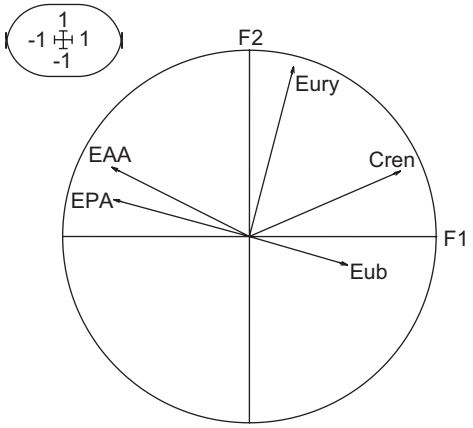

(B)

	Bact	Cren	Eury	EAA	EPA
Bact	1.00				
Cren	0.35*	1.00			
Eury	-0.02	0.35*	1.00		
EAA	-0.33*	-0.31*	0.02	1.00	
EPA	-0.03	-0.49*	0.02	0.49*	1.00

(C)

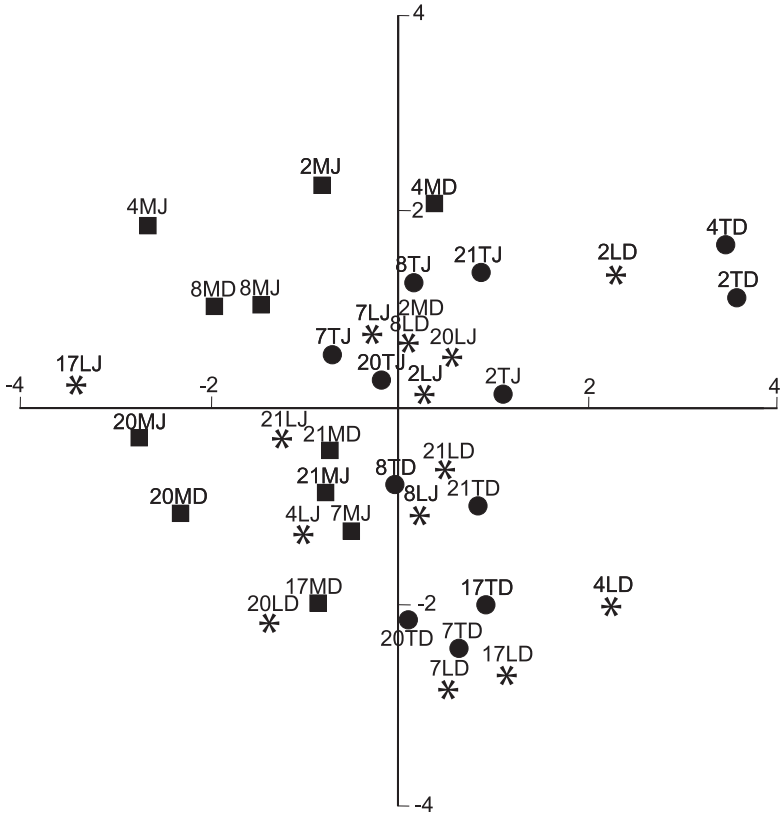

Fig. 6. Normed principal components analysis (PCA) computed on phosphatase (EPA) and aminopeptidase (EAA) activities, and on percent of Bacteria (Bact), Crenarchaeta (Cren), Euryarchaeta (Eury): (A) Correlation circle; (B) Pearson correlation coefficients calculated between all the variables considered. All significant values ($p<0.05$) are marked by an asterisk; (C) projection of the samples on the first factorial plane (samples are labeled firstly by the number of the station, secondly by a letter for water mass—M for MAW, L for LIW and T for TDW—and thirdly by a letter for the season—J for July and D for December). Samples are symbolized by water mass—square for MAW, star for LIW and full circle for TDW.

Firstly, from the projection of the samples on the first factorial plane (Fig. 6C), high heterogeneity is apparent within each station considering the five variables. Secondly, several samples can be distinguished from the others both according to their ectoenzymatic activity and relative abundance. For instance, the samples 4 MJ or 20 MD appeared different from the others due to their relatively high ectoenzymatic activity. In contrast, samples 4 and 2 TD presented low ectoenzymatic activity and were characterized by high relative abundance of Crenarchaeota. Similarly, the samples 2 MJ and 4 MD appeared to have a relatively high abundance of Euryarchaeota, while the samples 7 LD, 7 TD and 17 LD presented relatively low values. Finally, it appeared that the samples along the first factor was characterized by the water mass to which they belong (Fig. 6C), in particular the samples with relatively high ectoenzymatic activity belong mainly to the MAW (Fig. 6C), with the exception of sample 17 LJ which belongs to LIW. This confirms a bathymetric effect on the ectoenzymatic activity.

3.3.3. *Heterotrophic prokaryotic production and dark CO_2 fixation*

These measurements were performed only in July 2005, focusing particularly in the deep-sea realm activity (Table 4) and in an attempt to compare heterotrophic prokaryotic production

Table 5
Ratio of undecompressed to decompressed rate measurements for aminopeptidase activity, phosphatase activity, heterotrophic prokaryotic production and rates of dark fixation of CO_2.

Season (cruise)	Station	Aminopeptidase	Phosphatase	Heterotrophic prokaryotic production	Dark fixation of CO_2
July 2005 (CIESM-Sub1)	Station 2	–	1.6	2.5	–
	Station 4	–	–	8.3	0.6
	Station 8	1.7	2.1	10.9	2.3
	Station 17	–	–	–	–
	Station 20	2.0	5.8	–	–
December 2005 (CIESM-Sub2)	Station 7	–	1.4	–	–

and dark CO_2 fixation. Heterotrophic prokaryotic production was two orders of magnitude higher in the surface waters than in the deep realm as already found in the Ligurian (Tamburini et al., 2002) and Ionian areas (Tamburini, 2002) of the Mediterranean Sea.

3.3.4. *Effect of hydrostatic pressure conditions on prokaryotic activity*

Measurements done under *in situ* pressure conditions (Table 5) confirmed that decompression resulted in underestimation of the real rates of heterotrophic prokaryotic production in deep-sea waters (Tamburini, 2006 and reference therein). Pressure effects (thereafter called Pe, being ratio of undecompressed to decompressed rate measurements) on prokaryotic activity were highly variable according to the activity considered (Table 5) as previously discussed in Tamburini (2006). The Pe average and its associated standard error of all activities were equal to 3.3 ± 3.4 ($n = 10$). According to the activity, the Pe average and its associated standard error were 2.6 ± 1.8 ($n = 5$) for ectoenzymatic activity (both aminopeptidase and phosphatase activities), 7.2 ± 4.3 ($n = 3$) for heterotrophic prokaryotic production ($n = 3$), 1.5 ± 1.2 ($n = 2$) for dark fixation of CO_2.

Only two attempts (in duplicates) were performed and successful in comparing dark CO_2 fixation under *in situ* pressure conditions and their decompressed counterparts. As this was the first time that these measurements were performed, it is not possible to come to any conclusions regarding the effect of pressure on dark CO_2 fixation (Table 5), but it does permit us to validate the feasibility of these measurements under *in situ* pressure conditions.

4. Discussion

The overall aim of the CIESM-SUB campaign was to define the main diversity patterns of an understudied zone of the Mediterranean Sea, namely the Southern Tyrrhenian area that represents a key area for investigating the effects of large-scale atmospheric systems on the western Mediterranean basin. The prokaryotic structure and activities throughout the water column, in relation to the physico-chemical data, have been studied during two cruises (in July and December 2005), coinciding with stratified and mixed water conditions, respectively.

CARD-FISH was used to detect and quantify Bacteria, Crenarchaeota and Euryarchaeota cells. Cells targeted by CARD-FISH in July and December 2005, respectively, was equal to $49.3 \pm 18.4\%$ and $63.6 \pm 19.5\%$ (mean $\pm$ SE) of the total DAPI-stained cells (sum of percentage of Bacteria, Crenarchaeota and Euryarchaeota). This total percentage of hybridized cells is in the same range than recovery efficiency (between 41% and 66%) found by Varela et al. (2007) in the eastern North Atlantic waters. These authors hypothesized that low recovery efficiency might be caused by the low overall activity of the prokaryotic community they estimated. So, it could be possible to hypothesize than the very low content of rRNA per cell content is a consequence of a low overall prokaryotic activity that resulted in lower hybridization efficiency as suggested by Bouvier and del Giorgio (2003) using the FISH method. Another explanation, proposed by Varela et al. (2007), is the presence of specific group not targeted by oligonucleotide probes used in this study and in particular concerning Crenarchaeota. As Varela et al. (2007), using a Cren537 probe, we refer in this study exclusively to marine Crenarchaeota group I. In addition, it has been recently shown that the use of Eub338 might be insufficient to detect all Bacteria because it does not target members of the Verrucomicrobia and Planctomycetales (Daims et al., 1999).

First demonstrations that Crenarchaeota are nearly as abundant as Bacteria at about 1000 m depth in the North Pacific (Karner et al., 2001) have been confirmed in the Antarctic waters (Church et al., 2003), in the North Atlantic (Herndl et al., 2005; Teira et al., 2006; Varela et al., 2007), and in Arctic waters (Kirchman et al., 2007). Our data (Fig. 3B and C), obtained in Tyrrhenian Sea, are not in concordance with these prior oceanic results since the percentage of Bacteria was always higher than that of Crenarchaeota and higher than that of Euryarchaeota through the water column, during both seasons investigated. The proportion of Crenarchaeota to the total prokaryotic community increases on average with depth (as previously demonstrated), from 5% in MAW to 14% in TDW in July and from 7% in MAW to 16% in TDW in December but without reaching proportion of Bacteria. The percentage of Euryarchaeota appears constant (around 10%) throughout the water column in the Tyrrhenian Sea both in July and December 2005. Percentages of Euryarchaeota can be substantial in the North Atlantic, reaching 25% of total prokaryotic abundance in some deep-sea waters (Teira et al., 2006) even if averaging 17% in the Antarctic circumpolar deep-sea waters and 9% in the eastern North Atlantic (Varela et al., 2007). Recently, a study using a metagenomic fosmid library from a 3000-m-depth sample collected in November 2004 in the Ionian Sea detected among Archaea around 60% of Crenarchaeota and 40% of Euryarchaeota (Martin-Cuadrado et al., 2007). In the North Pacific, another study based on metagenomic data showed that Crenarchaeota and Euryarchaeota are equally common from 500 m depth (DeLong et al., 2006). DNA (16S rRNA genes) clone libraries performed at the station 4 at 3000 m depth in December 2005, showed that Archaea community was dominated by Crenarchaeota Marine Group I (52–64%) while Euryarchaeota Marine Group II represented only 22% of the Archaea community (La Cono et al., 2008). However, no clone relatives of Euryarchaeota Marine Group II were detected in RNA-based libraries, suggesting the dormant state of these organisms in deep-sea environment (La Cono et al., 2008).

Variability between and within the different stations according to their prokaryotic activity and relative abundance also has been checked using a PCA analysis to obtain an overall view. We have shown a high heterogeneity within and between stations according to their characteristics (relative abundance and activity). Five stations represented a strong contribution to the analysis (namely stations 2, 4, 7, 17 and 20) due to very high ectoenzyme activity or high relative abundance of prokaryotes. The three water masses considered during this study are very different in terms of activity and/or relative abundance of prokaryotes, but note that many samples with high ectoenzymatic activity belong to MAW stations (cf. PCA results in Section 3.3.2).

Cell-specific activity of phosphatase and aminopeptidase activities (expressed in amol cell^{-1} h^{-1}, Hoppe and Ullrich, 1999) as being the ratio of potential activity (expressed in nmol l^{-1} h^{-1}) to total cells counts (DAPI counts) were represented using Box-and-Whisker plots (Fig. 7). Cell-specific activity of phosphatase in the deep-sea waters (TDW) is higher than in surface (MAW) and intermediate waters (LIW) both in July and December 2005. The same pattern was found only in July 2005 but not in December 2005 (Fig. 7) for the cell-specific activity of aminopeptidase. In July, the relatively high ectoenzyme activity might lead to higher energy expenditure resulting from higher respiration activity due to a lack of organic matter in the intermediate and deep-sea layers in concordance with higher respiration rates (using ETS activity measurements) in July than in December (M. Azzaro, pers. comm.). These results are consistent with previous results where we demonstrated a decoupling between ectoenzymatic activity and prokaryotic production, glutamic acid assimilation and respiration in the Ligurian Sea in spring and fall 2002 (Tamburini et al., 2002, 2003). In these latter studies, ectoenzymatic activity was found to be higher than prokaryotic carbon demand during a period of low particle flux (in fall 2002), suggesting that in periods of low availability of easy-to-use organic matter, prokaryotes in the deep sea deployed very high levels of ectoenzymatic activity to recover carbon and energy coming from refractory organic matter. Hoppe and Ullrich (1999) suggested that that their observation of phosphatase increase in the deep Indian Ocean was related to the strict C-limitation of bacteria in deep-sea and not to the P-demand. The deep-sea environment is characterized by a low quantity of organic matter or, more exactly, by a very refractory part of the organic matter being constituted of complex polymers (Hedges et al., 2000; Wakeham et al., 1997). Recently, it has been demonstrated that the piezophilic strain *Photobacterium profundum* SS9 is able to degrade complex polymers such as chitin, pullulan and cellulose (Vezzi et al., 2005). Probably other deep-sea microbes are also able to utilize complex carbon compounds under high hydrostatic conditions as suggested by higher ectoenzyme activity measured under *in situ* pressure condition (comparatively to decompressed samples incubated at atmospheric pressure condition, Table 5). Metagenomic studies of the deep-sea waters of the North Pacific Subtropical Gyre (Delong et al., 2006) and of the Mediterranean Sea (Martin-Cuadrado et al., 2007) highlighted that specific metabolic genes encountered in the deep-sea realm were related to degradation of refractory pools of organic matter. High cell-specific ectoenzymatic activities in the deep-sea waters reinforce the idea that deep-sea microorganisms are adapted to degrade recalcitrant pools of organic matter.

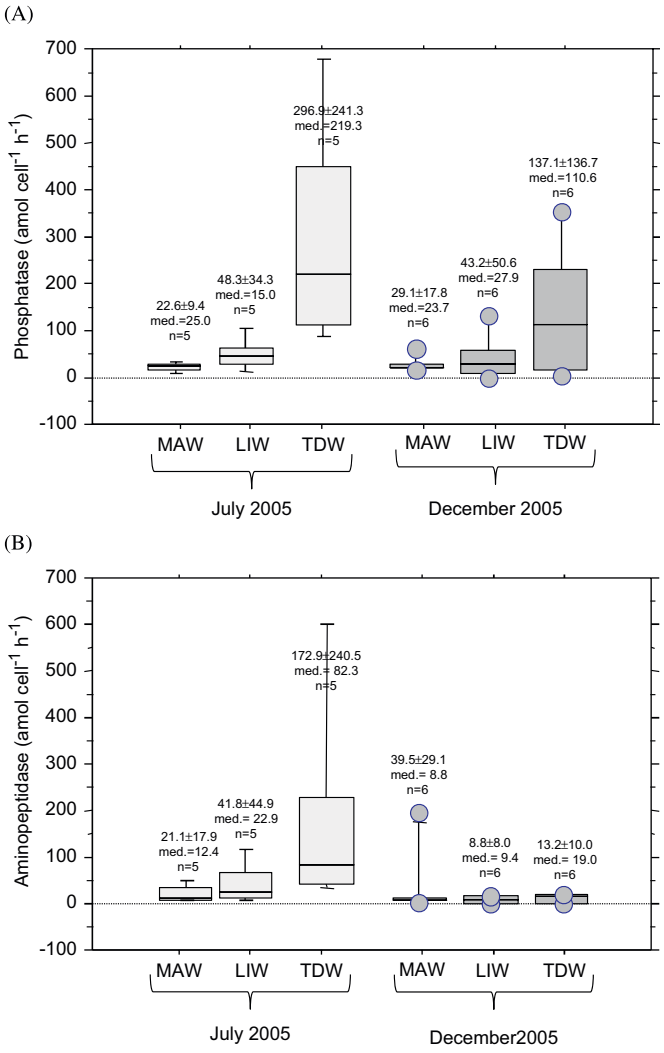

Fig. 7. Box-and-Whisker plot of the cell-specific activities of (A) phosphatase and (B) aminopeptidase (amol cell^{-1} h^{-1}) in the different water masses in July and December 2005 in the Tyrrhenian Sea. MAW: Modified Atlantic Water; LIW: Levantine Intermediate Water; TDW: Tyrrhenian Deep-sea Water. The top and bottom of each box-plot represent 75% and 25% of all values, respectively. The horizontal line is the median. The lower and upper bars represent the 10% and 90% limits, respectively. The outliers are shown as full circles.

During the first cruise in July 2005, we also investigated the effect of pressure on measured activity (Table 5). As previously demonstrated in other parts of the Mediterranean (Ligurian Sea; Bianchi and Garcin, 1993; Bianchi et al., 1999; Tamburini et al., 2002; Tholosan et al., 1999) and in the Ionian Sea (Tamburini, 2002), ectoenzymatic activity and heterotrophic prokaryotic production in the Tyrrhenian Sea measured under ambient pressure revealed higher values than their decompressed counterparts. In this study, we have found high-pressure effect (up to 10) regarding prokaryotic production. This is exceptionally high comparatively to previous data obtained around 2000 m depth essentially in the Ligurian Sea (Tamburini et al., 2002, 2003) but the high-pressure effect was already found in the Ionian Sea at 3000 m depth (Tamburini, 2002). This indicates a gap of knowledge about prokaryotic production in the deep-sea waters, in particular because we do not understand up to date how it is possible to sustain this prokaryotic production higher that the apparent carbon available in the deep-sea realm. This confirms the necessity to improve our effort to better understand biogeochemical cycles in the deep sea. Herndl et al. (2006) have shown that the autotrophic use of inorganic carbon might be far from negligible. However, this important new feature was demonstrated from decompressed samples incubated at atmospheric pressure condition, and so it was important to assess it under ambient pressure conditions. For the first time, measurements of dark fixation of CO_2 were performed under ambient pressure conditions using our high-pressure retrieval system.

On the basis of only these two attempts, hydrostatic pressure appears to have an impact on fixation rates even if it is not possible to speculate about the effect of pressure on bulk dark fixation of CO_2, but future research may be focused on collecting data for this purpose.

Deep-sea activity measurements performed at ambient pressure for prokaryotic production, dark CO_2 fixation and ectoenzyme activity confirmed the necessity of working to improve our understanding of the pressure effects on deep-sea Bacteria and Archaea and their role in marine biogeochemistry. Microbial rates measured under *in situ* conditions (e.g., high pressure, low temperature, ambient food availability) do realistic calculations of the flow of matter and energy as mediated by microbes become possible for the deep sea. By combining such rate measurements with recent developments on single-cell approaches and new insights highlighting possible chemoheterotrophy, we can expect to better understand elemental cycles in the mesopelagic and bathypelagic zones.

Acknowledgements

We thank the captains and crew of R/V *Urania* and R/V *Universitatis* for their help and their welcoming attitude. We also thank Violetta La Cono for help in collecting samples, Chiara Santinelli for her help in providing DOC data and comments, France Van Wambeke for her critical comments and Michael Paul for improving the English of the manuscript. Also sincere thanks to Laura Giuliano on behalf of the CIESM for the organization of these two cruises (www.ciesm.org/marine/campaigns/index.htm). This work was funded by the ANR-POTES (www.com.univ-mrs.fr/LMGEM/potes) program (ANR-05-BLAN-0161-01 awarded to CT) supported by the Agence Nationale de la Recherche (ANR, France).

References

Amann, R., Ludwig, W., Schleifer, K., 1995. Phylogenetic identification and in situ detection of individual microbial cells without cultivation. Microbiological Reviews 59 (1), 143–169.

Amann, R.I., Binder, B.J., Olson, R.J., Chisholm, S.W., Devereux, R., Stahl, D.A., 1990. Combination of 16S rRNA-targeted oligonucleotide probes with flow cytometry for analyzing mixed microbial populations. Applied and Environmental Microbiology 56 (6), 1919–1925.

Astraldi, M., Gasparini, G.P., 1994. The seasonal characteristics of the circulation in the Tyrrhenian Sea. In: La Violette, P.E. (Ed.), The Seasonal and Interannual Variability of the Western Mediterranean Sea, Coastal and Estuarine Studies. AGU, WA, pp. 115–134.

Astraldi, M., Balopoulos, S., Candela, J., Font, J., Gacic, M., Gasparini, G.P., Manca, M., Theocharis, A., Tintore, J., 1999. The role of straits and channels in understanding the characteristics of Mediterranean circulation. Progress in Oceanography 44, 65–108.

Bartlett, D.H., Wright, M., Yayanos, A.A., Silverman, M., 1989. Isolation of a gene regulated by hydrostatic pressure in a deep-sea bacterium. Nature 342 (6249), 572–574.

Bianchi, A., Garcin, J., 1993. In stratified waters the metabolic rate of deep-sea bacteria decreases with decompression. Deep-Sea Research I 40 (8), 1703–1710.

Bianchi, A., Garcin, J., Tholosan, O., 1999. A high-pressure serial sampler to measure microbial activity in the deep sea. Deep-Sea Research I 46 (12), 2129–2142.

Bouvier, T., del Giorgio, P.A., 2003. Factors influencing the detection of bacterial cells using in situ hybridization (FISH): a quantitative review of published reports. FEMS Microbiology Ecology 1485, 1–13.

Church, M.J., Delong, E.F., Ducklow, H.W., Karner, M.B., Preston, C.M., Karl, D.M., 2003. Abundance and distribution of planktonic *Archaea* and *Bacteria* in the waters west of the Antarctic Peninsula. Limnology and Oceanography 48 (5), 1893–1902.

Daims, H., Brühl, A., Amann, R., Schleifer, K.-H., Wagner, M., 1999. The domain-specific probe EUB338 is insufficient for the detection of all Bacteria: development and evaluation of a more comprehensive probe set. Systematic and Applied Microbiology 22, 434–444.

del Giorgio, P.A., Cole, J.J., Cimbleris, A., 1997. Respiration rates in bacteria exceed phytoplankton production in unproductive aquatic systems. Nature 385, 148–151.

DeLong, E.F., Preston, C.M., Mincer, T., Rich, V., Hallam, S.J., Frigaard, N.-U., Martinez, A., Sullivan, M.B., Edwards, R., Brito, B.R., Chisholm, S.W., Karl, D.M., 2006. Community genomics among stratified microbial assemblages in the Ocean's interior. Science 311 (5760), 496–503.

Deming, J.W., Tabor, P.S., Colwell, R.R., 1980. Deep ocean microbiology. In: Diemer, F., Vernberg, J., Mirkes, D. (Eds.), Advanced Concepts in Ocean Measurements for Marine Biology. University of South Carolina Press, Columbia State, pp. 285–305.

Francis, C.A., Roberts, K.J., Beman, J.M., Santoro, A.E., Oakley, B.B., 2005. Ubiquity and diversity of ammonia-oxidizing archaea in water columns and sediments of the ocean. Proceedings of the National Academy of Sciences 102 (41), 14683–14688.

Hedges, J.I., Eglinton, G., Hatcher, P.G., Kirchman, D.L., Arnosti, C., Derenne, S., Evershed, R.P., Kögel-Knabner, I., de Leeuw, J.W., Littke, R., Michaelis, W., Rullkötter, J., 2000. The molecularly-uncharacterized component of nonliving organic matter in natural environments. Organic Geochemistry 31 (10), 945–958.

Herndl, G.J., Reinthaler, T., Teira, E., van Aken, H., Veth, C., Pernthaler, A., Pernthaler, J., 2005. Contribution of Archaea to total prokaryotic production in the deep Atlantic Ocean. Applied and Environmental Microbiology 71 (5), 2303–2309.

Hoppe, H.-G., 1993. Use of fluorogenic model substrates for extracellular enzyme activity measurement of bacteria. In: Kemp, P.F., Sherr, B.F., Sherr, E.B., Cole, J.J. (Eds.), Handbooks of Methods in Aquatic Microbial Ecology. Lewis Publishers, Boca Raton, FL, pp. 423–431.

Hoppe, H.-G., Ullrich, S., 1999. Profiles of ectoenzymes in the Indian Ocean: phenomena of phosphatase activity in the mesopelagic zone. Aquatic Microbial Ecology 19 (2), 139–148.

Ihaka, R., Gentleman, R., 1996. R: a language for data analysis and graphics. Journal of Computational and Graphical Statistics 5, 299–314.

Ingalls, A.E., Shah, S.R., Hansman, R.L., Aluwihare, L.I., Santos, G.M., Druffel, E.R., Pearson, A., 2006. Quantifying archaeal community autotrophy in the mesopelagic ocean using natural radiocarbon. Proceedings of the National Academy of Sciences 103 (17), 6442–6447.

Jannasch, H.W., Wirsen, C.O., 1982. Microbial activities in undecompressed microbial populations from the deep seawater samples. Applied and Environmental Microbiology 43, 1116–1124.

Karner, M., Fuhrman, J., 1997. Determination of active marine bacterioplankton: a comparison of universal 16S rRNA probes, autoradiography, and nucleoid staining. Applied and Environmental Microbiology 63 (4), 1208–1213.

Karner, M.B., DeLong, E.F., Karl, D.M., 2001. Archaeal dominance in the mesopelagic zone of the Pacific Ocean. Nature 409 (6819), 507–510.

Kato, C., Suzuki, S., Hata, S., Ito, T., Horikoshi, K., 1995. The properties of a protease activated by high pressure from *Sporosarcina* sp. strainDSK25 isolated from deep-sea sediment. Jamstecr 32, 7–13.

Kirchman, D.L., 1993. Leucine incorporation as a measure of biomass production by heterotrophic bacteria. In: Kemp, P.F., Sherr, B.F., Sherr, E.B., Cole, J.J. (Eds.), Handbooks of Methods in Aquatic Microbial Ecology. Lewis Publishers, Boca Raton, Ann Arbor, London, Tokyo, pp. 509–512.

Kirchman, D.L., Elifantz, H., Dittel, A.I., Malmstrom, R.R., Cottrell, M.T., 2007. Standing stocks and activity of Archaea and Bacteria in the western Arctic Ocean. Limnology and Oceanography 52 (2), 495–507.

Konneke, M., Bernhard, A.E., de la Torre, J.R., Walker, C.B., Waterbury, J.B., Stahl, D.A., 2005. Isolation of an autotrophic ammonia-oxidizing marine archaeon. Nature 437 (7058), 543–546.

La Cono, V., Tamburini, C., Genovese, L., La Spada, G., Denaro, R., Yakimov, M.M., 2008. Cultivation-independent assessment of the bathypelagic archaeal diversity of Tyrrhenian Sea: comparative study of rDNA and rRNA-derived libraries and influence of sample decompression. Deep-Sea Research II, this issue [doi:10.1016/j.dsr2.2008.07.025].

Lauro, F., Bartlett, D., 2007. Prokaryotic lifestyles in deep sea habitats. Extremophiles 12 (1), 15–25.

Lefèvre, D., Denis, M., Lambert, C.E., Miquel, J.-C., 1996. Is DOC the main source of organic matter remineralization in the ocean water column? Journal of Marine Systems 201, 281–291.

Martin-Cuadrado, A.B., Lopez-Garcia, P., Alba, J.C., Moreira, D., Monticelli, L., Strittmatter, A., Gottschalk, G., Rodriguez-Valera, F., 2007. Metagenomics of the deep Mediterranean, a warm bathypelagic habitat. PLoS ONE 2 (9), e914.

Millot, C., Taupier-Lepage, I., 2005. Circulation in the Mediterranean Sea. In: Saliot, A. (Ed.), The Handbook of Environmental Chemistry. Springer, Heidelberg, pp. 29–66.

Ouverney, C.C., Fuhrman, J.A., 2000. Marine planktonic archaea take up amino acids. Applied and Environmental Microbiology 66 (11), 4829–4833.

Pierini, S., Simioli, A., 1998. A wind-driven circulation model of the Tyrrhenian Sea. Journal of Marine Systems 18, 161–178.

Qureshi, M.H., Kato, C., Horikoshi, K., 1998. Purification of two pressure-regulated c-type cytochromes from a deep-sea barophilic bacterium, *Shewanella* sp. strain DB-172F. FEMS Microbiology Letters 161, 93–99.

Robinson, A.R., Leslie, W.G., Theocharis, A., Lascaratos, A., 2001. Mediterranean Sea Circulation. OCEAN CURRENTS/Mediterranean Sea Circulation. Academic Press, New York, pp. 1–19.

Sekar, R., Pernthaler, A., Pernthaler, J., Warnecke, F., Posch, T., Amann, R., 2003. An improved protocol for quantification of freshwater Actinobacteria by fluorescence *in situ* hybridization. Applied and Environmental Microbiology 69 (5), 2928–2935.

Simon, M., Azam, F., 1989. Protein content and protein synthesis rates of planktonic marine bacteria. Marine Ecology—Progress Series 51, 201–213.

Sparnocchia, S., Gasparini, G.P., Astrali, M., Borghini, M., Pistek, P., 1999. Dynamics and mixing of the Eastern Mediterranean outflow in the Tyrrhenian Basin. Journal of Marine Systems 20, 301–317.

Tabor, P., Colwell, R.R., 1976. Initial investigation with a deep ocean in situ sampler. In: W.D. (Ed.), Proceedings of the MTS/IEEE OCEANS'76, pp. 13D-11–13D-14.

Tabor, P.S., Deming, J.W., Ohwada, K., Davis, H., Waxman, M., Colwell, R.R., 1981. A pressure-retaining deep ocean sampler and transfer system for measurement of microbial activity in the deep sea. Microbial Ecology 7, 51–65.

Tamburini, C., 2002. La dégradation du matériel organique profond par les microflores profondes: de la mesure des vitesses potentielles au flux de CO_2 généré *in situ*. Université de la Méditerranée, Marseille.

Tamburini, C., 2006. Life under Pressure. Deep-Sea Microbial Ecology. Life as We Know It. Series: Cellular Origin and Life in Extreme Habitats and Astrobiology. Springer, Dordrecht, The Netherlands, pp. 125–143.

Tamburini, C., Garcin, J., Ragot, M., Bianchi, A., 2002. Biopolymer hydrolysis and bacterial production under ambient hydrostatic pressure through a 2000 m water column in the NW Mediterranean. Deep-Sea Research II 49 (11), 2109–2123.

Tamburini, C., Garcin, J., Bianchi, A., 2003. Role of deep-sea bacteria in organic matter mineralization and adaptation to hydrostatic pressure conditions in the NW Mediterranean Sea. Aquatic Microbial Ecology 32 (3), 209–218.

Tamburini, C., Garcin, J., Grégori, G., Leblanc, K., Rimmelin, P., Kirchman, D.L., 2006. Pressure effects on surface Mediterranean prokaryotes and biogenic silica dissolution during a diatom sinking experiment. Aquatic Microbial Ecology 43 (3), 267–276.

Teira, E., Reinthaler, T., Pernthaler, A., Pernthaler, J., Herndl, G.J., 2004. Combining catalyzed reporter deposition-fluorescence in situ hybridization and micro-autoradiography to detect substrate utilization by bacteria and Archaea in the deep ocean. Applied and Environmental Microbiology 70 (7), 4411–4414.

Teira, E., Lebaron, P., vanAken, H., Herndl, G.J., 2006. Distribution and activity of Bacteria and Archaea in the deep water masses of the North Atlantic. Limonology and Oceanography 51 (5), 2131–2144.

Tholosan, O., Garcin, J., Bianchi, A., 1999. Effects of hydrostatic pressure on microbial activity through a 2000 m deep water column in the NW Mediterranean Sea. Marine Ecology—Progress Series 183, 49–57.

Varela, M.M., van Aken, H.M., Sintes, E., Herndl, G.J., 2007. Latitudinal trends of Crenarchaeota and Bacteria in the meso- and bathypelagic water masses of the Eastern North Atlantic. Environmental Microbiology, 1–15.

Vezzi, A., Campanaro, S., D'Angelo, M., Simonato, F., Vitulo, N., Lauro, F.M., Cestaro, A., Malacrida, G., Simionati, B., Cannata, N., Romualdi, C., Bartlett, D.H., Valle, G., 2005. Life at depth: *Photobacterium profundum* genome sequence and expression analysis. Science 307 (5714), 1459–1461.

Wakeham, S.G., Lee, C., Hedges, J.I., Hernes, P.J., Peterson, M.L., 1997. Molecular indicators of diagenetic status in marine organic matter. Geochimica et Cosmochimica Acta 61 (24), 5363–5369.

Wright, R.T., Hobbie, J.E., 1966. Use of glucose and acetate by bacteria and algae in aquatic ecosystems. Ecology 47, 447–464.

Wuchter, C., Schouten, S., Boschker, H.T.S., Sinninghe Damste, J.S., 2003. Bicarbonate uptake by marine Crenarchaeota. FEMS Microbiology Letters 219 (2), 203–207.

Yamada, M., Nakasone, K., Tamegai, H., Kato, C., Usami, R., Horikoshi, K., 2000. Pressure regulation of soluble cytochromes c in a deep-sea piezophilic bacterium, *Shewanella violacea*. Journal of Bacteriology 182 (10), 2945–2952.

ZoBell, C.E., 1970. Pressure effects on morphology and life processes of bacteria. In: Zimmerman, H.M. (Ed.), High Pressure Effects on Cellular Processes. Academic Press, New York, pp. 85–130.

Deep-Sea Research II 56 (2009) 713–724

Contents lists available at ScienceDirect

Deep-Sea Research II

journal homepage: www.elsevier.com/locate/dsr2

Persistence of an eddy signature in the central Tyrrhenian basin

G. Budillon [a,*], G.P. Gasparini [b], K. Schroeder [b]

[a] Università degli Studi di Napoli "Parthenope", Dipartimento di Scienze per l'Ambiente, Napoli, Italy
[b] Consiglio Nazionale delle Ricerche—Istituto di Scienze Marine, 19032 Pozzuolo di Lerici, Italy

ARTICLE INFO

Article history:
Accepted 8 July 2008
Available online 17 November 2008

Keywords:
Gyres
Hydrology
Mesoscale features
Seamounts
Bottom topography effects
Intermediate water masses

ABSTRACT

During July and December 2005 two basin-scale hydrographic cruises were performed in the Tyrrhenian basin to monitor hydrographic conditions after the significant changes observed during previous decades. A detailed investigation of the surface layer suggested the presence of a mesoscale structure in the central basin, off Naples. Its principal feature is a subsurface cold lens of Western Intermediate Water, a water mass produced in the Northwestern Mediterranean during the winter season. The lens, which appears as an anticyclonic eddy, was detected for the first time in July. Five months later an eddy signature was detected in the same position with the same hydrographic characteristics. The positive altimetric anomaly in correspondence with the observed structure suggests that the anticyclonic circulation lasted for a long period and its persistence was related to the presence of a seamount in the region. For the first time the importance of isolated topography in influencing the interior Tyrrhenian circulation is highlighted: the Vavilov Seamount, jointly with the weak mean current, seems to be responsible for the persistence of eddy structures in the region. The topographic effect is discussed on the basis of the eddy properties and theoretical findings.

1. Introduction

The Tyrrhenian Sea is the deepest and the most isolated basin of the Western Mediterranean (Fig. 1). It communicates with other sub-basins through the Corsica channel in the north and through the Sardinia–Sicily opening in the south. In spite of its marginal position, it plays an important role in the Mediterranean circulation because of several water masses crossing this basin. An important branch of Atlantic Water (AW) enters the basin mainly along the southern boundary: it is identified by a subsurface salinity minimum and typically occupies the upper 100–200 m of the water column. Leaving the Algerian basin, the AW branch splits into two; while the majority of the flow enters the Sicily Channel towards the Eastern Mediterranean, part of it moves along the northern coast of Sicily (Astraldi et al., 2002).

Below the AW layer a relative minimum of temperature is often detected. It has been frequently associated with the residual signature of the winter cooling (Hopkins, 1988), even if it can be also due to the presence of Western Intermediate Water (WIW). This water mass originates in the Northwestern Mediterranean (Salat and Font, 1987) during winter convection processes and successively flows towards the southern part of the Western Mediterranean. Typically the WIW does not have a continuous presence, but is generally organized in subsurface isolated vortex (Gasparini et al., 1999), advected along the basin by the large-scale current. For its characteristics that resemble the Mediterranean lenses observed in the Atlantic ocean (Meddies), they are called "Weddies" (Millot, 1999). Weddies are frequently found in the Algero–Provençal basin at a nominal depth of 150–200 m. Lenses of WIW were also observed in the Sardinia channel (Bouzinac et al., 1999) and at the entrance of the Sicily Channel. Its detection in the Sardinia channel suggests that the WIW is able to travel thousands of kilometers and to survive for a long time, preserving the identity of the source water.

At subsurface levels the Tyrrhenian basin is the first western basin reached by the Levantine Intermediate Water (LIW). Coming from the Eastern Mediterranean through the Sicily Channel, the LIW enters the Tyrrhenian Sea along the Sicily slope and leaves it mainly along the Sardinia side of the Sardinia–Sicily section. The Western Mediterranean Deep Water (WMDW) enters the basin throughout the deep part of the same section, filling the Tyrrhenian abyssal layer.

The relatively low dynamics inside the basin and the presence of gyre structures are favourable conditions for vertical exchanges (Astraldi and Gasparini, 1994), resulting in the creation of a peculiar water type, the Tyrrhenian Deep Water (TDW), a product of the mixing between LIW and WMDW. It is positioned below 1000 m depth and leaves the basin through the southern opening.

The overall circulation in the Tyrrhenian is cyclonic along the boundaries, according to the general Mediterranean circulation,

* Corresponding author.
E-mail address: giorgio.budillon@uniparthenope.it (G. Budillon).

0967-0645/$ - see front matter © 2008 Elsevier Ltd. All rights reserved.
doi:10.1016/j.dsr2.2008.07.027

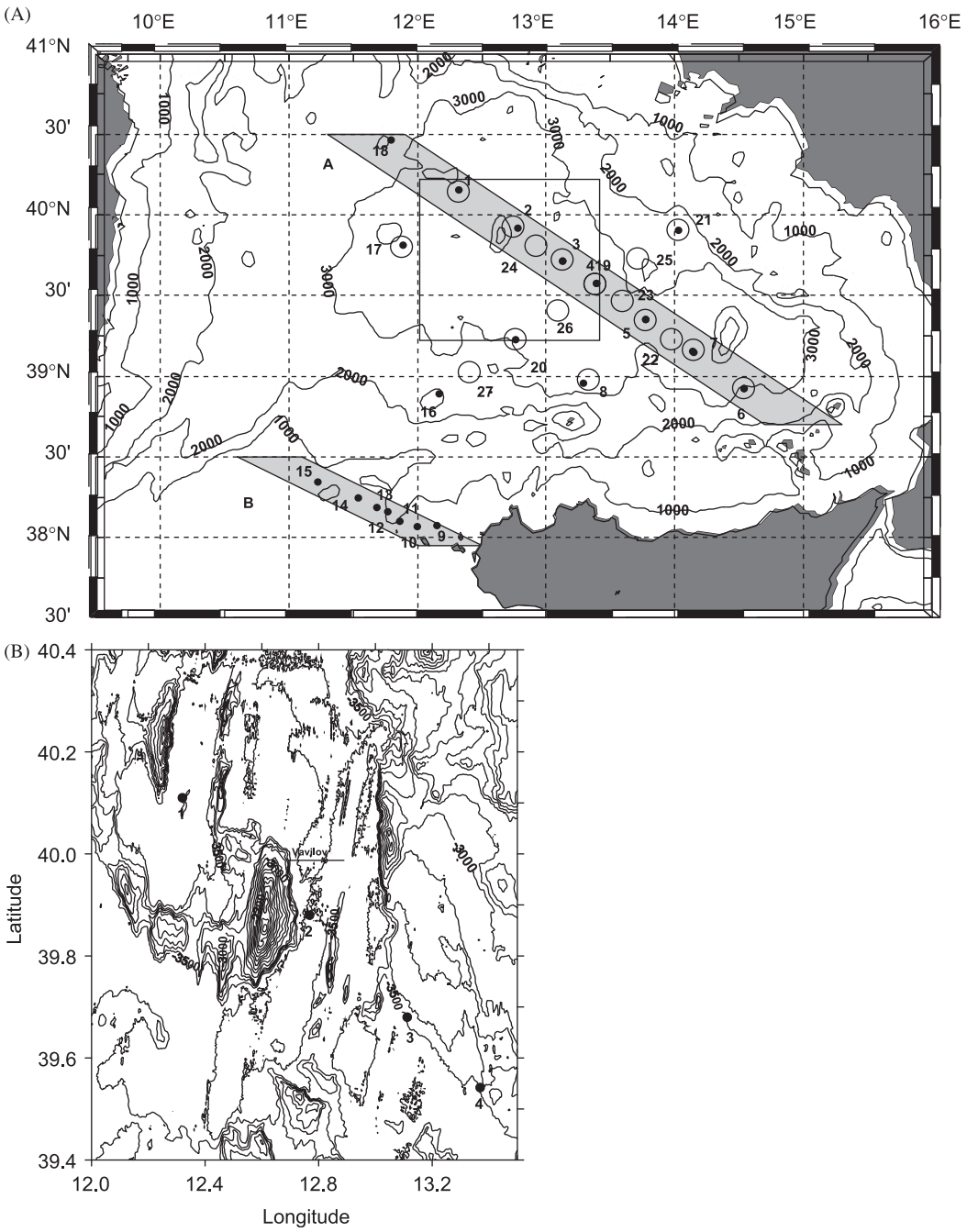

Fig. 1. The Tyrrhenian basin. (a) Hydrographic stations performed during July 2005 (dots), and during December 2005 (open circles); the inner box indicates the area shown in panel b; and (b) detailed topography around the Vavilov Seamount (Marani et al., 2004). Depths are in meters.

but several closed structures can be detected both in the northern and southern regions. Especially in the surface layer, these structures are generally wind driven and are related to its variability in space. The most known structure is the quasi-permanent cyclonic–anticyclonic system in front of the Bonifacio Strait, originated by the wind jet blowing through the Strait (Artale et al., 1994). A similar wind effect is probably responsible for a cyclonic gyre frequently observed at the southern edge of Sardinia. The first indications of gyre structures were provided by Krivosheya and Ovchinnikov (1973). SST satellite images also evidence the presence of cold and warm structures, some quasi-permanent, other intermittent (Marullo et al., 1994). Nevertheless, there are only few detailed studies on their formation and evolution (Artale et al., 1994; Pierini and Simioli, 1998).

The dynamics of the basin can account for some energy along the coastal boundaries, but is generally weak in the interior region, as confirmed by the relative importance of small-scale diffusive processes (Zodiatis and Gasparini, 1996). The weak dynamics induces long residence times, enough to permit the prevalence of small-scale mixing processes; the TDW is a result of these processes. Largely unknown is also the role played by the mean flow and the topographic effect, considering the high variability of the Tyrrhenian topography, with the presence of several seamounts. In the following we will examine hydrography and currents in the central region of the basin, addressing the attention on a persistent eddy structure, particularly evident during the investigation periods.

2. Observations

Two multidisciplinary surveys were conducted in July (21–31) and December (13–22) 2005 to investigate the central and southern Tyrrhenian Sea, on board, the R/V Universitatis (owned by the Italian Consortium of University for the Marine Sciences—CoNISMa) and the R/V Urania (owned by the Italian National Council for the Research—CNR), respectively. The study, supported by the Commission Internationale pour l'Exploration Scientifique de la Mer Mediterranée (CIESM), was intended to update the knowledge of the basin, whose hydrographic structure has been subject to important changes over the last 20 years (MEDAR Group, 2002; Gasparini et al., 2005; Schroeder et al., 2006, 2008).

The on-field data included traditional CTD measurements (temperature, conductivity, pressure, dissolved oxygen (DO), and fluorescence) using a SBE 9/11+ CTD probe together with water samples for the detection of chemical and biological parameters. In the following, attention will be devoted to the physical aspects of the water column, while other investigations concerning chemical and biological characteristics are described in companion papers (e.g., Decembrini et al., 2008; Ribera et al., 2008; Tamburini et al., 2008). In both cruises the sampling strategy was similar; casts were organized along two main sections (Fig. 1a), intersecting each other in the deeper part of the Tyrrhenian basin; during the first cruise an additional section was visited along the southern part of the Sicily–Sardinia passage in order to monitor the characteristics of the inflowing waters. It is worth mentioning that the whole region is characterized by a complex bottom topography, which plays an important role in forcing the internal dynamics. Some of the central stations are very close to the Vavilov Seamount, which rises from 3300–3500 m to 750 m depth, and its contour resembles an elliptic shape with the major and the minor axis of about 45 and 15 km, respectively (Fig. 1b).

In situ hydrological measurements were integrated by satellite altimeter data, to delineate surface and subsurface eddy activity (Stammer et al., 1991; Le Traon and Dibarboure, 1999). The Mean Surface Level Anomaly (MSLA) maps of the Tyrrhenian Sea used for this study were produced by the AVISO Group (Archiving Validation and Interpretation of Satellite Oceanographic data; www.aviso.oceanobs.com). In particular we analyzed the updated version (July 2007) of Data Unification and Altimeter Combination System (DUACS) data set obtained by processing data from all altimeter missions: Jason-1, T/P, ENVISAT, GFO, ERS1/2, and even GEOSAT.

Finally a satellite-tracked drifter was used, which is classified as ENEA Drifter b0006 in the Mediterranean drifter database (http://doga.ogs.trieste.it/drifter/database_med/html/). It is a TRISTAR drifter, with a shallow drogue (10 m) in the form of a corner-radar reflector, deployed near the Vavilov Seamount (39°49.2′N, 12°42.5′E) in autumn 1991. The typical position accuracy was 300 m, with a position fix approximately every 3–4 h.

3. Hydrographic characteristics

3.1. θ/S diagrams

The cumulative potential temperature (θ) versus salinity (S) diagrams in Fig. 2 summarize the hydrographic characteristics of the water column in the Tyrrhenian Sea observed in July (Fig. 2a) and December (Fig. 2b) 2005. During the summer cruise, the surface layer was characterized by θ greater than 14 °C (with a maximum of 28 °C) and S spanning between 37.3 and 38.4. Below this warm and relatively salty upper layer, the AW extended its influence in the first 100–150 m of the water column (Fig. 2a). During the second cruise (Fig. 2b), the surface temperature did not exceed 16 °C and all stations where characterized by a surface layer of about 50 m, with smaller ranges in temperature ($\theta \approx 14.0$–15.5 °C) and salinity ($S \approx 37.85$–38.2). This layer was slightly saltier and warmer than the AW core, which was detected at about 80 m depth ($\theta \approx 13.6$ °C, $S \approx 38.05$).

The lowest salinity ($S = 37.33$) was found in the Tyrrhenian entrance (stations 10 and 11). In the basin interior, during both cruises at stations 8 and 6, salinities lower than 37.5 were found. This confirms the direct influence of the AW in the southern sector of the Tyrrhenian Sea: after entering through the Sardinia channel, it moves close to the Sicilian coasts, consistent with the classical picture of a basin-scale cyclonic surface circulation.

A second significant signature is a relative minimum of θ ($T_{\min}$) in correspondence with the bottom of the surface layer (Fig. 2c). It is positioned between 120 and 160 m, but it also can be deeper. Its signature changes significantly in space, being well developed and colder at the Tyrrhenian entrance and in some northern stations, but less present and warmer in the central and southern stations. The presence of $T_{\min}$ is usually related to the winter cooling of the previous year (Hopkins, 1988), but locally we also observe the WIW signature. While in correspondence with the isopycnal 28.7, there is a common $T_{\min}$ for almost all stations, the $T_{\min}$ corresponding to approximately $\sigma_\theta = 28.5$ indicates the WIW presence. Its characteristics are very similar to the water observed by Bouzinac et al. (1999) along the western side of the Sardinia channel.

Moving deeper we identify an intermediate layer (traditionally occupied by the LIW) characterized by a maximum of salinity (Fig. 2c). At station 11, we can distinguish a profile (the rightmost in the diagram) with a significantly higher salt content, which corresponds to the Eastern Mediterranean Outflow entering the Tyrrhenian (Gasparini et al., 2005).

Going deeper, the basin interior is filled by TDW. This water mass exhibits a nearly isopycnal behavior, decreasing at the same time its temperature and salinity towards the WMDW characteristics and reaching the lowest values close to the bottom ($S < 38.5$ and $\theta < 13.0$ °C for depths greater than 3000–3500 m).

3.2. Vertical sections

The vertical distribution of the thermohaline parameters along the southern side of the Sardinia–Sicily passage (section B of Fig. 1a) is shown in Fig. 3. This section extends from Sicily (on the right side of the section) for 90 km, and indicates the entrance of the AW and the LIW in the Tyrrhenian basin. Below the thermocline, two cores of relatively fresh water (AW) are identified at 25 m depth (Fig. 3b). The core closer to the Sicily coast shows a salinity lower than 37.4. The LIW core ($S_{\max} > 38.70$) is found close to the Sicilian slope, between 250 and 800 m depth.

Between the AW and LIW, at a depth of 100–150 m, a significant portion of the section shows the presence of a cold structure ($\theta < 13.5$ °C), to which corresponds a salinity of 38.25–38.35, a density of 28.85, and oxygen concentrations of about 5.0 ml/l, which can be identified as WIW (Fig. 2c). This signature occupies a wide portion of the section, suggesting a noteworthy presence of this water mass in correspondence of the Tyrrhenian entrance. The winter conditions in 2005 were very severe and led to a large WMDW production (Lopez-Jurado et al., 2005; Schroeder et al., 2006, 2008) and the relevant presence of WIW appears in agreement with conditions observed in the Algero–Provencal basin during the first half of 2005.

Moving towards the basin interior (section A in Fig. 1a) the stratified conditions in the upper layer are well evident in the

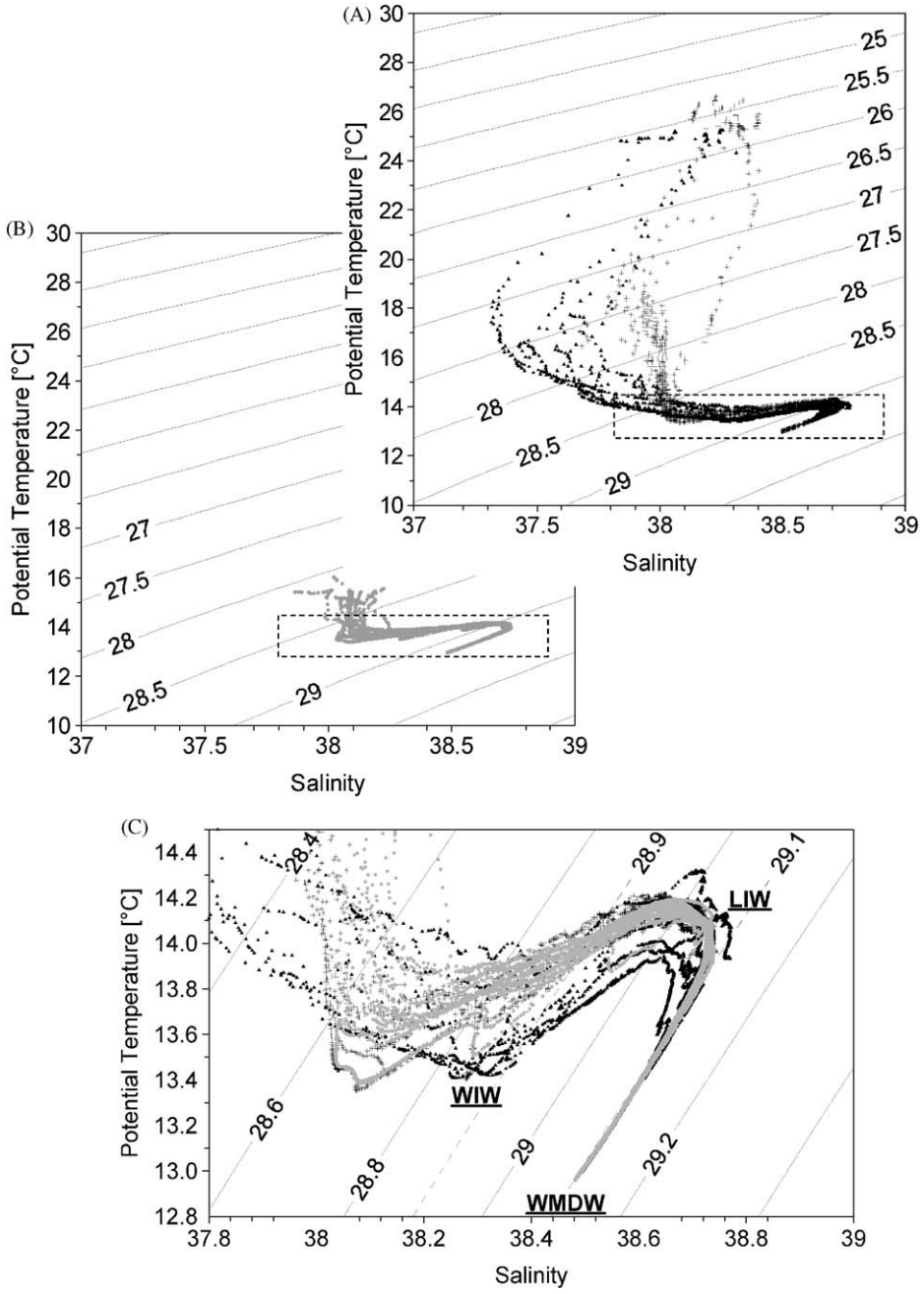

Fig. 2. Cumulative θ/S diagrams of the data collected (a) in July 2005 along transect A (black triangles) and B (black crosses), (b) in December 2005 (gray dots), and (c) with a higher detail in both periods.

temperature field (Fig. 4a) during the first survey (July 2005). Warm surface water (25–26 °C) is confined to the surface mixed layer, with the thermocline at about 30–40 m depth. The vertical section of salinity (Fig. 4b) indicates the salinity minimum (S_{min}) at about 50 m and the thickness of the AW water core can be estimated as about 50 m. Going deeper, both temperature and salinity indicate an isolated structure, characterized by lower values of temperature and salinity. Particularly evident in the first 400 m of depth, its signature can be observed down to 1000 m depth.

The vertical section of potential density (Fig. 4c) reproduces almost the same feature: isopycnals are almost horizontal in the southern region, but become steep at station 2, characterized by lower density. A similar signature is observed in the DO distribution (Fig. 4d); the sinking pattern is well evident in correspondence with station 2, where concentrations typical at 100 m are found 100–150 m deeper. The structure can be delimited by the 13.5 and 14.0 °C isotherms, corresponding to the 38.0 and 38.4 isohalines and the 5.4 and 4.8 ml/l isolines of DO. Examining the density, the same structure is seen between the 28.7 and 28.9 isopycnals. The displacement of these colder, fresher, and lighter characteristics suggests the presence of an anticyclonic eddy. Concerning the water masses involved, we can clearly distinguish the AW and the LIW on the border, while the cold signature has very similar characteristics to the WIW, previously seen at the Tyrrhenian entrance (Figs. 2 and 3).

Fig. 5 shows the same section (section A) 5 months later (in December). Rather unexpectedly, the thermohaline field does not exhibit substantial changes along section A. With the

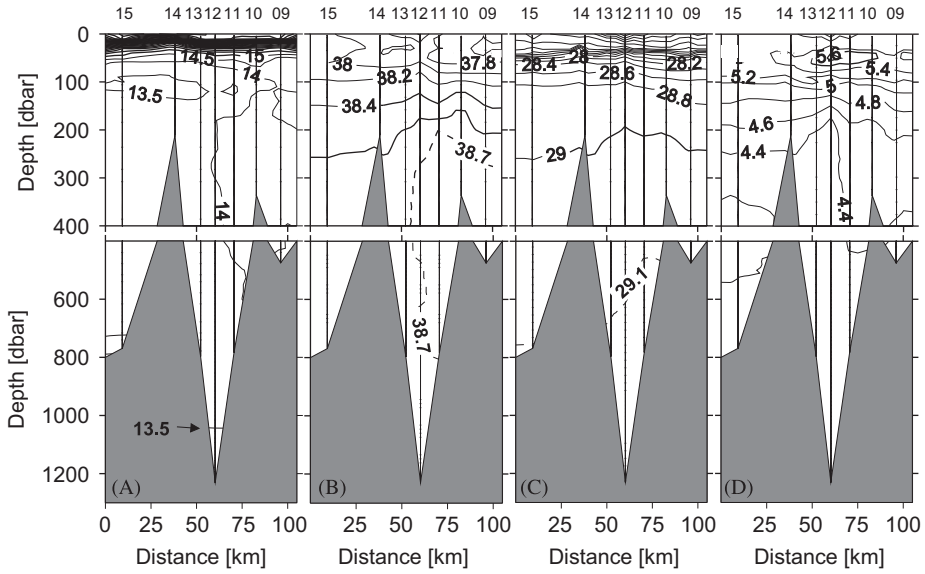

Fig. 3. Vertical hydrographic sections at the Tyrrhenian entrance during July 2005 (transect B in Fig. 1a) of (a) potential temperature (°C), (b) salinity, (c) potential density ($kg\,m^{-3}$), and (d) dissolved oxygen ($ml\,l^{-1}$).

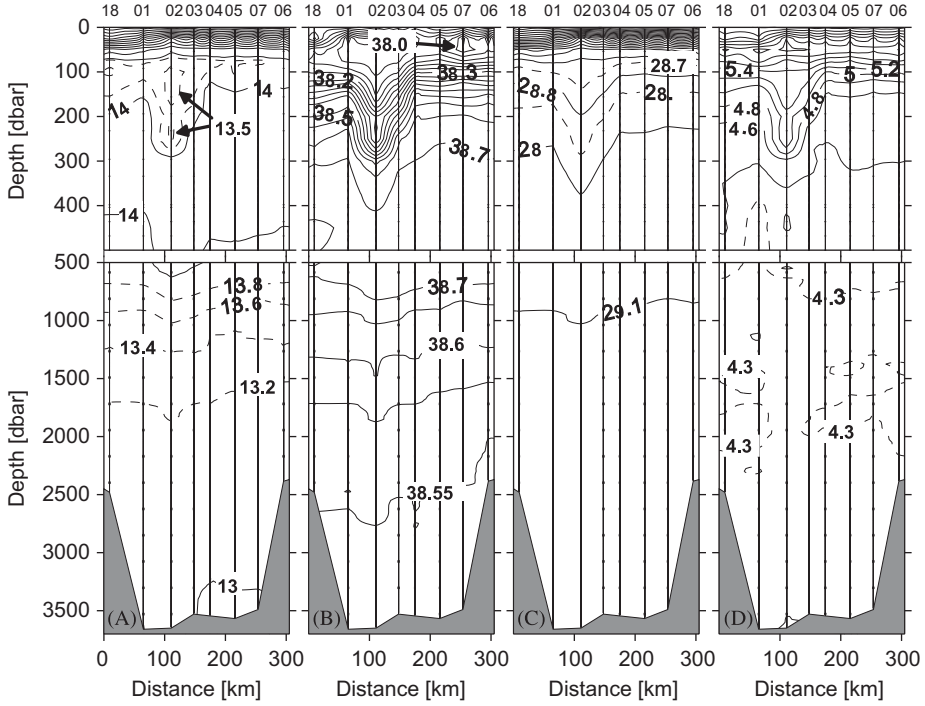

Fig. 4. Vertical hydrographic sections in the central basin during July 2005 (transect A in Fig. 1a) of (a) potential temperature (°C), (b) salinity, (c) potential density ($kg\,m^{-3}$), and (d) dissolved oxygen ($ml\,l^{-1}$).

exception of the surface layer, which shows the deepening of the thermocline, at 70 m depth, the same cold feature observed in July is still present in the same position. The similar deepening of isotherms, isohalines, and isopycnals suggests the existence of the anticyclonic eddy in December as well. The only significant difference is shown in the DO distribution (Fig. 5d), which does not reproduce the same structure, but which could be partially related to the fewer samples available during that period, due to a probe sensor failure. A detailed description of the θ–S characteristics of station 2 shows the same structure in both periods: we can observe the same θ/S shape with only a small change between July and December (Fig. 6). Furthermore the characteristics of station 2 are very similar to the water entering the Tyrrhenian basin near Sicily.

Moving deeper, no significant changes are observed if compared with the hydrographic conditions found during the previous July cruise (Figs. 2 and 4), indicating the negligible seasonal influence in the intermediate and deep layers.

4. Eddy description

In the following the eddy is described with some detail, but we must emphasize that the available data (only one section crosses

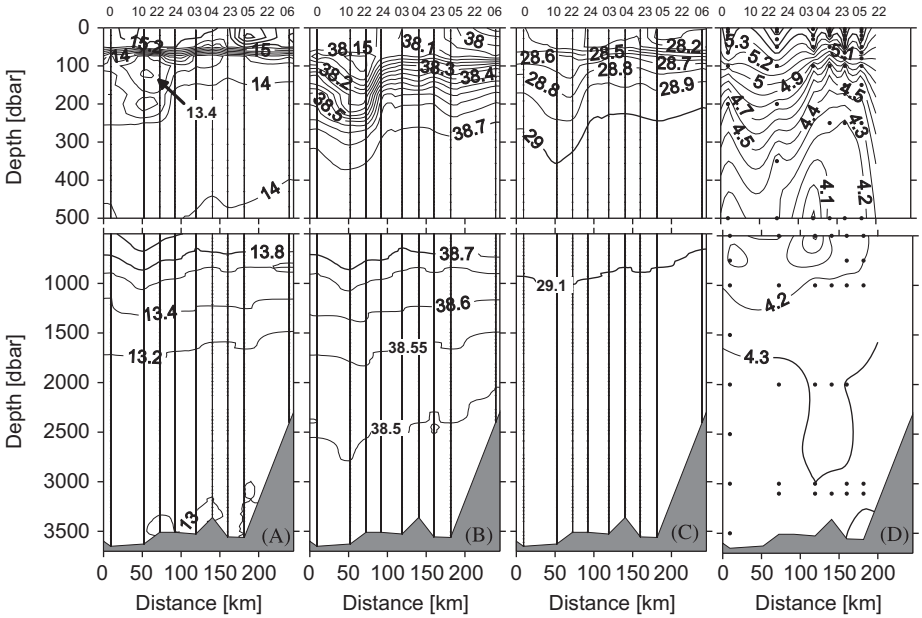

Fig. 5. Vertical hydrographic sections in the central basin during December 2005 (transect A in Fig. 1b) of (a) potential temperature (°C), (b) salinity, (c) potential density (kg m^{-3}), and (d) dissolved oxygen (ml l^{-1}).

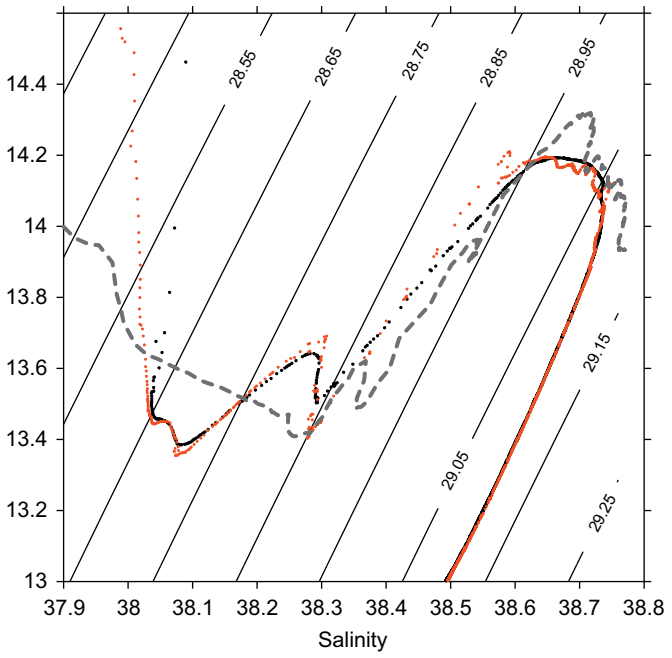

Fig. 6. θ/S diagram of the central station of the eddy (station 2) during July (red) and December (black). The gray line indicates station 11 along section B, at the Tyrrhenian entrance.

the eddy, with a mean distance between CTD stations of about 40–45 km) permit only a partial estimate of the eddy's characteristics.

4.1. Hydrographic structure

Anomaly estimates of heat, salt, and other water properties are useful because their magnitude, relative to the surrounding water, permits better evidence of the eddy's properties and characteristics. The differential temperature anomaly (°C) is defined by

$$T_{anomal} = T - T_{ref} \quad (1)$$

where T is the vertical profile of temperature at an eddy station and T_{ref} the reference vertical profile of temperature constructed as the arithmetic average of the temperature profiles far from the eddy (as far stations, we considered stations 5 and 17 in Fig. 1). The distribution of T_{anomal} (Fig. 7a) indicates that the negative values are concentrated horizontally between stations 1 and 4 and in the depth range 50–300 m. The distributions of salinity and oxygen anomalies (Figs. 7b, d) are quite similar. Conversely, the density anomaly seems to reach greater depths (Fig. 7c), suggesting that the observed structure extends to the intermediate layer as well. The hydrographic differences with the background water at station 2 are −0.5 °C, −0.4, and +0.6 ml/l for temperature, salinity, and DO, respectively. All these features are consistent with the presence of a WIW anticyclonic lens. The vertical scale of the lens (h) is about 200 m, while the horizontal scale ($2L$), which is given by the external lens margins, is estimated to be 75 km.

A dynamic body is considered dynamically stable when $L > R_d$ (Armi and Zenk, 1984), where L is the scale of the lens radius and R_d the internal Rossby radius of deformation. The R_d associated with the lens can be defined as

$$R_d = (g\,\Delta\rho\,h/\rho_0)^{0.5}/f \quad (2)$$

where g is the gravity acceleration, h the vertical scale of the lens, $f = 9.35 \times 10^{-5}$ the Coriolis parameter, $\Delta\rho = \rho_1 - \rho_2$, $\rho_0 = (\rho_1 + \rho_2)/2$ the average density, with $\rho_1 = 1029$ kg m^{-3} and $\rho_2 = 1028.852$ kg m^{-3} being the mean background density and the mean lens density, respectively. Assuming $\Delta\rho = 0.148$ kg/m^3 and $h = 200$ m, R_d is about 6 km, while L is on the order of 35–40 km. Thus, as $L > R_d$, the identified lens structure can be considered as a mesoscale, stable eddy.

5. The velocity field

To estimate the eddy velocity field it is necessary to start with the geostrophic assumption, which in cylindrical coordinates is (Olson, 1980)

$$fV_g = (1/\rho)\,\partial p/\partial r \quad (3)$$

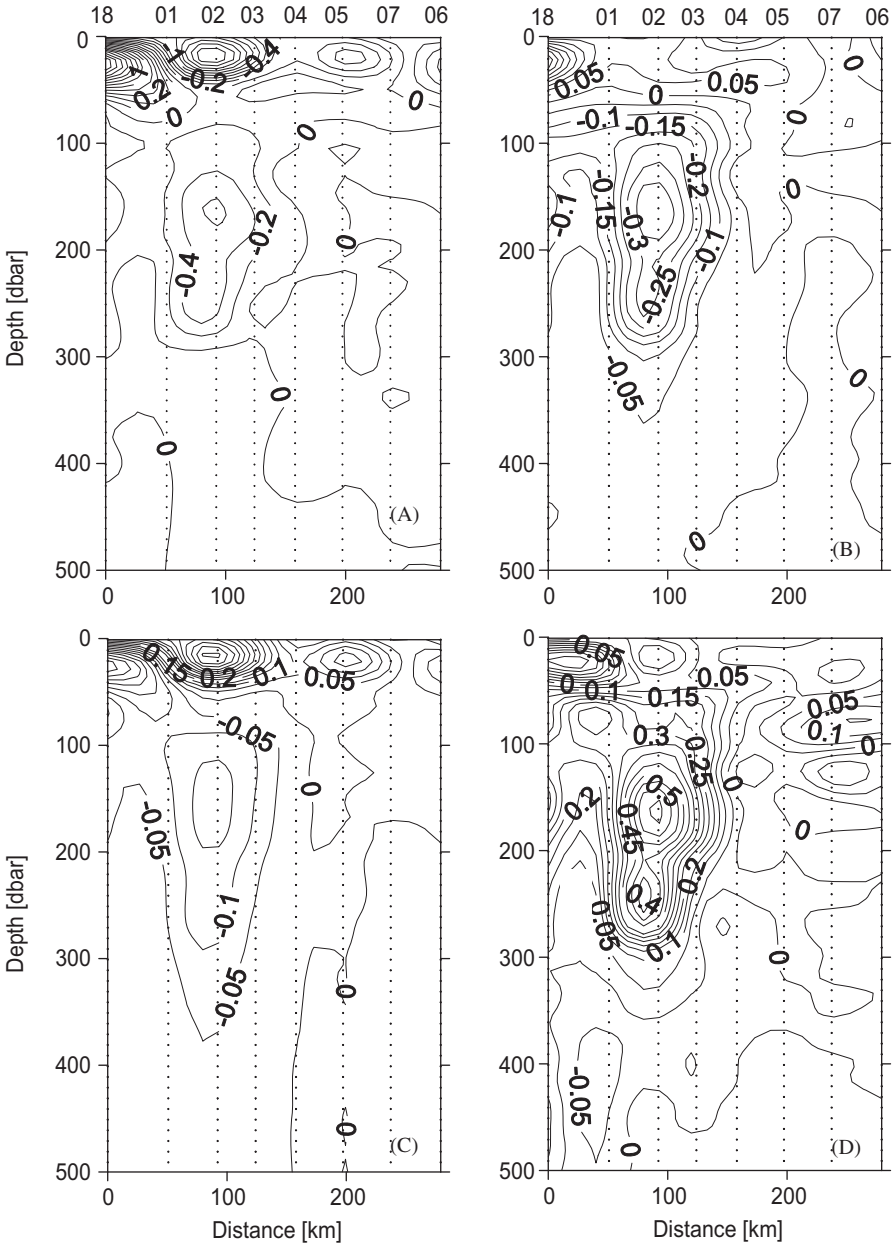

Fig. 7. Anomalies along the central section A, between 0 and 500 m, during July 2005. (a) Potential temperature (°C), (b) salinity, (c) potential density (kg m^{-3}), and (d) dissolved oxygen (ml l^{-1}).

where p is the vertical pressure and r the distance from the center of the eddy. As indicated above, the center of the eddy was assumed to be located at station 2 in Fig. 1a. Furthermore, due to the high curvature of the structure, the centrifugal force may be important. For an inviscid and almost stationary eddy, the gradient velocity V_θ can be computed from the gradient current balance:

$$V_\theta^2/r + V_\theta f = (1/\rho)\,\partial p/\partial r = fV_g \tag{4}$$

The gradient velocity V_θ can thus be obtained by solving the quadratic equation, where r is taken as the mean radius of the station pairs used in the calculation:

$$V_\theta = -fr/2 + (f^2r^2/4 + (r/\rho)\,\partial p/\partial r)^{1/2} \tag{5}$$

The few available profiles describing the eddy (stations 1–3 of section A) gave a too coarse estimate of the derivatives along the radial direction. For this reason, between two existing profiles a further profile corresponding to their mean has been introduced and a reconstructed section A has been considered for all parameters estimated in the following.

The vertical section of the gradient velocity V_θ (Fig. 8) shows a well-developed anticyclonic circulation, which extends from the surface to a depth of at least 500 m. A pronounced velocity jet, with speeds of about 8–9 cm/s, occurs at a depth of 90 m. On average, the gradient velocity is only a few per cent larger than the geostrophic velocity.

6. Vorticity distribution

The potential vorticity in cylindrical coordinates can be approximated by (Olson, 1980)

$$\pi \approx (\partial\rho/\partial z)(v/r + \partial\rho/\partial r + f) \tag{6}$$

where $v/r+\partial v/\partial r$ is the relative vorticity ζ.

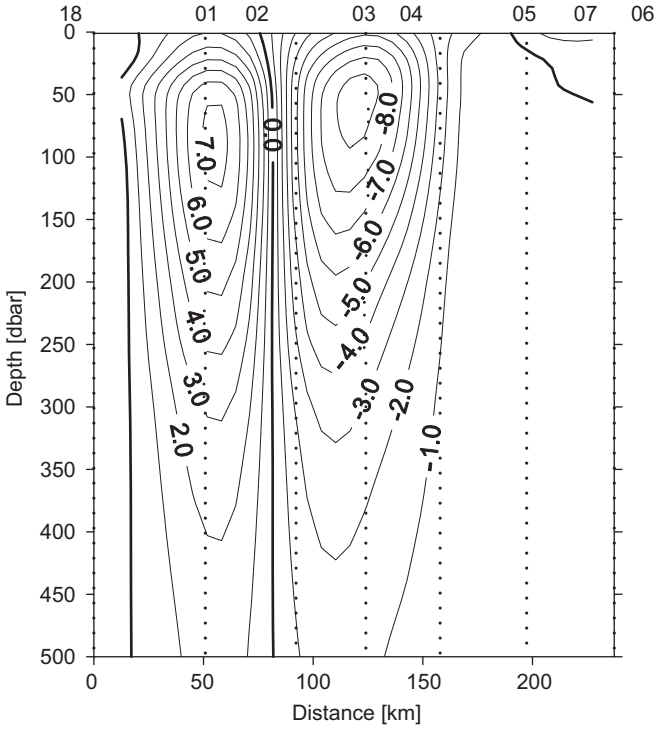

Fig. 8. Gradient velocity along section A in Fig. 1a, between 0 and 500 m depth, during July 2005. Reference level at 2000 db. Units are cm s^{-1}.

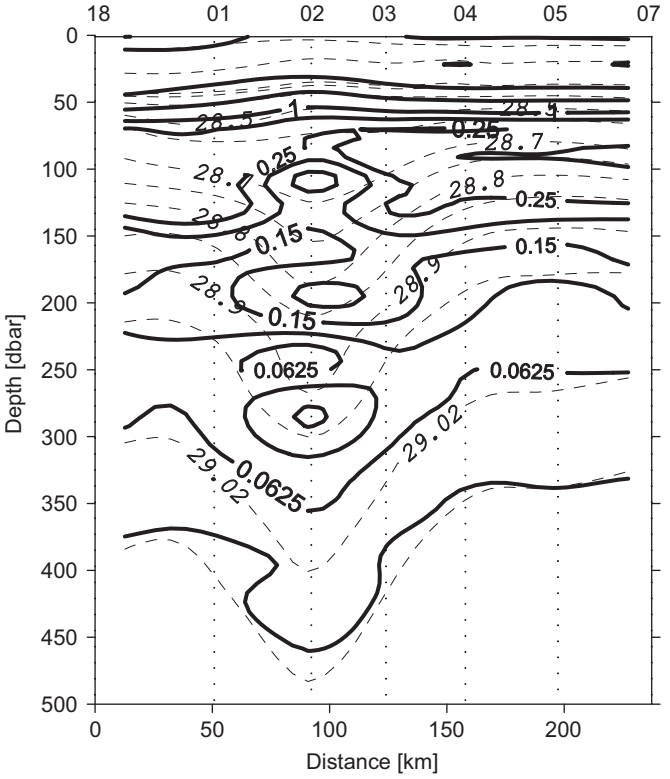

Fig. 9. Potential vorticity distribution $\pi \times 10^{-6}$ (kg m^{-4} s^{-1}; solid lines) superimposed on the potential density field (dashed lines) along section A of Fig. 1 during July 2005.

The relative vorticity field within the eddy consists of a region of negative values, more pronounced in its central part. The distribution tends to be axially symmetric, even if an intensification in the southern side can be observed. However, it is important to note that the values are of the order of 10^{-6} kg m^{-4} s^{-1}, two orders of magnitude lower than the planetary vorticity f. For this reason the driving parameter is the planetary vorticity.

The potential vorticity π should be conserved by a parcel of fluid as it circulates around the eddy. Hence, the orientation of isopleths of potential vorticity relative to isopycnals indicates where mixing between the eddy and the background waters may have occurred. Specifically, radial motion along isopycnal surfaces may have occurred in those regions where the isopleths of π are parallel to the isopycnals. If the isopleths of π intersect the isopycnals obliquely, the exchange is inhibited (Olson, 1980). Vertical distribution of π (solid lines) and of isopycnals (dashed lines) are shown in Fig. 9. It is well evident how the lens core maintains isolated from the background waters, suggesting a high stability of this structure. Conversely, moving up (to depths less than 75 m) and down (to depths larger than 275 m) the isopleths are almost parallel to the isopycnals and exchanges are permitted. Due to the reduced importance of the relative vorticity ζ, the potential vorticity π is controlled by the stratification, i.e. by the hydrographic characteristics of the lens.

7. Eddy persistency

7.1. Scalar properties

As described previously, 5 months after the July cruise, a subsequent cruise repeated most of the same hydrographic stations and, more specifically, a northwest–southeast section A (Fig. 1a). One noteworthy result was that the lens found before was still present (Fig. 5), approximately in the same position and with very similar characteristics (Fig. 6). Geostrophic velocities computed for December (Fig. 10) showed higher values, up to 15 cm/s; while in July significantly reduced values were observed close to the surface, in December high values involved the mixed layer (0–75 m) as well. During this period the current field was much more complex, with the presence of another mesoscale feature (probably a cyclonic eddy shifted towards the southern part of the section). Neglecting this effect, mainly confined in the surface layer (approximately a velocity reduction of 5 cm/s), the velocity field of the investigated eddy does not seem to be significantly different from the one observed in July.

To explain the high persistence of this structure, both in terms of hydrographic and dynamic conditions, it is important to observe that the abyssal plane near the eddy is marked by Vavilov Seamount, an isolated topographic feature that rises from a depth of 3300–3500 m to about 750 m (Fig. 1b). It is known that seamounts can greatly affect physical and biological processes, generating mesoscale circulation features. The dominant principle is the conservation of potential vorticity along a particle trajectory; as a column of water moves over an obstacle, vortex compression requires a decrease in local vorticity, resulting in anticyclonic currents, while the vortex stretching when moving away from the feature produces cyclonic rotation. Several studies have considered this process through laboratory and numerical models investigating the barotropic conditions, the stratification effect, or the interaction of an existing vortex structure with a seamount (Verron and Le Provost, 1985; Chapman and Haidvogel, 1992; Herbette et al., 2003). All authors, starting from a transient regime, looked for possible steady conditions. The primary mechanisms determining the flow pattern are the strength and time dependence of the background flow, the stratification of the

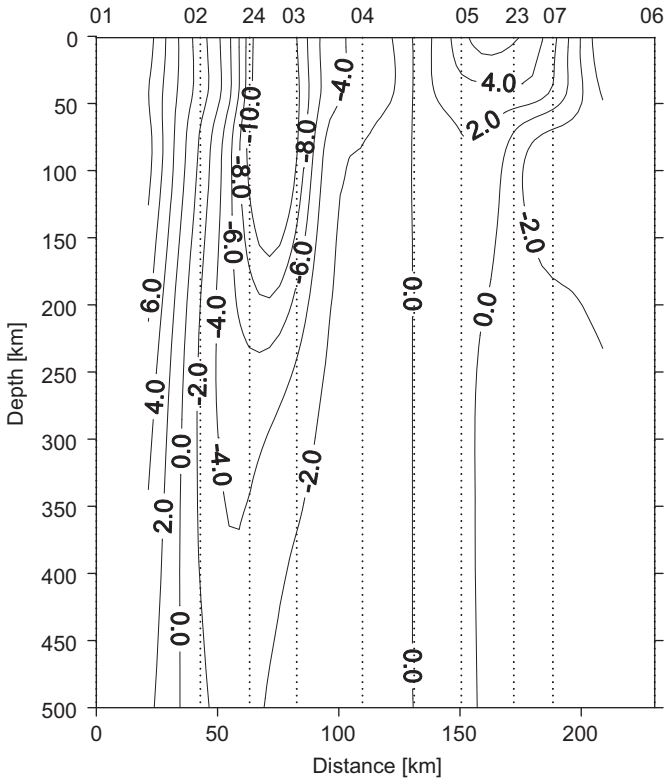

Fig. 10. Geostrophic velocity along section A of Fig. 1 during December 2005, between 0 and 500 m. Reference level at 2000 db. Units are in cm s^{-1}.

water column, and the geometry of the obstacle. The relative importance of each mechanism can be quantified with non-dimensional parameters (Verron and Le Provost, 1985; Chapman and Haidvogel, 1992), estimated in correspondence with the seamount region; the Rossby number, *Ro*, which determines the relative importance of advective (non-linear) effects compared to the Coriolis effect, and the Burger number, *Bu*, which is a measure of the stratification (baroclinicity) of the water column:

$$Ro = Uo/fD; \quad Bu = NH/fD \tag{7}$$

where *Uo* is the mean background flow, *f* the Coriolis parameter, *D* the seamount length scale (assumed as its major radius), *N* the Brunt–Vaisala frequency ($N^2 = (g/\rho_o)\partial\rho/\partial z$), and *H* the mean water depth. In particular, it was found that the resulting flow regime is most sensitive to variations of *Ro*.

Another relevant quantity that permits estimation of the topographic dynamical effect is the seamount fractional height $\delta = h/H$, where *h* is the obstacle height.

If in the barotropic case a blocking parameter that determines the possibility to have a trapped fluid over a seamount can be estimated as (Verron and Le Provost, 1985)

$$\mu = \delta/Ro \tag{8}$$

for the baroclinic case the situation appears more complex (Chapman and Haidvogel, 1992). The stratification tends to reduce the seamount's effect and its vertical extend above the bottom can be estimated by the vertical trapping scale (Chapman and Haidvogel, 1992):

$$h_v = Df/N \tag{9}$$

Information about temporal evolution of the observed structures can be obtained by estimating the advective timescale, $t_a = D/U_0$, *D* and U_0 being the characteristic motion scales. It is generally assumed that steady state is reached after a period covering several advective time scales.

The values presented in Table 1 summarize the conditions corresponding to the investigated region. Looking first at the topographic characteristics, we consider that the Vavilov volcano raises to about 750 m from a seafloor of approximately 3300–3500 m; the fractional height δ therefore is about 0.77–0.79, which means that we are in a tall seamount condition (Chapman and Haidvogel, 1992).

Examining the geostrophic current estimated from hydrography, we find usually weak values. The highest values are inside the eddy while outside the currents they do not exceed 5 cm/s. Nevertheless in the present estimate we considered U_0 to range between 5 and 15 cm/s (Table 1). The corresponding values of *Ro*, always $\ll 1$, are compatible with eddy generation. For the barotropic case the high value reached by the blocking parameter (always $\mu = 17$ or greater) suggests that, for the observed mean current, the circulation structure evolves towards a trapped anticyclonic structure (Verron and Le Provost, 1985). Nevertheless the Burger number ($Bu = 3$) indicates a certain relevance of stratification, thus suggesting baroclinic conditions. Chapman and Haidvogel (1992) indicate that for reduced *Ro* and high fractional height ($\delta > 0.7$) a seamount-trapped structure is possible, but with lower *Bu* ($= 1$). However the vertical trapping scale h_v (>2000 m) indicates a seamount influence larger than the effective seamount depth (750 m), and suggests that the trapping effect might affect the entire water column above the seamount. Consequently, the combination of a reduced Rossby number (also considering high velocity) and the observed stratification are compatible with a long eddy persistence.

The previous conditions mainly refer to the steady state, which means that they predict the trapping phenomena after several timescales t_a since its beginning (Verron and Le Provost, 1985; Chapman and Haidvogel, 1992). Starting from July, all examined parameters seem to support a steady condition, which would converge towards a long trapping anticyclonic eddy and justify the continuity between the July and December observations.

7.2. Surface signature

The MSLA derived from the DUACS data set can give further insights on the observed features. The MSLA during the cruise periods reveals a somewhat different behavior. During the second half of July 2005 (Fig. 11a), the Tyrrhenian Sea was dominated by a positive anomaly, centered at 40°N and 12.5°E (i.e. close to station 2), which during the following days intensified and moved to the east–southeast. The same feature was present until the end of the cruise but expanded its dimension and modified its shape, generating a three-lobe structure (Fig. 11c). During the second cruise the altimetry revealed a more complex pattern (Figs. 11d–f), where it was difficult to detect the anticyclonic feature present in the water column: the southern Tyrrhenian Sea showed a large cyclonic structure with some cyclonic and anticyclonic eddies superimposed. Fig. 11 shows also the gentle gradient of the MSLA, which characterized the region in December compared to the one observed in July.

In order to illustrate the long-term characteristics of the sea-level anomaly in the eddy region, we analyzed 14 years (from 1993 to 2006) of altimetry data. In particular, using the weekly DUACS data set, we evaluated the monthly averaged MSLA for two different areas (see also Fig. 1):

(a) the MSLA in the small box defined by the coordinate $\varphi = 39.5$–$40.0°$, $\lambda = 12.5$–$13.0°$ corresponding to the area eastwards to the Vavilov Seamount (which is located 39°52.00′N and 12°36.00′E) and centered over the area where the Weddy was detected ($MSLA_{Vav}$);

Table 1
Dimensional and non-dimensional parameters characterizing the Vavilov Seamount region: D is the seamount major length scale, H the bottom depth, δ the seamount fractional height, U_0 the mean background velocity, Ro the Rossby number, μ the blocking parameter, N the Brunt–Vaisala frequency, Bu the Burger number, h_v the vertical trapping scale, and t_a the advective timescale.

D (km)	H (m)	δ	U_o (cm s^{-1})	Ro	μ	N (s^{-1})	Bu	h_v (m)	t_a (days)
35	3300–3500	0.77–0.79	5–15	0.02–0.05	50–17	$\leqslant$0.003	3	2160	16–5

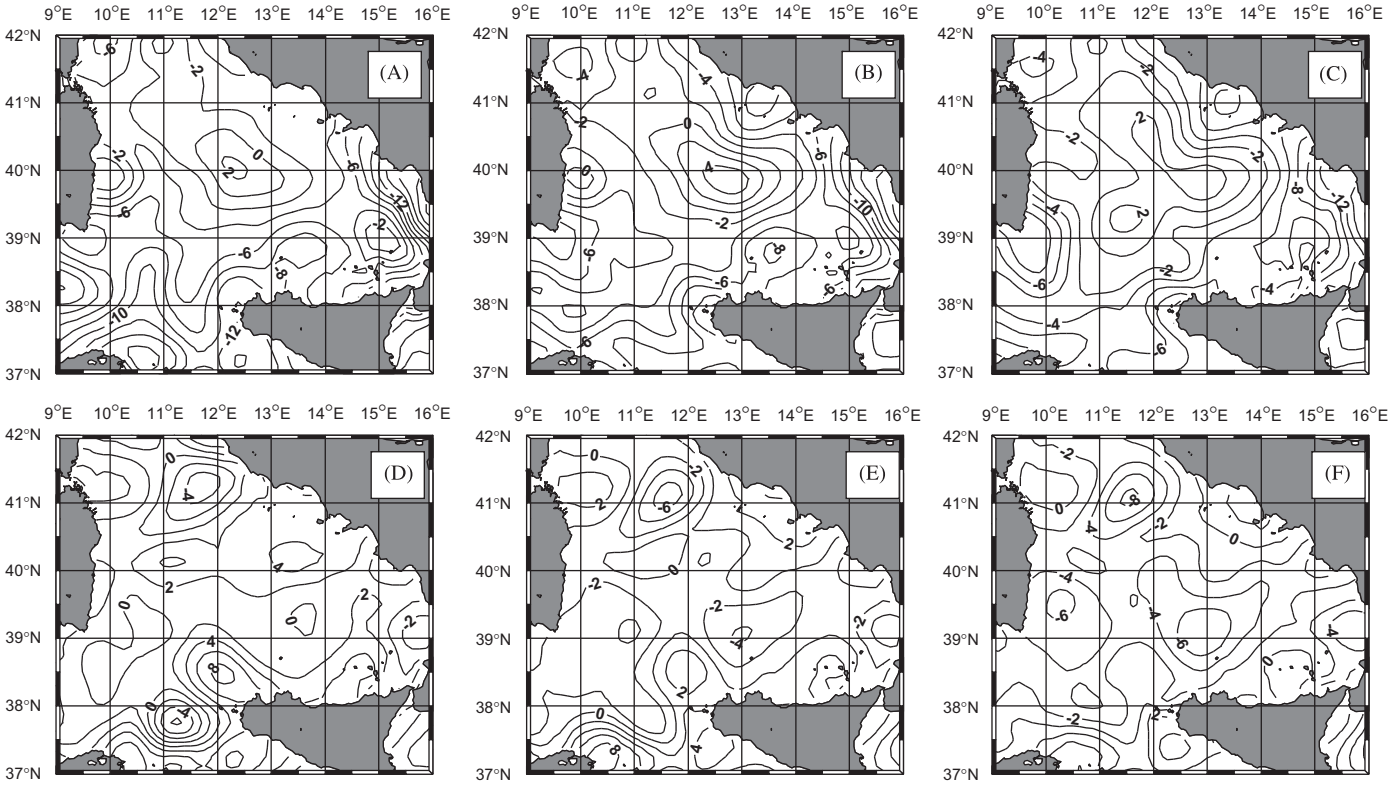

Fig. 11. Mean Sea Level Anomaly (MSLA) of the central-southern Tyrrhenian basin during the measurement program: (a) 20, (b) 23, and (c) 27 July 2005; (d) 17, (e) 21, and (f) 24 December 2005.

(b) the MSLA in a larger region of coordinate $\varphi = 38.5$–41.0°, $\lambda = 10.0$–15.0°, which includes the central and southern Tyrrhenian Sea ($MSLA_{Tyr}$).

In order to filter the seasonal variability of the steric component from each time series we subtracted from the weekly data the averaged MSLA computed for the corresponding week in the period 1993–2006. Subsequently we computed the difference

$$\Delta_{VT} = MSLA_{Vav} - MSLA_{Tyr} \quad (10)$$

Positive values of Δ_{VT} indicate a presence of a higher MSLA in the Vavilov region than in the central-southern Tyrrhenian basin.

The evolution of Δ_{VT} is shown in Fig. 12. Although a short-term variability is present in its evolution, probably related to the mesoscale activity, the evolution of Δ_{VT} clearly evidences the prevalence of positive anomalies, which may last for very long periods. More specifically, positive anomalies covered all 2005 and extended into 2006. This result seems to agree with the role of the Vavilov mount to trap anticyclonic structures. However, the positive anomaly is not a permanent feature; we can observe long periods when it disappears. Furthermore its presence seems to be independent of the seasonal evolution of stratification and dynamics. Its long persistence during the 1996–1997 period is remarkable, when it lasted for almost 24 months. These results support the hypothesis that the evolution of the observed Weddy is probably due to a combined effect of hydrographic and dynamic conditions, subject to the seamount's topographic influence.

A further evidence of the Vavilov Seamount trapping effect comes from a surface drifter trajectory (Fig. 13), even if the time period is different. Between 13 November 1991 and 8 January 1992, the drifter, released in proximity of the seamount, was retained in an anticyclonic circulation for 57 days before leaving it. Several details can be deduced from the drifter trajectory: its rotational speed was about 15 cm/s while the eddy length scale ($2L$) was of the order of 50–70 km, not far from the 2005 eddy characteristics. Its trajectory showed four almost regular loops, corresponding to a periodicity of about 14 days. The almost stable eddy position suggests that we are observing a stationary phase. The drifter departure after 8 January 1992 does not seem to be due to the eddy dissipation, but due to some external forcing able to transfer the drifter outside the eddy influence.

8. Discussion and conclusion

Two hydrographic cruises performed in July and December 2005 in the central Tyrrhenian region provided new information

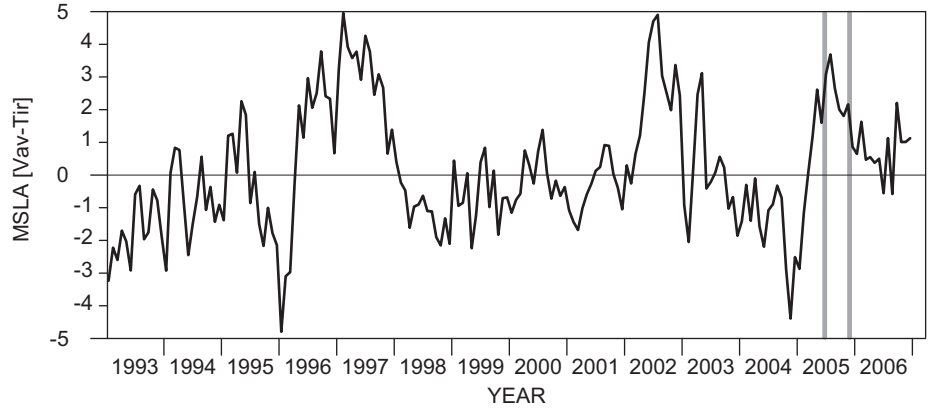

Fig. 12. Difference from 1993 to 2006 between the MSLA in the "Vavilov" and the Tyrrhenian regions. Vertical gray bars indicate the period of the two field surveys in 2005.

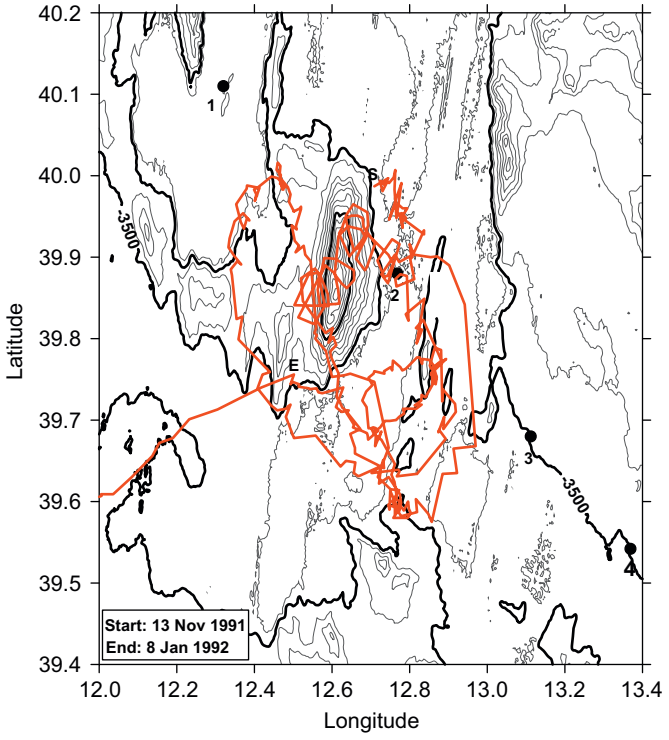

Fig. 13. Trajectory of a shallow drogued (10 m) drifter (ENEA Drifter b0006, Mediterranean drifter database http://doga.ogs.trieste.it/drifter/database_med/html/). *S* indicates the deployment position and *E* indicates the departure from the vortex. Dots indicate the hydrographic stations of the 2005 cruises.

on the hydrographic conditions of the entire water column and indicate how the water masses are modifying their characteristics during the previous 20 years (Gasparini et al., 2005). Furthermore they provided evidence of a peculiar persistent feature, recognized as an anticyclonic eddy. The collection of several CTD profiles in the same positions during the two cruises showed that the anticyclonic signature was stably positioned very close to the Vavilov Seamount, maintaining almost the same hydrographic properties.

Several parameters describing the relevance of topographic effect on eddy existence and persistence indicate that the topographic effect is possibly responsible for the eddy presence in the region in both periods, in agreement with laboratory and numerical modelling simulations (Verron and Le Provost, 1985; Chapman and Haidvogel, 1992).

The observational data (hydrographic properties and dynamical parameters) seem to support the hypothesis that we were observing the same structure in both periods. The concurrent and long-term presence of a positive altimetric anomaly in the eddy area suggests that the anticyclonic signature might persist for a long period. A further evidence of the possibility of a long-term presence in the region of an anticyclonic eddy comes from a drifter trajectory.

If the topographic effect is responsible for the permanence of the eddy in the region, it is important to understand if the observed eddy was locally generated or was advected in the region by large-scale circulation. From the previous discussion we found that its hydrographic properties were very similar to those of the WIW, which originates during the winter period in the Northwestern Mediterranean (Salat and Font, 1987). This might suggest that the eddy observed in the Tyrrhenian already existed and had a remote origin. WIW patches have been detected in different regions of the Western Mediterranean, sometimes with an eddy structure (Weddy; Millot, 1999), whose diameter can reach 100 km or more, allowing the Weddies to endure erosion processes and to cover long distances without losing their peculiarity. The severe winter conditions and the huge deep-water production during winter 2005 (Lopez-Jurado et al., 2005; Schroeder et al., 2006) strongly support a wider WIW presence in the Western Mediterranean during the examined period.

Theoretical studies on the interaction between an anticyclonic vortex and an isolated topography indicate the complexity of such a process, which appears sensitive to several environmental conditions; besides stratification and mean flow, the length scales of the incoming vortex in relation to the seamount length scales and their distance are determinants for its evolution and survival (Herbette et al., 2003). In our case the sparsely available information does not permit us to follow the evolution of this process.

The main intent of this work was to evidence, for the first time, the critical role played by isolated topography in influencing the interior Tyrrhenian circulation, generally characterized by weak dynamics. Until now the main responsibility of vortex activity has been attributed to the meteorological forcing, while topographic effects have been largely neglected. Several isolated seamounts are present in the Tyrrhenian basin, some of them reaching into the photic zone; with their associated vertical exchanges, they may provide an important role in modifying water properties, nutrient distribution, and biological activity.

By travelling for long distances, remote Weddy structures may be efficient vectors of chemical and biological properties. In the highly oligotrophic Tyrrhenian region, Weddy advection may be a mechanism for introducing nutrients or biological species, which

are more abundant in the more productive Western Mediterranean regions. The interaction between remote structures and isolated topography further enhances possible effects on distribution of biochemical parameters and the way they can influence the trophic chain of the Tyrrhenian basin.

Acknowledgements

The authors thank Yuri Cotroneo and Massimo De Stefano (University of Napoli "Parthenope"), Giuseppe Siena (CoNISMa), and the crew of the R/Vs Universitatis and Urania for their invaluable assistance in the field activity. Oxygen samples were provided by the Stazione Zoologica "A. Dohrn" of Napoli.

References

Armi, L., Zenk, W., 1984. Large lenses of highly saline Mediterranean water. Journal of Physical Oceanography 14, 1560–1576.

Artale, V., Astraldi, M., Buffoni, G., Gasparini, G.P., 1994. Seasonal variability of gyre-scale circulation in the Northern Tyrrhenian Sea. Journal of Geophysical Research 99, 14127–14137.

Astraldi, M., Gasparini, G.P., 1994. The seasonal characteristics of the circulation in the Tyrrhenian Sea. In: Seasonal and Interannual Variability of the Western Mediterranean Sea, Coastal and Estuarine Studies, vol. 46. AGU, Washington, DC, pp. 115–134.

Astraldi, M., Gasparini, G.P., Vetrano, A., Vignudelli, S., 2002. Hydrographic characteristics and interannual variability of water masses in the central Mediterranean: a sensitivity test for long-term changes in the Mediterranean Sea. Deep-Sea Research I 49, 661–680.

Bouzinac, C., Font, J., Millot, C., 1999. Hydrology and currents observed in the channel of Sardinia during PRIMO-1 experiment from November 1993 to October 1994. Journal of Marine Systems 20, 333–355.

Chapman, C.C., Haidvogel, D.B., 1992. Formation of Taylor caps over a tall isolated seamount in a stratified ocean. Geophysical and Astrophysical Fluid Dynamics 64, 31–65.

Decembrini, F., Caroppo, C., Azzaro, M., 2008. Size structure and production of phytoplankton community and carbon pathways channelling in the Southern Tyrrhenian Sea (Western Mediterranean). Deep-Sea Research II, this issue [doi:10.1016/j.dsr2.2008.07.022].

Gasparini, G.P., Zodiatis, G., Astraldi, M., Galli, C., Sparnocchia, S., 1999. Winter intermediate water lenses in the Ligurian Sea. Journal of Marine Systems 20, 319–332.

Gasparini, G.P., Ortona, A., Budillon, G., Astrali, M., Sansone, E., 2005. The effect of the Eastern Mediterranean transient on the hydrographic characteristics in the Strait of Sicily and in the Tyrrhenian Sea. Deep-Sea Research I 52, 915–935.

Herbette, S., Morel, Y., Arhian, M., 2003. Erosion of a surface vortex by a seamount. Journal of Physical Oceanography 33, 1664–1679.

Hopkins, T.S., 1988. Recent observations on the intermediate and deep water circulation in the southern Tyrrhenian Sea. Oceanologica Acta, SP, 41–50.

Krivosheya, V.G., Ovchinnikov, I.M., 1973. Peculiarities in the geostrophic circulation of the water of the Tyrrhenian Sea. Oceanology 13, 822–827.

Le Traon, P.-Y., Dibarboure, G., 1999. Mesoscale mapping capabilities of multi-satellite altimeter missions. Journal of Atmospheric and Oceanic Technology 16 (9), 1208–1223.

Lopez-Jurado, J.-L., González-Pola, C., Vélez-Belchí, P., 2005. Observation of an abrupt disruption of the long-term warming trend at the Balearic Sea, Western Mediterranean Sea, in summer 2005. Geophysical Research Letters 32, L24606.

Marani M., Gamberi F., Bonatti E. (Eds.), 2004. From seafloor to deep mantle: architecture of the Tyrrhenian back-arc basin, Memoria Descrittiva Carta Geologica d'Italia, LXIV, pp. 195.

Marullo, S., Santoleri, R., Bignami, F., 1994. The surface characteristics of the Tyrrhenian Sea: historical satellite data analysis. In: Seasonal and Interannual Variability of the Western Mediterranean Sea, Coastal and Estuarine Studies, vol. 46. AGU, Washington, DC, pp. 135–154.

MEDAR Group, 2002. Mediterranean and Black Sea Database of Temperature, Salinity and Biochemical Parameters and Climatological Atlas [4 CD-ROMs], Ifremer Ed., Plouzane, France. Available at 〈http://www.ifremer.fr/sismer/program/medar/〉.

Millot, C., 1999. Circulation in the Western Mediterranean. Journal of Marine Systems 20, 423–442.

Olson, D.B., 1980. The physical oceanography of two rings observed by the cyclonic ring experiment. Part II: dynamics. Journal of Physical Oceanography 10, 514–528.

Pierini, S., Simioli, A., 1998. A wind-driven circulation model of the Tyrrhenian Sea area. Journal of Marine Systems 18, 161–178.

Ribera d'Alcalà, M., Brunet, C., Conversano, F., Corato, F., Lavezza, R., 2008. Nutrient and pigment distributions in the Southern Tyrrhenian Sea during mid Summer and late fall 2005. Deep-Sea Research II, this issue [doi:10.1016/j.dsr2.2008.07.028].

Salat, J., Font, J., 1987. Water mass structure near and offshore the Catalan coast during the winters of 1982 and 1983. Annales Geophysicae 1B, 49–54.

Schroeder, K., Gasparini, G.P., Tangherlini, M., Astraldi, M., 2006. Deep and intermediate water in the Western Mediterranean under the influence of the Eastern Mediterranean Transient. Geophysical Research Letters 33, L21607.

Schroeder, K., Tailandier, V., Vetrano, A., Gasparini, G.P., 2008. The circulation of the Western Mediterranean Sea in spring 2005 as inferred from observations and from model outputs. Deep-Sea Research I 55, 947–965.

Stammer, D., Hinrichsen, H.H., Kase, R.H., 1991. Can Meddies be detected by satellite altimetry? Journal of Geophysical Research 96 (C4), 7005–7014.

Tamburini, C., Garel, M., Ali, B.A., Mérigot, B., Kriwy, P., Charrière, B., Budillon, G., 2008. Distribution and activity of Bacteria and Archaea in the different water masses of the Tyrrhenian Sea. Deep-Sea Research II, this issue [doi:10.1016/j.dsr2.2008.07.021].

Verron, J., Le Provost, C., 1985. A numerical study of a quasi-geostrophic flow over isolated topography. Journal of Fluid Mechanics 154, 231–252.

Zodiatis, G., Gasparini, G.P., 1996. Thermohaline staircase formations in the Tyrrhenian Sea. Deep-Sea Research I 43, 655–678.

Deep-Sea Research II 56 (2009) 725–737

Contents lists available at ScienceDirect

Deep-Sea Research II

journal homepage: www.elsevier.com/locate/dsr2

Integrated stratigraphic reconstruction for the last 80 kyr in a deep sector of the Sardinia Channel (Western Mediterranean)

F. Budillon [a,*], F. Lirer [a], M. Iorio [a], P. Macrí [b], L. Sagnotti [b], M. Vallefuoco [a], L. Ferraro [a], S. Garziglia [c], S. Innangi [a], M. Sahabi [d], R. Tonielli [a]

[a] Istituto per l'Ambiente Marino Costiero, IAMC, Consiglio Nazionale delle Ricerche, Calata Porta di Massa 80, I-80133 Napoli, Italy
[b] Istituto Nazionale di Geofisica e Vulcanologia, INGV, Via di Vigna Murata 605, I-00143 Rome, Italy
[c] Géosciences-Azur, CNRS, BP 48, Fr-06235,Villefranche sur Mer, France
[d] Faculté des Sciences, BP 20, 24000 El Jadida, Morocco

ARTICLE INFO

Article history:
Accepted 9 July 2008
Available online 7 November 2008

Keywords:
Integrated stratigraphy
Late Neogene marine record
Eco-bio-events
Reflectance 550 nm %
Sardinia Channel
Western Mediterranean

ABSTRACT

A quantitative analysis of planktonic foraminifera, coupled with petrophysical and paleomagnetic measurements and ^{14}C-AMS calibrations, was carried out on a deep core recovered in the Sardinia Channel (Western Mediterranean Sea), during the CIESM Sub2 survey, providing an integrated stratigraphic time-framework over the last 80 kyr. Significant changes in the quantitative distribution of planktonic foraminifera allowed the identification of several eco-bioevents useful to accurately mark the boundaries of the eco-biozones widely recognized in the Western Mediterranean records and used for large-scale correlations. Namely, 10 eco-biozones were identified based on the relative abundance of selected climate-sensitive planktonic foraminiferal species. Sixteen codified eco-bioevents were correlated with Alboran Sea planktonic foraminiferal data and several climatic global events (Sapropel S1, Younger Dryas, Greenland Isotope Interstadial 1, Greenland Isotope Stadial 2, Heinrich event H1–H6) were recognized.

The eco-bioevents together with the ^{14}C-AMS calibrations allowed us to define an accurate age model, spanning between 2 and 83 kyr. The reliability of the age model was confirmed by comparing the colour reflectance (550 nm%) data of the studied record with the astronomically tuned record from the Ionian Sea (ODP-Site 964). A mean sedimentation rate of about 7 cm/kyr included three turbidite event beds that were chronologically constrained within the relative low stand and regressive sea-level phases of MIS 4 and 3. The deep-sea sedimentary record includes a distinct tephra occurring at the base of the core that dates 78 ka cal. BP.

The paleomagnetic data provide a well-defined record of the characteristic remanent magnetization that may be used to reconstruct the geomagnetic paleosecular variation for the Mediterranean back to 83 kyr.

1. Introduction

Since climate excursions recorded in Northern Hemisphere in the Greenland GISP and GRIP ice cores (GRIP members, 1993) over the last 100 kyr had more or less synchronous effects in the Mediterranean area, many researches have focused on Mediterranean marine cores, with the aim to detect their intensity and impact on the marine environment. During the last glacial period the Mediterranean region experienced rapid modifications in hydrographic conditions in response to fast climatic excursions, such as Heinrich (HE) and Dansgaard–Oeschger (D–O) Stadials (cold) and Interstadials (warm) events (Heinrich, 1988; Dansgaard et al., 1993). In particular, Rohling et al. (1998) and Cacho et al. (1999, 2000) have proved that the millennial scale D–O and HE directly control the winds and precipitation system on the northern Mediterranean basin. Even during the Holocene the principal climatic events and oscillations of the northern Hemisphere have been clearly traceable in different sectors of the Mediterranean basin sedimentary records (Cacho et al., 1999, 2000, 2001; Rohling et al., 2002; Sprovieri et al., 2003, 2006; Perez-Folgado et al., 2003, 2004; Geraga et al., 2005).

A detailed outline of the paleo-environmental changes and their control on marine communities, calibrated by several independent proxies (tephra, sapropel, ^{14}C geochronology), is now available for the Mediterranean area (Buccheri et al., 2002; Ducassou et al., 2007; Emeis et al., 2003; Narcisi and Vezzoli,

* Corresponding author. Tel.: +390 81 542 3839; fax: +390 81 542 3888.
E-mail address: francesca.budillon@iamc.cnr.it (F. Budillon).

0967-0645/$ - see front matter © 2008 Elsevier Ltd. All rights reserved.
doi:10.1016/j.dsr2.2008.07.026

1999; Lourens, 2004; Principato et al., 2003; Rohling et al., 2003; Sangiorgi et al., 2006; Sprovieri et al., 2003, 2006, and reference therein). Several codified eco-bioevents, if clearly detected in marine records, can be used as tie points to chronologically constrain the late Pleistocene–Holocene Mediterranean marine sequence. Nevertheless, even if many reference records are available from deep-sea sites, most of them span a short time interval and lack a high resolution detail of the paleo-environmental and paleo-ecological changes before 40 kyr. Recently, Perez-Folgado et al. (2003, 2004) carried out a high-resolution study of the ODP-Site 977, located in the western part of the Alboran Sea, and identified several planktonic foraminiferal eco-bioevents that occurred during the marine isotope stages (MIS) 1–5. These eco-bioevents represent the best tool to correlate deep marine records from different Mediterranean sites.

Many recent studies emphasize the challenge when studying deep-sea records to establish a reliable chronology, even for the deposition of turbidites (Walker, 1992; Beaudouin et al., 2004; Ducassou et al., 2007), and underline the utility to support conventional dating methodologies with different constraints. It is widely accepted that one of the main factors controlling and enhancing turbidite deposition along deep-sea fan is the regression and low stand of sea-level, whereas sea-level rise and highstand phases reduce terrigenous supply to deep-sea systems (Walker, 1992; Richards et al., 1998; Normark et al., 1998).

The CIESM core C08 is located at the mouth of the Bizerte Canyon in the Sentinelle Valley in a key position of paleoceanographic and geological significance (Fig. 1). The Sardinia Channel connects the Alboran to the Tyrrhenian Basin and offers a stratigraphic record with the potential to link the eco-stratigraphic and paleoceanographic observations between the Western, Central and Eastern Mediterranean late Pleistocene–Holocene marine records (Perez-Folgado et al., 2004; Sbaffi et al., 2004; Geraga et al., 2005; Asioli et al., 2001; Ariztegui et al., 2000). In fact, a portion of the Modified Atlantic Water (MAW) coming from the Strait of Gibraltar (Bryden and Kinder, 1991), diverges from the part that enters the Eastern Mediterranean and flows through the Sardinia Channel into the Tyrrhenian Sea along the northern Sicilian coast (Millot, 1987), forming a secondary circulation gyre. The circulation system in this sector of the Tyrrhenian Sea is counter-clockwise, with the Levantine Intermediate Water (LIW) inflows lapping on the northern Sicilian coast and the outflow occurring along the eastern Sardinia coast (Pinardi and Masetti, 2000 and references therein).

The core site is also in a strategic position to check the efficiency of a submarine canyon in driving density flow to the deep-sea environment (see below), even if not directly connected to any emerged sector nor to continental shelf (Reading and Richards, 1994). Thus the possibility that such a type of canyon would form a fan can be evaluated, even verifying the significance and the timing of the turbidite deposition.

The aim of this study is to provide a record of integrated stratigraphic data spanning back to about 80 kyr, relative to a deep basin area, based on eco-biozones, ^{14}C-dated ages, event stratigraphy, lithostratigraphy, petrophysical properties and paleomagnetic measurements. Furthermore, the reliability of the reflectance parameter 550 nm% is evaluated as an independent correlation tool for tuning marine records.

2. Geological setting

Core C08 was collected in the Sentinelle Valley of the Sardinia Channel, 55 km from the mouth of the Bizerte Canyon, equidistant

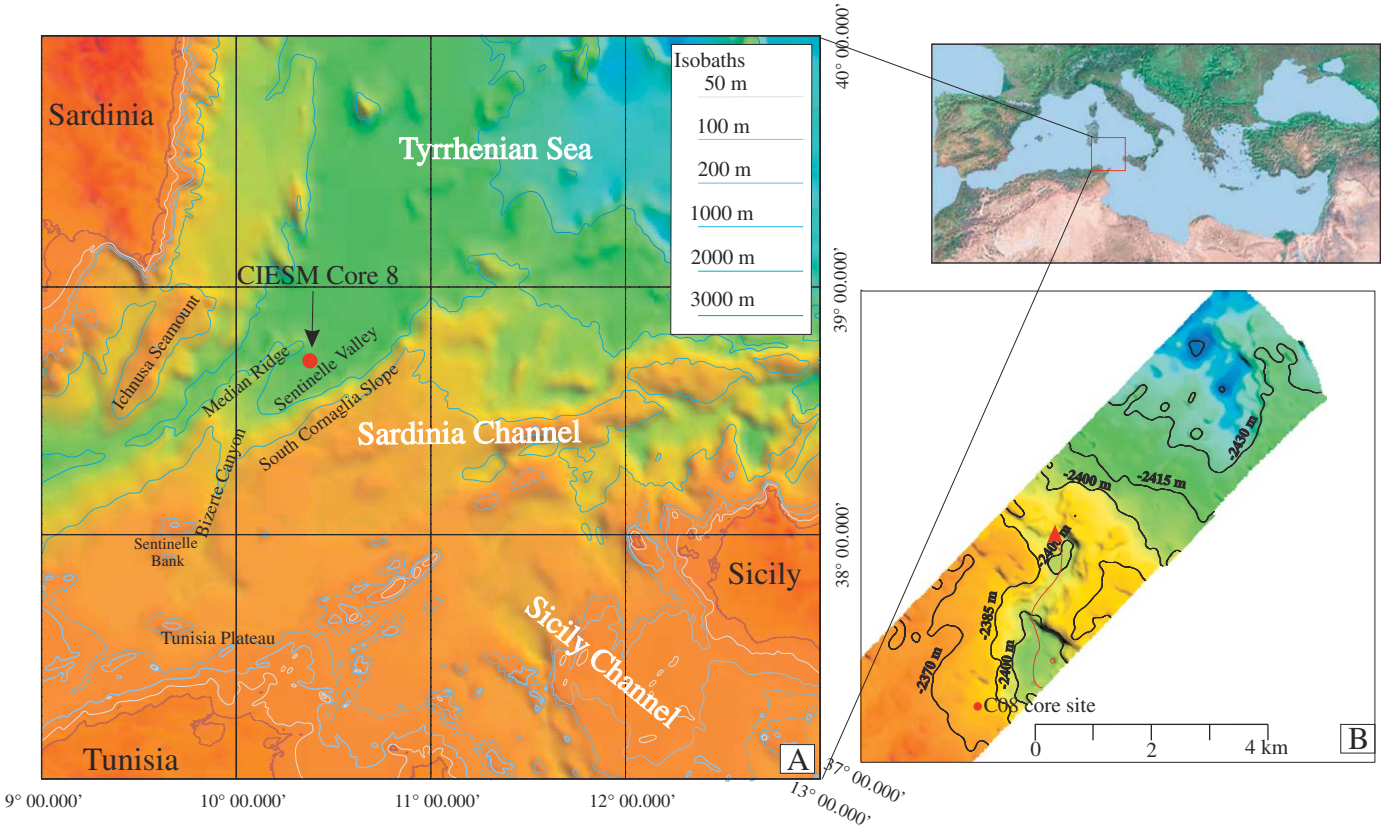

Fig. 1. (A) Location map of CIESM core C08. Bathymetry from GEBCO (1997); (B) bathymetric detail of core site, close to a channel South–North oriented (red arrow).

from Sicily, Sardinia and Tunisia (Fig. 1), during the cruise CIESM Sub2 onboard the R/V *Urania* in December 2005 (38°38.5364′N, 10°21.5576′E—2370 m water depth). In this area a 400-km-long submerged sector of the Apennine–Maghrebian branch of the Alpine orogen separates the Tyrrhenian (Plio-Pleistocene in age) and the Algero Provençal (Miocene in age) oceanic basins. This sector of the chain was not completely fragmented during the opening of the basins (Mascle et al., 2004). Due to the relatively minor post-orogenic extension and the good preservation of morpho-structural features, the Sardinia Channel is an important area for the reconstruction of the geodynamic evolution of the Western Mediterranean sector and was recently investigated through submersible surveys (Mascle et al., 2001a, 2004). The triangular-shaped valley is bounded by a NE–SW-oriented Median Ridge on its northwestern side and by the South Cornaglia slope to the southeast. The southwestern sector of the Sentinelle Valley receives the sedimentary contribution from the Bizerte Canyon, which cuts the Tunisian Plateau and the south margin of the Sentinelle Bank (Mascle et al., 2001b). The canyon head appears disconnected from the Tunisian shelf margin and extends over an area of about 1000 km^2 at an average depth of about 500 m (Fig. 1). It represents a particular type of canyons since it is not fed by an emerged areas or by a fluvio-deltaic systems (Reading and Richards, 1994; Prins et al., 2000; Kenyon et al., 2002;), but it drains a wide submarine plateau.

3. Material and methods

The gravity corer entered the uppermost portion of a sedimentary sequence made up with lateral continuous parallel and thin reflectors (Sartori et al., 2001), possibly related to hemipelagic and turbiditic deposition. It recovered about 5.40 m of hemipelagic mud interlayered with three fine-to-medium sand turbidite layers of increasing thickness towards the top of the core (Fig. 2).

3.1. Physical property measurements

The physical properties of the core were measured at 1-cm steps in a fully automated GEOTEK Multi-Sensor Core Logger (MSCL), in the petrophysical laboratories of IAMC in Naples (Italy). The MSCL system includes a Bartington MS2E Point sensor, to measure the low-field magnetic susceptibility (MS) with a spatial resolution of 0.4 cm and a Minolta Spectrophotometer CM 2002 that records at 0.8-cm steps, the percentage of reflected energy (RSC) at 31 wavelengths in 10-nm steps, over the visible spectrum (from 400 to 700 nm). MS and RSC measurements were taken on the archive half, ~1 h after the core had been split. The split core was covered with cling film to protect the glass cover of the Minolta aperture while measuring. Both measurements, log plotted, were visually compared to detect similar trends and

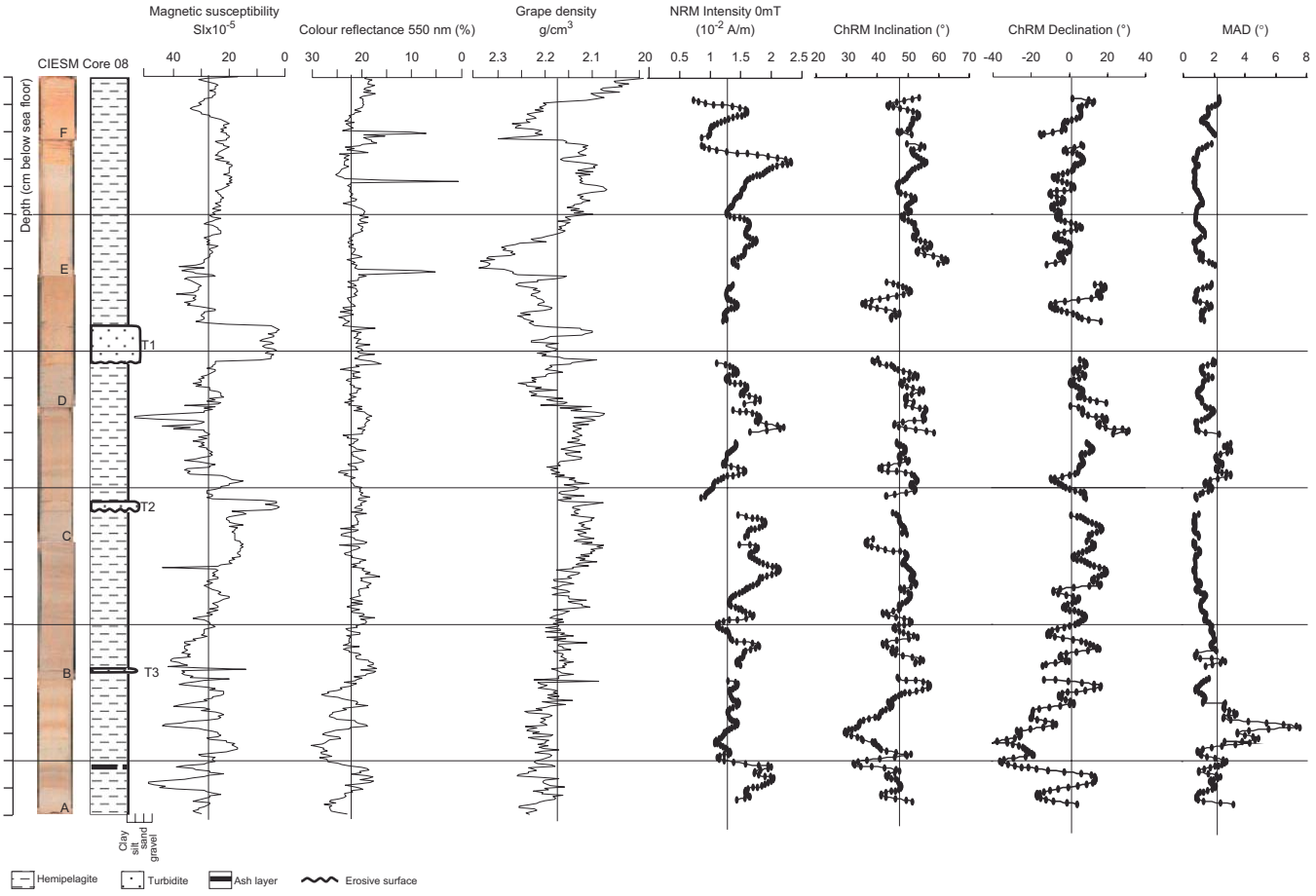

Fig. 2. Core CIESM 08: photography, lithologic log, petrophysical properties curves (magnetic susceptibility, reflectance 550 nm%, Grape density), paleomagnetic measurements curves (NRM intensity, ChRM inclination, ChRM declination, MAD) plotted against depth (cm below sea floor). In the paleomagnetic curves each dot represents a single measurement taken at 1-cm spacing. NRM: natural remanent magnetization; ChRM: characteristic remanent magnetization determined by principal component analysis on the demagnetization data; MAD: maximum angular deviation. The piston core was not azimuthally oriented, but a fiducial mark ensured the reciprocal orientation of each section from which u-channels were collected. The declination of each u-channel was rotated to bring the average value at 0°.

tentatively group the data according to their physical properties and corresponding stratigraphy (Wolf-Welling et al., 2001).

3.2. Paleomagnetic analysis

For the paleomagnetic study, 1-m-long u-channel specimens were sampled from archive halves of the CIESM 08 core. Only the turbiditic sandy interval at 182–208 cm depth was not suitable for u-channel sampling due to its coarse-grained and unconsolidated texture. The u-channels, sampled from the archive sections of the core, were measured in a magnetically shielded room at the paleomagnetic laboratory at the Istituto Nazionale di Geofisica e Vulcanologia in Rome, using an automated pass through a 2-G Enterprises DC SQUID cryogenic magnetometer system. For each u-channel the natural remanent magnetization (NRM) was measured at 1-cm steps. It is emphasized, however, that, due to the intrinsic response functions of the SQUID sensors, remanence measurements may be considered truly independent only every ca. 5 cm. The NRM was progressively demagnetized by the alternating field (AF) in nine steps up to a maximum field peak of 100 mT, by translating the u-channel through a set of three perpendicular AF coils at a speed of 10 cm/s. The remanence was measured at the same 1-cm spacing after each demagnetization step. Demagnetization data from u-channels were analysed on orthogonal vector projections and the paleomagnetic data obtained generally provided straightforward demagnetization diagrams, indicating that the sediments carry an almost single-component NRM. In fact, during the AF demagnetization a complete removal of any coring overprint and/or laboratory-induced remanences was achieved at low AF peaks (10 mT), and the characteristic remanent magnetization (ChRMs) of the sediments was clearly identified and determined by principal component analysis (Kirschvink, 1980). For each u-channel the uppermost and lowermost few cm were disregarded for the paleomagnetic analysis, to avoid any likely deflection of the remanence direction due to disturbances that may have been introduced during sampling. As stated before, no paleomagnetic data were collected for the coarse-grained level at 182–208 cm depth, and the NRM demagnetization diagrams did not allow a clear identification of a ChRM at 137–151 cm and 309–317 cm depth intervals.

3.3. Planktonic assemblage analysis

The analysis of planktonic foraminifera was conducted on 216 samples. Sampling spacing was 2 cm from the top of the core down to the base. Each wet sample of about 20 g was dried at 50 °C and washed over sieves with mesh-width size of 63 μm. Quantitative planktonic analyses were carried out on the fraction >125-μm. The adopted taxonomic units were those reported by Jorissen et al. (1993) and Capotondi et al. (1999). According to these authors, we introduced some supraspecific categories (which remain unchanged even under bad preservation conditions), reducing the number of species actually occurring in the planktonic foraminiferal assemblages.

3.4. ^{14}C Radiocarbon calibrations

About 10 mg of *Globigerina bulloides* and *Globorotalia inflata* were picked from three samples in the first 2 m beneath the sea floor (at the core top, at 0.44 and 1.43 mbsf) and were AMS radiocarbon dated at the Centre for Isotopic Research on Cultural and Environmental Heritage (CIRCE) radiocarbon laboratory, Caserta, (Italy). The CIRCE Accelerator Mass Spectrometry (AMS) system, based on the 3MV 9SDH-2 Pelletron accelerator, provides a mean overall precision of 0.63% (Passariello et al., 2007). All radiocarbon dates were calibrated using the CALIB 5.0 Program and a mean ΔR value of 48 ± 21 yr (calculated among six of the Tyrrhenian Sea, from the marine data base of Stuiver and Reimer, 1993). The AMS RC age at 1.430 mbsf (21,590 ± 120 a), close to the lower limit of the calibration curves, was not used for the age model.

4. Results

4.1. Lithostratigraphy and petrophysical properties

The sediment consists for the 95% of hemipelagic mud, ranging in colour from reddish and ochre to light, olive and dark grey; the remaining 5% are turbiditic sand layers (Fig. 2).

The uppermost 0.50 m consists of a reddish mud pervasively oxidized, then about 0.11 m of alternating dark grey and ochre laminated mud, and further below, 0.05 m of fine laminated ochre mud. From about 0.66 m down to 2.40 m olive grey mud occurs with rare dark patches, probably due to bioturbation, while from 2.40 m to the bottom of the core an alternation of several mud intervals occur, whose thickness range from cm to dm, showing different shades from light grey to dark grey. Three turbidite sand beds are interlayered in the mud sequence and occur from 1.82 to 2.08 m (T1), 3.10 to 3.17 m (T2) and 4.33 to 4.34 m (T3). They constitute 5% of the whole stratigraphic thickness of the core and are all characterized by low values of magnetic susceptibility. The turbidite layer T1 is marked by a sharp erosive contact and consists of a thin layer of oxidized sand, and then of a massive fine to medium sand with a high percentage of shell fragments; the upper boundary is sharp and the grain-size populations between fine sand and clay, which usually pertains to "b, c, d, e" divisions of the classical Bouma sequence (Bouma, 1962), are missing, as evidenced by the abrupt decrease of MS and Grape density values, which are a function of grain size and lithology. A sharp contact marks the onset of the turbidite layer T2, which contains a thin layer of well-sorted dark fine sand passing to a massive layer of well-sorted bioclastic fine sand; also in this case the upper boundary is sharp and the passage from massive and structureless sand to the hemipelagic mud is abrupt. Turbidite layer T3 has well-defined sharp boundaries and starts at the base with a thin layer of dark sand passing to light grey bioclastic sand. The thickness of the turbidites increases upward, but no sand layers occur in the uppermost 0.18 m of the core. A discrete fine ash layer, dark stained and characterized by diffuse boundaries occurs at 5.08 m and is marked by a MS peak value of 37 SI $\times 10^{-5}$. This tephra layer consists mainly of white pumice, dark green to yellowish glass shards, and few dark scoria; lithic elements are scarce (S. Tamburrino, pers. comm. 2007).

The lithologic features of the cored sediment are clearly detected by the petrophysical properties measured at a 1-cm steps: the volume magnetic susceptibility (MS) traces even thin tephra layers (Iorio et al., 2004), the GRAPE density is a compelling proxy for lithology and grain size (Wolf-Welling et al., 2001), and the reflectance at 550 nm% wavelength provides a quantitative evaluation of variations in sediment colour and can serve as a powerful correlation tool between long-distance core sites (Peterson et al., 2000). For instance, the meter composite depth of ODP-Sites records (ODP-Leg 154, Curry et al., 1995) is composed on the variation in natural gamma rays, reflectance and magnetic susceptibility parameters, to identify sedimentary patterns and to calibrate marine records to the standard variation of astronomical parameters (Lourens et al., 1998; Palike et al., 2006).

The three turbidites are well evidenced by low MS values (T1 and T2 measuring less than 5 SI $\times 10^{-5}$, T3 of 12 SI $\times 10^{-5}$) and by GRAPE density value (close to 2.1 g/cm^3), but are not highlighted by RSC. The RSC parameter traces well the changes in shade colour throughout the core, and in particular it points out those occurring at the core top (due to the pervasive seabed sediment oxidation) and in the deepest 1.4 m (Fig. 2). Along this latter interval the wide oscillations in the RSC parameter, ranging between 15% and 30%, correspond to analogous oscillations in MS values.

4.2. Paleomagnetism

The main paleomagnetic results are plotted in Fig. 2, which shows the stratigraphic trend of the NRM intensity, the ChRM inclination and declination and the maximum angular deviation (MAD). The NRM is weak and unstable in the topmost 0.15 m of the core and will not be discussed in the following. The data from below 0.15 m show that NRM intensity is relatively high and characterized by a limited variation, with values oscillating between 0.6 and 2.3 (10^{-2} A/m). The ChRM inclination oscillates from 30° to 60°, with an average value of 48° that is about 10° lower than the expected value (58°) at the latitude of the coring site. Such a kind of shallow bias, or inclination error, has been found in laboratory redeposition experiments and in some modern natural sediments. The sedimentary inclination shallowing is a well-known process linked to the deposition of magnetic particles and subsequent sediment compaction (see Tauxe and Kent, 1984, 2004; Arason and Levi, 1990; Deamer and Kodama 1990; Tan et al., 2003; Tan and Kodama, 2003). The piston core was not azimuthally oriented, but a fiducial mark ensured the reciprocal orientation of each section from which u-channels were collected. The ChRM declination of each u-channel was rotated to bring the core average at 0°. Under this transformation the ChRM declination oscillates between −30° and +30°, which is in the range of the expected geomagnetic secular variation. The principal component analysis of the demagnetization data shows a MAD always well below 3.3° along the core, which indicates a well-defined paleomagnetic direction, except a positive peak, up to a maximum of 7.5°, measured in the 0.47–0.48 m interval. This interval corresponds to the largest oscillations in the ChRM inclination and declination values, suggesting that some uncompensated lithological factor affects the paleomagnetic signal in that stratigraphic interval.

4.3. Quantitative distribution of planktonic foraminifera

A number of 13 species or groups of species were distinguished: *Globigerina bulloides* (including extremely rare specimens of *G. falconensis*); *Globigerinoides quadrilobatus* (including *G. trilobus* and very subordinate *G. sacculifer*); *Globigerinoides ruber* (including white and pink varieties, the latter extremely rare), *Globigerinoides elongatus* (very rare) and *Globigerinoides gomitolus* (very rare); *Globorotalia truncatulinoides* sl. right (very rare) and left coiling; *Globorotalia inflata* left coiling; *Globorotalia scitula* right and left coiling; *Globigerinoides tenellus* (rare); *Neogloboquadrina pachyderma* right and left coiling (extremely rare); *Globigerinita glutinata*; *Orbulina universa*; *Turborotalita quinqueloba*; *Globigerinatella siphoniphera* (rare) including *G. calida* (very rare); *Globoturborotalita rubescens* (rare).

The planktonic foraminifera, characterized by modern assemblages, are abundant and well-preserved, and the percentages of foraminiferal fragments are very low and do not alter the composition of the planktonic assemblage.

The long-term trend in planktonic foraminifera reveals that the faunal composition of the studied interval does not show drastic changes in the abundance patterns (Fig. 3). In particular, among the taxa that have a continuous distribution patterns, *G. bulloides*, *G. ruber*, *G. inflata* left coiled, *G. scitula* right coiled, *G. glutinata*, *N. pachyderma* right coiled and *T. quinqueloba* show long-term oscillation (trend) superimposed on short-term fluctuations possibly related to high-frequency climatic oscillations (Fig. 3).

Among the planktonic species having discontinuous distribution, *G. quadrilobatus*, *G. truncatulinoides* left coiled, *G tenellus*, only occasionally reach significant percentages (Fig. 3).

5. Discussion

5.1. Planktonic foraminiferal eco-biozonation

Significant changes in the quantitative distribution of the planktonic foraminifera species allowed several authors (Asioli et al., 1999, 2001; Capotondi et al., 1999; Casford et al., 2002; Principato et al., 2003; Sprovieri et al., 2003; Ducassou et al., 2007) to define eco-biozones useful for fine-scale subdividing of the stratigraphic record. The eco-biozone boundaries are characterized by the temporary appearance or disappearance and/or evident abundance peaks of different taxa. In the present work, we refer the stratigraphic record to a slightly modified eco-biostratigraphic classification by Sprovieri et al. (2003). At present, the eco-biostratigraphic classification of Sprovieri et al. (2003) proposes nine eco-biozones over the last 23 kyr. Here, we propose to mark the base of eco-biozone nine with the strong increase of *G. inflata*, occurring in the Mediterranean area at about 30 ka (Ducassou et al., 2007; Geraga et al., 2005), and to extend eco-biozone 10 back to ~80 kyr. Actually, using the quantitative distribution pattern of the most abundant planktonic foraminifera species counted throughout C08, we identified 10 evident eco-biozones from top to bottom (Fig. 3).

The uppermost part of the studied record attributed to eco-biozone 1, which extends down to 0.08 m, is characterized by a decrease in abundance of *G. quadrilobatus* and the end of *G. truncatulinoides* right coiled. This attribution is also supported by a ^{14}C-AMS calibration, which dates 2.18 ka cal. BP (Fig. 3; Table 1).

Eco-biozone 2 is defined by the concomitant abundance of *G. quadrilobatus* and *G. truncatulinoides* left and right coiled and low abundance values of *N. pachyderma* right coiled in the lower part. A strong increase of *G. truncatulinoides* left coiled marks the base of the eco-biozone (Fig. 3).

The short interval represented by eco-biozone 3, whose base is at 0.31 m, is marked by the end of the micropaleontological signature of sapropel S1 and is characterized by low abundances of *T. quinqueloba, G. quadrilobatus*, and *G. truncatulinoides* left coiled.

Eco-biozone 4 corresponds to the time interval of sapropel S1 deposition, although no lithological evidence was found except for colour shades (Fig. 2). *G. ruber* oscillations allowed a reliable identification of the faunal signature of the climatic events associated with the deposition of sapropel S1 (Fig. 3). In particular, two distinct peaks in *G. ruber* mark the two short-term warm oscillations (S1a and S1b, Sprovieri et al., 2003), separated by a cold phase (Fig. 3). A ^{14}C-AMS datum at 0.44 mbsf (within the cold phase) gives an age of 8.79 ka cal. BP (Table 1), coincident with an increase in abundance of *G. tenellus* and *G. quadrilobatus* (Sprovieri et al., 2003).

Eco-biozone 5 is defined by the concomitant occurrence of *G. ruber* and *G. inflata*, by a distinct peak of *G. truncatulinoides* left

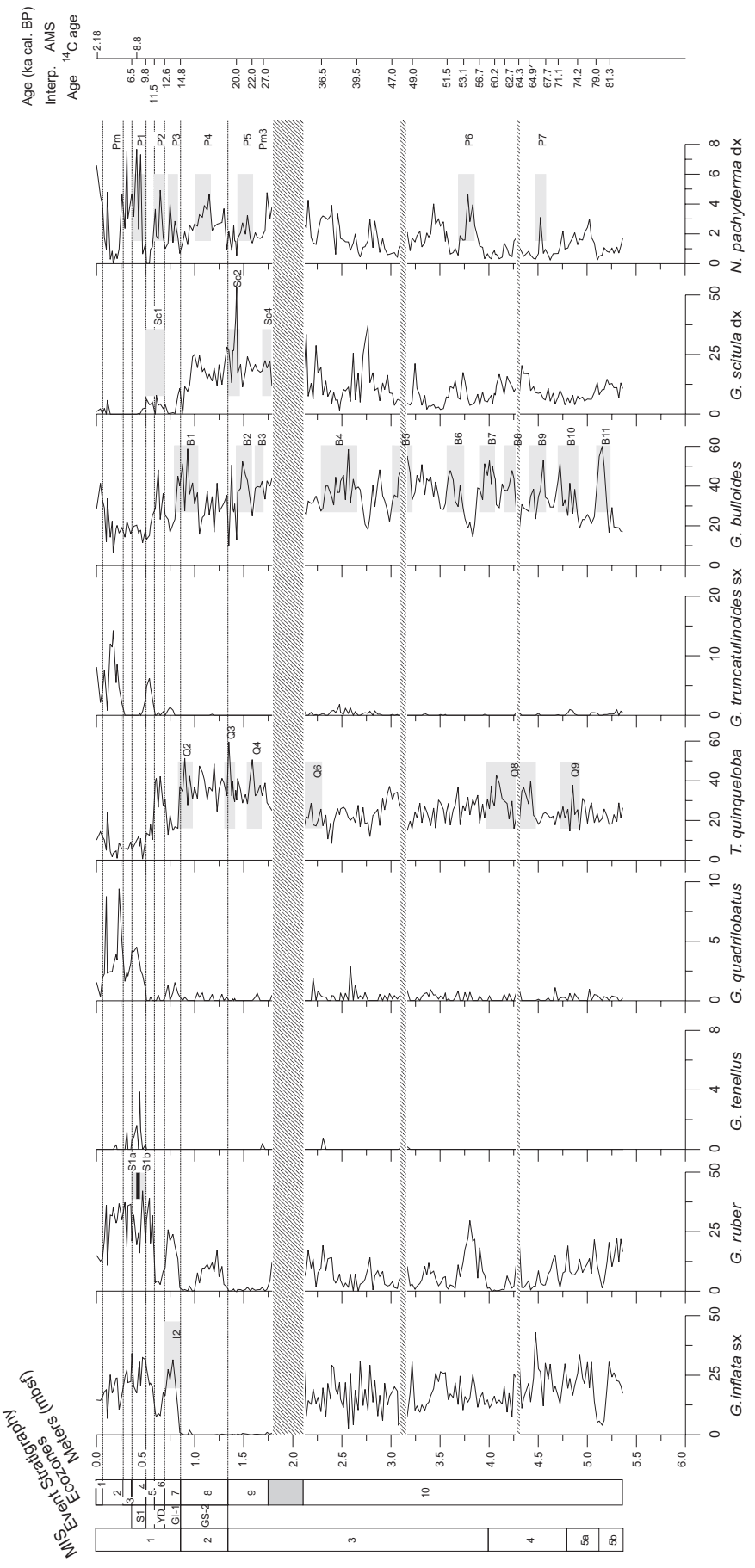
Age (ka cal. BP)
Interp. Age
AMS ^{14}C age
MIS Event Stratigraphy Ecozones Meters (mbsf)
G.inflata sx
G. ruber
G. tenellus
G. quadrilobatus
T. quinqueloba
G. truncatulinoides sx
G. bulloides
G. scitula dx
N. pachyderma dx
Pm
P1
P2
P3
P4
P5
Pm3
P6
P7
Sc1
Sc2
Sc4
B1
B2
B3
B4
B5
B6
B7
B8
B9
B10
B11
Q2
Q3
Q4
Q6
Q8
Q9
S1a
S1b
I2
S1
YD
GI-1
GS-2

Table 1
Tie points used for age–depth profile of core C08.

Events	mbsf	Age (ka cal. BP)	References
AMS ^{14}C–	0	2.18	This work
Top S1	0.360	6.5	Casford et al. (2002) (Aegean Sea)
AMS ^{14}C–	0.440	8.8	This work
Base S1	0.470	9.8	Casford et al. (2002) (Aegean Sea)
Top YD	0.570	11.5	Asioli et al. (2001) (Adriatic Sea)
Base YD	0.700	12.6	Asioli et al. (2001) (Adriatic Sea)
Base GI-1	0.850	14.8	Asioli et al. (2001) (Adriatic Sea)
Base GS-2	1.350	20	Andersen et al. (2006) (Greenland Ice core)
AMS ^{14}C–	1.430	25.1	This work (not used in the age model)
Base B2	1.540	22	Pérez-Folgado et al. (2003) (Alboran Sea)
Top B3	1.620	25.3	Perez-Folgado et al. (2004) (Alboran Sea)
Base B3	1.720	27	Pérez-Folgado et al. (2003) (Alboran Sea)
Top B4	2.360	36.50	Perez-Folgado et al. (2004) (Alboran Sea)
Base B4	2.690	39.50	Perez-Folgado et al. (2004) (Alboran Sea)
Top B5	3.040	47.00	Perez-Folgado et al. (2004) (Alboran Sea)
Base B5	3.200	49.00	Perez-Folgado et al. (2004) (Alboran Sea)
Top B6	3.570	51.50	Perez-Folgado et al. (2004) (Alboran Sea)
Base B6	3.740	53.10	Perez-Folgado et al. (2004) (Alboran Sea)
Top B7	3.875	56.70	Perez-Folgado et al. (2004) (Alboran Sea)
Base B7	4.075	60.20	Perez-Folgado et al. (2004) (Alboran Sea)
Top B8	4.125	62.70	Perez-Folgado et al. (2004) (Alboran Sea)
Base B8	4.275	64.30	Perez-Folgado et al. (2004) (Alboran Sea)
Top B9	4.430	64.90	Perez-Folgado et al. (2004) (Alboran Sea)
Base B9	4.610	67.70	Perez-Folgado et al. (2004) (Alboran Sea)
Top B10	4.680	71.10	Perez-Folgado et al. (2004) (Alboran Sea)
Base B10	4.910	74.20	Perez-Folgado et al. (2004) (Alboran Sea)
Top B11	5.080	79.00	Perez-Folgado et al. (2004) (Alboran Sea)
Base B11	5.210	81.30	Perez-Folgado et al. (2004) (Alboran Sea)

The *Globigerina bulloides* eco-bioevents B3–B11 follow Perez-Folgado et al. (2003, 2004).

coiled, and by the absence of *N. pachyderma* right coiled and very low amounts of *T. quinqueloba*.

The eco-biozone 6 is marked by the absence of *G. ruber* and *G. inflata* left coiled, by distinct peaks of *T. quinqueloba* and *N. pachyderma* right coiled. This eco-biozone corresponds to the Younger Dryas event, according to Sprovieri et al. (2003).

Eco-biozone 7 is defined by the increase in the abundance of *G. ruber* and *G. inflata*, by the absence of *T. quinqueloba*, and by a distinct peak of *G. quadrilobatus*, corresponding to the warmer (interstadial) GI-1.

According to Sprovieri et al. (2003) in eco-biozone 8 the persistent high abundance of cold species permit correlation of this interval with the GRIP GS-2 period. In particular this eco-biozone is dominated by *T. quinqueloba*, *N. pachyderma* right coiled, *G. scitula*, and by absence of *G. inflata* left coiled and rare *G. ruber*. The base of this eco-biozone approximates to the base of MIS 2 (Pérez-Folgado et al., 2003) (Fig. 3).

Eco-biozone 9 is characterized by the concomitant absence of *G. inflata* left coiled and *G. ruber*, by low abundance of *N. pachyderma* right coiled, and by high abundance of *T. quinqueloba* and *G. scitula* right coiled.

Eco-biozone 10 is clearly marked by the progressive downward increase in abundance of *G. inflata* left coiled and *G. ruber* and the progressive decrease of *G. scitula* right coiled, *T. quinqueloba*, *N. pachyderma* right coiled and *N. dutertrei* right coiled (Fig. 3). No distinctive or drastic events in the planktonic faunal patterns are visible towards the base of the studied record but only short-term oscillation in *G. bulloides* (B3–B11 eco-bioevents; the adopted sampling resolution unfortunately did not allow the recognition of the *G. bulloides* B8 eco-bioevent), *G. inflata* left coiled (I3–I5 eco-bioevents), *T. quinqueloba* (Q4–Q9 eco-bioevents) and *N. pachyderma* right coiled (P5–P7 eco-bioevents), clearly associated to the millennial climatic oscillations occurring in the last 80 kyr (Perez-Folgado et al., 2004). According to Perez-Folgado et al. (2004) *G. bulloides* eco-bioevents B7 and B10 are placed at the MIS 4/MIS 3 and MIS4/MIS 5a transitions, respectively. Finally, also according to Perez-Folgado et al. (2004), the lowermost part of the studied record lies within the eco-bioevent B11 and within the uppermost part of MIS 5b (Fig. 3).

5.2. Age model

The identified foraminiferal marker events, regarded to reflect major changes in oceanographic conditions and already recognized in the central and Western Mediterranean (Jorissen et al., 1993; Capotondi et al., 1999; Asioli et al., 2001; Sbaffi et al., 2004; Sprovieri et al., 2003; Perez-Folgado et al., 2004; Geraga et al., 2005), were used, together with two ^{14}C-AMS dates (Table 1), to constrain the age of core CIESM C08 and strengthen the correlations between the various Mediterranean sites. In particular, we used the age model proposed by Perez-Folgado et al. (2003, 2004) for the Alboran Sea to recognize the top and base of the eco-bioevents recorded in the core C08, the age model proposed by Asioli et al. (2001) for the Adriatic Sea, to identify the Younger Dryas and the base of the Greenland isotope interstadial 1 (GI-1), and the age model of Andersen et al. (2006) for the NGRIP record to distinguish the Greenland isotope stadial 2 (GS-2) (Table 1).

During the recovery of the core, a small amount of the core top may have been lost, which is seen by the ^{14}C-AMS dating of 2.18 ka cal. BP at the top of the core and by comparing the planktonic foraminiferal contents of the studied record with those reported by Sprovieri et al. (2003) for ODP-Site 963 (Sicily Channel). This seems to confirm that the sedimentation of the last 2000 years is not preserved in CIESM C08 core.

The turbidite layers T1, T2 and T3 have been taken into account to construct the age model curve and to estimate sedimentation rates. A second-order polynomial is needed to describe the age–depth relationship for the studied record, indicating an average sedimentation rate of ~7 cm/kyr from the base to the top and four main excursions (Fig. 4).

In order to confirm the reliability of the proposed age model, a three-step validation process was performed. First, the visual comparison, in time domain, between *G. bulloides* distribution pattern of Perez-Folgado et al. (2004) for the Alboran Sea and the patterns in core CIESM C08 (Fig. 4), confirmed the tuning accuracy.

The second step consisted of the comparison of colour reflectance record at 550 nm (%) of core CIESM C08 with the record of the ODP-Site 964 (Fig. 5), drilled in the Ionian Sea at 3650 mbsl and astronomically calibrated (Lourens, 2004). Using the proposed age–depth profile (Fig. 4), the colour reflectance record of the studied core was plotted against time by a cubic spline interpolation method. This comparison (Fig. 5) shows that the large-scale reflectance fluctuations in core CIESM C08 not only have a similar pattern to those reported in the Ionian Sea record but also encompass absolute values in the same range ($\pm$10 nm).

Fig. 3. Relative abundance of selected planktonic foraminifera from core CIESM C08 plotted vs depth (m bsf). Eco-biozones 1–10 are identified, according to Sprovieri et al. (2003), slightly modified. Grey bands show the selected eco-bioevents proposed by Perez-Folgado et al. (2003, 2004). Event stratigraphy according to GRIP. MIS and age scale according to Perez-Folgado et al. (2003, 2004). Associated with the *G. ruber* curve, two grey bands interbedded with the black one correspond to the position of sapropel 1 equivalent with S1a and S1b. The banded areas indicate the position of the turbidite layers.

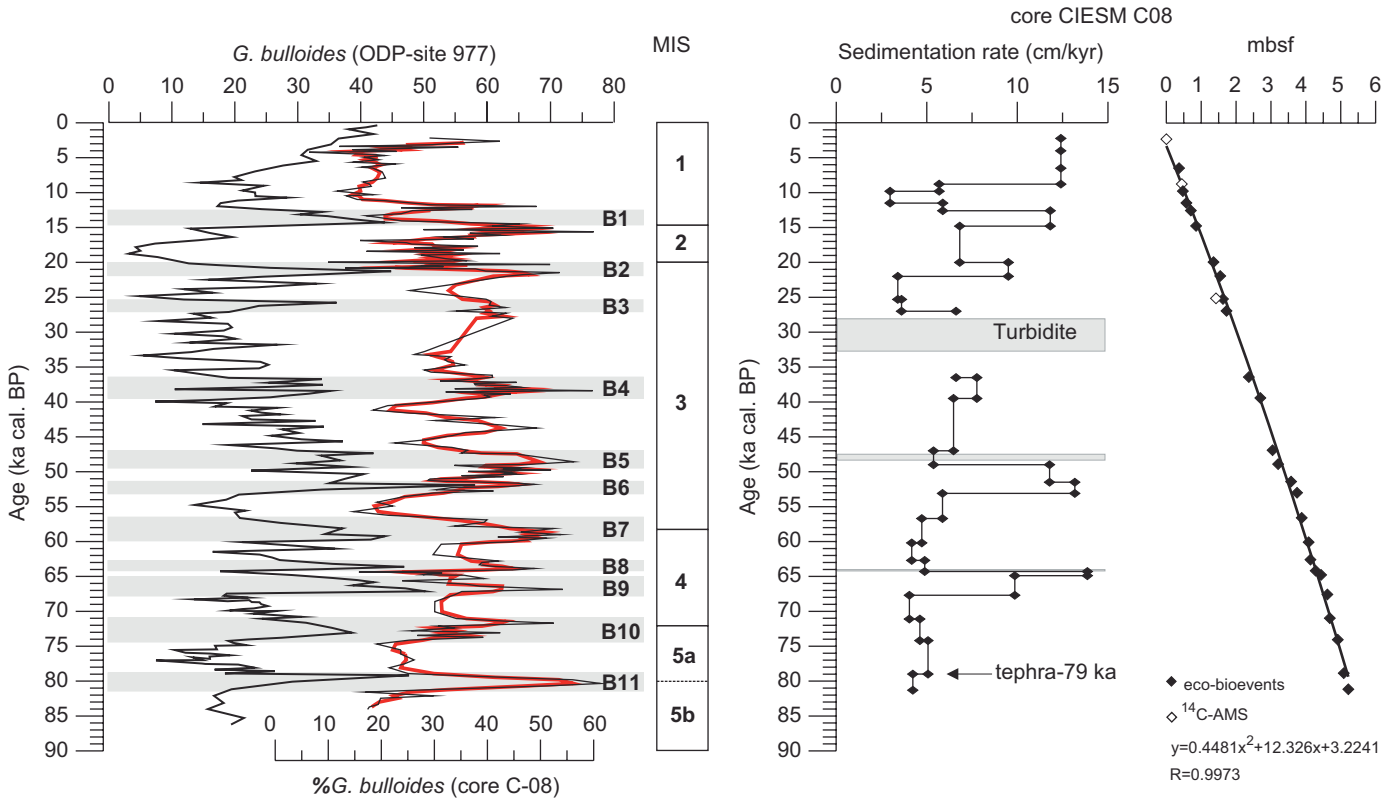

Fig. 4. From left to right: comparison in time domain between the distribution pattern of *G. bulloides* from ODP-Site 977 (Perez-Folgado et al., 2004) and the studied core CIESM C08 (the red curve represents a 3-point average). The grey bands and the labels B1 to B11 are from Perez-Folgado et al., (2004). Age–depth profile and sedimentation rates of core CIESM C08. The adopted tie-points by eco-bioevents and by ^{14}C-AMS data are shown respectively with black boxes and white boxes.

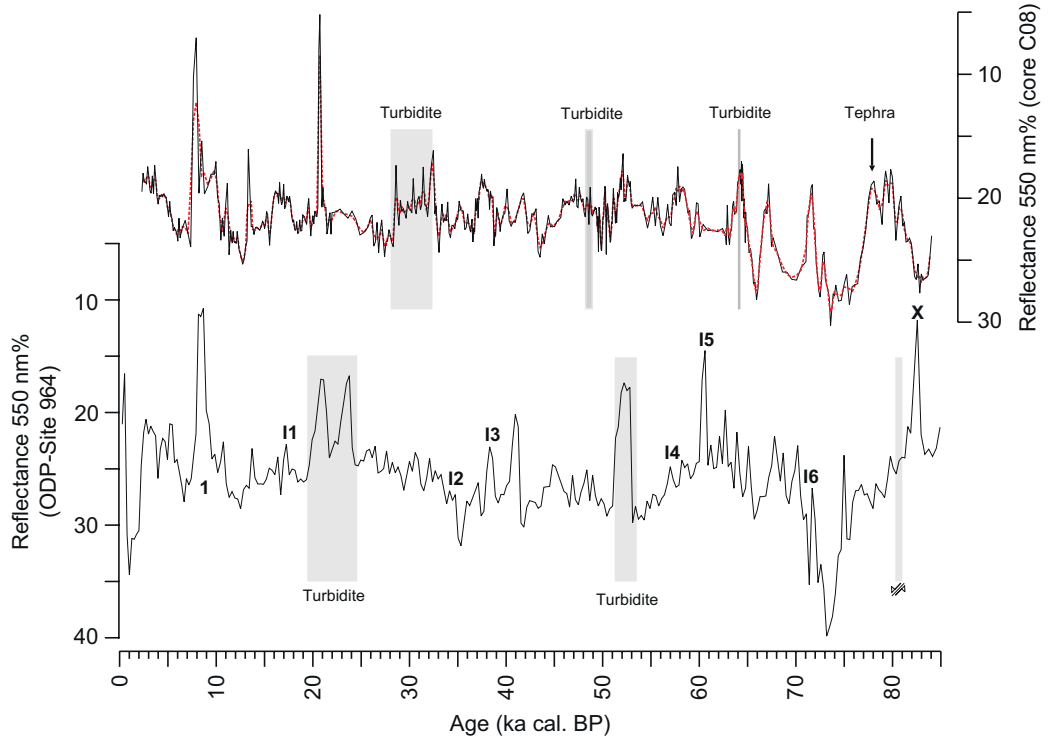

Fig. 5. Comparison in time domain of colour reflectance data of core CIESM C08 (black curve, with 3-point average, red dotted curve) with reflectance data after Lourens (2004) for ODP-Site 964 (thin black curve) in the Ionian Sea. The numbers I1-I6 indicate tephra layers in ODP-Site 964, and 1 and X indicate the position of the sapropel 1 and X, respectively.

Lourens (2004) used the reflectance parameter to detect sapropel and tephra layers in the Ionian Sea (Mediterranean area), which in turn, are tuned to the insolation curve of Laskar et al. (2004). According to Hilgen et al. (2003 and references therein), the Neogene marine successions (on land and in ODP-sites) in the Mediterranean area are often characterized by the cyclic recurrence of sapropels layers and sedimentary patterns, clearly forced by variation in astronomical parameters (Hilgen, 1991a, b; Hilgen et al., 1999, 2003; Hilgen and Krijgsman, 1999; Lourens et al., 1996a, b, 1998 and references therein). Therefore it is not surprising that the cyclic patterns in the colour reflectance records relative to two adjacent deep environmental Mediterranean areas are similar. There is also a strong similarity between the colour reflectance signature of the sapropel S1 equivalent, recorded in the studied core, with the sapropel S1 colour reflectance signature in the Ionian basin. Nevertheless, some of the minimum peaks of the ODP-Site 964 reflectance record, related to the occurrence of tephra layers, are not present in the studied core. This is clearly due to the different spatial distribution of the tephra layers in the Mediterranean. On the whole, the good visual correlation obtained between the two records supports the validity of the age model based on the identified eco-bioevents and ^{14}C-AMS calibrations.

The third control step consisted in the comparison of the *G. ruber* distribution with the δ^{18}O NGRIP ice core record. The ecological features of *G. ruber* associated with warm and oligotrophic surface waters have been established in several oceanographic settings (Hemleben et al., 1989; Pujol and Vergnaud-Grazzini, 1995; Watkins et al., 1996; Zaric et al., 2005). Moreover, several authors (Sprovieri, 1991; Sanvoisin et al., 1993; Sprovieri et al., 2003, 2006) have confirmed the utility of relative abundance fluctuations of *G. ruber* as recorders of climatic variability and for age model proxies. The *G. ruber* and δ^{18}O NGRIP ice core records exhibit a remarkable agreement, with the identification of the Heinrich events (H1–H6) and of the Younger Dryas (YD) in the studied record, which further supports the reliability of our tuning (Fig. 6). The observed strong link between δ^{18}O of Greenland ice cores, a proxy for Greenland air temperature, and the thermal character of surface water masses of Mediterranean area has been previously established in several papers and is usually explained by teleconnective phenomena (Rohling et al., 1998; Cacho et al., 1999, 2000; Sbaffi et al., 2004; Combourieu Nebout et al., 2002; Moreno et al., 2002; Rohling et al., 2002).

The proposed age model also was adopted to plot paleomagnetic data against time (Fig. 7). We note that the time interval spanned by the core encompasses three known geomagnetic excursions (the Mono Lake, dated at 33 ± 1 ka; the Laschamp, dated at 41 ± 1 ka; the Norwegian-Greenland Sea, dated at 61 ± 2 ka; see Lund et al., 2006). Nevertheless in the paleomagnetic record of CIESM C08 core there is no clear marked oscillation that can be ascribed to any of such excursions. The lack of paleomagnetic evidence for geomagnetic excursions in this record may be due to a relatively low sedimentation rate (cf. 5.1, Fig. 4), which may have resulted in a prolonged time interval for the lock-in of the natural remanence of the sediments (Roberts and Winklhofer, 2004; Sagnotti et al., 2005), as well as response functions of the SQUID sensors in the magnetometer (i.e. Oda and Shibuya, 1996; Guyodo et al., 2002). Despite the suggested smoothing of the paleomagnetic signal, the well-defined paleomagnetic data of core CIESM-08 provide an original source of information to improve the confidence of geomagnetic paleosecular variation reconstructions in the Mediterranean for the last 83 kyr.

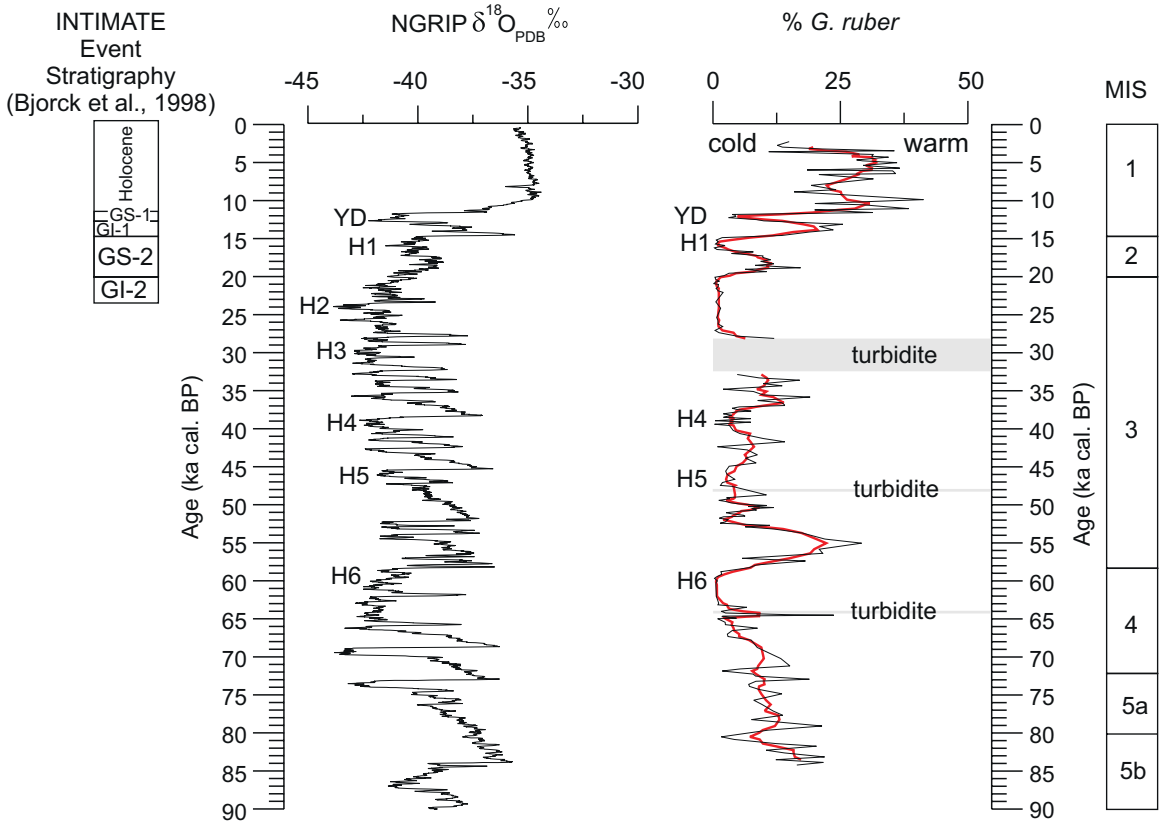

Fig. 6. Distribution pattern of *G. ruber* (thin black line) with 3-point average (red line) of core CIESM C08 plotted versus δ^{18}O NGRIP (NGRIP members, 2004) record, with 7-point average, in time domain. Labels H1 to H6 indicate the position of Heinrich events and the label YD the position of the Younger Dryas.

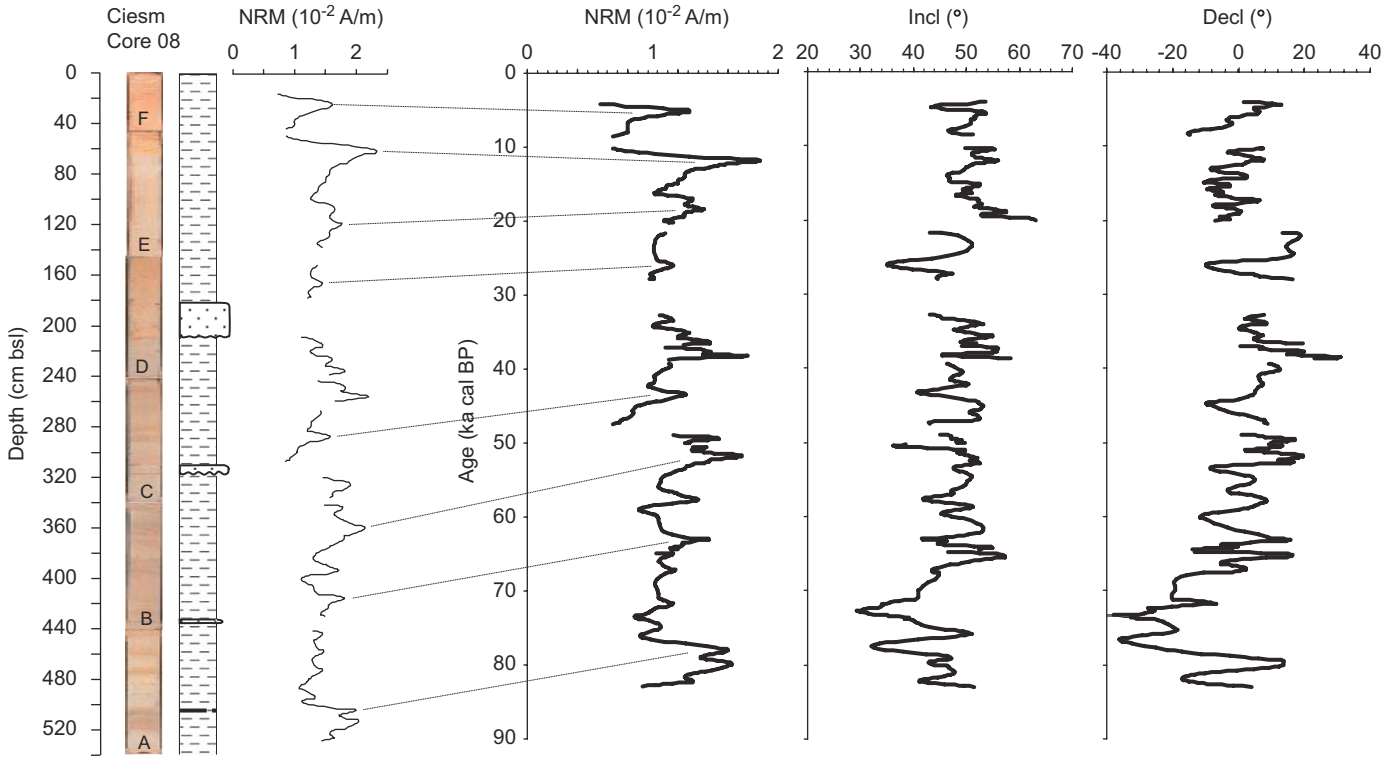

Fig. 7. Downcore plot of paleomagnetic data. The NRM intensity plotted versus stratigraphic depth is shown beside to the main paleomagnetic data (NRM, inclination and declination of the characteristic remanent magnetization) plotted versus age, according to the independently derived age model discussed in this study.

5.3. *Provenance and ages of turbidite events*

The size population of grains, the grain fabric, the high content in bioclasts (gastropod, bivalve and echinoderm debris) and the features of the surfaces bounding T1, T2 and T3 turbidites lead us to infer a distant source of transported material, since it seems to have been remobilized from areas of high productivity. Both the slope of the Median Ridge and the southern Cornaglia slope (Fig. 1) can be ruled out as possible source areas for these sand-rich bioclastic turbidites, since they are too deep, respectively 1300 and 1000 mbsl. Sartucya 6 diving survey (Mascle et al., 2001a) showed that the base of the southern slope of the Median Ridge (2270–1940 mbsl) is draped with mud, shaped by current bed-forms, while the upper slope (1990–1640 mbsl) is characterized by conglomerates and sandstone layers outcropping from the mud, then volcanic rocks. The lithology to the southern Cornaglia slope was described during the Sarcya 2 submersible diving (Mascle et al., 2001a) by the occurrence of pelagic mud at 2500–2250 mbsl, and cemented coarse material on the steep slopes (2250–2060 mbsl). Although several canyons are noted along the Southern Cornaglia slope (Brocard, 2001), they enter the Sentinelle Valley seaward to the core site and thus they possibly feed the deepest parts of the basin.

Thus, we must infer that the Bizerte Canyon acted as the main conduit to transport the bioclastic sand from high productivity areas on the Tunisian plateau (Fig. 1), inferring transport of more than 50 km before sedimenting. As highlighted by many authors (Walker, 1967; Normark et al., 1984; Reading and Richards, 1994) gentle gradient slopes or pre-existing slope conduits can drive very efficient density currents (Damuth and Flood, 1984; Richards et al., 1998) able to cover long distances quickly and to "segregate the original grain populations into distinct and relatively well-sorted facies types with distances" (Mutti et al., 1999). The beds occurring in C08 core, in particular T1 and T2, could correspond to the facies tract F7 in Mutti et al. (1999), composed predominantly of medium to fine grained well-sorted sand. In fact in this model, which associates the horizontal grain-size partition of the deposit with the different degrees of flow efficiency, the F7 facies tract consists of medium to fine sand overlying a mm-thick traction carpet that accounts for the development of an erosion surface at the base. This model may explain why T1 and T2 turbidites lack parallel and ripple lamination and pelitic division and why a wide stratigraphic gap occurs at the T1 base (and likely at the T2 base).

The turbidite layers in CIESM core C08 are confined in the lower 4 m of the core and their thicknesses increase upward, peaking at T1 (Fig. 2) and pointing to a general regressive trend. Through the age model scheme of CIESM C08 core here proposed, it is possible to date T layers, respectively, at 28 ka cal. BP (T1), 48 ka cal. BP (T2) and 64 ka cal. BP (T3) (Fig. 5), thus during the MIS 4 and MIS 3. The emplacement of T1 event bed caused the removal of an undefined thickness of hemipelagic mud corresponding to a time span of about 4 kyr (Fig. 4).

Plotting their inferred age on sea-level curve relative to the last 100 kyr (Waelbroeck et al., 2002; Imbrie et al., 1984), T2 and T3 turbidite event beds appear to correlate with two relative sea-level low stands, and T1 with regressing sea level that led to the maximum low stand at ~20 kyr (Fig. 8). This observation seems to agree with the most accepted stratigraphic models of deep-sea deposition (Normark et al., 1998). Thus, the part of the basin fan intercepted by the CIESM core C08 was actively fed with bioclastic sand deposition during the relative sea-level minimum and increased its transport efficiency following the sea level lowering. Nevertheless the CIESM core C08 does not record any further sand deposition during the MIS 2 sea-level low stand. A rapid starvation in detritus supply occurred in this area beginning at 28 ka cal. BP and this sector of the fan fossilized below a drape of hemipelagic mud. It is reasonable to suppose that during this phase, this sector of the fan acted mainly as a bypass area. Thus, any possible sand flow would have been deposited basinward.

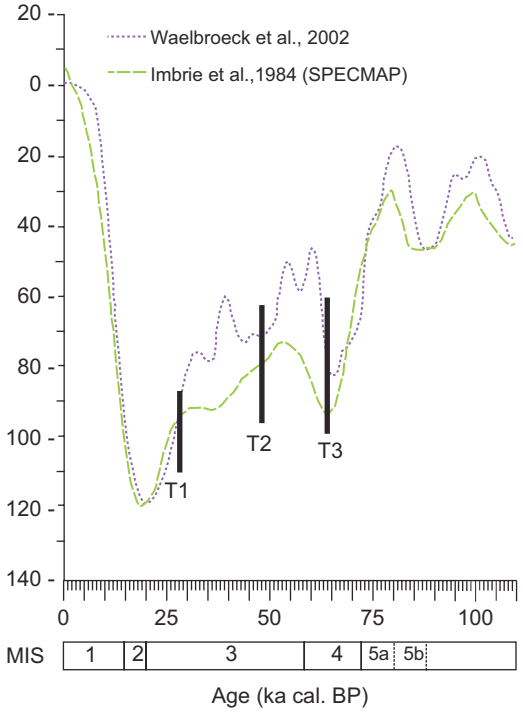

Fig. 8. The inferred age of turbidite sand beds is plotted relative to the sea level over the past 100 kyr (from Antonioli et al., 2004, modified). T2 and T3 turbidites occur during two relative low-stand phases of MIS 4 and 3, while the T1 turbidite falls during the last sea level lowering of MIS 3.

6. Conclusions

The multidisciplinary study of core C08, recovered from the deep sector of the Sardinia Channel, based on planktonic foraminiferal assemblages, petrophysical (MS, Grape density, 550 nm% reflectance) and paleomagnetic (NRM Intensity, ChRM Inclination, ChRM Declination) data, provides an integrated stratigraphic reference record for the Western Mediterranean Sea that spans back for about 83 kyr. The most important eco-bioevents widely used for large-scale correlation in the Western Mediterranean area provide a detailed correlation with the eco-stratigraphic reconstruction proposed by Perez-Folgado et al. (2003, 2004) for the Alboran Sea.

In particular, the relative abundance of selected climate-sensitive planktonic foraminiferal species have led us to identify several eco-bioevents in *G. bulloides* (B3–B11 eco-bioevents), *G. inflata* left coiled (I3–I5 eco-bioevents), *T. quinqueloba* (Q4–Q9 eco-bioevents) and *N. pachyderma* right coiled (P5–P7 eco-bioevents). According to Perez-Folgado et al. (2003, 2004), the documented short-term oscillations in the planktonic foraminiferal fauna are clearly associated with the stadial/interstadial excursions over the last 80 kyr, allowing the identification in core C08 of the S1, YD, GI-1 and GS-2 climatic events in the last 23 kyr. Furthermore, the comparison between the $\delta^{18}O$ NGRIP ice core record and *G. ruber* distribution in core C08 suggests that the Heinrich events (H1–H6) and the Younger Dryas (YD) are also recorded.

The eco-bioevents chronology combined with ^{14}C-AMS data were used to define a detailed age model that was compared by means of reflectance parameters to the astronomically tuned age model proposed for the Ionian Sea ODP-Site 964 (Lourens, 2004). The similarity between the two reflectance records plotted vs time validates the age model of the studied record, especially in the time intervals between 2–25 and 60–83 kyr. This methodology, if confirmed with further study, could prove a powerful tool for reliably correlating marine records between comparable deep-sea settings.

The sector of the Sentinelle Valley intercepted by the CIESM core C08 has been sporadically fed by sand turbidite flows, likely driven along the Bizerte Canyon from the northern sector of the Tunisian Plateau, during relative sea-level minimum and sea-level fall of MIS 4 and 3. This sector of the basin was reached by three sand deposition events of increasing thickness between 64 and 28 kyr. After about 28 kyr this part of the fan was deactivated and fossilized beneath a carpet of hemipelagic mud at a sedimentation rate of about 7 cm/kyr.

The combined logging of sedimentological, petrophysical and paleomagnetic data of core CIESM C08, integrated with eco-biozone stratigraphy, could provide an important source of information to improve the confidence of correlations in the Mediterranean over the last 83 kyr. In this framework, future efforts will be focused on the comparison of the ChRM directions obtained for the core with the other available European geomagnetic paleosecular variation records, as well as on the reconstruction of a relative geomagnetic paleointensity curve, to establish a Mediterranean paleomagnetic reference record to be used as an original dating tool for coeval sequences of this region.

Acknowledgements

The authors gratefully acknowledge Lucas J. Lourens of the University of Utrecht for original reflectance data of Ionian cores and Carmine Lubritto of CIRCE Radiocarbon Laboratory, (Caserta, Italy) for ^{14}C-AMS dates. Sincere thanks are also due to Laura Giuliano, who involved some of us in CIESM SUB2 cruise. Captain Vincenzo Lubrano di Lavadera and the crew of R/V *Urania*, who sailed despite a very rough sea, are kindly acknowledged. Two anonymous reviewers and Patricia Scalfani are sincerely thanked for the comments and the English revision to the manuscript.

References

Andersen, K.K., Svensson, A., Johnsen, S.J., Rasmussen, S.O., Bigler, M., Rothlisberger, R., Ruth, U., Siggaard-Andersen, M.L., Steffensen, J.P., Dahl-Jensen, D., Vinther, B.M., Clausen, H.B., 2006. The Greenland ice core chronology 2005, 15–42 ka. Part 1: Constructing the time scale. Quaternary Science Reviews 25, 3246–3257.

Antonioli, F., Bard, E., Potter, E.K., Silenzi, S., Improta, S., 2004. 215-ka history of sea-level oscillations from marine and continental layers in Argentarola Cave speleothems (Italy). Global and Planetary Change 43 (1–2), 57–78.

Arason, P., Levi, S., 1990. Models of inclination shallowing during sediment compaction. Journal of Geophysical Research 95, 4481–4499.

Ariztegui, D., Asioli, A., Lowe, J.J., Trincardi, F., Vigliotti, L., Tamburini, F., Chondrogianni, C., Accorsi, C.A., Bandini Mazzanti, M., Mercuri, A.M., Van der Kaars, S., McKenzie, J.A., Oldfield, F., 2000. Palaeoclimate and the formation of sapropel S1: inferences from Late Quaternary lacustrine and marine sequences in the central Mediterranean region. Palaeogeography, Palaeoclimatology, Palaeoecology 158, 215–240.

Asioli, A., Trincardi, F., Lowe, J.J., Oldfield, F., 1999. Short-term climate changes during the last Glacial–Holocene transition: comparison between Mediterranean and North Atlantic records. Journal of Quaternary Science 4, 3732–3781.

Asioli, A., Trincardi, F., Lowe, J.J., Ariztegui, D., Langone, L., Oldfield, F., 2001. Sub-millennial scale climatic oscillations in the central Adriatic during the Lateglacial. Paleoceanographic implications. Quarternary Science Review 20, 1201–1221.

Beaudouin, C., Dennielou, B., Melki, T., Guichard, F., Kallel, N., Berné, S., Huchon, A., 2004. The Late-Quaternary climatic signal recorded in a deep-sea turbiditic levee (Rhône Neofan, Gulf of Lions, NW Mediterranean): palynological constraints. Sedimentary Geology 172 (1–2), 85–97.

Bouma, A.H., 1962. Sedimentology of Some Flysch Deposits, a Graphic Approach to Facies Interpretation. Elsevier, Amsterdam.

Brocard, G., 2001. Le canal de Sardaigne au Néogène: analyse morphologique et structurale. Apports de la bathymétrie multifaisceaux et des plongées Sarcya et Sartucya. In: Mascle, G., Tricart, P. (Eds.), Le Canal de Sardaigne: les plongées Cyana, vol. 34. Geologie Alpine, Mém. H.S., pp. 115–166.

Bryden, H.L., Kinder, T.H., 1991. Steady two-layer exchange through the Strait of Gibraltar. Deep-Sea Research 38 (1), S445–S463.

Buccheri, G., Capretto, G., Di Donato, V., Esposito, P., Ferruzza, G., Pescatore, T.S., Russo Ermolli, E., Senatore, M.R., Sprovieri, M., Bertoldo, M., Carella, D., Madonia, G., 2002. A high resolution record of the last deglaciation in the southern Tyrrhenian Sea: environmental and climatic evolution. Marine Geology 186, 447–470.

Cacho, I., Grimalt, J.O., Pelejero, C., Canals, M., Sierro, F.J., Flores, J.A., Shackleton, N., 1999. Dansgaard–Oeschger and Heinrich event imprints in Alboran Sea paleotemperatures. Paleoceanography 14 (6), 698–705.

Cacho, I., Grimalt, J.O., Sierro, F.J., Shackleton, N.J., Canals, M., 2000. Evidence for enhanced Mediterranean thermohaline circulation during rapid climate coolings. Earth and Planetary Science Letters 183, 417–429.

Cacho, I., Grimalt, J.O., Canals, M., Sbaffi, L., Shackleton, N.J., Schönfeld, J., Zahn, R., 2001. Variability of the western Mediterranean Sea surface temperature during the last 25,000 years and its connection with the Northern Hemisphere climatic changes. Paleoceanography 16, 40–52.

Capotondi, L., Borsetti, A.M., Morigi, C., 1999. Foraminiferal eco-biozones, a high resolution proxy for the late Quaternari biochronology in the central mediterranean. Marine Geology 153, 253–274.

Casford, J.S.L., Rohling, E.J., Abu-Zied, R., Cooke, S., Fontanier, C., Leng, M., Lykousis, V., 2002. Circulation changes and nutrient concentrations in the late Quaternary Aegean Sea: a nonsteady state concept for sapropel formation. Paleoceanography 17, 1–11.

Combourieu Nebout, N., Turon, J.L., Zahn, R., Capotondi, L., Londeix, L., Pahnke, K., 2002. Enhanced aridity and atmospheric high-pressure stability over the western Mediterranean during the North Atlantic cold events of the past 50 kyr. Geology 30, 863–866.

Curry, W.B., Shackleton, N.J., Richter, C., Bralower, T.J., 1995. Shipboard Scientific Party. In: Proceedings of the Ocean Drilling Program, Initial Reports, 154, College Station, TX, Ocean Drilling Program, 1111pp.

Damuth, J.E., Flood, R.D., 1984. Morphology, sedimentation processes, and growth pattern of the Amazon Deep-Sea fan. Geo-Marine Letters 3 (2–4), 109–117.

Dansgaard, W., Johnsen, S.J., Clausen, H.B., Dahl-Jensen, D., Gunderstrup, N.S., Hammer, C.V., Hvidberg, C.S., Steffensen, J.P., Sveinbjornsdottin, A.E., Jouzel, J., Bard, G., 1993. Evidence for general instability of past climate from a 250 kyr ice-core record. Nature 364, 218–220.

Deamer, G.A., Kodama, K.P., 1990. Compaction-induced inclination shallowing in synthetic and natural clayrich sediments. Journal of Geophysical Research 95, 4511–4529.

Ducassou, E., Capotondi, L., Murat, A., Bernasconi, S., Mulder, T., Gonthier, E., Migeon, S., Duprat, J., Giraudeau, J., Mascle, J., 2007. Multiproxy Late Quaternary stratigraphy of the Nile deep-sea turbidite system—towards a chronology of deep-sea terrigeneous systems. Sedimentary Geology 200 (1–2), 1–13.

Emeis, K.C., Emeis, H., Schulz, U., Struck, M., Rossignol-Strick, H., Erlenkeuser, M.W., Howell, D., Kroon, A., Mackensen, S., Ishizuka, T., Oba, T., Sakamoto, I., Koizumi, I., 2003. Eastern Mediterranean surface water temperatures and δO^{18} composition during deposition of sapropels in the late Quaternary. Paleoceanography 18, 1–18.

GEBCO, 1997. General Bathymetric Chart of the Oceans, British Oceanographic Data Centre, British Cartographic Data Centre, http://www.bodc.ac.uk/projects/international/gebco/.

Geraga, M., Tsaila-Monopolis, S., Ioakim, C., Papatheodorou, G., Ferentinos, G., 2005. Short-term climate changes in the southern Aegean Sea over the last 48,000 years. Palaeogeography, Palaeoclimatology, Palaeoecology 220, 311–332.

GRIP members, 1993. Greenland Ice-Core Project (GRIP) members, Climate instability during the last interglacial period recorded in the GRIP ice core. Nature 364, 203–207.

Guyodo, Y., Channell, J.E.T., Thomas Ray, G., 2002. Deconvolution of u-channel paleomagnetic data near geomagnetic reversals and short events. Geophysical Research Letters 29 (17), 1845.

Hemleben, C., Spindler, M., Anderson, O.R., 1989. Modern Planktonic Foraminifera. Springer, New York (pp. 1–363).

Heinrich, H., 1988. Origin and consequences of cyclic ice rafting in the Northeast Atlantic Ocean during the past 130,000 years. Quaternary Research 29, 142–152.

Hilgen, F.J., 1991a. Astronomical calibration of Gauss to Matuyama sapropels in the Mediterranean and implication for the geomagnetic polarity timescale. Earth Planetary Science Letters 104, 226–244.

Hilgen, F.J., 1991b. Extension of the astronomically calibrated (polarity) timescale to the Miocene–Pliocene boundary. Earth Planetary Science Letters 107, 349–368.

Hilgen, F.J., Krijgsman, W., 1999. Cyclostratigraphy and astrochronology of the Tripoli diatomite Formation (pre-evaporite Messinian Sicily, Italy). Terra Nova 11, 16–22.

Hilgen, F.J., Abdul Aziz, H., Krijgsman, W., Langereis, C.G., Lourens, L.J., Meulenkamp, J.E., Raffi, I., Steenbrink, J., Turco, E., van Vugt, N., Wijbrans, J.R., Zachariasse, W.J., 1999. Present status of the astronomical (polarity) time-scale for the Mediterranean Late Neogene. Philosophical Transactions of the Royal Society of London Series A (The Royal Society) 357, 1931–1947.

Hilgen, F.J., Abdul Aziz, H., Krijgsman, W., Raffi, I., Turco, E., 2003. Integrated stratigraphy and astronomical tuning of the Serravallian and lower Tortonian at Monte dei Corvi (Middle–Upper Miocene, northern Italy). Palaeogeography, Palaeoclimatology, Palaeoecology 199, 229–264.

Imbrie, J., Hays, J.D., Martinson, D.G., McIntyre, A., Mix, A.C., Morley, J.J., Pisias, N.G., Prell, W.L., Shackleton, N.J., 1984. The orbital theory of Pleistocene climate: support from a revised chronology of the marine δO^{18} record. In: Berger, A.L., et al. (Eds.), Milankovitch and Climate, Part I. Reidel, Dordrecht, pp. 269–305.

Iorio, M., Sagnotti, L., Angelino, A., Budillon, F., D'Argenio, B., Dinare's-Turell, J., Macrí, P., Marsella, E., 2004. High-resolution petrophysical and palaeomagnetic study of late-Holocene shelf sediments, Salerno Gulf, Tyrrhenian Sea. The Holocene 14 (3), 426–435.

Jorissen, F.J., Asioli, A., Borsetti, A.M., de Visser, L., Hilgen, F.J., Rohiling, E.J., van der Borg, K., Vergnaud-Grazzini, C., Zachariasse, W.J., 1993. Late Quaternary central Mediterranean biochronology. Marine Micropaleontology 21, 169–189.

Kenyon, N.H., Klaucke, I., Millington, J., Ivanov, M.K., 2002. Sandy submarine canyon-mouth lobes on the western margin of Corsica and Sardinia, Mediterranean Sea. Marine Geology 184, 69–84.

Kirschvink, J.L., 1980. The least-square line and plane and the analysis of paleomagnetic data. Geophysical Journal of the Royal Astronomical Society 62, 699–718.

Laskar, M., Gastineau, F., Joutel, B., Levrard, P., Robutel, 2004. A new astronomical solution for the long term evolution of the insolation quantities of Mars. Lunar and Planetary Science XXXV, 1–2.

Lourens, L.J., 2004. Revised tuning of Ocean Drilling Program Site 964 and KC01B (Mediterranean) and implication for the $\delta^{18}O$, tephra, calcareous nannofossil, and geomagnetic reversal chronologies of the past 1.1 Myr. Paleocenography 19, 3010.

Lourens, L.J., Hilgen, F.J., Zachariasse, W.J., Van Hoof, A.A.M., Antonarakou, A., Vergnaud-Grazzini, C., 1996a. Evaluation of the Plio-Pleistocene astronomical time scale. Paleoceanography 11, 391–413.

Lourens, L.J., Hilgen, F.J., Raffi, I., Vergnaud-Grazzini, C., 1996b. Early Pleistocene chronology of the Vrica section (Calabria, Italy). Paleoceanography 11, 797–812.

Lourens, L.J., Hilgen, F.J., Raffi, I., 1998. Base of large Gephyrocapsa and astronomical calibration of Early Pleistocene sapropels in site 967 and hole 969D: solving the chronology problem of the Vrica section (Calabria, Italy). In: Robertson, A.H.F., Emeis, K.C., Richter, C., Camerlinghi, A. (Eds.), Proceedings of the ODP, Scientific Results, vol. 160, pp. 191–197.

Lund, S., Stoner, J.S., Channell, J.E.T., Acton, G., 2006. A summary of Brunhes paleomagnetic field variability recorded in Ocean Drilling Program cores. Physics of the Earth and Planetary Interiors 156, 194–204.

Mascle, G.H., Tricart, P., Bouillin, J.P., Compagnoni, R., Depardon, S., Mascle, J., Pecher, A., Peis, D., Rekhiss, F., Rolfo, F., Torelli, L., 2001a. Données de campagne des plongées Cyana Sarcya-Sartucya. In: Mascle, G., Tricart, P. (Eds.), Le Canal de Sardaigne: les plongées Cyana, Vol. 34. Geologie Alpine, Mém. H.S., pp. 7–113.

Mascle, G.H., Tricart, P., Torelli, L., Bouillin, J.P., Rolfo, F., Lapierre, H., Monié, P., Depardon, S., Mascle J., PeisD., 2001b. Evolution of the Sardinia Channel (Western Mediterranean): new constraints from a diving survey on Cornacya seamount off SE Sardinia. Marine Geology 179 (3–4), 179–201.

Mascle, G.H., Tricart, P., Torelli, L., Bouillin, J.P., Compagnoni, R., Depardon, S., Mascle, J., Pecher, A., Peis, D., Rekhiss, F., Rolfo, F., Bellon, H., Brocard, G., Lapierre, H., Monié, P., Poupeau, G., 2004. Structure of the Sardinia Channel: crustal thinning and tardi-orogenic extension in the Apenninic-Maghrebian orogen; results of the Cyana submersible survey (SARCYA and SARTUCYA) in the Western Mediterranean. Bulletin de la Société Géologique de France 175 (6), 607–627.

Millot, C., 1987. Circulation in the western Mediterranean Sea. Oceanology Acta 10, 143–149.

Moreno, A., Cacho, I., Canals, M., Prins, M.A., Sanchez-Goni, M.-F., Grimalt, J.O., Weltje, G.J., 2002. Saharan dust transport and high latitude glacial climatic variability: the Alboran Sea record. Quaternary Research 58, 318–328.

Mutti, E., Tinterri, R., Remacha, E., Mavilla, N., Angella, Fava, L., 1999. An Introduction to the Analysis of Ancient Turbidite Basins From an Outcrop Perspective, Continuing Education Coursr Note Series, vol. 39. American Association Petroleum Geologists, Tulsa, OK.

NGRIP Members, 2004. High-resolution record of Northern Hemisphere climate extending into the last interglacial period. Nature 431, 147–151.

Narcisi, B., Vezzoli, L., 1999. Quaternary stratigraphy of distal tephra layers in the Mediterranean—an overview. Global Planetary Change 21, 31–50.

Normark, W.R., Barnes, N.E., Coumes, F., 1984. Rhone deep-sea fan: a review. Geo-Marine Letters 3 (2–4), 155–160.

Normark, W.R., Piper, D.J.W., Hiscott, R.N., 1998. Sea level control on the textural characteristics and depositional architecture of the Hueneme and associated fan systems, Santa Monica Basin, California. Sedimentology 26, 749–774.

Oda, H., Shibuya, H., 1996. Deconvolution of long-core paleomagnetic data of Ocean Drilling Program by Akaike's Bayesian information criterion minimization. Journal of Geophysical Research 101, 2815–2834.

Palike, H., Frazier, J., Zachos, J.C., 2006. Extended orbitally forced palaeoclimatic records from the equatorial Atlantic Ceara Rise. Quaternary Science Reviews 25, 3138–3149.

Passariello, I., Marzaioli, F., Lubritto, C., Rubino, M., D'Onofrio, A., De Cesare, N., Borriello, G., Casa, G., Palmieri, A., Rogalla, D., Sabbarese, C., Terrasi, F., 2007. Radiocarbon sample preparation at the Circe AMS laboratory in Caserta. Italy Radiocarbon 49 (2), 225–232.

Pérez-Folgado, M., Sierro, F.J., Flores, J.A., Cacho, I., Grimalt, J.O., Zahn, R., Shackleton, N., 2003. Western Mediterranean planktonic foraminifera events and millennial climatic variability during the last 70 kyr. Marine Micropaleontology 48 (1–2), 49–70.

Perez-Folgado, M., Sierro, F.J., Flores, J.A., Grimalt, J.O., Zahn, R., 2004. Paleoclimatic variations in foraminifer assemblages from the Alboran Sea (Western Mediterranean) during the last 150 ka in ODP Site 977. Marine Geology 212, 113–131.

Peterson, L.C., Haug, G.H., Hughen, K.A., Rohl, U., 2000. Rapid changes in the hydrologic cycle of the tropical Atlantic during the Last Glacial. Science 290, 1947–1951.

Pinardi, N., Masetti, E., 2000. Variability of the large scale general circulation of the Mediterranean Sea from observations and modelling: a review. Palaeogeography, Palaeoclimatology, Palaeoecology 158, 153–173.

Principato, M.S., Giunta, S., Corselli, C., Negri, A., 2003. Late Pleistocene–Holocene planktonic assemblages in three box-cores from the Mediterranean ridge area (west–southwest of Crete): palaeoecological and palaeoceanographic reconstruction of sapropel S1 interval. Palaeogeography, Palaeoclimatology, Palaeoecology 190, 61–77.

Prins, M.A., Postma, G., Cleveringa, J., Cramp, A., Kenyon, N.H., 2000. Controls on terrigenous supply to the Arabian Sea durin the Late Quaternary: the Indus Fan. Marine Geology 169, 327–349.

Pujol, C., Vergnaud-Grazzini, C., 1995. Distribution patterns of live planktonic foraminifers as related to regional hydrography and productive system of the Mediterranean Sea. Marine Micropaleontology 25, 187–217.

Reading, H.G., Richards, M.T., 1994. The classification of deep-water siliciclastic depositional systems by grain size and feeder system. American Association Petroleum Geologists Bulletin 78, 792–822.

Richards, M., Bowman, M., Reading, H., 1998. Submarine-fan systems. I: Characterization and stratigraphic prediction. Marine and Petroleum Geology 15 (7), 671–689.

Roberts, A.P., Winklhofer, M., 2004. Why are geomagnetic excursions not always recorded in sediments? Constraints from post-depositional remanent magnetization lock-in modelling. Earth and Planetary Science Letters 227 (3–4), 345–359.

Rohling, E.J., Hayes, A., Kroon, D., De Rijk, S., Zachariasse, W.J., Eisma, D., 1998. Abrupt cold spells in the NW Mediterranean. Paleoceanography 13, 316–322.

Rohling, E.J., Cane, T.R., Cooke, S., Sprovieri, M., Boulabassi, I., Emeis, K.C., Schiebel, R., Kroon, D., Jorissen, F.J., Lorre, A., Kemp, A.E.S., 2002. African monsoon variability during the previous interglacial maximum. Earth and Planetary Science Letters 202, 61–75.

Rohling, E.J., Mayewski, P.A., Challenor, P., 2003. On the timing and mechanism of millennial-scale climate variability during the last glacial cycle. Climate Dynamics 20, 257–267.

Sagnotti, L., Budillon, F., Dinarès-Turell, J., Iorio, M., Macrí, P., 2005. Evidence for a variable paleomagnetic lock-in depth in the Holocene sequence from the Salerno Gulf (Italy): implications for ''high-resolution'' paleomagnetic dating. Geochemistry, Geophysics, and Geosystems 6 (11), 1–11.

Sangiorgi, F., Dinelli, E., Maffioli, P., Capotondi, L., Giunta, S., Morigi, C., Principato, M.S., Negri, A., Emeis, K.C., Corselli, C., 2006. Geochemical and micropaleontological characterisation of a Mediterranean sapropel S5: a case study from core BAN89GC09 (south of Crete). Palaeogeography, Palaeoclimatology, Palaeoecology 235, 192–207.

Sanvoisin, R., D'Onofrio, S., Lucchi, R., Violanti, D., Castradori, D., 1993. 1Ma Paleoclimatic record from the Eastern Mediterranean-Marflux Project: the first results of micropaleontological and sedimentological investigation of a long piston core from the Calabrian Ridge. Il Quaternario 6, 169–188.

Sartori, R., Carrara, G., Torelli, L., Zitellini, N., 2001. Neogene evolution of the southwestern Tyrrhenian Sea (Sardinia Basin and western Bathyal plain). Marine Geology 1-4 (175), 47–66.

Sbaffi, L., Wezel, F.C., Curzi, G., Zoppi, U., 2004. Millennial- to centennial-scale palaeoclimatic variations during Termination I and the Holocene in the central Mediterranean Sea. Global and Planetary Change 40, 201–217.

Sprovieri, R., 1991. Plio-Pleistocene paleoclimatic evolution at ODP Leg 107 Site 653 (Tyrrhenian Sea, Western Mediterranean). Memorie della Societa' Geologica Italiana 44, 135–144.

Sprovieri, R., Di Stefano, E., Incarbona, A., Gargano, M.E., 2003. A high-resolution of the last deglaciation in the Sicily Channel based on foraminiferal and calcareous nannofossil quantitative distribution. Palaeogeography, Palaeoclimatology, Palaeoecology 202, 119–142.

Sprovieri, R., Di Stefano, E., Incarbona, A., Oppo, D.W., 2006. Suborbital climate variability during Marine Isotopic Stage 5 in the central Mediterranean basin: evidence from calcareous plankton record. Quaternary Science Reviews 25, 2332–2342.

Stuiver, M., Reimer, P.J., 1993. Extended ^{14}C data base and revised CALIB 3.0 ^{14}C Age calibration program. Radiocarbon 35 (1), 215–230.

Tan, X., Kodama, K.P., 2003. An analytical solution for correcting palaeomagnetic inclination error. Geophysical Journal International 152 (1), 228–236.

Tan, X., Kodama, K.P., Lin, H., Fang, D., Sun, D., Li, Y., 2003. Palaeomagnetism and magnetic anisotropy of Cretaceous red beds from the Tarim basin, northwest China: evidence for a rock magnetic cause of anomalously shallow palaeomagnetic inclinations from central Asia. Journal of Geophysical Research 108 (B2), 2107.

Tauxe, L., Kent, D.V., 1984. Properties of a detrital remanence carried by hematite from study of modern river deposits and laboratory redeposition experiments. Geophysical Journal of the Royal Astronomical Society 77, 543–561.

Tauxe, L., Kent, D.V., 2004. A simplified statistical model for the geomagnetic field and the detection of shallow bias in paleomagnetic inclinations: was the ancient magnetic field dipolar? In: Channell, J.E.T., et al. (Eds.), Timescales of the Paleomagnetic field, vol. 145. Geophysical Monograph, pp. 101–116.

Walker, R.G., 1967. Turbidite sedimentary structures and their relationship to proximal and distal depositional environments. Journal of Sedimentary Petrology 37 (1), 25–37.

Walker, R.G., 1992. Turbidites and submarine fans. In: Walker, R.G., James, N.P. (Eds.), Facies Model Response to Sea-level Change. Geological Association of Canada, Ontario, pp. 239–263.

Waelbroeck, C., Labeyrie, L., Michel, E., Duplessy, J.C., Lambeck, K., McManus, J.F., Balbon, E., Labracherie, M., 2002. Sea-level and deep water temperature changes derived from benthic foraminifera isotopic records. Quaternary Science Reviews 21, 295–305.

Watkins, J.M., Mix, A.C., Wilson, J., 1996. Living planktic foraminifera: tracers of circulation and productivity regimes in the central equatorial Pacific. Deep-Sea Research II 43, 1257–1282.

Wolf-Welling, T.C.W., Cowan, E.A., Daniels, J., Eyles, N., Maldonado, A., Pudsey, C.J., 2001. Diffuse spectral reflectance data from rise Sites 1095, 1096, 1101 and Palmer Deep Sites 1098 and 1099 (Leg 178, Western Antarctic Peninsula). In: Barker, P.F., Camerlenghi, A., Acton, G.D., Ramsay, A.T.S. (Eds.), Proceeding Ocean Drilling Program, Scientific Results, vol. 178, pp. 1–22.

Zaric, S., Donner, B., Fischer, G., Mulitza, S., Wefer, G., 2005. Sensitivity of planktic foraminifera to sea surface temperature and export production as derived from sediment trap data. Marine Micropaleontology 55, 75–105.

Deep-Sea Research II 56 (2009) 738–747

Contents lists available at ScienceDirect

Deep-Sea Research II

journal homepage: www.elsevier.com/locate/dsr2

Prokaryote diversity and viral production in deep-sea sediments and seamounts

Roberto Danovaro [a,*], Cinzia Corinaldesi [a], Gian Marco Luna [a], Mirko Magagnini [a], Elena Manini [b], Antonio Pusceddu [a]

[a] Department of Marine Science, Polytechnic University of Marche, Via Brecce Bianche, 60131 Ancona, Italy
[b] Institute of Marine Science (ISMAR), National Research Council, Ancona, Italy

ARTICLE INFO

Article history:
Accepted 15 July 2008
Available online 7 November 2008

Keywords:
Deep-sea viruses
Prokaryote diversity
Seamounts

ABSTRACT

Despite the fact that marine prokaryotes and viruses have been increasingly investigated over the last decade, knowledge on prokaryote diversity and viral production in bathyal sediments is limited. We investigated microbial variables in the deep-sea sediments around two seamounts at 3000-m depth in the Tyrrhenian Sea and sediments located at the same depth, but not affected by the presence of the seamounts. We hypothesized that seamounts altered significantly prokaryotes–viruses interactions in surrounding deep-sea sediments. Sediments surrounding seamounts were characterised by prokaryotic abundances significantly higher than those observed in non-seamount sediments. Benthic viral production was about double in sediments close to seamounts than in non-seamount sediments, where virus turnover was up to 3 times lower. Total Bacteria, as assessed by CARD-FISH, dominated prokaryotic community structure, whereas Archaea accounted on average for approximately 10%. The fraction of Crenarchaeota was always higher than Euryarchaeota. Bacterial diversity, estimated using ARISA, was high, with up to 127 different microbial operational taxonomic units (OTUs) in a single sample. Archaeal richness (determined using T-RFLP of the 16S rRNA gene) ranged from 12 to 20 OTUs, while Archaeal evenness was comprised between 0.529 ± 0.018 and 0.623 ± 0.08. Results represent a pointer for future investigations dealing with the interactions between viruses and prokaryotes in deep-sea sediments.

1. Introduction

Seamounts are usually isolated and typically cone-shaped elevations of the seafloor topography (Rogers, 2004). These structures interact with ocean currents (Boehlert and Genin, 1987) and, depending on current speed, water-column stratification and latitude and their morphology, they can trigger small- and meso-scale processes, such as the formation of eddies and circular currents (“Taylor column”), turbulent mixing, benthic boundary effects, and regional up- or down-welling (Fock et al., 2002; Heinz et al., 2004). These processes may influence locally, or on larger spatial scales, primary and secondary production, nutrient dynamics, the settlement of fauna, the presence of zooplankton and fish, and various ecosystem properties (Uchida and Tagami, 1984; Koslow, 1997; Dower and Perry, 2001; Diekmann et al., 2006).

Recent investigations on seamounts’ ecology have shown that they are also hot-spots of biodiversity for sessile macrobenthos, displaying a large number of endemic species (from 5% to 50% of the species richness) (Rogers, 1994; De Forges et al., 2000). For their complexity and inaccessibility, these environments are still poorly known both in terms of fauna living on their surface, and for the fauna inhabiting the bottom sediments around seamounts (Wilson and Kaufmann, 1987). Very little is known also on the microbial component associated with seamounts. The only available information deals with the microbial assemblages of deep corals or hydrothermal vents discovered on the top of seamounts (Emerson and Moyer, 2002; Nakagawa et al., 2004; Sunamura et al., 2004; Takai et al., 2004; Penn et al., 2006). Seamounts, for their dimensions and characteristics, influence biological and physical processes in large areas of the seafloor; for instance seamounts alter the hydrodynamic characteristics of the overlying waters, thus influencing sedimentation rates and inputs of organic material (Pitcher et al., 2007). However, information on the effects of seamounts on microbial assemblages in sediments surrounding the mountains is non-existent.

Benthic prokaryotes (Bacteria and Archaea) represent the numerically dominant component and the largest fraction of the biomass on a global scale (Whitman et al., 1998). Moreover, their quantitative importance with respect to the other living components increases with increasing water depth (Rex et al., 2006). The discovery of high metabolic activities and specific functional

* Corresponding author. Tel.: +39 071 2204654; fax: +39 071 2204650.
E-mail address: r.danovaro@univpm.it (R. Danovaro).

0967-0645/$ - see front matter © 2008 Elsevier Ltd. All rights reserved.
doi:10.1016/j.dsr2.2008.10.011

characteristics in deep-sea prokaryotes has lead to the conclusion that prokaryotes play a pivotal role in deep-sea food webs, carbon and nutrient cycling, and overall deep-sea ecosystem functioning (Boetius et al., 2000). In particular, recent studies have demonstrated that, conversely to what was previously hypothesized, Archaea are not confined to specific and extreme systems, but are present at all depths in the world's oceans (Fuhrman and Davis, 1997; Massana et al., 2000). Moreover, their quantitative importance apparently increases up to ~40% of total prokaryote abundance in meso- and bathypelagic waters (Karner et al., 2001). Since Archaea can take up both aminoacids and bicarbonate (Ouverney and Fuhrman, 1999; Wuchter et al., 2003) and contribute significantly to the overall deep-sea metabolism, their role cannot be neglected, especially in the deep sea. Unfortunately, available information on Archaea in deep-sea sediments is extremely limited, so that their overall ecological role in benthic domain remains unknown (Vetriani et al., 1999). Further studies have recently suggested that viruses could play an increasingly important role in meso-bathypelagic waters and sediments (Magagnini et al., 2007; Corinaldesi et al., 2007; Hewson and Fuhrman, 2007), possibly controlling prokaryote community structure, prokaryote production and mortality, thus influencing carbon cycling and other key biogeochemical processes (Fuhrman, 1999; Winter et al., 2004; Suttle, 2005; Danovaro et al., 2008).

Here, we report the abundance, biomass, production and diversity of benthic prokaryote assemblages and viral abundance and production in deep-sea sediments close to two seamounts (Palinuro and Marsili) of the South Tyrrhenian Sea. These results were compared with those obtained in sediments collected far from the seamounts, hereafter defined as "non-seamount" sediments. We investigated the effects of the presence of the seamounts on microbial variables (including prokaryotic and viral production) on surrounding deep-sea sediments.

2. Methods

2.1. Study site and sampling strategy

Sediment samples were collected in the Southern Tyrrhenian Sea (Western Mediterranean; Fig. 1), in the framework of the CIESM-SUB 1 cruise, from 21 to 31 July 2005, on board the R/V *Universitatis*. Four sites were investigated: two located in proximity to the Marsili and Palinuro seamounts and two located at about 50 miles from the seamounts (at depths comprised between 3430 and 3581 m). All sites were selected at similar depths to discount the effect of changing pressure and last two sites were used as the controls (hereafter defined as "Non-seamount" sites 1 and 2). At each site, undisturbed sediment samples were collected by repeated multicorer deployments ($n = 3–6$) (Bowers and Connelly, Mod. Mini), equipped with four liners (inner diameter, 6 cm).

In order to provide unbiased estimates of viral abundance induced by the use of preservatives, sediment aliquots (~1 cm^3) from the top 1 cm of each core were transferred into sterile tubes and supplemented with 4.5 sterile virus-free seawater (prefiltered

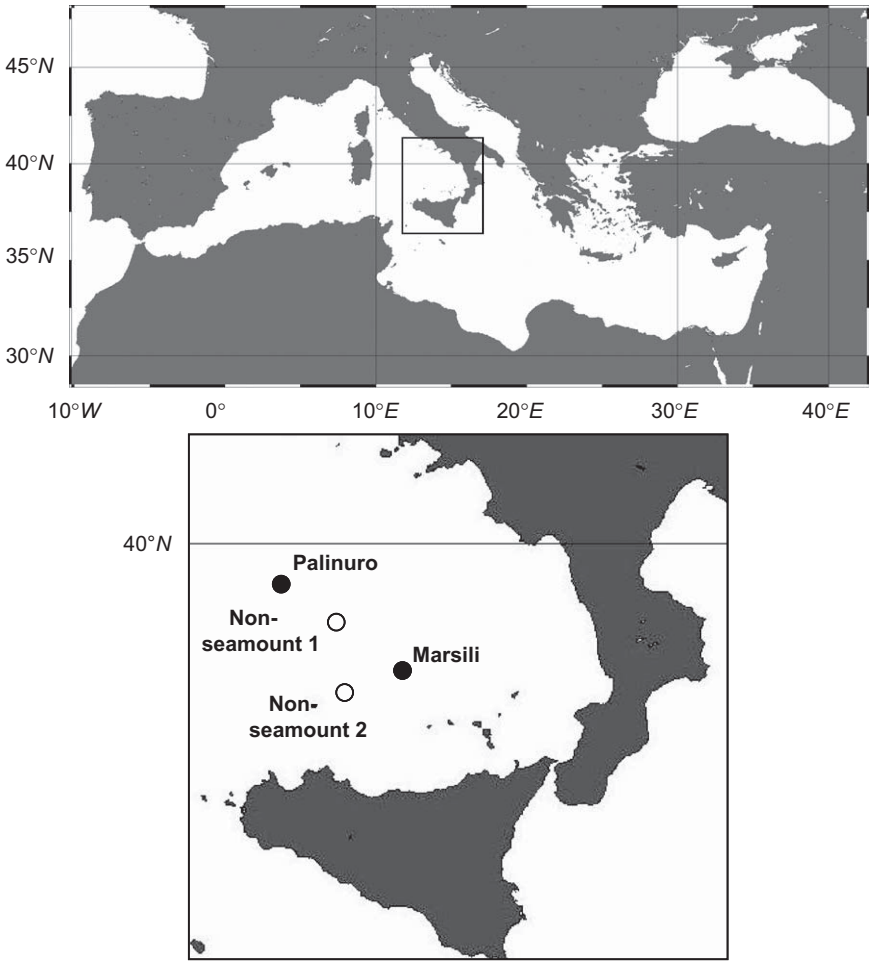

Fig. 1. The study area and the location of the sampling stations.

onto 0.02-μm membranes) and stored at −20 °C until analysis (within 1 week; Wen et al., 2004; Helton et al., 2006). For prokaryote counts, samples were fixed with 2% formalin as previously described and stored at 4 °C until processing (Manini and Danovaro, 2006).

For analysis of prokaryote community structure and diversity, aliquots (ca. 10 cm^3) from the top 1 cm of each core were immediately put into sterile tubes and stored at −20 °C.

2.2. Total prokaryote counts and active fraction

Total prokaryote numbers and the metabolically active fraction (as nucleoid-containing cells, NuCC) were determined according to Luna et al. (2002) and Manini and Danovaro (2006). It must be pointed out that the NuCC counts theoretically represent the maximum estimate of the number of active bacteria, since the presence of a nucleoid does not ensure that a bacterium is growing or even capable of growth (Zweifel and Hagström, 1995; Alonso, 2005). The determination of NuCC fraction is based on a staining/de-staining procedure (Zweifel and Hagström, 1995; Zampino et al., 2004). Replicate ($n = 3$) sediment sub-samples of 1 ml were sonicated three times (Branson Sonifier 2200; 60 W for 1 min). A pre-incubation of 1 h (with Acridine Orange) was performed according to Karner and Fuhrman (1997). After dilution, samples were incubated for 2 h in the dark with Acridine Orange (0.025% final concentration) and Triton X-100 (0.1% [vol:vol]) and then filtered onto 0.2-μm-pore size black-stained polycarbonate filters. Filters were washed with 10 ml of 2-propanol for 10 min, before mounting on microscopic slides. Total and nucleoid-containing prokaryote cells abundance was obtained by epifluorescence microscopy (Zeiss Axioskop 2, magnification 1000 ×) by examining at least 10 fields per slide, in order to count at least 200 cells per filter. According to the staining/de-staining procedure (Luna et al., 2002), each counted filter was removed from the slide using sterile forceps, mounted again on the filtration apparatus, stained with Acridine Orange (0.025% final concentration), washed twice with 5 ml of 0.2-μm-filtered Milli-Q water, let dry for some seconds and mounted onto a microscopic slide for subsequent total prokaryote counts. Prokaryotic counts recorded after this procedure were then compared with the NuCC counts recorded for the same filter. Data were normalized to sediment dry weight after desiccation (60 °C, 24 h).

2.3. Prokaryotic C production

Prokaryotic carbon production in the sediment was measured by ^{3}H-leucine incorporation following the procedure previously described by Manini et al. (2004). Sediment sub-samples (200 μl), supplemented with an aqueous solution of ^{3}H-leucine (0.2 nmol final concentration, specific activity of 72 Ci $mmol^{-1}$) were incubated for 1 h in the dark at in situ temperature. Sediment blanks ($n = 3$) were made adding ethanol immediately before [^{3}H]-leucine addition. After incubation, samples were supplemented with ethanol (80%) and stored at 4 °C until processing in the laboratory. Briefly, sediments were washed two times with ethanol (80%) by mixing, centrifuging and discarding the supernatant. The sediment was then re-suspended into ethanol (80%) and transferred onto a polycarbonate filter (0.2 μm pore size) using a filtration apparatus and a vacuum pump (Millipore). Subsequently, each filter was washed four times with 2 ml of 5% trichloroacetic acid (TCA), then each filter transferred into a Pyrex test tube containing 2 ml of NaOH (2 M) and subsequently heated for 2 h at 100 °C. After centrifugation to separate the sediment residual, 1 ml of supernatant was transferred to scintillation vials containing appropriate scintillation fluid. The incorporated radioactivity (as DPM) in sediment samples was measured by determining the counts per minute with a liquid scintillation counter (Packard Tri-Carb 300). For benthic prokaryote production, data were normalized to sediment dry weight after desiccation (60°, 24 h).

2.4. Viral abundance, production and decay

Viral counts were carried out as described by Danovaro et al. (2001) with some modifications. Sediment sub-samples (500 μl) were treated using pyrophosphate (5 mmol l^{-1} final concentration) and ultrasound treatment (three times for 1 min, Branson 2200, 60 W) to increase the extraction yields. In order to eliminate uncertainties in virus counting due to extracellular DNA interference, sub-samples were supplemented with DNase I from bovine pancreas (10 U ml^{-1} final concentration) and incubated for 15 min at room temperature (Danovaro et al., 2001). Sediment samples were diluted 250 times with 0.02-μm-pre-filtered Milli-Q sterile water, filtered on 0.02-μm-pore-size filters (Anodisc; diameter, 25 mm; Al_2O_3) and then stained with 20 μl of diluted SYBR Green I (i.e. the commercially-available 10,000 × stock solution was diluted 1:20). Filters were incubated in the dark for 20 min and then mounted on glass slides with 20 μl of 50% phosphate buffer (pH 7.8) and 50% glycerol containing 0.5% ascorbic acid. Viral counts were obtained by epifluorescence microscopy (Zeiss Axioskop 2, magnification 1000 ×) examining at least 10 fields per slide, in order to count at least 200 viral particles per filter. Slides were stored at −20 °C until counting, which were performed in laboratory within 1 week. Data were normalized to sediment dry weight (60 °C, 24 h).

Viral production was determined according to Mei and Danovaro (2004) and Corinaldesi et al. (2007). Immediately after sampling, sediment samples (about 25 ml, $n = 3$) were transferred in sterile Falcon tubes and supplemented with 25 ml of virus-free (0.02-μm pre-filtered) seawater. The slurries were incubated in the dark at *in situ* temperature. In order to estimate viral production and decay, 5-ml sub-samples were collected after 0, 2, 4, 8 and 12 h. Net viral production was determined as the maximum increment of viral abundance per gram of sediment per hour (Corinaldesi et al., 2007). Viral decay rates in all samples were determined following the same procedure used for the analysis of viral production without the addition of cellular metabolic inhibitors (e.g., KCN) in order to minimize biases due to sample manipulation. Viral decay was estimated as the maximum decrement of viral abundance observed during time-course experiments and expressed as viruses per gram of sediment per hour.

2.5. CARD-FISH: catalyzed reporter deposition—fluorescence in situ hybridization

The analysis of the benthic prokaryote community structure was performed as described by Teira et al. (2004) with a few modifications. Sediment samples were centrifuged (2500 rpm for 5 min), washed with phosphate-buffered saline (PBS, pH 7.8), then centrifuged and re-suspended in PBS and ethanol 96% for a total volume of 5 ml. Samples were then treated with ultrasounds three times for 1 min (Branson sonifier 2200, 60 W) and diluted (250 ×). Samples were then filtered onto 0.2-μm polycarbonate filters. Filters were dipped in low-gelling-point agarose (0.1% [wt/vol] in Milli-Q water), dried upside down on a glass Petri dish at 37 °C, and subsequently dehydrated in 95% (vol/vol) ethanol. For cell wall permeabilization, filters were incubated either with lysozyme (catalog number 7651, 10 mg/ml; Sigma) or with proteinase K (1844 U/mg, 10.9 mg/ml, catalog number 82456,

0.2 μl/ml; Fluka) solution (0.05 EDTA, 0.1 Tris–HCl [pH 8]) at 37 °C for 1 h. Subsequently, the filters were washed three times with Milli-Q water and incubated in 0.01 M HCl at room temperature for 20 min. Incubation in HCl inhibits intracellular enzymes. Previous attempts to use proteinase K treatment to detect *Archaea* failed (Pernthaler et al., 2002), probably because of the incomplete inactivation of the proteinase K after the permeabilization step. Complete inactivation of proteinase K is of crucial importance to avoid degradation of the HRP linked to the oligonucleotide probe. After incubation in HCl, filters were washed twice with Milli-Q water, dehydrated with 95% ethanol, and dried at room temperature. Filters were cut in sections for hybridization with the oligonucleotide probes Eub338 (5′-GCTGCCTCCCGTAGGAGT-3′ targeting *Bacteria*), Arch915 (5′-GTGCTCCCCCGCCAATTCCT-3′ targeting *Archaea*), Cren537 (5′ TGACCACTTGAGGTGCTG-3′; targeting *Crenarchaea*) and Eury806 (5′-CACAGCGTTTACACCTAG-3′; targeting *Euryarchaea*). The probes target the same sequences as the polynucleotide probes used in previous studies (De Long et al., 1999; Lee et al., 1999). To 200 μl of hybridization buffer (0.9 M NaCl, 20 mM Tris–HCl [pH 7.5], 10% [wt/vol] dextran sulfate, 0.02% [wt/vol] sodium dodecyl sulfate, 1% blocking reagent [Boehringer Mannheim, Germany], and 55% [vol/vol] formamide [for Eub338 and Arch915] or 20% [vol/vol] formamide [for Cren537 and Eury806]) were added with 2 μl of HRP-Probe (50 ng μl^{-1}). This hybridization mix was added to filter sections. The hybridization was performed at 35 °C for 2 h in a dynamic incubator. Thereafter, the sections were transferred into 50 ml of pre-warmed washing buffer (5 mM EDTA [pH 8], 20 mM Tris–HCl [pH 7.4–7.6], 0.01% [wt/vol] sodium dodecyl sulfate) at 37 °C for 10–15 min. Two different washing buffers were prepared, containing 13 mM NaCl (for Eub338 and Arch915) and 145 mM NaCl (for Cren537 and Eury806) (Pérez et al., 2003). Sections were then placed in PBS (pH 7.6) added with 0.05% Triton X-100 (PBS-T) at room temperature for 15 min. After removal of excess buffer, the filter sections were supplemented 150 μl of amplification buffer and 7.5 μl of tyramide CY3 (1:20) and incubated for 10–15 min in the dark at 37–46 °C. After amplification, filters were washed in PBS-T (room temperature, 15 min), Milli-Q water, and 95% ethanol. Finally, filter sections were air dried and stored at −20 °C until further analyses under epifluorescence microscope.

2.6. Analysis of bacterial and archaeal diversity using fingerprinting techniques: ARISA and T-RFLP

In this study, ARISA and T-RFLP were utilized for assessing patterns of bacterial and archaeal biodiversity in deep-sea sediments. Advantages and disadvantages of these two techniques have been previously discussed (Danovaro et al., 2006). We have utilized the technique ARISA for Bacteria and T-RFLP for Archaea, as ARISA is more efficient than TRFLP for the determination of bacterial diversity, but cannot be applied to Archaea, as they do not have an ITS region. At present, the only attempt of using ARISA on one group of Archaea (i.e. the halophilic Archaea) from stromatolites (Leuko et al., 2006) confirmed that several Archaea do not have the ITS region. In addition, little information is available on the range of variation within the 16S rDNA and the ITS in marine Archaea (Garcia-Martinez and Rodriguez-Valera, 2000). Despite T-RFLP analysis could fail in detecting all of the Archaeal taxonomic groups (e.g., euryarchaeotes sequenced to date lack of continuous or linked 16S and 23S genes), this technique has been preferred to others (e.g., DGGE) for its higher sensitivity (Hewson and Fuhrman, 2004). Before DNA extraction, 2.5 g of sediments were washed according to Fortin et al. (2004), in order to eliminate PCR-inhibiting compounds. This procedure is based on a three-steps washing of the sediment sample, each followed by a centrifugation step. According to epifluorescence microscopy estimates carried out on sediments before and after the washing procedure, we have found that this additional step does not result in a loss of cells from the sediment sample (data not shown). Conversely, this procedure strongly decreases the inhibition of the *Taq polymerase* in PCR reactions carried out on DNA extracted from deep-sea sediment samples. DNA was extracted from 1 g of sediment using the UltraClean Soil DNA Isolation kit (MoBio Laboratoires Inc., California, USA). Previous studies revealed that this kit provides estimates of bacterial diversity comparable to those obtained using other direct lysis procedures (Luna et al., 2006). In all samples, extracted DNA was quantified spectrophotometrically, using an UV 1700 spectrophotometer (Shimadzu).

For ARISA, 1 μl of DNA (corresponding to 1–5 ng) was amplified using universal bacterial primers 16S-1392F (5′-GYACACCGCCCGT-3′) and 23S-125R (5′-GGGTTBCCCCATTCRG-3′), which amplify the ITS1 region in the rRNA operon plus ca. 282 bases of the 16S and 23S rRNA (Hewson and Fuhrman, 2004). The primer 23S-125R was fluorescently labeled with the fluorochrome HEX (MWGspa BIOTECH). All PCR reactions were performed in a volume of 50 μl in a thermalcycler (Biometra, Germany) using the MasterTaq® kit (Eppendorf AG, Germany), which reduces the effects of PCR-inhibiting contaminants. Thirty PCR-cycles were used, consisting of 94 °C for 1 min, 55 °C for 1 min and 72 °C for 2 min, preceded by 3 min of denaturation at 94 °C and followed by a final extension of 10 min at 72 °C. To check for eventual contamination of the PCR reagents, negative controls containing the PCR-reaction mixture but without the DNA template were run during each amplification. Positive controls, containing genomic DNA of *Escherichia coli*, also were used. PCR products were checked on agarose-TBE gel (1%), containing ethidium bromide for DNA staining and visualization. Four different reactions were run for each sample and then combined to form two duplicate PCR reactions (Qiu et al., 2001), which were subsequently utilized for separate ARISA analyses. The two resulting PCR combined products were purified using the Wizard PCR clean-up system (Promega, Madison, WI), resuspended in 50 μl of milli-Q water supplied with the clean-up system and then quantified. About 5 ng of amplicons were mixed with 14-μl of internal size standard (GS2500-ROX; Applied Biosystems, Foster City, CA) in deionised formamide, then denatured at 94 °C for 2 min and immediately chilled in ice. Automated detection of ARISA fragments was carried out using an ABI Prism 3100 genetic analyzer (Applied Biosystems). ARISA fragments in the range 390–1400 bp were determined using Genescan analytical software 2.02 (ABI) and the results analyzed adopting the procedure described by Danovaro et al. (2006), which included standardization of fluorescence among samples, elimination of "shoulder" and non-replicated peaks, and cut-off criterion. According to available literature (Danovaro et al., 2006; Hewson and Fuhrman, 2006), we have set the accuracy in sizing at ±3 bp for ARISA fragments lesser than 700 bp, ±5 bp from 700–1000 bp and ±10 bp for greater than 1000 bp.

For T-RFLP analysis on Archaea, 1 μl of extracted DNA was amplified using archaeal universal primers ARCH 21for (5′-TTCYGGTTGATCCYGCCRGA-3′) and ARCH 958rev (5′-YCCGGCGTTGANTCCAATT-3′; e.g. De Long, 1992; Huber et al., 2002; Lanoil et al., 2005). The reverse primer ARCH 958rev had been labeled at the 5′ end with the fluorescent dye HEX (MWGspa BIOTECH). All PCR reactions were performed under the same conditions reported above for ARISA, using 55 °C and 30 s for the annealing step (Huber et al., 2002). Negative (containing the PCR mixture without DNA template) and positive (genomic DNA of *Methanococcous jannashii*) controls were run. PCR products were checked on agarose-TBE gel (1%) and four different PCRs for each sample were carried out as for ARISA. PCR products were purified using

the Wizard PCR clean-up system (Promega, Madison, WI), resuspended in 50 μl of milliQ water supplied with the clean-up system and then quantified as described above. About 300 ng of purified 16S rDNA amplicons from each of the two duplicate PCR were digested separately in a 20-μl reaction volume, containing 10 U of the enzyme *Alu I* (Promega), at 37 °C for 3 h. This specific restriction enzyme was selected because previous studies demonstrated that it is highly efficient in assessing phylotype richness and bacterial diversity in benthic assemblage (Luna et al., 2006). Restriction digestions were stopped by incubating at 65 °C for 20 min, and samples were then kept frozen at −20 °C until analysis. Aliquots from each digestion were analyzed using the ABI Prism 3100 genetic analyzer described above and GS1000-ROX (Applied Biosystems) as size standard. Terminal restriction fragment sizes were determined using Genescan analytical software 2.02 (Applied Biosystems) and T-RFLP profiles processed as described elsewhere (Danovaro et al., 2006). In this case, the accuracy in fragment sizing was ±1 bp.

2.7. Statistical analyses

To test for differences in all of the investigated variables between the sampling sites, one-way analysis of variance (ANOVA) was applied after testing for the homogeneity of variances using the Cochran test. When significant differences were encountered, Tukey's *post-hoc* comparison tests (at $\alpha = 0.05$) were also carried out, to ascertain in which station(s) the investigated parameters were significantly different. Using the ARISA datasets and assuming that the peak height associated with each fragment represented the relative abundance of each bacterial operational taxonomic unit (OTU) within the fingerprint, we investigated the similarity in community composition among the investigated areas. A Bray–Curtis similarity analysis was performed and a similarity matrix was used to obtain a multidimensional scaling (MDS) analysis. Statistical analyses were performed using the PRIMER program (Plymouth Marine Laboratory; Clarke, 1993).

3. Results

The values of the microbial variables investigated in the present study are reported in Table 1, while the results of the statistical analyses are summarized in Table 2.

3.1. Prokaryote abundance, biomass and C production

Prokaryote abundance and biomass in the sediments surrounding the seamounts "Palinuro" and "Marsili" displayed values significantly higher than those observed in "Non-seamount 1" and "Non-seamount 2" sediments (ANOVA, $p<0.001$). Conversely, bacterial biomass, prokaryote C production and the percentage of NuCC were significantly different among areas higher in "Non-seamounts" sediments (Table 2, ANOVA, $p<0.001$).

3.2. Viral abundance, production and decay

No significant differences in viral abundance and decay were observed among sampling sites. Conversely, significant differences were found comparing the values of viral production in sediments surrounding the two seamounts and in non-seamount sediments (Table 2), where viral production was about double than in sediments located close to seamounts (ANOVA, $p<0.01$). Viral production showed a linear increase during incubations, as shown in Fig. 2a and b. The virus to prokaryote abundance ratio (range 3.0–6.1) was ca. double in non-seamount sediments than at sites close to the seamounts (Table 2).

3.3. Prokaryote community structure

The fraction of prokaryotes detected using CARD-FISH (i.e. Total Bacterial abundance+Total Archaeal abundance) ranged from 71% to 82% of the total prokaryote abundance (Table 1). The highest abundance of Bacteria was observed in the Palinuro seamount ($2.07\pm0.19\times10^8$ cell g^{-1}; Tukey's test $p<0.05$). However, no significant differences in the total bacterial fraction were observed among sites (range 54–78%; ANOVA, $p>0.05$). Conversely, both total archaeal abundance and the total archaeal fraction were highest in the sediments of the Marsili seamount ($4.30\pm0.93\times10^7$ cell g^{-1} and 17%; Tukey's test $p<0.01$ and $p<0.05$, respectively), while they varied within a narrow range at all other sites (range: $1.34–1.81\times10^7$ cell g^{-1}).

Within the Archaeal domain, the abundance of Euryarchaeota was significantly higher at Non-seamount St. 2 ($5.82\pm1.27\times10^6$ cell g^{-1}, Tukey's test $p<0.01$) compared with the other sites (range: $0–3.39\times10^6$ cell g^{-1}). Conversely, abundance of Crenarchaeota did not display significant differences among all investigated sites. Within the Archaeal assemblages, the fraction of Crenarchaeota plus Euryarchaeota accounted for ca. 25–100% of the total assemblage. The contribution of Crenarchaeota to the Archaeal assemblages was generally ~3 times higher than Euryarchaeota (Table 1).

3.4. Bacterial and Archaeal OTU richness

Bacterial OTU richness ranged from 66 (Non-seamount 1) to 127 (Non-seamount 2) changed significantly among sites (Table 2, ANOVA, $p<0.001$), with values in the Non-seamount 1 significantly lower than those observed in the other sampled stations (Tukey's test $p<0.05$). Conversely, no significant differences in archaeal OTU richness among sampling sites were encountered.

Bacterial evenness displayed significant differences among sampling sites (ANOVA $p<0.01$), with values of the Pielou index significantly higher in Non-seamount St. 1 than in the other sites (Table 2). Conversely, no differences in archaeal evenness were observed among sampling sites.

4. Discussion

4.1. Prokaryote and viriobenthos in deep-sea sediments

Benthic prokaryote abundance and biomass reported here fall within the range of values reported in the literature for deep-sea sediments worldwide (Mei and Danovaro, 2004; Danovaro et al., 2002; Middelboe et al., 2006). Sediments surrounding seamounts were characterised by higher prokaryotic abundances, with values 2–3 times higher than in non-seamount sediments. Seamounts have important effects on local circulation and sedimentation processes. As reported in a publication related with the present research (Pusceddu et al., 2008), seamounts also can influence organic matter accumulation in surrounding sediments, which showed organic contents (<2 mg C g^{-1}) lower than non-seamount sediments. Therefore, the enhanced prokaryotic production in non-seamount sediments could be related to the higher amount of labile organic matter available. Besides the "bottom up" control described above, lower values of prokaryotic abundance and biomass could be due to viral predation ("top down" control). Estimates of viral production rates in deep-sea sediments are important to understand whether benthic viral shunt can be

Table 1
Microbial variables in the deep-sea sediments investigated.

Station	Unit	Seamount		Seamount	
		Marsili	Non-seamount 1	Palinuro	Non-seamount 2
Total prokaryotic abundance	cell g^{-1}	2.53E+08	1.78E+08	2.79E+08	2.21E+08
	std	1.57E+07	9.68E+06	1.48E+07	1.79E+06
Nucleoid-containing cell (NuCC) fraction	%	53.8	65.1	63.3	81.5
Prokaryotic biomass	μg C g^{-1}	4.7	2.9	5.1	4.4
	std	0.3	0.1	0.3	0.2
Prokaryotic C production	ng C g^{-1} h^{-1}	2.01	3.10	n.a.	4.28
	std	0.51	0.68	n.a.	0.99
Viral abundance	VLP g^{-1}	7.51E+08	1.08E+09	1.01E+09	9.20E+08
	std	7.67E+07	1.39E+08	1.39E+08	1.94E+08
Virus–prokaryote ratio		3.0	6.1	3.6	4.2
Viral production	VLP g^{-1} h^{-1}	5.07E+07	2.23E+07	8.76E+07	4.75E+07
	Std	1.94E+07	4.38E+06	3.40E+07	2.07E+06
Viral turnover	d^{-1}	1.6	0.5	2.1	1.2
Viral decay	VLP g^{-1} h^{-1}	1.91E+07	3.93E+07	1.41E+07	3.82E+07
	std	4.66E+06	n.a.	6.39E+06	2.13E+07
Total Bacterial abundance (CARD-FISH)	cell g^{-1}	1.37E+08	1.39E+08	2.07E+08	1.49E+08
	std	2.38E+07	2.56E+07	1.92E+07	2.16E+07
Total Archaeal abundance (CARD-FISH)	cell g^{-1}	4.30E+07	1.34E+07	1.81E+07	1.73E+07
	std	9.34E+06	1.01E+06	4.79E+06	8.44E+06
Crenarchaeota abundance (CARD-FISH)	cell g^{-1}	1.27E+07	3.35E+06	5.36E+06	1.16E+07
	std	1.02E+06	1.01E+06	1.07E+06	8.33E+06
Euryarchaeota abundance (CARD-FISH)	cell g^{-1}	3.39E+06	0.00E+00	0.00E+00	5.82E+06
	std	2.22E+06	0.00E+00	0.00E+00	1.27E+06
Bacterial contribution to total abundance	%	54.13	78.47	74.09	67.44
	std	9.41	14.44	6.87	9.78
Archaeal contribution to total abundance	%	17.00	7.55	6.48	7.83
	std	3.69	2.98	1.72	3.82
Crenarchaeota contribution to total Archaea	%	5.00	1.89	1.92	5.23
	std	4.02	0.32	0.66	3.77
Euryarchaeota contribution to total Archaea	%	1.34	0.00	0.00	2.63
	std	0.88	0.00	0.00	0.99
Bacterial diversity	OTU richness	100	66	118	127
Bacterial evenness	J	0.929	0.965	0.954	0.949
	std	0.007	0.003	0.003	0.002
Archaeal diversity	OTU richness	15	12	20	14
Archaeal evenness	J	0.553	0.630	0.529	0.623
	std	0.027	0.126	0.018	0.008

n.a.: result not available.
std = standard deviations among replicate samples ($n = 3$–5).

Table 2
Summary of the one-way analysis of variance results, conducted to test for differences between sampling sites.

	F	*p*-Level	Tukey's *post hoc* test (at *p* level <0.05)
Total prokaryotic abundance	40.684	<0.0001	Seamounts > Non-seamounts
Total prokaryotic biomass	56.673	<0.0001	Seamounts > Non-seamounts
Prokaryote C production	5.342	<0.01	Non-seamounts > Seamounts
Nucleoid containing cell (NuCC) fraction	35.751	<0.0001	Non-seamounts > Seamounts
Viral abundance	2.943	ns	–
Viral production	5.596	<0.01	Seamounts > Non-seamounts
Viral decay	3.898	ns	–
Total Bacterial abundance (CARD-FISH)	6.288	<0.05	Palinuro > Non-seamounts-Marsili
Total Archaeal abundance (CARD-FISH)	12.040	<0.01	Marsili > Non-seamounts-Palinuro
Abundance of Crenarchaeota	3.451	ns	–
Abundance of Euryarchaeota	14.774	<0.01	Non-seamount 2 > Non-seamount 1-Marsili-Palinuro
Bacterial contribution to total abundance	3.0739	ns	–
Archaeal contribution to total abundance	7.1749	<0.05	Marsili > Non-seamounts-Palinuro
Crenarchaeota contribution to total Archaea	1.3372	ns	–
Euryarchaeota contribution to total Archaea	10.916	<0.01	Non-seamount 2 > Marsili-Non-seamount 1-Palinuro
Bacterial diversity	–	<0.01	Marsili-Non-seamount 2-Palinuro > Non-seamount 1
Bacterial evenness	43.188	<0.0001	Non-seamount 1 > Marsili-Non-seamount 2-Palinuro
Archaeal diversity	–	ns	–
Archaeal evenness	1.806	ns	–

Reported are also the results of the Tukey's *post-hoc* test for significant differences.

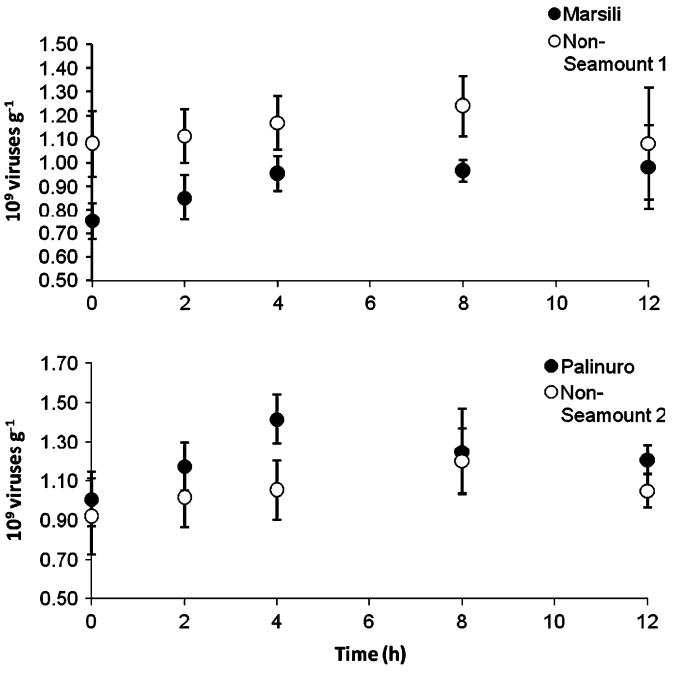

Fig. 2. Viral production experiments: viral abundance during the time-course experiments in the four investigated areas.

responsible for a significant reduction of benthic prokaryote production and to quantify the impact of viruses in biogeochemical cycling of organic matter. Despite the potential importance of this variable, information on viral production in the deep sea is very scant (Corinaldesi et al., 2007). This also can be due to methodological and technological problems related with working in the deep sea. Recent studies, however, suggest that in meso-bathypelagic waters and deep-sea sediments large virus numbers are present, thus leading to hypothesize high viral-induced prokaryote mortalities (Danovaro et al., 2001; Hewson and Fuhrman, 2003; Magagnini et al., 2007). We found that values of viral production in all deep-sea sediments investigated here were higher in comparison with other values reported so far for deep-sea sediments (Middelboe et al., 2006; Middelboe and Glud, 2006). This difference could be due to the different methodologies utilized (i.e. dilution technique vs Würgler bags incubations). The high values reported here are comparable with those measured, using the same methodology, in highly productive coastal sediments (Mei and Danovaro, 2004). Benthic viral production was about double in sediments close to seamounts than in non-seamount sediments where virus turnover was up to 3 times lower. Virus replication is known to depend upon abundance and growth rates of host cells (Wommack and Colwell, 2000), so that information on the metabolic activity of prokaryote assemblages (such as carbon production) is important. The fraction of metabolically active bacteria can be another important variable to take into consideration for evaluating the interaction between viruses and their hosts. In all of the investigated sediments, the active prokaryotic fraction was >50% and the largest active fractions were observed in non-seamount sediments.

Viral production was therefore significantly higher in sediments close to seamounts, which displayed a larger, but slightly less active prokaryote biomass (i.e. in non-seamount sites). These results taken together let hypothesize that viral dynamics were coupled with prokaryote abundance and biomass.

Data reported here for viral decay rates are the first available in literature for deep-sea viriobenthos. Our results indicate that rates of viral decay in deep-sea sediments were high in comparison with values reported so far for coastal sediments (Glud and Middelboe, 2004; Mei and Danovaro, 2004), suggesting that viral decay could be an important factor controlling virus abundance in deep-sea sediments, especially where viral production is low. Moreover, our data suggest that the presence of seamounts did not alter benthic viral decay when compared with the non-seamount sediments. The uncoupling between viral variables suggests that factors influencing viral decay rates may be different from those controlling viral production.

In all investigated sediments, prokaryote community was dominated by Bacteria. Archaea represented an important fraction of total prokaryote abundance only in deep-sea sediments close to the Marsili seamount (ca. 17%). Within the Archaea domain, the fraction of Crenarchaeota was higher than Euryarchaeota, but no significant differences were observed among sites. Recent studies on Crenarchaeota and Euryarchaeota suggested that Crenarchaeota typically dominate deep waters (De Long et al., 1999; Karner

et al., 2001) and account for 3–18% of total prokaryotic production (Herndl et al., 2005). Unfortunately, data on prokaryotic community structure in deep-sea sediments are extremely scant and this hampers a proper comparison and a deep understanding of our findings. However, data reported here would suggest that, overall, Archaea represent a minor fraction of the benthic prokaryote assemblage.

The results of the ARISA and T-RFLP analyses indicated that the deep Tyrrhenian sediments harbor highly diverse microbial assemblages (up to 127 different microbial OTUs). As fingerprinting techniques, such as ARISA and T-RFLP, do not allow identifying rare or the less abundant taxa in the sample (Bent et al., 2007), it can be hypothesized that prokaryotic diversity in these areas can be even higher. Values of deep-sea benthic bacterial diversity are high if compared with those published so far and based on the T-RFLP technique (Luna et al., 2004; Danovaro et al., 2006). High values of deep-sea benthic bacterial diversity (estimated using the T-RFLP technique) have been previously reported in the Tokio Bay, at depths ranging from 1133 to 4023 m by Urakawa et al. (2000), which found from 27 to 73 TRFs and by Luna et al. (2004) in the deep Mediterranean sediments. At the same time, values of ARISA richness reported here are comparable with the highest reported so far in deep-sea sediments (Hewson and Fuhrman, 2007). Luna et al. (2004) reported that the number of OTUs was coupled with the abundance and relative importance of the active bacterial fraction, which in turn were associated with high concentration of potentially available substrates. They suggested that the higher nutrient availability sustained a higher deep-sea microbial diversity. Values of bacterial diversity can depend also on the methodology utilized. Recent studies have demonstrated that ARISA is more efficient than T-RFLP in measuring bacterial diversity, as it appears to be more efficient in detecting rare OTUs (Brown et al., 2005; Danovaro et al., 2006). At the same time, being ARISA and T-RFLP based on different approaches, a direct comparison among Bacterial and Archaeal OTUs richness cannot be made. Nonetheless, we found that patterns of Archaeal OTU richness did not reflect that of bacterial OTUs, possibly indicating that the diversity of the two domains is controlled by different environmental/ecological factors.

A multi-dimensional scaling analysis of bacterial community structure revealed that the bacterial assemblages in the sediments close to Palinuro seamount and Non-seamount 2 clustered together, and differed from those obtained for the Marsili seamount and Non-seamount 1 (Fig. 3). This indicates that, besides the differences in the microbial variables, consistently observed comparing seamount and non-seamount sediments, there are also differences between southern and northern sites in terms of bacterial community composition. Further investigations are therefore needed for understanding the biogeographic patterns of the bacterial assemblages.

We also found a much lower evenness (i.e., equitability of distribution of the OTUs among species) in Archaea than in Bacteria, which suggests that few archaeal OTUs were dominant in the deep-sea sediments investigated, whereas a much more equitable distribution characterized deep-sea bacterial assemblages. Overall, these findings indicate that the highest number of archaeal OTUs were observed in sediments close to the seamounts, where the lowest evenness and the highest viral production were observed.

Although based on a still limited data set and without the use of a manipulative experimental approach, results reported in the present study represent a pointer for future studies, which should to be focused on the interactions between viruses and prokaryotes in deep-sea sediments in order to elucidate the ecological factors which control the patterns of microbial biodiversity in deep-sea sediments.

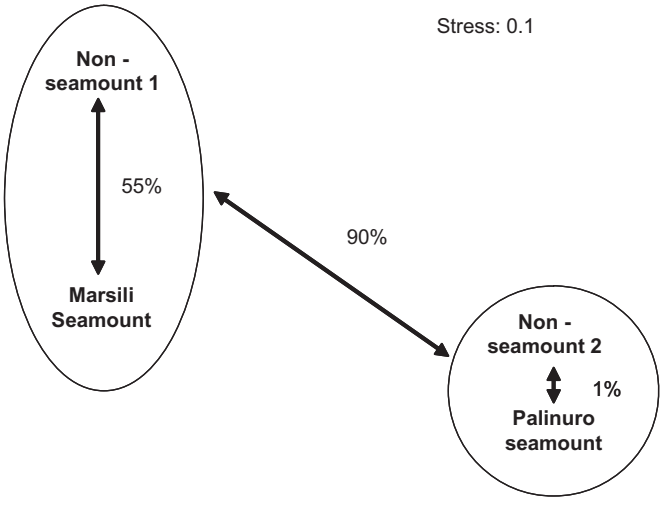

Fig. 3. A multi-dimensional scaling (MDS) obtained using data on bacterial community composition.

Acknowledgments

This study was carried out within the framework of the CIESM-SUB (CIESM *Sur-Un-Bateau* Cruise-I) programme, and was financially supported by the program Hotspot Ecosystem Research on the Margins of European Seas (HERMES, Contract no. GOCE-CT-2005-511234-1). We thank Dr. Laura Giuliano for making this research possible and Ian Hewson for providing useful comments and suggestions.

References

Alonso, C., 2005. Identity and activity of marine microbial populations as revealed by single cell techniques. Ph.D. Dissertation, Bremen.

Bent, S.J., Pierson, J.D., Forney, L.J., Danovaro, R., Luna, G.M., Dell'Anno, A., Pietrangeli, B., 2007. Measuring species richness based on microbial community fingerprints: the emperor has no clothes. Applied Environmental Microbiology 73, 2399–2401.

Boehlert, G.W., Genin, A., 1987. A review of the effects of seamounts on biological processes. In: Keating, B.H., Fryer, P., Batiza, R., Boehlert, G.W. (Eds.), Seamounts, Islands and Atolls. American Geophysical Union, Geophysical Monograph 43, pp. 319–334.

Boetius, A., Ferdelman, T., Lochte, K., 2000. Bacterial activity in sediments of the deep Arabian Sea in relation to vertical flux. Deep Sea Research II 47, 2835–2875.

Brown, M.V., Schwalbach, M.S., Hewson, I., Fuhrman, J.A., 2005. Coupling 16S-ITS rDNA clone libraries and automated ribosomal intergenic spacer analysis to show marine microbial diversity: development and application to a time series. Environmental Microbiology 7, 1466–1479.

Clarke, K.R., 1993. Non parametric multivariate analyses of changes in community structure. Australian Journal of Ecology 18, 117–143.

Corinaldesi, C., Dell'Anno, A., Danovaro, R., 2007. Viral infection plays a key role in extracellular DNA dynamics in marine anoxic systems. Limnology and Oceanography 52, 508–516.

Danovaro, R., Dell'Anno, A., Trucco, A., Vannucci, S., 2001. Determination of virus abundance in marine sediments. Applied and Environmental Microbiology 67, 1384–1387.

Danovaro, R., Manini, E., Dell'Anno, A., 2002. Higher abundance of bacteria than viruses in deep Mediterranean sediments. Applied and Environmental Microbiology 68, 1468–1472.

Danovaro, R., Luna, G.M., Dell'anno, A., Pietrangeli, B., 2006. Comparison of two fingerprinting techniques, terminal restriction fragment length polymorphism and automated ribosomal intergenic spacer analysis, for determination of bacterial diversity in aquatic environments. Applied and Environmental Microbiology 72, 5982–5989.

Danovaro, R., Dell'Anno, A., Corinaldesi, C., Magagnini, M., Noble, R., Tamburini, C., Weinbauer, M., 2008. Major viral impact on the functioning of benthic deep-sea ecosystems. Nature 454, 1084–1087.

De Forges, B.R., Koslow, J.A., Poore, G.C.B., 2000. Diversity and endemism of the benthic seamount fauna in the southwest Pacific. Nature 405, 944–947.
De Long, E.F., 1992. Archaea in coastal marine environments. Proceedings of the National Academy of Sciences 89, 5685–5689.
De Long, E.F., Taylor, L.T., Marsh, T.L., Preston, C.M., 1999. Visualization and enumeration of marine planktonic Archaea and Bacteria by using polyribonucleotide probes and fluorescent in situ hybridization. Applied Environmental Microbiology 65, 5554–5563.
Diekmann, R., Nellen, W., Piatkowski, U., 2006. A multivariate analysis of larval fish and paralarval cephalopod assemblages at Great Meteor Seamount. Deep-Sea Research I 53, 1635–1657.
Dower, J.F., Perry, R.I., 2001. High abundances of larval rockfish over Cobb Seamount, an isolated seamount in the Northeast Pacific. Fisheries Oceanography 10, 268–274.
Emerson, D., Moyer, C.L., 2002. Neutrophilic Fe-oxidizing bacteria are abundant at the Loihi Seamount hydrothermal vents and play a major role in Fe oxide deposition. Applied and Environmental Microbiology 68, 3085–3093.
Fock, H., Uiblein, F., Köster, F., von Westernhag, H., 2002. Biodiversity and species–environment relationships of the demersal fish assemblage at the Great Meteor Seamount (subtropical NE Atlantic), sampled by different trawls. Marine Biology 141, 185–199.
Fortin, N., Beaumier, D., Lee, K., Greer, C.W., 2004. Soil washing improves the recovery of total community DNA from polluted and high organic content sediments. Journal of Microbiological Methods 56, 181–191.
Fuhrman, J.A., 1999. Marine viruses and their biogeochemical and ecological effects. Nature 399, 541–548.
Fuhrman, J.A., Davis, A.A., 1997. Widespread Archaea and novel Bacteria from the deep sea as shown by 16S rRNA gene sequences. Marine Ecology Progress Series 150, 275–285.
Garcia-Martinez, J., Rodriguez-Valera, F., 2000. Microdiversity of uncultured marine prokaryotes: the SAR11 cluster and the marine Archaea of Group I. Molecular Ecology 9, 935–948.
Glud, R.N., Middelboe, M., 2004. Virus and bacteria dynamics of a coastal sediment: implications for benthic carbon cycling. Limnology and Oceanography 49, 2073–2081.
Heinz, P., Ruepp, D., Hemleben, C., 2004. Benthic foraminifera assemblages at Great Meteor Seamount. Marine Biology 144, 985–998.
Helton, R.R., Liu, L., Wommack, K.E., 2006. Assessment of factors influencing direct enumeration of viruses within estuarine sediments. Applied and Environmental Microbiology 72, 4767–4774.
Herndl, G.J., Reinthaler, T., Teira, E., van Aken, H., Veth, C., Pernthaler, A., Pernthaler, J., 2005. Contribution of Archaea to total prokaryotic production in the deep Atlantic Ocean. Applied and Environmental Microbiology 71, 2303–2309.
Hewson, I., Fuhrman, J.A., 2003. Viriobenthos production and virioplankton sorptive scavenging by suspended sediment particles in coastal and pelagic waters. Microbial Ecology 46, 337–347.
Hewson, I., Fuhrman, J.A., 2004. Richness and diversity of bacterioplankton species along an estuarine gradient in Moreton Bay, Australia. Applied and Environmental Microbiology 70, 3425–3433.
Hewson, I., Fuhrman, J.A., 2006. Improved strategy for comparing microbial assemblage fingerprints. Microbial Ecology 51, 147–153.
Hewson, I., Fuhrman, J.A., 2007. Covariation of viral parameters with bacterial assemblage richness and diversity in the water column and sediments. Deep-Sea Research I 54, 811–830.
Huber, J.A., Butterfield, D.A., Baross, J.A., 2002. Temporal changes in archaeal diversity and chemistry in a mid-ocean ridge subseafloor habitat. Applied and Environmental Microbiology 68, 1585–1594.
Karner, M., Fuhrman, J.A., 1997. Determination of active marine bacterioplankton: a comparison of universal 16S rRNA probes autoradiography, and nucleoid staining. Applied and Environmental Microbiology 63, 1208–1213.
Karner, M.B., DeLong, E.F., Karl, D.M., 2001. Archaeal dominance in the mesopelagic zone of the Pacific Ocean. Nature 409, 507–510.
Koslow, J.A., 1997. Seamounts and the ecology of deep-sea fisheries. American Scientist 85, 168–176.
Lanoil, B.D., La Duc, M.T., Wright, M., Kastner, M., Nealson, K.H., Bartlett, D., 2005. Archaeal diversity in ODP legacy borehole 892b and associated seawater and sediments of the Cascadia Margin. FEMS Microbiology Ecology 54, 167–177.
Lee, N., Nielsen, P.H., Andreasen, K.H., Juretschko, S., Nielsen, J.L., Schleifer, K.H., Wagner, M., 1999. Combination of fluorescent in situ hybridization and microautoradiography—a new tool for structure-function analyses in microbial ecology. Applied and Environmental Microbiology 65, 1289–1297.
Leuko, S., Goh, F., Allen, M.A., Burns, B.P., Walter, M.R., Neilan, B.A., 2006. Analysis of intergenic spacer region length polymorphisms to investigate the halophilic archaeal diversity of stromatolites and microbial mats. Extremophiles 11, 203–210.
Luna, G.M., Manini, E., Danovaro, R., 2002. Large fraction of dead and inactive bacteria in coastal marine sediments: comparison of protocols for determination and ecological significance. Applied and Environmental Microbiology 68, 3509–3513.
Luna, G.M., Dell'Anno, A., Giuliano, L., Danovaro, R., 2004. Bacterial diversity in deep Mediterranean sediments: relationship with the active bacterial fraction and substrate availability. Environmental Microbiology 6, 745–753.
Luna, G.M., Dell'Anno, A., Danovaro, R., 2006. DNA extraction procedure: a critical issue for bacterial diversity assessment in marine sediments. Environmental Microbiology 8, 308–320.
Magagnini, M., Corinaldesi, C., Monticelli, L.S., De Domenico, E., Danovaro, R., 2007. Viral abundance and distribution in mesopelagic and bathypelagic waters of the Mediterranean Sea. Deep-Sea Research I 54, 1209–1220.
Manini, E., Danovaro, R., 2006. Synoptic determination of living/dead and active/dormant bacterial fractions in marine sediments. FEMS Microbiology Ecology 55, 416–423.
Manini, E., Luna, G.M., Danovaro, R., 2004. Benthic bacterial response to variable estuarine water inputs. FEMS Microbiology Ecology 50, 185–194.
Massana, R., De Long, E.F., Pedros-Alio, C., 2000. A few cosmopolitan phylotypes dominate planktonic archaeal assemblages in widely different oceanic provinces. Applied and Environmental Microbiology 66, 1777–1787.
Mei, M.L., Danovaro, R., 2004. Virus production and life strategies in aquatic sediments. Limnology and Oceanography 49, 459–470.
Middelboe, M., Glud, R., 2006. Viral activity along a trophic gradient in continental margin sediments off central Chile. Marine Biology Research 2, 41–51.
Middelboe, M., Glud, R.N., Wenzhöfer, F., Ogurib, K., Kitazato, H., 2006. Spatial distribution and activity of viruses in the deep-sea sediments of Sagami Bay, Japan. Deep-Sea Research I 53, 1–13.
Nakagawa, T., Ishibashi, J.I., Maruyama, A., Yamanaka, T., Morimoto, Y., Kimura, H., Urabe, T., Fukui, M., 2004. Analysis of dissimilatory sulfite reductase and 16S rRNA gene fragments from deep-sea hydrothermal sites of the Suiyo Seamount, Izu-Bonin Arc, Western Pacific. Applied and Environmental Microbiology 70, 393–403.
Ouverney, C.C., Fuhrman, J.A., 1999. Marine planktonic Archaea take up amino acids. Applied and Environmental Microbiology 66, 4829–4833.
Penn, K., Wu, D., Eisen, J.A., Ward, N., 2006. Characterization of bacterial communities associated with deep-sea corals on Gulf of Alaska seamounts. Applied and Environmental Microbiology 72, 1680–1683.
Pérez, M.T., Pausz, C., Herndl, G.J., 2003. Major shift in bacterioplankton utilization of enantiomeric amino acids between surface waters and the ocean's interior. Limnology and Oceanography 48, 755–763.
Pernthaler, A., Pernthaler, J., Amann, R., 2002. Fluorescence in situ hybridization and catalyzed reporter deposition for the identification of marine bacteria. Applied and Environmental Microbiology 68, 3094–3101.
Pitcher, T.J., Morato, T., Hart, P.J.B., Clark, M.R., Haggan, N., Santos, R.S., 2007. Seamounts: Ecology, Fisheries & Conservation, Fish and Aquatic Resources Series 12. Blackwell Publishing, Oxford, 520pp.
Pusceddu, A., Gambi, C., Zeppilli, D., Bianchelli, S., Danovaro, R., 2008. Organic matter composition, meiofauna and nematode biodiversity in deep-sea sediments surrounding two seamounts. Deep-Sea Research II, this volume [doi:10.1016/j.dsr2.2008.10.012].
Qiu, X., Wu, L., Huang, H., McDonel, P.E., Palumbo, A.V., Tiedje, J.M., Zhou, J., 2001. Evaluation of PCR-generated chimeras, mutations, and heteroduplexes with 16S rRNA gene-based cloning. Applied and Environmental Microbiology 67, 880–887.
Rex, M.A., Etter, R.J., Morris, J.S., Crouse, J., McClain, C.R., Johnson, N.A., Stuart, C.T., Deming, J.W., Thies, R., Avery, R., 2006. Global bathymetric patterns of standing stock and body size in the deep-sea benthos. Marine Ecology Progress Series 317, 1–8.
Rogers, A.D., 1994. The biology of seamounts. Advances in Marine Biology 30, 305–350.
Rogers, A.D., 2004. The Biology, ecology and vulnerability of seamount communities. Report for the World Conservation Union for the 7th Convention of Parties, Convention for Biodiversity, Kuala Lumpur, 8–19 February, 8pp.
Sunamura, M., Higashi, Y., Miyako, C., Ishibashi, J., Maruyama, A., 2004. Two bacteria phylotypes are predominant in the Suiyo Seamount hydrothermal plume. Applied and Environmental Microbiology 70, 1190–1198.
Suttle, C.A., 2005. Viruses in the sea. Nature 437, 356–361.
Takai, K., Gamo, T., Tsunogai, U., Nakayama, N., Hirayama, H., Nealson, K.H., Horikoshi, K., 2004. Geochemical and microbiological evidence for a hydrogen-based, hyperthermophilic subsurface lithoautotrophic microbial ecosystem (HyperSLiME) beneath an active deep-sea hydrothermal field. Extremophiles 8, 269–282.
Teira, E., Reinthaler, T., Pernthaler, A., Pernthaler, J., Herndl, G., 2004. Combining catalyzed reporter deposition-fluorescence in situ hybridization and microautoradiography to detect substrate utilization by *Bacteria* and *Archaea* in the deep ocean. Applied and Environmental Microbiology 70, 4411–4414.
Uchida, R.N., Tagami, D.T., 1984. Groundfish fisheries and research in the vicinity of seamounts in the North Pacific Ocean. Marine Fisheries Review 46, 1–17.
Urakawa, H., Yoshida, T., Nishimura, M., Ohwada, K., 2000. Characterization of depth-related population variation in microbial communities of a coastal marine sediment using 16S rDNA-based approaches and quinone profiling. Environmental Microbiology 2, 542–554.
Vetriani, C., Jannasch, H.W., MacGregor, B.J., Stahl, D.A., Reysenbach, A.L., 1999. Population structure and phylogenetic characterization of marine benthic Archaea in deep-sea sediments. Applied and Environmental Microbiology 65, 4375–4384.
Wen, K., Ortmann, A.C., Suttle, C.A., 2004. Accurate estimation of viral abundance by epifluorescence microscopy. Applied and Environmental Microbiology 70, 3862–3867.
Whitman, W.B., Coleman, D.C., Wiebe, W.J., 1998. Prokaryotes: the unseen majority. PNAS 95, 6578–6583.
Wilson, R.R., Kaufmann, R.S., 1987. Seamount biota and biogeography. In: Keating, B.H., Fryer, P., Batiza, R., Boehlert, G.W. (Eds.), Seamounts, Islands and Atolls. American Geophysical Union, Geophysical Monograph 43, Washington, DC, pp. 355–377.

Winter, C., Smit, A., Herndl, G.J., Weinbauer, M.G., 2004. Impact of virioplankton on archaeal and bacterial community richness as assessed in seawater batch cultures. Applied and Environmental Microbiology 70, 804–813.
Wommack, K.E., Colwell, R.L., 2000. Virioplankton: viruses in aquatic ecosystems. Microbiology and Molecular Biology Review 64, 69–114.
Wuchter, C., Schouten, S., Boschker, H.T.S., Damsté, J.S.S., 2003. Bicarbonate uptake by marine Crenarchaeota. FEMS Microbiology Letters 219, 203–207.
Zampino, D., Zaccone, R., La Ferla, R., 2004. Determination of living and active bacterioplankton: a comparison of methods. Chemistry and Ecology 20, 411–422.
Zweifel, U.L., Hagström, A., 1995. Total counts of marine bacteria include a large fraction of non-nucleoid-containing bacteria (ghosts). Applied and Environmental Microbiology 61, 2180–2185.

Deep-Sea Research II 56 (2009) 748–754

Contents lists available at ScienceDirect

Deep-Sea Research II

journal homepage: www.elsevier.com/locate/dsr2

A first insight into the occurrence and expression of functional *amo*A and *acc*A genes of autotrophic and ammonia-oxidizing bathypelagic *Crenarchaeota* of Tyrrhenian Sea

Michail M. Yakimov *, Violetta La Cono, Renata Denaro

Institute for Coastal Marine Environment (IAMC), CNR, Molecular Microbiology and Ecology, Spianata S. Raineri 86, 98122 Messina, Italy

ARTICLE INFO

Article history:
Accepted 8 July 2008
Available online 5 November 2008

Keywords:
Autotrophic ammonia-oxidizing *Crenarchaeota*
Deep Marine Group I
Putative ammonia mono-oxygenase *amo*A
Putative acetyl-CoA carboxylase *acc*A

ABSTRACT

The autotrophic and ammonia-oxidizing crenarchaeal assemblage at offshore site located in the deep Mediterranean (Tyrrhenian Sea, depth 3000 m) water was studied by PCR amplification of the key functional genes involved in energy (ammonia mono-oxygenase alpha subunit, *amo*A) and central metabolism (acetyl-CoA carboxylase alpha subunit, *acc*A). Using two recently annotated genomes of marine crenarchaeons, an initial set of primers targeting archaeal *acc*A-like genes was designed. Approximately 300 clones were analyzed, of which 100% of *amo*A library and almost 70% of *acc*A library were unambiguously related to the corresponding genes from marine *Crenarchaeota*. Even though the acetyl-CoA carboxylase is phylogenetically not well conserved and the remaining clones were affiliated to various bacterial acetyl-CoA/propionyl-CoA carboxylase genes, the pool of archaeal sequences was applied for development of quantitative PCR analysis of *acc*A-like distribution using TaqMan® methodolgy. The archaeal *acc*A gene fragments, together with alignable gene fragments from the Sargasso Sea and North Pacific Subtropical Gyre (ALOHA Station) metagenome databases, were analyzed by multiple sequence alignment. Two *acc*A-like sequences, found in ALOHA Station at the depth of 4000 m, formed a deeply branched clade with 64% of all archaeal Tyrrhenian clones. No close relatives for residual 36% of clones, except of those recovered from Eastern Mediterranean, was found, suggesting the existence of a specific lineage of the crenarchaeal *acc*A genes in deep Mediterranean water. Alignment of Mediterranean *amo*A sequences defined four cosmopolitan phylotypes of *Crenarchaeota* putative ammonia mono-oxygenase subunit A gene occurring in the water sample from the 3000 m depth. Without exception all phylotypes fell into Deep Marine Group I cluster that contain the vast majority of known sequences recovered from global deep-sea environment. Remarkably, three phylotypes accounted for 91% of all Mediterranean *amo*A clones and corresponded to the sequences retrieved from the less deep compartments of the world's ocean, most likely reflecting the higher temperature at the depth of the Mediterranean Sea. In order to verify whether these phylotypes might represent important *Crenarchaeota* in the functioning of the Mediterranean bathypelagic ecosystem, expression of crenarchaeal *amo*A gene was monitored by direct RNA retrieval and following analysis of *amo*A-related mRNA transcripts. Surprisingly, all mRNA-derived sequences formed a tight monophyletic group, which fell into large Shallow Marine Group I cluster with sequences retrieved from shallow (up to 200 m) waters, sediments and corals. This group was not detected in DNA-based clone library, obviously, due to an overwhelming dominance of the Deep Marine Group I. The failure to recover the *amo*A transcripts, related to Deep Marine Group I of *Crenarchaeota*, was unanticipated and likely resulted from the physiology of these strongly adapted deep-sea organisms. As far as all seawater samples were treated on-board under atmospheric pressure conditions and sunlight, the decompression and/or photoinhibition likely affected their metabolic activity, followed by the strong decay of gene expression.

1. Introduction

The bathypelagic and abyssal realms of the world oceans are the important and less understood microbial ecosystems on Earth. Most marine microbiology studies so far have been devoted to the photic zone (0–200 m), which is considered as an ecosystem

* Corresponding author. Tel.:+39090669003; fax:+39090669007.
E-mail address: michail.yakimov@iamc.cnr.it (M.M. Yakimov).

0967-0645/$ - see front matter © 2008 Elsevier Ltd. All rights reserved.
doi:10.1016/j.dsr2.2008.07.024

where most primary production occurs. The role of deeper microbial communities of deeper water bodies in carbon cycling has been linked exclusively to degradation of complex organic molecules, and thus heterotrophy was coined as the predominant lifestyle for deep-sea prokaryotes (Martin-Cuadrado et al., 2007). Apparently, new 'players' in the C cycle, however, have recently been identified as autotrophic (Herndl et al., 2005; DeLong, 2006; Ingalls et al., 2006), and they are among the most widely distributed and abundant groups of microorganisms on the planet—the mesophilic *Crenarchaeota*. Although archaea were previously characterized as extremophiles, mesophilic archaea are now recognized to be an ubiquitous component of marine plankton (DeLong, 1992, 1998; Fuhrman and Davis, 1997), with the marine 'Group 1' clade of *Crenarchaeota* alone comprising over 20% of picoplankton in the world ocean (Karner et al., 2001). Giving the vast dimensions of the oceans, occupying nearly two thirds of the planet's surface and reaching an average depth of 3800 m, marine *Crenarchaeota* obviously play a fundamental role in global biochemical cycling. These organisms are estimated to number a staggering 10^{28} cells in total, but, because of our inability to cultivate them, for the last 15 years our understanding of their physiology and biogeochemical function has remained mostly speculative.

Analyzing metagenomic data obtained from the photic layers of the Sargasso Sea, Venter et al. (2004) identified an putative ammonia mono-oxygenase (*amo*A-like) gene on an archaeal-associated scaffold, and suggested the genetic capacity for ammonia oxidation. More direct indication on archaeal origin of *amo*A-like genes was obtained by analyzing the soil metagenome, when a similar gene was found on 43-kb soil DNA fragment harboring 16S rRNA gene of the group 1.1b *Crenarchaeota* (Treusch et al., 2005).

The definitive link between these novel *amo*A-like genes and archaeal ammonia oxidation was recently and convincingly established by cultivation of an ammonia-oxidizing crenarchaeon—designated *Nitrosopumilus maritimus*—from a saltwater aquarium (Könneke et al., 2005). The 16S rRNA phylogeny analysis placed this organism into the Marine Group 1 of *Crenarchaeota,* the first cultivated representative from this exceptionally abundant archaeal group. The putative ammonia mono-oxygenase genes *amo*A, *amo*B and *amo*C also were revealed in this organism. The energy gained from the near-stoichiometric conversion of ammonia into nitrite allows this crenarchaeon to use dissolved bicarbonate chemoautotrophically as a principal carbon source. Moreover, *N. maritimus* likely belongs to the obligate oligotrophic CO_2-fixing organisms, since the addition of organic carbon actually inhibits its growth (Könneke et al., 2005). Compared with recent molecular evidences demonstrating the archaeal *amo*A gene to be pervasive in various areas and ecosystems of the ocean (Francis et al., 2006, 2007), the molecular tools to monitor the occurrence and diversity of genetic determinants of CO_2-fixation are still to be developed.

Metagenomic analysis of the only other established species within the marine group 1 *Crenarchaeota*, the uncultivated sponge symbiont *Cenarchaeum symbiosum* A, identified multiple components of a modified 3-hydroxypropionate cycle (for autotrophic carbon assimilation) as well as genes predicted to encode a nearly complete oxidative tricarboxylic acid cycle (consistent with organic carbon consumption) in *C. symbiosum*, suggesting that this organism has the potential to function either as a strict autotroph or as a mixotroph utilizing both CO_2 and organic material as carbon sources (Hallam et al., 2006a, b). In fact, organic geochemical evidence indicated that either of these metabolic lifestyles or even both are real possibilities. On the basis of an isotopic mass balance model, 83% of *in situ* archaeal production at 670 m water depth was estimated to be chemoautotrophic, and the balance heterotrophic (Ingalls et al., 2006). It remains to be determined if either the archaeal mixotrophs, or a mixed community of autotrophic and heterotrophic archaea dominated by autotrophs, are the dominant organisms in these environments. The 3-hydroxypropionate pathway employs several enzymes typically associated with bacterial fatty acid biosynthesis, including the biotin-dependent acetyl-CoA/propionyl-CoA carboxylase (Moss and Lane, 1971). Since archaeal lipids are typically devoid of fatty acids, the presence of acetyl-CoA carboxylase in *Crenarchaeota* is necessary evidence for autotrophic carbon assimilation by the 3-hydroxypropionate cycle.

Here, for the first time, we present the development and application of molecular tool for specific 'fishing' of archaeal acetyl-CoA carboxylase *acc*A gene from the deep-sea environment. The study site is located offshore in the Tyrrhenian Sea and is characterized as having highly oligotrophic, bathypelagic conditions at the depth below 1000 m. The samples were taken from 3000 m depth. Functional characterization of ammonia-oxidizing autotrophic *Crenarchaeota* also has been accomplished with DNA and mRNA studies of archaeal ammonia mono-oxygenase *amo*A gene isolated from the same water samples. The further phylogenetic analysis has demonstrated the existence of Mediterranean-specific 'ecotypes' of both analysed genes, confirming the uniqueness of this warm deep-sea microbial habitat (Zaballos et al., 2006; Martin-Cuadrado et al., 2007).

2. Methods

2.1. Sampling site and sample collection

Seawater from two 10 L Niskin bottles housed on a rosette with conductivity–temperature–depth (CTD) sensors were sampled during the CIESM-SUB2 cruise (December 2005, RV *Urania*) from the depth of 3000 m at Station 4 (VECTOR), located in the southern Tyrrhenian Sea area at 39°32.050′N, 13°22.280′E. The water mass at this depth is named the Tyrrhenian Dense Water (TDW), which results from the mixing of oligotrophic Eastern overflow water with waters resident in the western basin when they cascade down to ~2000 m from the channel of Sicily (Millot et al., 2006). Twenty litre samples of seawater were filtered through 47 mm diameter, 0.2 μm pore-size Nuclepore filters (Millipore, Billerica, MA, USA). Collected material was resuspended in 100 μL of TE buffer (pH 8.0) containing lysozyme (5 mg/mL), lysed by adition of 300 μL of lysis buffer QRL1 (Qiagen, Milan, Italy) and stored at −20 °C until processing.

2.2. DNA, RNA extraction and reverse transcription RT-PCR

Total genomic DNA and RNA were extracted from filters using Qiagen RNA/DNA Mini Kit (Qiagen, Milan, Italy). The extraction was carried out according to the manufacturer's instructions. DNA and RNA were stored in isopropanol at −20 °C before the precipitation. RNA was treated with "DNA-free" kit (Ambion). The quality of the RNA sample was examined by agarose electrophoresis, and concentrations were determined using the NanoDrop® ND-1000 Spectrophotometer (Wilmington, DE, USA). cDNA synthesis of *amo*A gene were performed using SuperScript II Reverse Transcriptase (Invitrogen, Carlsbad, CA, USA) as described elsewhere (Yakimov et al., 2007). Mixture (final volume 20 μL) for each reaction contained 4 μL of 5X First-Strand Buffer, 3 μL of template RNA, 1 μL of random primers (50–250 ng), dNTP (10 mM each) and 1 μL of SuperScript II RT (200 units). The reaction was carried out in a MasterCycler 5331 Gradient (Eppendorf, Hamburg, Germany), after initial incubation at 25 °C for 10 min, the cDNA synthesis was at 42 °C for 50 min. The reaction was

stopped by heating at 80 °C for 5 min. The cDNA was used as the template for a further PCR amplification. Possible DNA contamination of RNA templates was routinely monitored by PCR amplification of RNA aliquots that were not reverse transcribed. No contaminating DNA was detected in any of these reactions.

2.3. Amplification of amoA and accA genes, cloning and sequencing

Total DNA and the cDNA synthetized were used for the amplification of ammonia mono-oxygenase subunit A (*amo*A) and acetyl-CoA carboxylase alpha subunit (*acc*A) gene. *amo*A gene was amplified using a specific primers set ArcamoAF (5′-STAATGGTCTGGCTTAGACG-3′) and ArcamoAR (5′-GCGGCC ATCCATCTGTATGT-3′) (Francis et al., 2005). The sets of specific primers for *acc*A gene were designed based on the alignment of all the known sequences of the acetyl-CoA carboxylase (*acc*) gene and depicted in Table 1. PCR products were visualized on an 1% agarose gel, specific bands (635 and 883 bp-long amplicons for *amo*A and *acc*A genes, respectively) were cut out and purified using QIAquick gel extraction kit (Qiagen, Milan, Italy). The purified PCR products were ligated into pGEM plasmid vector (Promega, Madison WI, USA) and transformed by electroporation into the *Escherichia coli* DH10B cells (Invitrogen, Carlsbad, CA, USA). Transformants were selected on LB containing 100 mg/mL of ampicillin under blue–white selection. The clone libraries were screened by direct colony PCR amplification. The reaction was carried out in a MasterCycler 5331 Gradient PCR (Eppendorf, Hamburg, Germany) as follows: initial denaturation at 94 °C for 5 min; 35 cycles of 1 min at 94 °C, 1 min at 50 °C, and 2 min at 72 °C; final extension step of 10 min at 72 °C. Sequencing reaction were performed using the ABI Prism Big Dye 3.1 Terminator Cycle sequencing kit and an ABI Prism 3100 Avant (Applied Biosystems).

2.4. Sequencing and phylogenetic analysis

Sequence analysis was performed as previously described (Hallsworth et al., 2007; Yakimov et al., 2007). Briefly, all sequences were edited with MacVector Software (Accelrys, San Diego, CA) version 7.2.2 (Rajagopal, 2000) and compared with DNA or amino acid sequences in the public domain through the Basic Local Alignment Search Tool (BLAST) (Altschul et al., 1997; Pearson, 1990). Phylogenetic trees were constructed using the Neighbor Joining method and Jukes-Cantor distance matrix; 1000 bootstrap resamplings were performed to estimate the reproducibility of the tree. Random order input of sequences, single jumbling and the global rearrangement option were used. A multiple sequence alignment and the phylogeny of AmoA and AccA protein homologues were constructed using MacVector 7.2.2 software with BLOSUM matrix, open and extend gap penalties of 10.0 and 0.05, respectively. The alignment file was then analysed with the same software for calculation of the distance matrix. Neighbor Joining algorithm and Poisson correction of distances were used to construct the phylogenetic tree; 1000 bootstrap resamplings were performed to estimate the reproducibility of the tree.

Table 1
Acetyl-CoA carboxylase alpha subunit-specific primers used for detection and quantitative analysis of *acc*A-like genes attributed to marine *Crenarchaeota*.

Primer	Annealing site[a]	Sequence (5′–3′)
PcB_388F	388–410	GGB GGB GCM MGW ATW CAR GAR GG
PcB_1271R	1252–1271	GGC CAH GCR TAR TTN AYR TC
Crena_529F	529–552	GCW ATG ACW GAY TTT GTY RTA ATG
Crena_981R	961–981	TGG WTK RYT TGC AAY TAT WCC
AccAF573	573–592	GTT YGT YAC DGG DCC YGA YG
AccAR279	697–718	TGA TRT RRT CCA TRC AHT CRT A
TaqMan® AccTaq183	620–646	TTT CRW TBG AYG AWY TDG GTG GAG CWA

[a] C. *symbiosum* (CENSYa_1660) and *N. maritimus* (NmarDRAFT_1629) *acc*A genes numbering.

2.5. Nucleotide sequence accession numbers

Sequence data have been submitted in the DDBJ/EMBL/GenBank data bases under AM901402–AM901411 (*accA*) and AM901412–AM901420 (*amo*A).

3. Results and discussion

Autotrophic carbon assimilation in prokaryotic organisms implies five known pathways of autotrophic CO_2 fixation: (a) the unidirectional reductive pentose phosphate cycle, (b) the bidirectional reductive acetyl coenzyme A (CoA) pathway, (c) the reductive tricarboxylic acid pathway, (d) the unidirectional 3-hydroxypropionate cycle and € e) reductive monocarboxylic acid cycle. Genes predicted to encode components of eight steps mediating the 3-hydroxypropionate cycle, including acetyl-CoA/propionyl-CoA carboxylase, were unambiguously identified in the *C. symbiosum* A genome fosmid sequences (Hallam et al., 2006a, b). Although four additional steps represented by malonyl-CoA reductase and propionyl-CoA synthase could not be definitively annotated, the presence of acetyl-CoA carboxylase in *C. symbiosum* A is necessary evidence that *C. symbiosum* A has the genetic potential to encode a modified version of the 3-hydroxypropionate cycle for CO_2 incorporation into biomass.

To have an initial insight in distribution of archaeal *acc*A-like genes in marine environments, an attempt to develop a highly specific PCR-based approach was performed. Using the recently annotated genome of *C. symbiosum* with circular chromosome as a single contig of 2,045,086 bp and draft genome of second marine crenarchaeon, Candidatus *Nitrosopumilus maritimus* SCM1, with a linear contig of 1,311,773 bp (available online at the GenBank website as RefSeq. DP000238 and NZ_ABEO01000001, respectively), we sought the archaeal *acc*A-like sequences in whole genome shotgun (WGS) of Sargasso Sea (Venter et al., 2004) and metagenomic library of the water column at the North Pacific Subtropical Gyre ALOHA station (DeLong et al., 2006; Mincer et al., 2007). By using the CENSYa_1660 and NmarDRAFT_1629 sequences encoding for putative acyl-Co-A carboxylases as the template, four and two WGS sequences were identified in Sargasso Sea and deep Pacific (4000 m) metagenomes. A set of degenerated oligonucleotides (PcB_388F ad PcB_1271R) designed from these sequences was used for PCR amplification and cloning of *acc*A homologues from isolated DNA.

Phylogenetic affiliation of deduced amino acid sequences of 96 PCR products revealed significant similarities between acetyl-CoA/propionyl-CoA carboxylase genes in bacteria and archaea. Almost 70% of all Tyrrhenian clones harboring *acc*A-like genes were partitioned between two distinct clades, unambiguously affiliated within group of marine *Crenarchaeota*, whereas the balance was represented by various bacterial AccA/PccB-like sequences (Fig. 1). Even though dramatically divergent at the nucleotide level ($\geqslant$64% sequence similarity), all marine *Crenarchaeota acc*A-like genes shared striking homology at the level of deduced amino acid sequences ($\geqslant$79% and $\geqslant$90% of identity and similarity, respectively). This kinship appears to scale across oceanic provinces from the Antarctic, Atlantic and Pacific oceans to the Mediterranean basin.

Fig. 1. Phylogenetic affiliation of putative acyl- and propionyl-CoA carboxylases AccA/PccB recovered from deep Tyrrhenian Sea (3000 m) as determined by neighbor-joining analysis and Poisson correction of distances. The clones attributed to *Crenarchaeota* are shown as two phylogenetically related lineages, Cluster_1 and Cluster_2. Their unambiguous affiliation is depicted in more detail in Fig. 2. The scale bar represents 10% amino acid sequence divergence.

Similar topology of phylogenetic tree, constructed at nucleotide level, confirmed the distribution of 67 Tyrrhenian 'archaeal' clones into two clades with six subgroups sharing ⩾98% nucleotide sequence identity (Fig. 2). The majority of Tyrrhenian *acc*A-like clones (46,3%) formed an 'Ecotype_1a' distantly related to the HOTS_Contig48812 and HOTS_Contig54507, the WGS sequences retrieved from seawater (4000 m depth) from North Pacific Subtropical Gyre, Hawaii Ocean Time Series station ALOHA (Delong et al., 2006; Mincer et al., 2007). The sequences similar to the rest of Tyrrhenian *acc*A-like clones were recovered only from meso- and bathypelagic seawater in the Eastern Mediterranean (Lat. 35°18.27′N and 21°23.46′E). Taking into account the masses of Tyrrhenian Dense Water are mainly composed of cascaded Eastern Overflow Water (Millot et al., 2006), the presence of endemic monophyletic 'Ecotypes' 1b and 2, adapted to this particular environment (the densest, oldest, highly oligotrophic and warm, deep water masses), is suggested.

Further analysis of alignment with metagenomic WGS reads containing crenarchaeal sequences allowed us to design the set of primers, Crena_529F and Crena_975R, specifically targeting *acc*A-like genes attributed to marine *Crenarchaeota*-specific. Moreover, the conserved region at 573–718 bp position (CENSYa_1660 and NmarDRAFT_1629 numbering) was applied to develop TaqMan® methodolgy for quantitative PCR analysis of

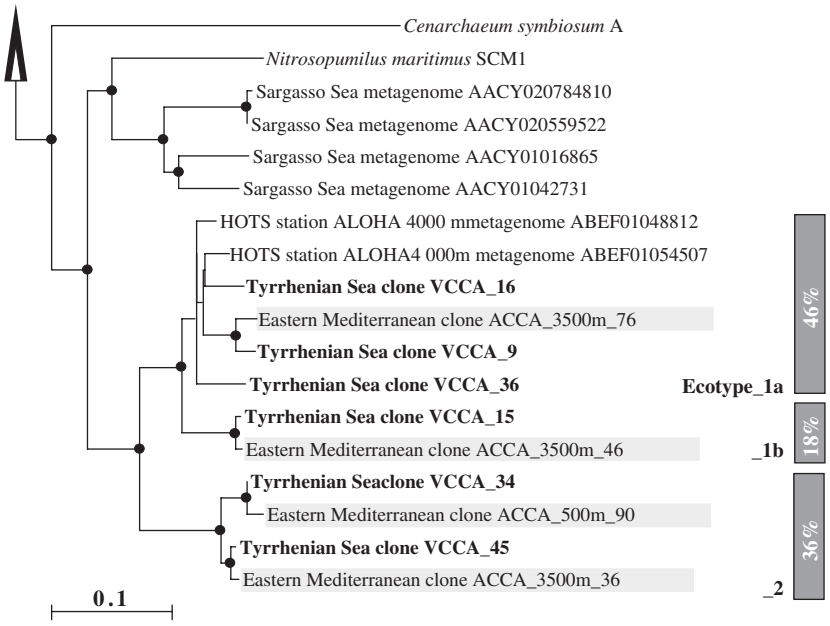

Fig. 2. Phylogenetic relationships of the three crenarchaeal *acc*A-like 'ecotypes' retrieved from deep Tyrrhenian Sea (3000 m) and from Eastern Mediterranean (35°18.27′N and 21°23.46′E) waters at 500 and 3500 m. The tree was constructed using sequences of *acc*A genes of *N. maritimus* SCM1 (NZ_ABEO01000001) and *C. symbiosum* A (DP000238) together with alignable gene fragments from the Sargasso Sea and North Pacific Subtropical Gyre (HOTS station ALOHA) metagenome databases. The tree is rooted and out-grouped with *acc*A genes of *Haloquadratum walsbyi* DSM 16790 (NC_008212) and *Caldicellulosiruptor saccharolyticus* DSM 8903 (CP000679), respectively. Neighbor-joining analysis using 1000 bootstrap replicates was used to infer tree topology, and the nodes with the percentage of bootstrap re-sampling above 75% are indicated by filled cycles. All clones retrieved from Tyrrhenian Sea are listed in bold, whereas Eastern Mediterranean clones are gray shaded. The scale bar represents 10% sequence divergence. Additionally, the percentage of the Tyrrhenian clones attributed to each phylotypes (1a, 1b and 2) found is shown as stack column.

*acc*A-like gene distribution (Table 1). The pool of crenarchaeal *acc*A-like genes examined by this approach showed their high abundance at the 3000-m-depth sample, 2083 ± 312 copies mL^{-1}. Taking into account that *acc*A gene presents as a single copy in two sequenced genomes, the number of *acc*A-harboring cells covered 33–76% of all *Crenarchaeota*, determined by CARD-FISH counting in the same sampling compartment (4250 ± 1090 cells mL^{-1}). This ~1:1 ratio between crenarchaeal cell number and *acc*A gene copies suggests an absolute dominance of the deep-sea planktonic autotrophic *Crenarchaea* in the bathypelagic realm of Tyrrhenian Sea.

To explore further the potential link between autotrophic fixation of CO_2 and energy metabolism, the diversity and abundance of crenarchael ammonia mono-oxygenase *amo*A gene were studied. A PCR-based approach for detection of *amo*A-like genes in deep Mediterranean Sea was used through the study (Yakimov et al., 2007). Archaeal library was constructed from total DNA pool isolated from the same seawater sample used for *acc*A analysis. A total of 96 clones were sequenced and their phylogenetic affiliation was estimated. All DNA-derived sequences are distributed between four subgroups with internal sequence similarities over 98%, and without any exceptions fell into Deep Marine Group I cluster (Hallam et al., 2006b) that contain the vast majority of known sequences recovered from global deep-sea environments (Fig. 3). This finding offers further evidence for the environmental specificity of crenarchaeal *amo*A sequences at the DNA level (Beman et al., 2007; Francis et al., 2007) and supports the idea that bathypelagic and abyssal *Crenarchaeota* are distinct from their shallow-water counterparts (Hallam et al., 2006b; Mincer et al., 2007).

As detected by TaqMan® approach (Yakimov et al., 2007), the number of *amo*A-like gene copies in the deep Tyrrhenian Sea, 5600 ± 504 copies mL^{-1}, was essentially the same as the number of CARD-FISH counted crenarchaeal cells, suggesting that ammonia oxidation is a pivotal energy-gaining pathway required to sustain the metabolic activity of marine *Crenarchaeota*.

As far as the expression of any gene is considered to be an unambiguous indicator of its corresponding enzymatic activity, the presence of *amo*A mRNA transcripts in the deep Tyrrhenian Sea water sample was therefore determined. After reverse transcription of mRNA with *amo*A-specific primer, cDNA was amplified and cloned. A total of 96 clones were sequenced and their phylogenetic affiliation estimated. Surprisingly, all mRNA-derived sequences formed a tight monophyletic group, which fell into a large cluster Shallow Marine Group I with sequences retrieved from shallow (up to 200 m) waters, sediments and corals (Beman et al., 2007). This cluster also contains two archaeal *amo*A-like sequences recovered from the depth of 3400 m in the Eastern Mediterranean (Yakimov et al., 2007). Such dramatic variation in crenarchaeal ammonia mono-oxygenase *amo*A with nature of nucleic acid is probably not introduced by PCR-derived biases, but likely reflects the differences in sensitivity of two groups marine *Crenarchaeota* to the changes of environmental conditions during cast recovery and subsequent seawater sample filtration. As proposed recently (Mincer et al., 2007), the significant phylogenetic partioning of putative *amo*A genes attributed to shallow and deep marine groups of *Crenarchaeota* could be due to photoinhibition-resistance adaptations. As *amo* genes are known to be membrane-spanning, this enzymatic complex could experience significant exposure to light and particular residue substitutions could compensate for this. As far as the deep-sea samples were decompressed and exposed to the light, the decompression and/or photoinhibition likely have affected the metabolic activity of deep-sea adapted Deep Marine Group I, followed by the strong decay of gene expression. As a consequence, inherently unstable macromolecules having very short half-lives, like mRNA, may not be detected in the stressed, deep-sea adapted cells, whereas more stable macromolecules, such as dsDNA, could effectively be retrieved. In contrast, proliferation of Shallow Marine Group I in bathypelagic realm was probably prevented by high pressure/pO_2 concentrations

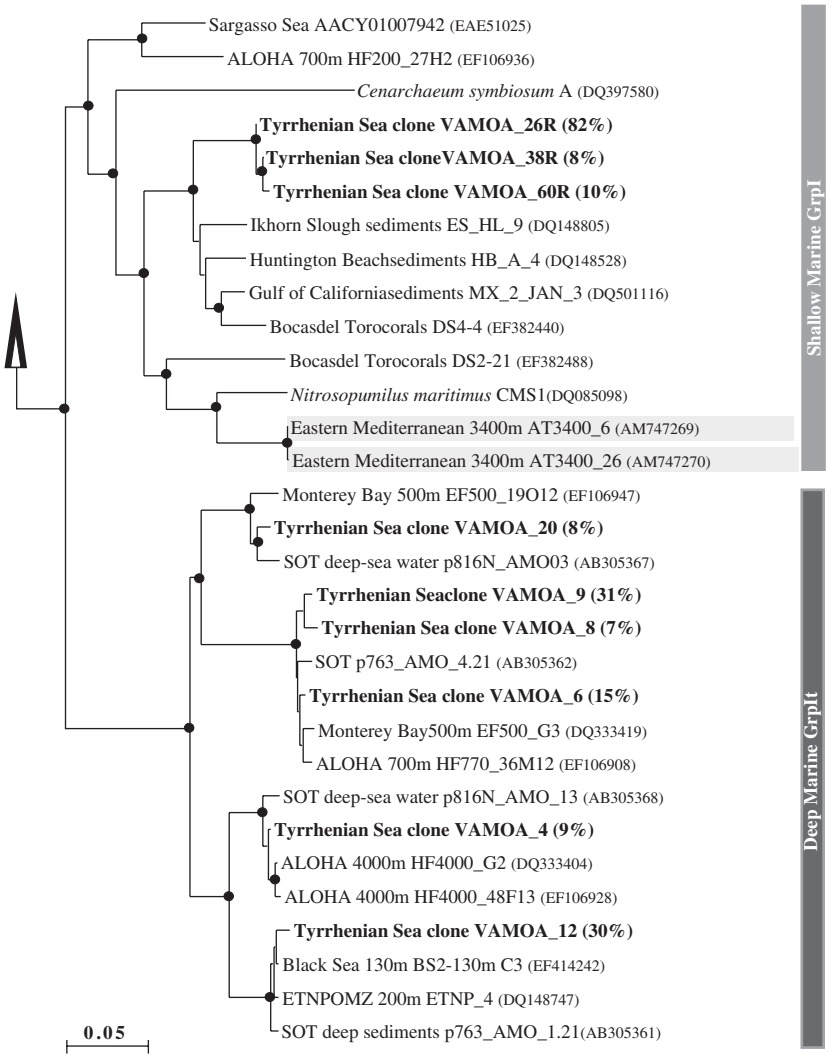

Fig. 3. Phylogenetic relationships of crenarchaeal *amo*A-like sequences retrieved from deep Tyrrhenian Sea (3000 m). The clones obtained by RT-PCR of *amo*A mRNA have the letter R at the end of name. The tree was constructed using sequences of comparable regions of the *amo*A gene sequences available in public databases. The tree is rooted with putative ammonia mono-oxygenase subunit A (*amo*A) gene found in soil metagenome (AJ627422). Neighbor-joining analysis using 1000 bootstrap replicates was used to infer tree topology and the nodes with the percentage of bootstrap re-sampling above 75% is indicated by filled circles. All clones retrieved from Tyrrhenian Sea are listed in bold, whereas Eastern Mediterranean (35°18.27′N and 21°23.46′E) clones are gray-shaded. The scale bar represents 5% sequence divergence. Additionally, the abundance of similar sequences among Tyrrhenian clones in corresponding DNA and mRNA libraries is shown as percentage. Abbreviation used: ALOHA, North Pacific Subtropical Gyre ALOHA station; SOT, Southern Okinawa Trough; ETNPOMZ, Eastern Tropical North Pacific Oxygen Minimum Zone.

(Hallam et al., 2006b). But these organisms, overwhelming in bathypelagic ecosystems by Deep Marine Group I, tolerated the decrease of pressure during cast recovery and following filtration, and thus their metabolic activity could be registered by the presence of mRNA transcripts. Clearly, more work needs to be done on marine crenarchaeons to test this hypothesis directly in the world's ocean. Further research also will be needed to infer the genetic, biochemical and physiological properties of this enigmatic group of prokaryotes, simply because archaeal autotrophy may be a general and quantitatively important (dark) ocean process. Marine *Crenarchaeota* may represent a significant global sink for inorganic carbon and form an important but as yet unrecognized component of the global carbon cycle.

Acknowledgments

This study was supported by the CIESM under CIESM-SUB activity and as a part of the European Science Foundation EUROCORES Programme EURODEEP supported by funds from the CNR and the EC Sixth Framework Programme under MIDDLE (06-EuroDEEP-FP-004 MIDDLE) project. We thank the captain and the crew of RV *Urania* for their expert handling of our casts and equipment in the Tyrrhenian Sea and for highly productive oceanographic cruises CIESM-SUB1 and CIESM-SUB2.

References

Altschul, S.F., Madden, T.L., Schaffer, A.A., Zhang, J., Zhang, Z., Miller, W., Lipman, D.J., 1997. Gapped BLAST and PSI-BLAST: A new generation of protein database search programs. Nucleic Acids Research 25, 3389–3402.

Beman, J.M., Roberts, K.J., Wegley, L., Rohwer, F., Francis, C.A., 2007. Distribution and diversity of archaeal ammonia monooxygenase genes associated with corals. Applied and Environmental Microbiology 73, 5642–5647.

DeLong, E.F., 1992. Archaea in coastal marine environments. In: Proceedings of the National Academy of Sciences of the United States of America. Vol. 89. pp. 5685–9.

DeLong, E.F., 1998. Everything in moderation: Archaea as 'non-extremophiles'. Current Opinions in Genetics & Development 8, 649–654.

DeLong, E.F., 2006. Archaeal mysteries of the deep revealed. In: Proceedings of the National Academy of Sciences of the United States of America. Vol. 103. pp. 6417–8.

Delong, E.F., Preston, C.M., Mincer, T., Rich, V., Hallam, S.J., Frigaard, N.U., Martinez, A., Sullivan, M.B., Edwards, R., Brito, B.R., Chisholm, S.W., Karl, D.M., 2006. Community genomics among stratified microbial assemblages in the ocean's interior. Science 311, 496–503.

Francis, C.A., Roberts, K.J., Beman, J.M., Santoro, A.E., Oakley, B.B., 2005. Ubiquity and diversity of ammonia-oxidizing archaea in water columns and sediments of the ocean. In: Proceedings of the National Academy of Sciences of the United States of America. Vol. 102. pp. 14683–8.

Francis, C.A., Beman, J.M., Kuypers, M.M.M., 2007. New processes and players in the nitrogen cycle: the microbial ecology of anaerobic and archaeal ammonia oxidation. The ISME Journal 1, 19–27.

Fuhrman, J.A., Davis, A.A., 1997. Widespread *Archaea* and novel *Bacteria* from the deep-sea as shown by 16S rRNA gene sequences. Marine Ecology Progress Series 150, 275–285.

Hallam, S.J., Konstantinidis, K.T., Putnam, N., Schleper, C., Watanabe, Y., Sugahara, J., Preston, C., de la Torre, J., Richardson, P.M., Delong, E.F., 2006a. Genomic analysis of the uncultivated marine crenarchaeote Cenarchaeum symbiosum. In: Proceedings of the National Academy of Sciences of the United States of America. Vol. 103. pp. 18296–301.

Hallam, S.J., Mincer, T.J., Schleper, C., Preston, C.M., Roberts, K., Richardson, P.M., Delong, E.F., 2006b. Pathways of carbon assimilation and ammonia oxidation suggested by environmental genomic analyses of marine *Crenarchaeota*. Public Library of Science: Biology 4 (4), e95.

Hallsworth, J.E., Yakimov, M.M., Golyshin, P.N., Gillion, J.L., D'Auria, G., de Lima, A.F., La Cono, V., Genovese, M., McKew, B., Hayes, S.L., Harris, G., Giuliano, L., Timmis, K.N., McGenity, T.J., 2007. Limits of life in $MgCl_2$-containing environments: Chaotropicity defines the window. Environmental Microbiology 9, 801–813.

Herndl, G.J., Reinthaler, T., Teira, E., van Aken, H., Veth, C., Pernthaler, A., Penthaler, J., 2005. Contribution of *Archaea* to total prokaryotic production in the deep Atlantic Ocean. Applied and Environmental Microbiology 71, 2303–2309.

Ingalls, A.E., Shah, S.R., Hansman, R.L., Aluwihare, L.I., Santos, G.M., Druffel, E.R., Pearson, A., 2006. Quantifying archaeal community autotrophy in the mesopelagic ocean using natural radiocarbon. In: Proceedings of the National Academy of Sciences of the United States of America. Vol. 103. pp. 6442–7.

Karner, M.B., DeLong, E.F., Karl, D.M., 2001. Archaeal dominance in the mesopelagic zone of the Pacific Ocean. Nature 409, 507–510.

Könneke, M., Bernhard, A.E., de la Torre, J.R., Walker, C.B., Waterbury, J.B., Stahl, D.A., 2005. Isolation of an autotrophic ammonia-oxidizing marine archaeon. Nature 437, 543–546.

Martin-Cuadrado, A.-B., Lòpez-Garcia, P., Alba, J.-C., Moreira, D., Monticelli, L., Srittmatter, A., Gottschalk, G., Rodriguez-Valera, F., 2007. Metagenomics of the deep Mediterranean, a warm bathypelagic habitat. Public Library of Science: One 9, e914.

Millot, C., Candela, J., Fuda, J.-L., Tber, Y., 2006. Large warming and salinification of the Mediterranean outflow due to changes in its composition. Deep-Sea Research I 53, 656–666.

Mincer, T.J., Church, M.J., Taylor, L.T., Preston, C., Karl, D.M., DeLong, E.F., 2007. Quantitative distribution of presumptive archaeal and bacterial nitrifiers in Monterey Bay and the North Pacific Subtropical Gyre. Environmental Microbiology 9, 1116–1175.

Moss, J., Lane, M.D., 1971. The biotin-dependent enzymes. Advances in Enzymology Related Areas: Molecular Biology 35, 321–442.

Pearson, W.R., 1990. Rapid and sensitive sequence comparison with FASTP and FASTA. Methods in Enzymology 183, 63–98.

Rajagopal, I., 2000. Software: Genomics made easy. Science 290, 474.

Treusch, A.H., Leininger, S., Kletzin, A., Schuster, S.C., Klenk, H.-P., Schleper, C., 2005. Novel genes for nitrite reductase and Amo-related proteins indicate a role of uncultivated mesophilic crenarchaeota in nitrogen cycling. Environmental Microbiology 7, 1985–1995.

Venter, J.C., Remington, K., Heidelberg, J.F., Halpern, A.L., Rusch, D., Eisen, J.A., Wu, D., Paulsen, I., Nelson, K.E., Nelson, W., Fouts, D.E., Levy, S., Knap, A.H., Lomas, M.W., Nealson, K., White, O., Peterson, J., Hoffman, J., Parsons, R., Baden-Tillson, H., Pfannkoch, C., Rogers, Y.H., Smith, H.O., 2004. Environmental genome shotgun sequencing of the Sargasso Sea. Science 304, 66–74.

Yakimov, M.M., La Cono, V., Denaro, R., D'Auria, G., Decembrini, F., Timmis, K.N., Golyshin, P.N., Giuliano, L., 2007. Primary producing prokaryotic communities of brine, interface and seawater above the halocline of deep anoxic lake L'Atalante, Eastern Mediterranean Sea. The ISME Journal 1, 743–755.

Zaballos, M., López-López, A., Ovreas, L., Bartual, S.G., D'Auria, G., Alba, J.C., Legault, B., Pushker, R., Daae, F.L., Rodríguez-Valera, F., 2006. Comparison of prokaryotic diversity at offshore oceanic locations reveals a different microbiota in the Mediterranean Sea. FEMS Microbiology Ecology 56, 389–405.

Deep-Sea Research II 56 (2009) 755–762

Contents lists available at ScienceDirect

Deep-Sea Research II

journal homepage: www.elsevier.com/locate/dsr2

Organic matter composition, metazoan meiofauna and nematode biodiversity in Mediterranean deep-sea sediments

Antonio Pusceddu *, Cristina Gambi, Daniela Zeppilli, Silvia Bianchelli, Roberto Danovaro

Dipartimento di Scienze del Mare, Università Politecnica delle Marche, Via Brecce Bianche, 60131 Ancona, Italy

ARTICLE INFO

Article history:
Accepted 7 August 2008
Available online 8 November 2008

Keywords:
Deep-sea sediments
Organic matter
Meiofauna
Nematodes
Mediterranean Sea
Seamounts

ABSTRACT

To identify the relationships between the abundance and biodiversity of deep-sea meiofauna and their food resources in the Tyrrhenian Sea (Mediterranean Sea), we have investigated the quantity and biochemical composition of sediment organic matter, the metazoan meiofauna abundance and biomass, and the nematode biodiversity at meso- (>50 km) and/or local (<1 km) scales. Sediment samples were collected at four deep-sea sites (from 3430 to 3581 m in depth), two of which were close to two seamounts. The analysis of variance revealed significant differences at both the meso- and local scales (i.e. between sites and between stations at each site), and showed that the variability at the mesoscale was much higher than that at the local scale. The values of all of the investigated variables were generally lowest in sediments surrounding the seamounts, suggesting a role for these submersed structures in the abundance of the metazoan meiofauna and their resources. The nematode assemblage composition changed significantly across the four sites. Among the 96 identified nematode species, 14 were exclusively seen in sediments around the two seamounts, and only three species were present at all sampling stations. Differences in the trophic structures of the nematode assemblages were also linked with differences in the biochemical composition of sediment organic matter. These results indicate that high β-diversity in soft sediments around deep seamounts is associated with diversification of the benthic food webs, and suggest that while making the sediments poorer for food availability for benthic consumers, the presence of seamounts enhances the biodiversity in neighbouring sediments.

1. Introduction

Over the last few decades, evidence has accumulated demonstrating that the deep-ocean floor is characterised by a high spatial heterogeneity. Along the continental margins, the canyons, slumps, open slopes and seamounts are characterised by widely variable topographic features (Weaver et al., 2004), which can contribute locally to the heterogeneous distribution of nutrients and biota (Palanques et al., 2005; Canals et al., 2006). An increasing number of deep-sea sites have been found to host hot-spots of organic matter, biomass and biodiversity (Boetius et al., 1996; Danovaro et al., 2002, 2003, 2008), thus challenging the 'paradigm' of decreasing abundance and biomass of macro- and meiobenthic organisms with increasing depth (Rex et al., 2006). Recently, Gambi and Danovaro (2006) demonstrated that the influence of energy availability on the deep-sea fauna distribution changes on different spatial scales, and that the analysis of spatial variability at the mesoscale is crucial for an understanding of the relationships between deep-sea benthic fauna and environmental drivers. Despite this, the spatial heterogeneity and the role that the different topographic features have concerning deep-sea biological features have remained little investigated.

Due to its paleo-ecological, topographic and environmental features, the Mediterranean Sea is characterised by strong trophic gradients and is a hot-spot of marine biodiversity (Myers et al., 2000; Danovaro and Pusceddu, 2007). Therefore, it represents a model for investigating the patterns of deep-sea biomass and biodiversity and their relationships with the available energy. Recently, Danovaro et al. (2008) indicated that biodiversity patterns in the deep Mediterranean Sea are not controlled by the amount of food resources, but, instead, that bioavailability is the key factor. They also indicated that the deep Mediterranean Sea is characterised by an extremely high turnover diversity (β-diversity), both among sites at different depths, as well as at similar depths at different longitudes or within the same basin.

The present study was aimed at investigating the relationships between food availability and the abundance, biomass and taxa richness of the meiofauna and the biodiversity of nematodes in the deep Tyrrhenian Sea (western Mediterranean Sea). We initially hypothesised that: (i) the variability of the quantity and quality of organic matter and of meiofauna assemblage attributes does not change at either local (within 100 m) or meso- (at more

* Corresponding author. Tel.: +39 71 2204335; fax: +39 71 2204650.
E-mail address: a.pusceddu@univpm.it (A. Pusceddu).

0967-0645/$ - see front matter © 2008 Elsevier Ltd. All rights reserved.
doi:10.1016/j.dsr2.2008.10.012

than 50 km distance) scales; and (ii) the nematode biodiversity and trophic structure do not change at the meso-scale (i.e. between sites at more than 50 km distance in the same basin). Moreover, with the aim of providing new insights into the possible roles of seamounts for the deep-sea meiofauna inhabiting neighbouring sediments, two of the four investigated sites were located close to the Palinuro and Marsili seamounts.

2. Methods

2.1. Study sites and sampling strategy

The sampling area was located in the southern Tyrrhenian Sea (Mediterranean Sea) (Fig. 1A, B). Sediment samples were collected in the framework of the CIESM-SUB 1 cruise, from 21 to 31 July, 2005, on board the R/V *Universitatis*. The sampling strategy included a set of four sites that were located at similar depths (from 3430 to 3581 m), about 50 km distance from each other. Two of these sites were located close to the Palinuro (site 1 at 3581 m in depth) and the Marsili (site 2 at 3430 m in depth) seamounts. At each of the four sites, undisturbed sediment samples were collected by three independent deployments of a multicorer (Bowers and Connelly, Mod. Mini) that was equipped with four liners (inner diameter, 6 cm). For all of the biochemical variables, and for meiofauna abundance and biomass, three replicate measurements from each of the three different liners obtained from separate deployments were made, for a total of 36 determinations per variable. For nematode biodiversity and trophic structure, three replicate measurements were made for the single deployment per site (i.e. only at the mesoscale), for a total of 12 determinations (Fig. 1C).

For the analyses of the biochemical composition of the organic matter in the sediment, the top first cm of three replicate liners from each multicorer deployment was frozen at −20 °C until analysis (completed within 30 days of the end of the cruise).

For the metazoan meiofauna variables and the analysis of nematode diversity, liners were vertically sectioned into different sediment horizons (0–1, 1–3, 3–5, 5–10, 10–15 cm), preserved in buffered 4% formalin solution, and stained with Rose Bengal. Since more than 90% of all of the meiofauna specimens were found in the first 3 cm, we report here only the values integrated down to 15 cm in depth.

2.2. Analysis of potential food sources

Chlorophyll-*a* and phaeopigment analyses were carried out according to Lorenzen and Jeffrey (1980) and the concentrations are reported as $\mu g\,g\,DW^{-1}$. The total phytopigments were defined as the sum of chlorophyll-*a* and phaeopigments.

The protein, carbohydrate and lipid contents of the sediments were determined spectrophotometrically, and their concentrations are expressed as bovine serum albumin, glucose and tripalmitine equivalents, respectively (Pusceddu et al., 2004). For each biochemical assay, blanks were obtained using pre-combusted sediments (450 °C for 4 h). All of the analyses were performed as three replicates, with about 1 g of sediment per sample. The protein, carbohydrate and lipid sediment contents were converted into carbon equivalents using the conversion factors of 0.49, 0.40 and $0.75\,\mu g\,C\,\mu g^{-1}$, respectively, and their sum was defined as the biopolymeric organic carbon (Fabiano et al., 1995).

2.3. Meiofauna

For the meiofauna extraction, the sediment samples were sieved through a 1000-μm mesh, and a 20-μm mesh was then used to retain the smallest organisms. The fraction remaining on the latter sieve was re-suspended and centrifuged three times with Ludox HS40 (density $1.31\,g\,cm^{-3}$), according to Heip et al. (1985). All of the meiobenthic animals were counted and classified according to taxon, under a stereomicroscope and after staining with Rose Bengal ($0.5\,g\,l^{-1}$). Since the analysis of soft-bodied organisms can be difficult in formalin-preserved samples, some fresh samples were analysed immediately after sampling, to identify the characteristics of the different meiofauna taxa. All of the soft-bodied organisms from the preserved samples were mounted on slides and viewed at 1000 × magnification.

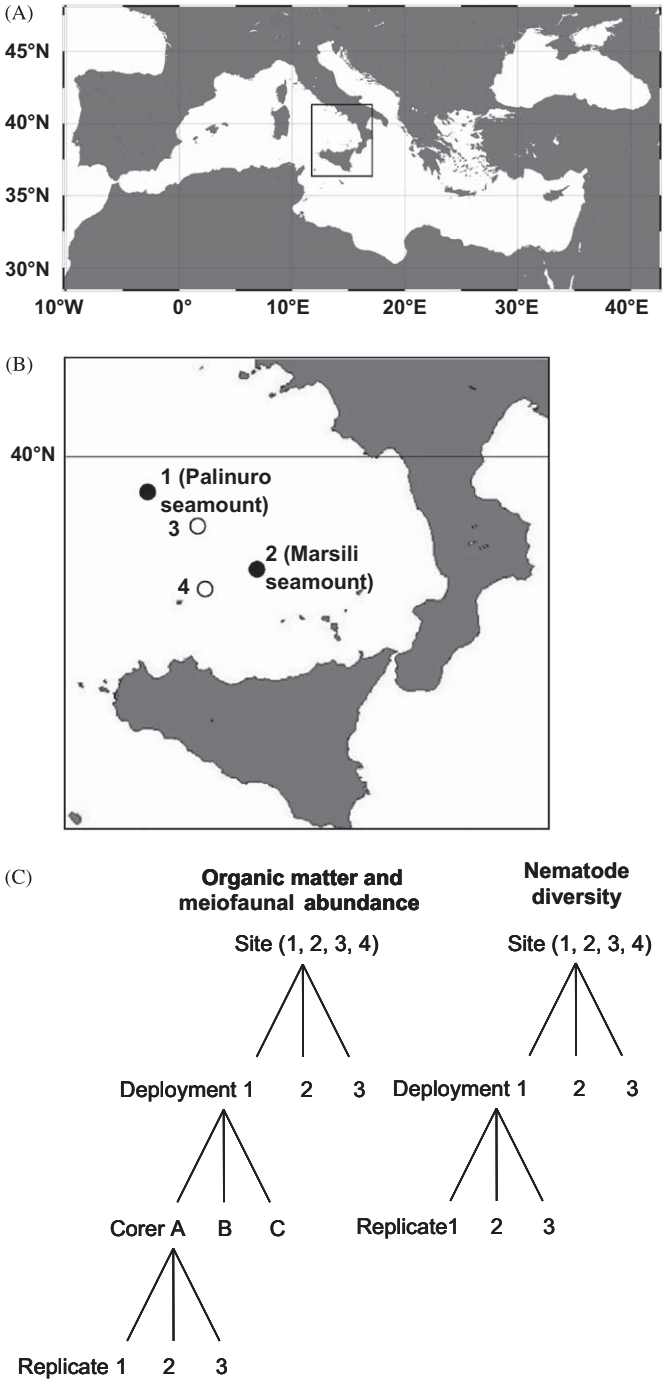

Fig. 1. The study area (A), the location of the four sampling sites (B), and the sampling strategy (C) adopted for organic loads and meiofauna assemblages (left panel) and nematode biodiversity and trophic structure (right panel).

Nematode biomass was calculated from the biovolume, which was estimated from all of the specimens using the Andrassy (1956) formula ($V = L \times W^2 \times 0.063 \times 10^{-5}$, in which body length, L, and width, W, were expressed in μm). The biovolumes of all of the specimens of other taxa encountered were calculated using the formula $V = L \times W^2 \times C$, where L and W were expressed in mm, and C is the approximate conversion factor for each meiofauna taxon, as reported by Feller and Warwick (1988). The total biovolume was multiplied by a mean density of $1.13\,g\,cm^{-3}$ to estimate the wet weight. The dry weight was calculated as 25% of the wet weight (Wieser, 1960) and converted into carbon content, which was assumed to be 40% of the dry weight (Feller and Warwick, 1988).

2.4. Nematode biodiversity

For the biodiversity analysis, following the use of the formalin–ethanol–glycerol technique described by Seinhorst (1959) to prevent dehydration, all of the nematodes (from three independent replicates) were withdrawn and mounted on slides. The nematodes were identified to the species level (whenever possible, due to the presence of several unknown species), according to Platt and Warwick (1983, 1988), Warwick et al. (1998) and the recent literature dealing with new nematode genera and species.

Species diversity (H', as log-base 2) was measured using the Shannon information function (Shannon and Weaver, 1949) and the evenness as J' (Pielou, 1975). The species richness (SR) was calculated as the total number of species collected at each station, and the Margalef index (D) was estimated as $D = (S-1)/\ln N$, where S is the number of species and N is the number of individuals in the sample (Margalef, 1958). Moreover, at each site, the species abundance data were converted into rarefaction diversity indices (Sanders, 1968, as modified by Hurlbert, 1971). The expected number of species for a theoretical sample of 51 specimens, ES(51), was selected. The β-diversity (i.e. turnover diversity) was estimated through the SIMPER analysis (Gray, 2000). A ranked matrix of Bray–Curtis similarities obtained on a presence-absence raw matrix was used as input for this test. All of these indices and analyses were performed using PRIMER v5 (Plymouth Marine Laboratory, UK; Clarke, 1993).

The trophic composition was defined according to Wieser (1953). The nematodes were divided into four original groups, as follows: (1A) no buccal cavity or a fine tubular one: selective (bacterial) feeders; (1B) large but unarmed buccal cavity: non-selective deposit feeders; (2A) buccal cavity with scraping tooth or teeth: epistrate or epigrowth (diatom) feeders; (2B) buccal cavity with large jaws: predators/omnivores. Moens and Vincx (1997) and Moens et al. (1999) proposed a modified feeding-type classification based on: (1) microvores; (2) ciliate feeders; (3) deposit feeders *sensu strictu*; (4) epigrowth feeders; (5) facultative predators; and (6) predators. However, in the present study, the Wieser classification was preferred because it is still widely used and because no information was available for most of the genera encountered in these deep-sea systems.

2.5. Statistical analyses

To test for differences in organic matter quantity and meiofauna abundance and biomass between the four sampling sites and the three deployments, a two-way analysis of variance (ANOVA) was applied using the GMAV 5.0 software (University of Sydney, Australia). Sites and deployments (nested in sites) were treated as random factors with four and three levels, respectively.

To test for differences in nematode diversity and the trophic structure between the four sampling sites (treated as random factors with four levels), a one-way analysis of variance (ANOVA) was applied using the GMAV 5.0 software (University of Sidney, Australia). Prior to analyses, the homogeneity of variance was tested by the Cochran test, and when necessary, the data were appropriately transformed.

To ascertain the potential relationships between meiofauna abundance and their food resources, a non-parametric multivariate multiple regression analysis based on Euclidean distances was also applied, using the routine DISTLM forward (Anderson, 2003). The forward selection of the predictor variables was carried out with tests by permutation. P values were obtained using 4999 permutations of raw data for the marginal tests (tests of individual variables), while for all of the conditional tests, the routine uses 4999 permutations of residuals under a reduced model.

3. Results

3.1. Food sources, meiofauna abundance, biomass and assemblage composition

The concentrations of all of the biochemical compounds and the meiofauna abundances and biomasses differed significantly both between sites, and within each site between deployments (Table 1). Generally, the organic matter concentrations and the meiofauna abundance and biomass in the sediments neighbouring the two seamounts (sites 1 and 2) were lower than those in the non-seamount sediments (sites 3 and 4; Fig. 2A–D). The biochemical compositions of the sediments also differed between the four sites, with site 1 having lower protein and higher carbohydrate fractions than the other three sites (Fig. 2B). For all of the biochemical variables (except carbohydrates) and the meiofauna abundance and biomass, the relative percentages of variance revealed that the variability between the sites was much higher than that between the deployments at each site (Table 1).

When fitting each variable individually, the marginal tests of the multiple regression analysis revealed that all of the investigated biochemical compounds were significantly related to the meiofauna abundance (Table 2a). The forward selection procedure indicated that the carbohydrates and proteins together explained about 86% of the meiofauna abundance variance, while the lipids and phytopigments together contributed only about 1% (Table 2b).

Overall, only five metazoan meiofauna taxa were found in the entire study area. Nematodes and copepods (including their nauplii) were seen at all of the sites, and together they represented the most abundant taxa (83–98% for nematodes and 1–11% for copepods). Polychaetes and tardigrades were seen only at site 3 (5% and 0.5%, respectively). Kinorhynchs were seen only at site 1.

In the two sites neighbouring the seamounts, the nematodes accounted for 35–51% of the total meiofauna biomass, while the copepods accounted for 43–65%. At the two non-seamount sites, the nematodes accounted for a mean of 45% of the total meiofauna biomass, followed by copepods (38%), polychaetes (25%) and all of the remaining taxa (less than 6% when pooled together). The differences in the meiofauna biomass between the sites were mostly attributable to the presence of polychaetes in site 3 (Fig. 2D).

3.2. Nematode biodiversity

The ANOVA revealed that none of the estimated diversity indices differed significantly among the sites, except the species

Table 1
Output of the two-way analysis of variance, including the computation of the variance components for the site and deployment effects.

Variable	Source	DF	MS	*F*	*P*	% Variance
Phytopigments	Site	3	15.216	262.88	***	99
	Deployment (site)	8	0.058	11.19	***	1
	Residuals	24	0.005			0
Protein	Site	3	6 623 726	41.18	***	91
	Deployment (site)	8	160 831	6.86	***	6
	Residuals	24	23 451			0
Carbohydrate	Site	3	3 042 878	130.32	***	100
	Deployment (site)	8	23 349	0.48	n.s.	0
	Residuals	24	48 723			
Lipid	Site	3	99 954	14.97	**	79
	Deployment (site)	8	6677	9.5	***	15
	Residuals	24	702			0
Biopolymeric C	Site	3	4 077 796	56.17	***	91
	Deployment (site)	8	72 599	2.44	*	3
	Residuals	24	29 796			0
Meiofauna abundance	Site	3	2803	6.06	**	61
	Deployment (site)	8	462	25.18	***	35
	Residuals	24	18.366			0
Meiofauna biomass	Site	3	11.940	48.64	***	94
	Deployment (site)	8	0.245	22.51	***	6
	Residuals	24	0.011			0

n.s., not significant.
* $P<0.05$.
** $P<0.01$.
*** $P<0.001$.

richness, which in sediments close to the two seamounts (sites 1 and 2) was from 1.4- to 4.3-fold higher than at sites 3 and 4 (Table 3).

Overall, 96 nematode species (belonging to 21 families) were identified. The highest number of families (17) and species (52) were seen at site 4, while the lowest (eight families and 12 species) were seen in the site 2 sediments, close to the Marsili seamount. Only five families (Desmoscolecidae, Linhomoeidae, Oxystominidae, Sphaerolaimidae and Xyalidae) were found at all four sites, while Enchelidiidae, Ironidae and Leptosomatidae were seen only at sites 1 and 2. Only three species were present at all of the sampling sites, with 14 species exclusively encountered in the sediments surrounding the seamounts, and 49 at the other two sites.

The SIMPER analysis revealed a high coefficient of dissimilarity between the four sites, with the highest dissimilarity (83%) seen between the sediments surrounding the two seamounts (Table 4). The ANOSIM analysis revealed that the compositions of the nematode assemblages significantly differed both between the sediments close to the two seamounts and between the other two sites.

At all of the investigated sites, the nematode assemblage was dominated by deposit feeders (altogether accounting for 50–64% of the total nematode abundance). In the sediments close to sites 1 (Palinuro seamount) and 3, epistrate feeders were more abundant than predator–omnivores, whereas the opposite was seen in the sediments close to sites 2 (Marsili seamount) and 4 (Fig. 3).

4. Discussion

4.1. Local versus mesoscale variability in quantity and quality of food resources and meiofauna

Low values of organic matter concentration are typical of deep-sea Mediterranean sediments (Gambi and Danovaro, 2006). Our data have shown that the organic matter concentrations in deep-sea sediments of the Tyrrhenian Sea are equivalent to about 50% of those reported for other locations at similar depths in the western Mediterranean (Gambi and Danovaro, 2006). These results are consistent with the gradient of trophic conditions reported to occur along the longitudinal axis of the Mediterranean Sea (Danovaro, 2003; Danovaro and Pusceddu, 2007). On the other hand, the abundance, biomass and taxa richness of the meiofauna in sediments of the deep Tyrrhenian Sea were very low, and similar or even lower than those encountered in the ultra-oligotrophic deep eastern Mediterranean Sea (Gambi and Danovaro, 2006).

Recently, Gambi and Danovaro (2006) demonstrated that the variability in meiofauna abundance of deep Mediterranean sediments on a local scale (i.e. <7 km) at similar depths (i.e. about 3000 m in depth) is lower than that seen at higher spatial scales (i.e. mesoscale, at about 30 km distance; and regional scale, between the western and eastern sectors of the basin).

Our results here indicate that all of the investigated variables showed significant differences between the sites as well as between the deployments at the same site. Moreover, in

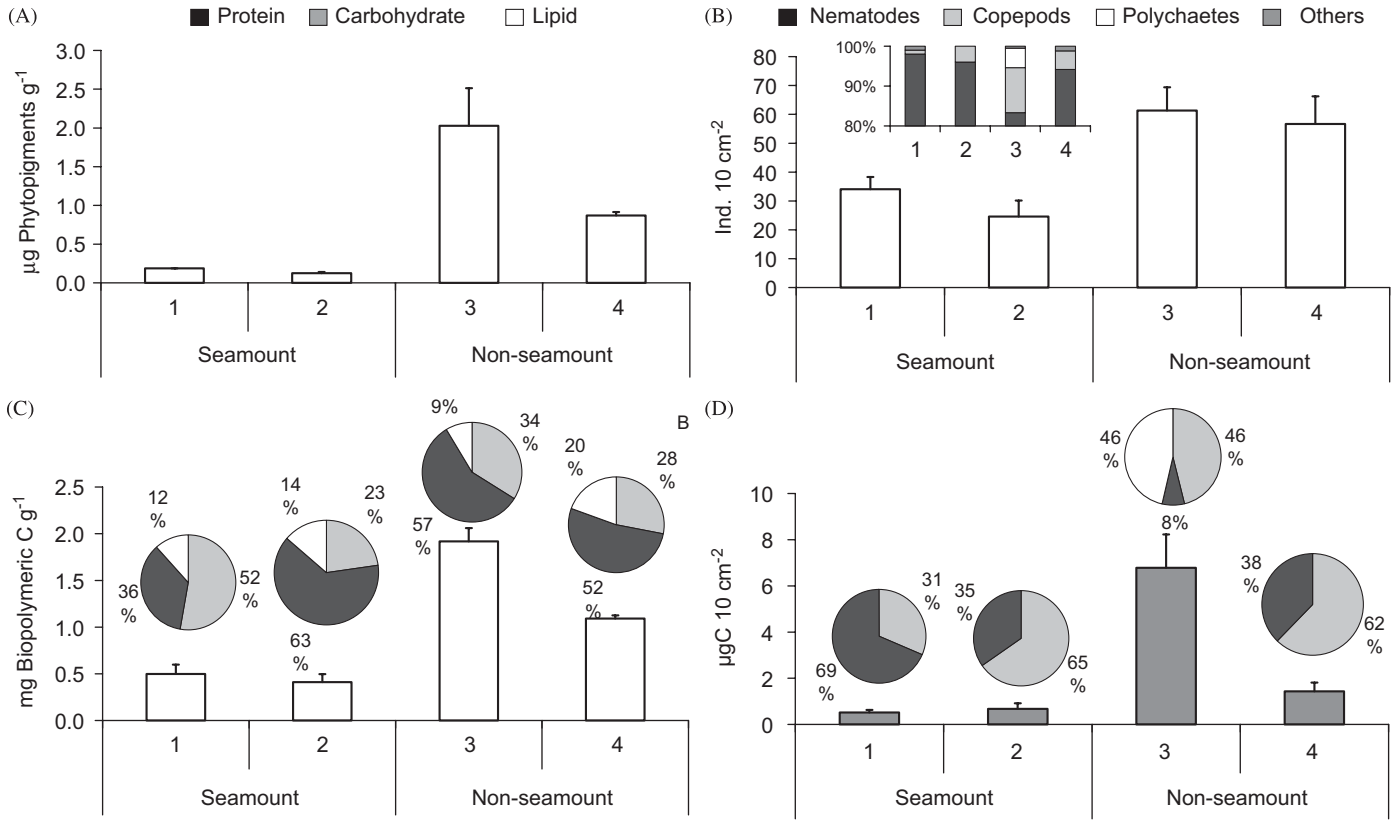

Fig. 2. Total phytopigment (A), biopolymeric C contents and its biochemical composition (B), total meiofauna abundance and its taxonomic composition (C), and meiofauna biomass and its taxonomic composition (D) in the sediments of the deep Tyrrhenian Sea. In panel D, the group "Others" includes Tardigrades and Kinorhynchs.

Table 2
Results of multiple regression analysis of organic compounds on meiofauna abundance.

(a) Marginal tests

Variable	*F*	*P*	% Variance
Carbohydrates	44.5092	0.0002	0.5669
Proteins	48.5444	0.0002	0.5881
Lipids	113.3852	0.0002	0.7693
Phytopigments	32.8985	0.0002	0.4918

(b) Conditional (sequential) tests

Variable	*F*	*P*	% Variance	% Variance cumulative
Carbohydrates	113.3852	0.0002	0.7693	0.7693
Proteins	21.5133	0.0002	0.0910	0.8604
Lipids	2.5330	0.1252	0.0102	0.8706
Phytopigments	0.0440	0.8468	0.0002	0.8708

(c) Correlations among variables

Variable	Carbohydrates	Proteins	Lipids	Phytopigments
Carbohydrates	–			
Proteins	0.8878	–		
Lipids	0.5776	0.7197	–	
Phytopigments	0.8926	0.9505	0.6158	–

% Variance: percentage of variance explained by the variable.
(a) Results of the marginal tests (i.e. fitting each variable individually, ignoring other variables).
(b) Results of the forward selection procedure with the conditional tests (i.e. fitting each variable one at a time, conditional on the variables that are already included in the model).
(c) The correlation matrix among all pairs of explanatory variables of meiofauna abundance deriving from the first analysis.

agreement with Gambi and Danovaro (2006) and Dell'Anno et al. (2003) for different regions of the Mediterranean basin, we report here that the variability of the quantity of the deep-sea meiofauna and organic matter at the mesoscale (i.e. at >50 km distance) is much higher than that on the small local scale (hundreds of metres distance). On the one hand, this allows consideration of the observed patterns as a typical feature of the deep Mediterranean Sea. On the other hand, together with the previous studies, our results indicate that the relationship between meiofauna abundance and their food resources is consistent at the basin scale, but changes at scales lower than the local one.

The results of the present study allowed us to definitely reject both the null hypotheses of no differences in (i) the quantity and quality of organic matter and of meiofauna assemblage at either local (within 100 m) and meso- (at more than 50 km distance) scales; and (ii) in the nematode biodiversity and trophic structure between sites within the same basin. This result confirms what previously reported for the Mediterranean Sea at a basin scale (Gambi and Danovaro, 2006), but also stimulates further investigations on these patterns at other different spatial scales.

4.2. Relationships between meiofauna abundance and food availability

There are several studies that have been conducted worldwide in deep-sea systems that have reported that differences in the sediment trophic conditions can be invoked to explain the differences in abundance and biomass of benthic assemblages (Cosson et al., 1997; Smith et al., 1997; Gooday et al., 1998. 2001; Galéron et al., 2000; Hughes and Gage, 2004). Similar results have been reported for the metazoan meiofauna, which respond rapidly

Table 3
Meiofauna taxon richness and indices of nematode diversity at all of the sampling sites.

Site	Number of taxa	SR	H'	D	J	ES(51)
1 (Palinuro seamount)	5	36	3.8±0.4	4.8±0.9	0.968	15.0±3.6
2 (Marsili seamount)	2	12	3.6±0.4	4.4±0.4	1.000	12.0±0.4
3 (Non-seamount)	5	50	4.0±0.8	5.7±2.1	0.951	20.3±9.6
4 (Non-seamount)	5	52	4.0±0.5	5.8±0.8	0.889	22.0±4.4
ANOVA results (df = 3)	nd	nd	$F = 0.36$ ns	$F = 0.94$ ns	nd	$F = 2.07$ ns

SR, species richness; H', index of Shannon; D, index of Margalef; J, index of Pielou; ES(51), expected species number.
The results of the one-way ANOVA testing for differences in nematode biodiversity between the sampling sites (i.e. at the mesoscale).
ns, not significant; nd, not determined.

Table 4
Percentage dissimilarity of nematode assemblages composition between the four sites after the SIMPER analysis.

Site	1 (Palinuro seamount)	2 (Marsili seamount)	3 (Non-seamount)	4 (Non-seamount)
1 (Palinuro seamount)	–			
2 (Marsili seamount)	83% (*)	–		
3 (Non-seamount)	76%	78%	–	
4 (Non-seamount)	76%	78%	79%*	–

* $P < 0.05$ level of statistical significance (ANOSIM).

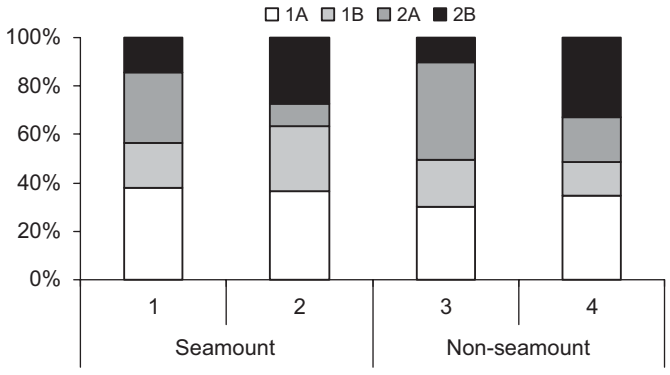

Fig. 3. Trophic structure of the Nematode assemblages at the four sites in the deep Tyrrhenian Sea. The percentage contributions are reported for selective deposit feeders (1A), non-selective deposit feeders (1B), epigrowth feeders (2A), and predators (2B).

to changes in food availability (Brown et al., 2001; Galéron et al., 2001; Danovaro et al., 2002; Gambi and Danovaro, 2006).

Our results here indicate that the meiofauna abundance is significantly related to all of the organic compounds, although up to 77% of its variance was explained by the carbohydrate concentrations alone. Moreover, our data also reveal that the total phytopigment content in sediments accounted for only a very small proportion of the meiofauna abundance variance. Both of these results are somewhat surprising. Carbohydrates are generally considered as refractory compounds (Tselepides et al., 2000), so that this positive relationship with the meiofauna abundance was not expected. Moreover, Danovaro et al. (2008) reported that for different sectors of the deep Mediterranean Sea, but not the Tyrrhenian Sea, most of the variability in the meiofauna abundance was related to the water-column depth and the total phytopigment concentrations. On the one side, the inconsistencies between our results and those reported from other Mediterranean regions suggest that the former are likely to be distinctive features of the deep Tyrrhenian region. On the other hand, the lack of a strong relationship between sedimentary phytopigment content and abundance of meiofauna can be at least partially explained by the presence of the particular hydrodynamic conditions that are typically associated with the presence of seamounts (as in sites 1 and 2). These include regional up- and down-welling processes, which can probably affect the export of material to the deep-sea basin surrounding the seamounts (Fock et al., 2002; Heinz et al., 2004; Diekmann et al., 2006).

4.3. Do seamounts have an effect on meiofauna distribution and biodiversity?

The water column surrounding seamounts is often characterised by the formation of eddies and circular currents (Taylor column), turbulent mixing of the benthic boundary layer, and regional up-wellings (Fock et al., 2002; Diekmann et al., 2006). These processes can influence primary and secondary production, organic matter fluxes down to the sea floor, and nutrient and fauna standing stocks on the top of the seamounts and in their proximity (Freeland, 1994; Parker and Tunnicliffe, 1994; Rogers, 1994; Vezina et al., 1995). These effects, however, might be site-specific, as Venrick (1991) reported for low chlorophyll-*a* concentrations above the Emperor Seamount Chain (western sub-arctic Pacific), which was attributed to the advection of pigment-depleted waters along the seamount chain rather than to *in-situ* changes. In contrast, Odate and Furuya (1998) reported two deep (75–90 m) chlorophyll maxima above the Komahashi No. 2 seamount (NW Pacific, offshore Japan), and related the first to the upward transport of nutrients caused by topography–current interactions over the seamount, as it coincided with uplifted isotherms, and the second to the lateral intrusion of an allochthonous water mass. Again, while some studies have suggested that over the top of seamounts the large-scale entrapment of water by topographically rectified currents can increase the downward flow of particulate organic matter to the sea floor (Brink, 1995; Mullineaux and Mills, 1997), others have reported lower levels of sedimentary organic carbon at the summit of seamounts, than on the adjacent slope and in the abyssal plain (Heinz et al., 2004; Weber et al., 2000).

Our study has here highlighted some differences in the ecological settings of seamount and non-seamount sediments, while it has also indicated that they were much higher between seamount sediments than between non-seamount sediments. For example, the biochemical compositions of non-seamount sediments were largely different from those at seamount site 1, but were rather similar to those at seamount site 2. Further studies are thus needed to clarify the factors, other than food availability, that may drive the meiofauna distribution around these systems.

Our data suggest here that the sediments close to the seamounts tend to harbour a low number of meiofauna taxa and a low nematode species richness, when compared with non-seamount sediments. At the same time, there were families and species exclusively present in the sediments close to the seamounts and absent in the other two sites, and *vice versa*. These findings suggest that the deep-sea nematode assemblages of the Tyrrhenian Sea are highly site-specific (i.e. they can vary at a regional scale within the same basin), and confirm previous studies that have indicated that the deep Mediterranean Sea can be characterised by extremely high turnover diversity (β-diversity) among sites within the same basin (Danovaro et al., 2008).

Seamounts are often characterized by their peculiar biological communities, when compared to adjacent systems (Boehlert and Genin, 1987; de Forges et al., 2000; Sassa et al., 2002), and our data at least partially support this concept also for the deep-sea sediments surrounding the Tyrrhenian Sea seamounts.

The nematode assemblages in the deep Tyrrhenian Sea were characterised by the dominance of Desmoscolescidae and Onchoilamidea, which are generally less abundant in bathyal sediments (Soetaert and Heip, 1989; Vanhove et al., 1999). In addition, the (few) specimens of Enchelidiidae, Ironidae and Leptosomatidae were exclusively found in the sediments surrounding the two seamounts. Again, among the 96 nematode species identified, only three were ubiquitous to all of the sampling stations, while 14 were exclusively from the sediments surrounding the two seamounts. This suggests a possible role of the seamounts in favouring the presence of particular assemblages.

The differences in biochemical composition of the organic matter between the sediments surrounding the two seamounts were reflected in the changes in the trophic structures of the nematode assemblages. Indeed, the sediments surrounding the Palinuro seamount were characterised by a low quantity and quality of potential food sources, and by the dominance of epistrate feeders. In contrast, the sediments surrounding the Marsili seamount were characterised by a higher food quality (i.e. a higher protein fraction), and the nematode assemblages were dominated by predators and omnivores. These data suggest that the presence of high-quality food items (i.e. with higher protein content) facilitates the energy transfer within the deep-sea nematode assemblages up to the predator level. This result is consistent with very recent findings reporting that the higher fraction of predators in the nematode assemblages of the deep Mediterranean Sea is associated with sediment organic matter that is characterised by higher protein contents (Danovaro et al., 2008).

Although there are tens of thousands of seamounts spread throughout the world oceans (Wessel, 2001), their biodiversity and their ecology are still little known. As we have here demonstrated for those of the Tyrrhenian Sea, our study suggests that, in addition, seamounts have a strong influence on the structure and functioning of the adjacent ecosystems, with these being reflected in their biodiversity patterns.

Acknowledgments

This study was carried out within the framework of the CIESM Sur-Un-Bateau Cruise programme. It was partially funded by the HERMES EU programme, and it is a contribution to the MARBEF EU Network of Excellence. We thank L. Giuliano for her key role in making this research possible, M. Magagnini (Polytechnic University of Marche) for valuable help during sampling, and S. Fraschetti (University of Lecce, Italy) for help with the statistical analyses. We are grateful to F. Briand and two anonymous referees for valuable comments on a previous version of the manuscript.

References

Anderson, M.J., 2003. DISTLM Forward: A FORTRAN Computer Program to Calculate a Distance-based Multivariate Analysis for a Linear Model using Forward Selection. Department of Statistics, University of Auckland, New Zealand.

Andrassy, I., 1956. The determination of volume and weight of nematodes. Acta Zoologica (Hungarian Academy of Science) 2, 1–15.

Boehlert, G.W., Genin, A., 1987. A review of the effects of seamounts on biological processes. In: Keating, B., Fryer, P., Batiza, R., Boehlert, G. (Eds.), Seamounts, Islands and Atolls. Geophysical Monographs 43, 319–334.

Boetius, A., Scheibej, S., Tselepides, A., Thiel, H., 1996. Microbial biomass and activities in deep-sea sediments of the Eastern Mediterranean: trenches are benthic hotspots. Deep-Sea Research I 43, 1439–1460.

Brink, K.H., 1995. Tidal and lower frequency currents above Fieberling Guyot. Journal of Geophysical Research 100, 10817–10832.

Brown, C.J., Lambshead, P.J.D., Smith, C.R., Hawkins, L.E., Farley, R., 2001. Phytodetritus and the abundance and biomass of abyssal nematodes in the central, equatorial Pacific. Deep-Sea Research I 48, 555–565.

Canals, M., Puig, P., Durrieu de Madron, X., Heussner, S., Palanques, A., Fabres, J., 2006. Flushing submarine canyons. Nature 444, 354–357.

Clarke, K.R., 1993. Non parametric multivariate analyses of changes in community structure. Australian Journal of Ecology 18, 117–143.

Cosson, N., Sibuet, M., Galéron, J., 1997. Community structure and spatial heterogeneity of the deep-sea macrofauna at three contrasting stations in the tropical northeast Atlantic. Deep-Sea Research I 44, 247–269.

Danovaro, R., 2003. Organic inputs and ecosystem efficiency in the deep Mediterranean Sea. Chemistry and Ecology 19, 391–398.

Danovaro, R., Pusceddu, A., 2007. Ecomanagement of biodiversity and ecosystem functioning in the Mediterranean Sea: concerns and strategies. Chemistry and Ecology 23, 347–360.

Danovaro, R., Gambi, C., Della Croce, N., 2002. Meiofauna hotspot in the Atacama Trench (southern Pacific Ocean). Deep-Sea Research I 49, 843–857.

Danovaro, R., Della Croce, N., Dell'Anno, A., Pusceddu, A., 2003. A depocenter of organic matter at 7800-m depth in the SE Pacific Ocean. Deep-Sea Research I 50, 1411–1420.

Danovaro, R., Gambi, C., Lampadariou, N., Tselepides, A., 2008. Deep-sea nematode biodiversity in the Mediterranean basin: testing for longitudinal, bathymetric and energetic gradients. Ecography 31, 231–244.

de Forges, B.R., Koslow, J.A., Poore, G.C.B., 2000. Diversity and endemism of the benthic seamount fauna in the southwest Pacific. Nature 405, 944–947.

Dell'Anno, A., Incera, M., Mei, M.L., Pusceddu, A., 2003. Mesoscale variability of organic matter composition in NW Adriatic sediments. Chemistry and Ecology 19, 33–45.

Diekmann, R., Nellen, W., Piatkowski, U., 2006. A multivariate analysis of larval fish and paralarval cephalopod assemblages at Great Meteor Seamount. Deep-Sea Research I 53, 1635–1657.

Fabiano, M., Danovaro, R., Fraschetti, S., 1995. A three-year time series of elemental and biochemical composition of organic matter in subtidal sandy sediments of the Ligurian Sea (north western Mediterranean). Continental Shelf Research 15, 1453–1469.

Feller, R.J., Warwick, R.M., 1988. Energetics. In: Higgins, R.P., Thiel, H. (Eds.), Introduction to the Study of Meiofauna. Smithsonian Institute Press, London, pp. 181–196.

Fock, H., Uiblein, F., Köster, F., von Westernhag, H., 2002. Biodiversity and species-environment relationships of the demersal fish assemblage at the Great Meteor Seamount (subtropical NE Atlantic), sampled by different trawls. Marine Biology 141, 185–199.

Freeland, H.J., 1994. Ocean circulation at and near Cobb Seamount. Deep-Sea Research I 41, 1715–1732.

Galéron, J., Sibuet, M., Mahaut, M.L., Dinet, A., 2000. Variation in structure and biomass of the benthic communities at three contrasting sites in the tropical northeast Atlantic. Marine Ecology Progress Series 197, 121–137.

Galéron, J., Sibuet, M., Vanreusel, A., Mackenzie, K., Gooday, A.J., Dinet, A., Wolff, G.A., 2001. Temporal patterns among meiofauna and macrofauna taxa related to changes in sediment geochemistry at an abyssal NE Atlantic site. Progress in Oceanography 50, 303–324.

Gambi, C., Danovaro, R., 2006. A multiple-scale analysis of metazoan meiofaunal distribution in the deep Mediterranean Sea. Deep-Sea Research I 53, 1117–1134.

Gooday, A.J., Bett, B.J., Shires, R., Lambshead, P.J.D., 1998. Deep-sea benthic foraminiferal species diversity in the NE Atlantic and NW Arabian sea: a synthesis. Deep-Sea Research I 45, 165–201.

Gooday, A.J., Huges, J.A., Levin, L.A., 2001. The foraminiferan macrofauna from three North Carolina (USA) slope sites with contrasting carbon flux: a comparison with the metazoan macrofauna. Deep-Sea Research I 48, 1709–1739.
Gray, J.S., 2000. The measurement of marine species diversity, with an application to the benthic fauna of the Norwegian continental shelf. Journal of Experimental Marine Biology and Ecology 250, 23–49.
Heinz, P., Ruepp, D., Hemleben, C., 2004. Benthic foraminifera assemblages at Great Meteor Seamount. Marine Biology 144, 985–998.
Heip, C., Vincx, M., Vranken, G., 1985. The ecology of marine nematodes. Oceanography and Marine Biology Annual Review 23, 399–489.
Hughes, D.J., Gage, J.D., 2004. Benthic metazoan biomass, community structure and bioturbation at three contrasting deep-water sites on the northwest European continental margin. Progress in Oceanography 63, 29–55.
Hurlbert, S.H., 1971. The non-concept of species diversity: a critique and alternative parameters. Ecology 52, 577–586.
Lorenzen, C., Jeffrey, J., 1980. Determination of chlorophyll in seawater. Technical Paper in Marine Science (UNESCO) 35, pp. 1–20.
Margalef, R., 1958. Information theory in ecology. General Systems 3, 36–71.
Moens, T., Vincx, M., 1997. Observations on the feeding ecology of estuarine nematodes. Journal of the Marine Biological Association of the United Kingdom 77, 211–227.
Moens, T., Verbeec, L.K., Vincx, M., 1999. Feeding biology of predatory and facultative predatory nematodes (*Enoploides longispiculosus* and *Adoncholaimus fucus*). Marine Biology 134, 585–593.
Mullineaux, L.S., Mills, S.W., 1997. A test of the larval retention hypothesis in semount-generated flows. Deep-Sea Research I 44, 745–770.
Myers, N., Mittermeier, R.A., Mittermeier, C.G., da Fonseca, G.A.B., Kent, J., 2000. Biodiversity hotspots for conservation priorities. Nature 403, 853–858.
Odate, T., Furuya, K., 1998. Well-developed subsurface chlorophyll maximum near Komahashi No. 2 Seamount in the summer of 1991. Deep-Sea Research 45, 1595–1607.
Palanques, A., García-Ladona, E., Gomis, D., Martín, J., Marcos, M., Pascual, A., Puig, P., Gili, J.-M., Emelianov, M., Monserrat, S., Guillén, J., Tintoré, J., Segura, M., Jordi, A., Ruiz, S., Basterretxea, G., Font, J., Blasco, D., Pagès, F., 2005. General patterns of circulation, sediment fluxes and ecology of the Palamós (La Fonera) submarine canyon, northwestern Mediterranean. Progress in Oceanography 66, 89–119.
Parker, T., Tunnicliffe, V.J., 1994. Dispersal strategies of the biota on an oceanic seamount: implications for ecology and biogeography. Biological Bulletin 187, 336–345.
Pielou, E.C., 1975. Ecological Diversity. Wiley, New York, p. 165.
Platt, H.M., Warwick, R.M., 1983. A Synopsis of the Free-Living Marine Nematodes. Part I: British Enoplids. Cambridge University Press, Cambridge, p. 307.
Platt, H.M., Warwick, R.M., 1988. A Synopsis of the Free-Living Marine Nematodes. Part II: British Chromadorids. Cambridge University Press, Cambridge, p. 502.
Pusceddu, A., Dell'Anno, A., Fabiano, M., Danovaro, R., 2004. Quantity and biochemical composition of organic matter in marine sediments. Biologia Marina Mediterranea 11 (Suppl. 1), 39–53.
Rex, M.A., Etter, R.J., Morris, J.S., Crouse, J., McClain, C.R., Johnson, N.A., Stuart, C.T., Deming, J.W., Thies, R., Avery, R., 2006. Global bathymetric patterns of standing stock and body size in the deep-sea benthos. Marine Ecology Progress Series 317, 1–8.
Rogers, A.D., 1994. The biology of seamounts. Advanced Marine Biology 30, 305–350.
Sanders, H.L., 1968. Marine benthic diversity: a comparative study. The American Naturalist 102, 243–282.
Sassa, C., Kawaguchi, K., Kinoshita, T., Watanabe, C., 2002. Assemblages of vertical migratory mesopelagic fish in the transitional region of the western North Pacific. Fisheries Oceanography 11, 193–204.
Seinhorst, J.W., 1959. A rapid method for the transfer of nematodes from fixative to unhydrous glycerine. Nematologica 4, 67–69.
Shannon, C.E., Weaver, W., 1949. The Mathematical Theory of Communication. University of Illinois, Urbana, IL.
Smith, C.R., Berelson, W., Demaster, D.J., Dobbs, F.C., Hammound, D., Hoover, D.J., Pope, R.H., Stephens, M., 1997. Latitudinal variations in benthic processes in the abyssal equatorial Pacific: control by biogenic particle flux. Deep-Sea Research II 44, 2295–2317.
Soetaert, K., Heip, C., 1989. The size structure of nematode assemblages along the Mediterranean deep-sea transect. Deep-Sea Research 36, 93–102.
Tselepides, A., Polychronaki, T., Marrale, D., Akoumianaki, I., Dell'Anno, A., Pusceddu, A., Danovaro, R., 2000. Organic matter composition of the continental shelf and bathyal sediments of the Cretan Sea (NE Mediterranean). Progress in Oceanography 46, 311–344.
Vanhove, S., Arntz, W., Vincx, M., 1999. Comparative study of the nematode communities on the south-eastern Weddell Sea shelf and slope (Antarctica). Marine Ecology Progress Series 181, 237–256.
Venrick, E.L., 1991. Mid-ocean ridges and their influence on the large-scale patterns of chlorophyll and production in the North Pacific. Deep-Sea Research A 38, S83–S102.
Vezina, A.F., Comeau, L.A., Bourgeois, M., Juniper, S.K., 1995. Relationship between phytoplankton production and the physical structure of the water column near Cobb Seamount, northeast Pacific. Deep-Sea Research I 42, 993–1005.
Warwick, R.M., Howard, H.M., Somerfield, P.J., 1998. A Synopsis of the Free-Living Marine Nematodes. Part III: Monhysterids. Field Studies Council, Shrewsbury, p. 296.
Weaver, P.E., Billett, D.M., Boetius, A., Danovaro, R., Freiwald, A., Sibuet, M., 2004. Hotspot ecosystem research on Europe's deep-ocean margins. Oceanography 17, 132–143.
Weber, M.E., von Stackelberg, U., Marchig, V., Wiedicke, M., Grupe, B., 2000. Variability of surface sediments in the Peru basin: dependence on water depth, productivity, bottom water flow, and seafloor topography. Marine Geology 163, 169–184.
Wessel, P., 2001. Global distribution of seamounts inferred from gridded Geosat/ERS-1 altimetry. Journal of Geophysical Research 106, 19431–19442.
Wieser, W., 1953. Die Beziehung zwischen Mundhöhlengestalt, Ernährungsweise und Vorkommen bei freilebenden marinen Nematoden. Arkiv för Zoologi 2–4, 439–484.
Wieser, W., 1960. Benthic studies in Buzzards Bay. II The meiofauna. Limnology and Oceanography 5, 121–137.

Deep-Sea Research II 56 (2009) 763–767

Contents lists available at ScienceDirect

Deep-Sea Research II

journal homepage: www.elsevier.com/locate/dsr2

PCR-based detection of bioluminescent microbial populations in Tyrrhenian Sea

Gabriela Gentile [a,b], Massimo De Luca [a], Renata Denaro [b], Violetta La Cono [b], Francesco Smedile [a], Simona Scarfì [a], Emilio De Domenico [a], Maria De Domenico [a], Michail M. Yakimov [b,*]

[a] Department of Animal Biology and Marine Ecology, University of Messina, Salita Sperone, 31, 98166 Messina, Italy
[b] Institute for Coastal Marine Environment (IAMC), CNR, Spianata S. Raineri 86, 98122 Messina, Italy

ARTICLE INFO

Article history:
Accepted 8 July 2008
Available online 31 October 2008

Keywords:
Deep-sea microbial communities
Bioluminescent bacteria
luxA gene
Uncultured bacteria

ABSTRACT

The present study is focused on the development of a cultivation-independent molecular approach for specific detection of bioluminescent bacteria within microbial communities by direct amplification of *luxA* gene from environmental DNA. A new set of primers, specifically targeting free-living bioluminescent bacteria, was designed on the base of l*uxA* sequences available from the public database. Meso- and bathypelagic seawater samples were collected from two stations in Tyrrhenian Sea at the depths of 500 and 2750 m. The same seawater samples also were used to isolate bioluminescent bacteria that were further subjected to *luxA* and 16S rRNA gene sequencing. PCR products obtained by amplification with designed primers were cloned, and the phylogenetic affiliation of 40 clones was determined. All of them were clustered into three groups, only distantly related to the *Photobacterium phosphoreum* and *Photobacterium kishitanii* clades. The half of all clones formed a tight monophyletic clade, while the rest of clones were organized in "compartment"-specific, meso- and bathypelagic ecotypes. No matches with *luxA* gene sequences of four bioluminescent strains, isolated from the same seawater samples, were observed. These findings indicate that the PCR-based approach developed in present manuscript, allowed us to detect the novel, "yet to be cultivated" lineages of bioluminescent bacteria, which are likely specific for distinct warm bathypelagic realms of Mediterranean Sea.

1. Introduction

Luminous bacteria have been extensively studied and well described phylogenetically and ecologically (Hastings, 1996; Sukovataya and Tyulkova, 2001; Ast and Dunlap, 2005; Ast et al., 2007). They are grouped on the basis of their capability to generate visible light, and they possess *lux* genes for light production (Dunlap and Kita-Tsukamoto, 2001). These bacteria are ubiquitous in marine environment and are occasionally found in fresh water, brackish water, and soil environments (Nealson and Hastings, 1992; Dunlap and Kita-Tsukamoto, 2001). Marine bioluminescent bacteria have been isolated from seawater, sediment, and detritus (Reichelt and Baumann, 1973; Ramesh et al., 1990) and have a broad distribution in shallow coastal environments and deep pelagic water. The distribution of cultivable marine luminescent bacteria in Mediterranean Sea has been extensively studied (De Domenico et al., 2005, 2006) and these studies have shown strong, area-specific differences in their distribution. In particular, the Strait of Gibraltar along with Alboran Sea is characterized by high relative abundances of bioluminescent bacteria comparable to those observed in the proximal Atlantic Ocean (Orndorff and Colwell, 1980). In all these areas the luminescent microbial communities are dominated by *Vibrio* spp. Quantitative estimation of bioluminescent bacteria in the Strait of Sicily and Ionian Sea show significantly lower number of these microorganisms, with a predominance of *Photobacterium phophoreum* (87%), whereas luminescent *Vibrio* and *Shewanella* spp. are only occasionally encountered in the samples collected in northern areas (De Luca, 2006).

Bioluminescent bacteria can be associated with living and nonliving marine organisms and colonize marine animals as saprophytes, commensals, and parasites (Ramesh et al., 1990; Dunlap and Kita-Tsukamoto, 2001; Cussatlegras et al., 2001; Geistdoerfer and Cussatlegras, 2001; Nealson et al., 1993; Ruby et al., 2005). Some species are marine fish and squids symbionts and are harbored in highly specialized light organs (Nealson and Hastings, 1992; Dunlap and Kita-Tsukamoto, 2001).

All known luminous bacteria are phylogenetically affiliated to γ-proteobacteria with 14 species of marine origins, nine species belonging to *Vibrio*, three to *Photobacterium*, and two to *Shewanella* genus (Kita-Tsukamoto et al., 2006).

Previous ecological studies have been based on conventional strategies to identify taxonomically the luminescent isolates (Reichelt and Baumann, 1973; Nealson, 1978). Luciferase enzyme

* Corresponding author. Tel.: +39 090 669003; fax: +39 090 669007.
E-mail address: michail.yakimov@iamc.cnr.it (M.M. Yakimov).

0967-0645/$ - see front matter © 2008 Published by Elsevier Ltd.
doi:10.1016/j.dsr2.2008.07.023

catalyzes the light-emitting reaction in luminous bacteria and *luxA* gene encodes the *alpha* subunit of luciferase (Wimpee et al., 1991; Makemson et al., 1997). More recently, PCR primers, which are suitable for the amplification and sequencing of *luxA* have been used (Wimpee et al., 1991; Budsberg et al., 2003). An interesting ecological study could be based on identification of bioluminescent bacterial communities inhabiting different habitats by direct culture-independent analysis of environmental samples omitting the isolation of the strains.

In this study we describe the initial attempts to develop a PCR-based approach for specific detection of bioluminescent bacteria directly from seawater collected during CIESM-SUB2 cruise. A set of primers targeting the 0.6K bp *luxA* fragment was designed on the base of available *luxA* gene sequences.

2. Material and methods

2.1. Samples collection and on-field processing

Seawater samples were collected in the Tyrrhenian Sea during CIESM-SUB2 cruise (13–22 December 2005) using 10-l Niskin water samplers (General Oceanics Inc., Miami, FL, USA) fitted on "Rosette" frame. In detail, seawater samples were collected at the depth of 2750 m (Station 4: latitude 39.5400N, longitude 13.3700E) and at 500 m (Station 6: latitude 38.9000N, longitude 14.5000E). For culture-independent detection of bioluminescent microbes, 5 l of each sample were filtered through 47-mm diameter 0.2-μm pore-size Nucleopore filters (Millipore) and subsequently stored in RNA*later* (Ambion) at −20 °C until processing in laboratory. For isolation of bioluminescent bacteria, 30 mL of seawater samples were filtered through a polycarbonate filter with a pore size of 0.47 μm (Millipore). Each filter was then placed with the bacterial side up on a Petri dish containing SWC agar medium (seawater 75%, 0.38 M NaCl, 0.02 M $MgCl_2 \cdot 6H_2O$, 0.25 M $MgSO_4 \cdot 7H_2O$, 8 mM KCl, 0.5% peptone, 0.3% yeast extract, 0.3% glycerol) and incubated at 15 °C in the dark for 7 days. For colony-forming units (CFU) counting, ten 100 μl seawater subsamples collected at each stations were directly spread onto Difco™ Marine Agar 2216 plates. This operation was repeated three times, and 60 plates in total were stored at 15 °C in the dark for 7 days before counting.

2.2. Design of PCR primers

For *luxA* gene amplification, all *luxA*-like sequences available from the GeneBank database including whole genome shot-gun (WGS) and environmental sequences libraries were employed and aligned using MacVector program version 7.2.2 (Accelrys, San Diego, CA, USA) (Rajagopal, 2000). As a result, the pair of slightly degenerated primers was designed and used through this study (Table 1).

2.3. DNA extraction, PCR amplification, cloning, and screening of luxA clones

Extraction of DNA from the filters was performed using RNA/DNA mini kit (Qiagen, Hilden, Germany); the quality of total DNA and RNA samples was examined by agarose gel electrophoresis and concentrations were determined using the NanoDrop® ND-1000 Spectrophotometer (Wilmington, DE, USA). PCR amplification of total DNA was performed with a GeneAmp PCR System 2700 (Applied Biosystems) using designed primers (Table 1). The 50-μl mixture (total volume) contained 10 × Titanium™ Taq PCR Buffer, 1 μM of each primer, 10 μM dNTPs (Gibco, Invitrogen, Carlsbad, CA, USA), 2.0 μl (40–250 ng) of DNA template and 2.0 U of Titanium™ Taq DNA Polymerase (Clontech). The reaction started with 5 min of hot start at 95 °C, continued with 40 cycles of 30 s at 94 °C, 30 s at 50 °C, and 90 s at 72 °C, and finished with a 10 min extension at 72 °C. PCR products were analyzed on agarose gel and purified with QIAquick Gel Extraction Kit (Qiagen).

Amplified gene fragments were cloned into the pGEM®-T Easy Vector (Promega) according to the manufacturer's instructions. The resulting ligation products were used to transform *Escherichia coli* DH10B cells (Invitrogen). Ninety-six white colonies from each clone library were randomly picked, and the 20 randomly picked cells were directly used in a PCR reaction with standard M13f and M13r primers under the conditions described above. Amplified inserts of expected size were identified by gel electrophoresis.

2.4. 16S rRNA and luxA gene amplification from bioluminescent isolates

Total genomic DNA of each bioluminescent isolate was extracted from a 5-ml late-exponential phase cell culture using RNA/DNA mini kit (Qiagen, Hilden, Germany). PCR amplification of the 16S rRNA genes was performed using the primers 16F27 (5′-AGAGTTTGATCMTGGCTCAG-3′) and 16R1492 (5′-TACGGYTACCTTGTTACGACTT-3′). PCR was performed in 50 μl of mixture containing 1 × Q-solution (Qiagen, Hilden, Germany), 1 × Qiagen reaction buffer, 1 μM of each primer, 10 μM dNTPs (Gibco, Invitrogen, Carlsbad, CA, USA), 2 μl of DNA template (40–250 ng), and 2 U of Taq Polymerase (Qiagen). The reaction started with a 3 min hot start at 95 °C, continued with 30 cycles of 1 min at 94 °C, 1 min at 50 °C, and 2 min at 72 °C, and finished with a 10-min extension at 72 °C. PCR amplification of *luxA* gene isolates was performed using primers 66F and 611R (Table 1) under conditions described above. 16S rDNA and *luxA* genes amplified products

Table 1
Sequences of degenerated primers designed through this study and the mismatches with conserved regions of several *luxA* gene sequences of bioluminescent bacteria.

luxA sequence	Primer 66F CAAATGTCRAAAGGTCGTTTTAATTTTGG	Primer 611R AACRAAATCWYKCCATTGRCCTTTAT
Photobacterium isolates (4)[a]	.....	.....
Clones (40)[a]	.....	.....
P. phosphoreum (five strains)	.....	.....
P. kichitanii (five strains)	.....	.....
Vibrio fischeri (two strains)	.....	.....
P. phosphoreum X55458	.....A.....C.....	.....
P. leiognathi (two strains)	.....A.....C.....	T.....G.....G.
S. hanedai AB058949	.....T.....	T.....G.
Vibrio harveyi X58791	.....A..A..CCG.....	G.....
P. luminescens M57416	.....A..A...CGG.....	T.....G.....C.....

[a] Obtained in this study.

were purified with QIAquick Gel Extraction Kit (Qiagen) following the manufacturer's protocol.

2.5. Sequencing and phylogenetic analyses

Sequencing was performed with an ABI PRISM 3100-Avant Genetic Analyzer (PE Applied Biosystems, Foster City, CA, USA) using the ABI PRISM BigDye® Terminator v3.1 Cycle Sequencing Kit (PE Applied Biosystems). Sequence analyses were performed using the Basic Local Alignment Search Tool (BLAST) (Altschul et al., 1997). Analyses of nucleotide sequences were performed using MacVector software, version 7.2.2 (Accelrys, San Diego, CA, USA) (Rajagopal, 2000). This software also was used for construction of phylogenetic trees using Neighbour-Joining method and Jukes–Cantor distance matrix; 1000 bootstrap re-samplings were performed to estimate the reproducibility of the tree.

2.6. Nucleotide sequence and accession number

Sequence data have been submitted in the DDBJ/EMBL/GenBank data bases under accession numbers AM933561–AM933562 (16S rDNA), and AM933563–AM933577 (*lux*A).

3. Results

3.1. Screening of luxA clone libraries

In spite of isolation of bioluminescent bacteria from seawater samples of Stations 4 and 6, all attempts to simultaneously amplify the *luxA* genes from the same samples failed using different sets of primers published elsewhere (Budsberg et al., 2003). The complete sequencing of *luxA* gene of CIESM-2 isolates amplified with *luxA–luxB* primers revealed the presence of several

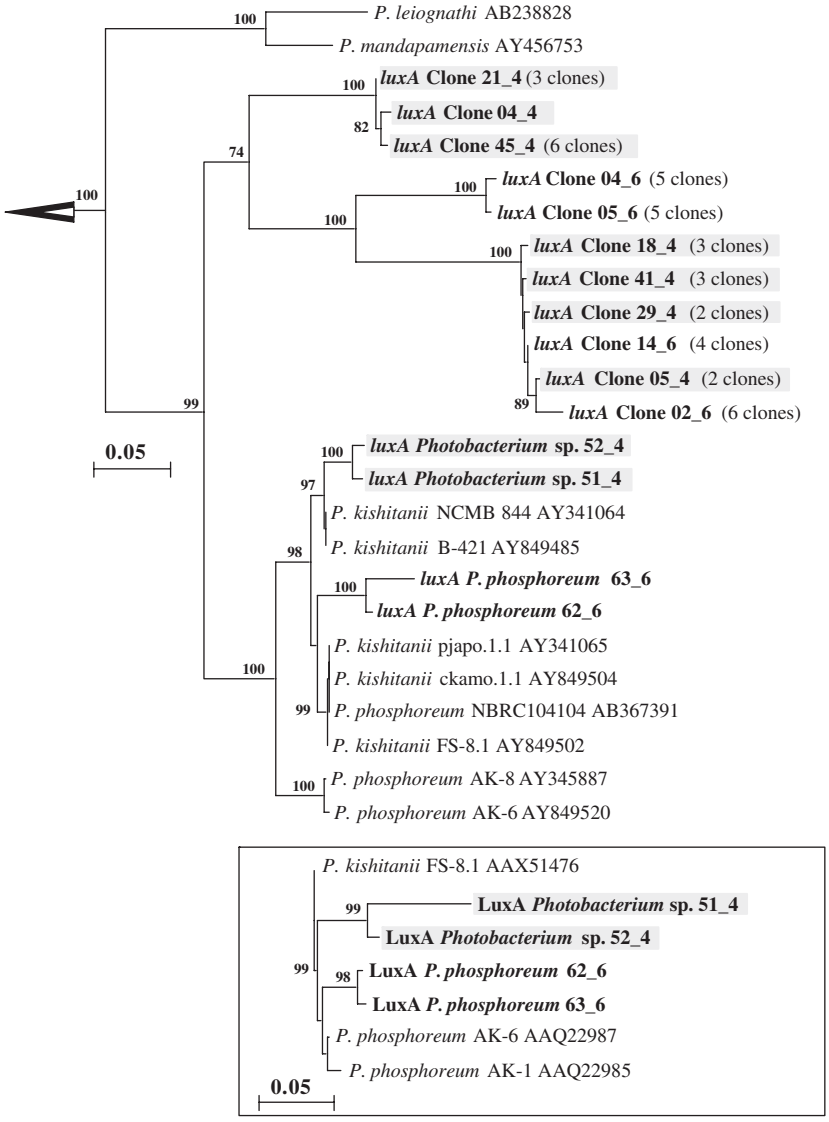

Fig. 1. Phylogenetic relationships of the three *lux*A-like "ecotypes" retrieved from clone libraries of meso- and bathypelagic water of Tyrrhenian Sea at 500 and 2750 m. The phylogenetic positioning of *luxA* gene sequences obtained from four bioliminescent stains isolated through this study is also present. The tree was rooted and out-grouped with *lux*A genes of *Shewanella hanedai* (AB058949) and *Vibrio fischeri* (AF170104), respectively. Neighbor-joining analysis using 1000 bootstrap replicates was used to infer tree topology and the percentage values of bootstrap re-sampling are shown at the proximity of the nodes. All clones and isolates retrieved from Tyrrhenian Sea are listed in bold and the 2750-m-derived sequences additionally evidenced as gray-shaded. The scale bar represents 5% sequence divergence. Inset: Phylogenetic affiliation of deduced sequence of LuxA protein of four bioluminescent isolates as determined by Neighbor-Joining analysis and Poisson correction of distances. The scale bar represents 5% amino acid sequence divergence.

mismatches in the targeted regions. Therefore a new set of *luxA*-specific primers (66F/611R) was designed to avoid this problem (Table 1). Further application of these primers was successful for amplification of 560-bp long product from total DNA isolated from seawater samples, although two additional PCR products with exceeding lengths were obtained from DNA of Station 4 (data not shown). All PCR products were further cloned and sequenced, and only those of expected size were affiliated to *luxA*-like genes. Phylogenetic analysis of 20 clones from each library revealed the presence of three distinct clusters with a high level of internal similarity (Fig. 1). Identical topology of the phylogenetic tree, produced on the base of deduced protein sequences (data not shown), establishes these clades as potential evolutionary distinct novel bacterial lineages.

3.2. Bioluminescent isolates 16S rRNA and luxA genes analysis

The concentration of DAPI-stained cells at 2800 m at Station 4 was 12,470 ± 1390 cells ml^{-1} and, as it was demonstrated by CARD-FISH counting, only half of them (48.6 ± 12.8%) were metabolically active (maintaining the ribosomes) bacterial cells (Tamburini et al., 2008). The similar situation was observed at 500 m at Station 6, where also only the half of 59,530 ± 6640 cells ml^{-1}, visualized by DAPI, were attributed to active bacterial cells. The obtained CFU counting was in accordance with low cultivability paradigm of marine bacterioplankton (Ferguson et al., 1984; Cho and Giovannoni, 2004) and only 0.8‰ and 0.4‰ of all prokaryotic cells, stained by DAPI, were successfully retrieved as growing colonies from the Stations 6 and 4, respectively.

SWC plate triplicates performed to obtain the bioluminescent colonies gave six isolates in total from each station. Taking into account the different CFU numbers, these strains correspondingly represent 0.14% and 1.33% of all cultivable bacterial cells from Stations 6 and 4. 16S rRNA genes from all isolates were amplified and their phylogenetic affiliation was determined. It was found that all isolates collected from the same station possess an identical 16S rRNA gene sequence. Based on these results, only two representative isolates from each station were further subjected to both phylogeny and *luxA* gene analyses. The almost complete 16S rRNA gene sequences of bioluminescent isolates retrieved from Station 6 (500 m depth) were unambiguously affiliated to the *Photobacterium phosphoreum* clade, while the isolates obtained from deeper water masses of Station 4 were distantly related to the clade of *Photobacterium kishitanii*, a new luminous marine bacterium symbiotic with deep-sea fishes (Ast et al., 2007) (Fig. 2).

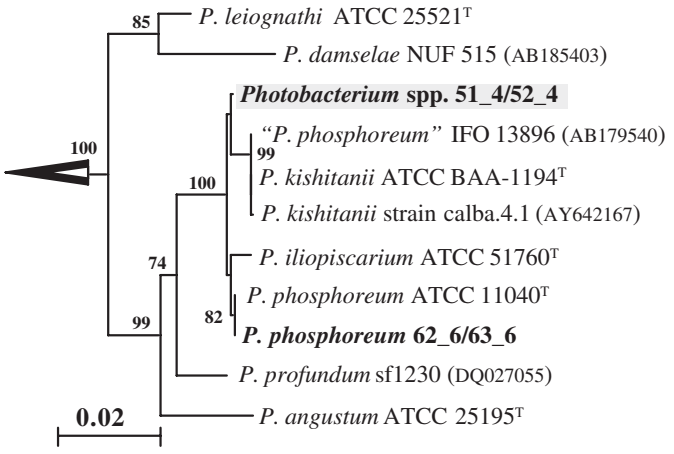

Fig. 2. Phylogenetic tree of *Photobacterium* including the four bioluminescent strains isolated in this study. The tree was rooted and out-grouped with 16S rRNA genes of *Cycloclasticus pugetii* (U57920) and *Vibrio fischeri* ATCC^T (X74702), respectively. Numbers at nodes are bootstrap support values based on 5000 resampling replicates. The scale bar represents 2% nucleotide sequence divergence.

Isolated strains were further subjected to a PCR amplification of *luxA* gene using 66F/611R set of primers. For each isolate, one gene fragment of expected size, corresponding to *luxA* gene, was amplified. Bidirectional sequencing of amplified inserts was performed to obtain the complete sequence of 561–567 bp lengths. As it shown in Fig. 1, phylogenetic analysis of the partial *luxA* nucleotide sequences confirmed the 16S-based placement of bioluminescent isolates into *phosphoreum/kishitanii* clades with a tendency to cluster closely with *kishitanii* clade. At the level of deduced protein, the LuxA sequences of isolates tested here were more affiliated to those of *P. phosphoreum* AK-6 and AK-8, isolated from the skin of the fishes (Ast and Dunlap, 2005) (Fig. 1, inset). No matches either at nucleotide or aa sequence levels were found with the environmental *luxA* clones retrieved from the same seawater samples.

4. Discussion

Numerous studies are mainly focused on the isolation and further characterization of bioluminescent bacteria inhabiting different environments (Budsberg et al., 2003; Wimpee et al., 1991; Makemson et al., 1997; Duncan et al., 1994), whereas very little is known about the distribution of bioluminescent bacteria within bacterioplankton communities actually thriving in marine ecosystems. At least for some pathogenic marine bacteria, the viable-but-not-culturable state is considered as a strategy of cellular response to adverse environmental conditions (Jones et al., 1991). It seems that this concept could be extended also to other marine bacteria, such as bioluminescent symbiotic species, that can find themselves as "free-living bacteria" in seawater rather than host tissue. Therefore, studies on distribution of bioluminescent microbial communities in marine habitats, such as Mediterranean Sea, and knowledge of their phylogeny and metabolic state are useful to understand their ecological significance and the role they carry out in environmental processes.

The present study is focused on development of PCR-based method oriented on specific detection of luminescent bacterial within bacterioplankton communities of two meso—and bathypelagic stations located in Tyrrhenian Sea during CIESM-SUB2 cruise (13–22 December 2005). A set of three degenerated primers was constructed on the basis of bacterial *luxA*-like gene sequences available from public databases The pair-wise alignment has demonstrated the sufficient annealing of designed set with the most important bioluminescent bacterial genera. Further on, the primers were used to amplify a fragment of *luxA* gene directly from total genomic DNA extracted from seawater samples and to construct corresponding clone libraries (192 clones in total). As revealed by sequence analysis of 20 clones from each library, the diversity of *luxA*-like genes was scarce and 95% and 100% phylotype coverage was obtained for clone library of Stations 4 and 6, respectively. The further phylogenetic affiliation of *luxA*-like genes revealed that half of all clones formed a tight monophyletic clade, while the rest were organized in "compartment"-specific meso- and bathypelagic groups. All these clades did not match with any of *luxA*-like genes, available from public databases including environmental and whole genome shot-gun sequence libraries (*E* values between $5e^{-18}$ and $1e^{-38}$). This finding indicates that the approach developed in present manuscript allowed us to detect the novel lineages of *luxA*-like genes, which could be, regarding their distant relation to known sequences, attributed to the bacteria, specific for warm bathypelagic realm of Mediterranean Sea.

Seawater samples used for DNA extraction were simultaneously subjected to the cultivation approach. Six identical bioluminescent strains were isolated from each station, and the 16S rRNA genes of four representative isolates were sequenced and analyzed. All isolates obtained from 500m-depth sample at Station 6 were related to the *P. phosphoreum* clade, while those obtained from bathypelagic seawater of Station 4 were distantly clustered with *P. kishitanii* strains. The further analysis of their *luxA*-like genes confirmed their taxonomical placement into *phosphoreum/kishitanii* clades. Thus the meso- and bathypelagic seawater in the sampled area of Mediterranean Sea (Tyrrhenian Sea) possesses the low diversity of "compartment"-specific cultivable bioluminescent bacteria.

None of the *luxA* sequences of the isolates matched with environmental *luxA*-like gene sequences retrieved from the same seawater used for cultivation approach. This finding directly demonstrates the strong limitation of cultivation-based approaches to study marine microbial ecology. Among *luxA*-like-possessing bacteria there are at least several, yet cultivation-resisting, lineages. In order to make these groups available for genome-enabled studies of physiology, the isolation approach will probably require approaches other than standard plating methods.

Acknowledgements

This study was supported by the CIESM under CIESM-SUB activity, by Project FIRB-MIUR under contract no. RBAU012K-XA008, by University of Messina under Project PRA 2003 and as a part of the European Science Foundation EUROCORES Programme EURODEEP under MIDDLE (06-EuroDEEP-FP-004 MIDDLE) project. We thank the captain and the crew of R.V. *Urania* for their expert handling of our casts and equipment in the Tyrrhenian Sea and for highly productive oceanographic cruises CIESM-SUB1 and CIESM-SUB2.

References

Altschul, S.F., Madden, T.L., Schaffer, A.A., Zhang, J., Zhang, Z., Miller, W., Lipman, D.J., 1997. Gapped BLAST and PSI-BLAST: a new generation of protein database search programs. Nucleic Acids Research 25, 3389–3402.

Ast, J.C., Dunlap, P.V., 2005. Phylogenetic resolution and habitat specificity of members of the *Photobacterium phosphoreum* species group. Environmental Microbiology 7, 1641–1654.

Ast, J.C., Cleenwerck, I., Engelbeen, K., Urbanczyk, H., Thompson, F.L., De Vos, P., Dunlap, P.V., 2007. *Photobacterium kishitanii* sp. nov., a luminous marine bacterium symbiotic with deep-sea fishes. International Journal of Systematic and Evolutionary Microbiology 57, 2073–2078.

Budsberg, K.J., Wimpee, C.F., Braddock, J.F., 2003. Isolation and identification of *Photobacterium phosphoreum* from an unexpected niche: migrating salmon. Applied and Environmental Microbiology 69 (11), 6938–6942.

Cho, J.-C., Giovannoni, S.J., 2004. Cultivation and growth characteristics of a diverse group of oligotrophic marine *Gammaproteobacteria*. Applied and Environmental Microbiology 70, 432–440.

Cussatlegras, A.S., Geistdoerfer, P., Prieur, L., 2001. Planktonic bioluminescence measurements in the frontal zone of Almeria-Oran (Mediterranean Sea). Oceanologica acta 24 (3), 239–250.

De Domenico, M., De Luca, M., Giuliano, L., Guadagno, D., Lo Giudice, A., Leonardi, M., Scarfì, S., De Domenico, E., 2005. Ulteriori indagini sulla distribuzione di batteri luminosi in acque pelagiche del Mare Ionio (Mar Mediterraneo). Biologia Marina Mediterranea 12 (1), 625–630.

De Domenico, M., De Luca, M., Gentile, G., Giuliano, L., Scarfí, S., De Domenico, E., 2006. Distribuzione di batteri luminescenti in acque pelagiche del Mar Tirreno Centro-Meridionale (Mar Mediterraneo). Biologia Marina Mediterranea 13 (2), 314–315.

De Luca, M., 2006. Marine luminescent bacteria in the Mediterranean Sea. Ph.D. Thesis, University of Genoa, 109pp., unpublished.

Duncan, S., Glover, L.A., Killham, K., Prosser, J.I., 1994. Luminescence-based detection of activity of starved and viable but nonculturable bacteria. Applied and Environmental Microbiology 60 (4), 1308–1316.

Dunlap, P.V., Kita-Tsukamoto, K., 2001. Luminous bacteria. In: Dworkin, M., Falkow, S., Rosenberg, E., Schleifer, K.H., Stackebrandt, E. (Eds.), The Prokaryotes. Academic Press, New York.

Ferguson, R.L., Buckley, E.N., Palombo, A.V., 1984. Response of marine bacterioplankton to differential filtration and confinement. Applied and Environmental Microbiology 47, 49–55.

Geistdoerfer, P., Cussatlegras, A.S., 2001. Variations nycthemerales de la bioluminescence marine en mediterranèe et dans l'atlantique nord-est. Comptes Rendus de l' Académie des Sciences, Series III, Sciences de la Vie 324, 1037–1044.

Hastings, J.W., 1996. Chemistries and colours of bioluminescent reactions: a review. Gene 173, 5–11.

Jones, D.M., Sutcliffe, E.M., Curry, A., 1991. Recovery of viable but non-culturable *Campylobacter jejuni*. Journal of General Microbiology 137, 2477–2482.

Kita-Tsukamoto, K., Yao, K., Kamiya, A., Yoshizawa, S., Uchiyama, N., Kogure, K., Wada, M., 2006. Rapid identification of marine bioluminescent bacteria by amplified 16S ribosomal RNA gene restriction analysis. FEMS Microbiology Letters 258 (2), 320.

Makemson, J.C., Fulayfil, N.R., Landry, W., Ert, L.M.V., Wimpee, C.F., Widder, E.A., Case, J.F., 1997. *Shewanella woodyi* sp. nov., an exclusively respiratory luminous bacterium isolated from the Alboran Sea. International Journal of Systematic Bacteriology 47, 1034–1039.

Nealson, K.H., 1978. Isolation, identification and manipulation of luminous bacteria. Methods in Enzymology 57, 153–166.

Nealson, K.H., Hastings, J.W., 1992. The luminous bacteria. In: Balows, A., Trüper, H.G., Dworkin, M., Harder, W., Schleifer, K.-H. (Eds.), The Prokaryotes, second ed. Springer, New York, pp. 625–639.

Nealson, K.H., Wimpee, B., Wimpee, C., 1993. Identification of *Vibrio splendidus* as a member of the planktonic luminous bacteria from the Persian Gulf and Kuwait Region with luxA probes. Applied and Environmental Microbiology 59 (8), 2684–2689.

Orndorff, S.A., Colwell, R.R., 1980. Distribution and identification of luminous bacteria from the Sargasso sea. Applied and Environmental Microbiology 39 (5), 983–987.

Rajagopal, I., 2000. SOFTWARE: Genomics Made Easy. Science 290 (5491), 474.

Ramesh, A.B., Loganathan, G., Venkateswaran, K., 1990. Ecological dynamics of marine luminous bacteria. Journal of Basic Microbiology 30, 686–703.

Reichelt, J.L., Baumann, P., 1973. Taxonomy of the marine luminous bacteria. Archives of Microbiology 94, 283–330.

Ruby, E.G., Urbanowski, M., Campbell, J., et al., 2005. Genome sequence of *Vibrio fischeri*: a symbiotic bacterium with pathogenic congeners. Proceedings of the National Academy of Sciences of the United States of America 102, 3004–3009.

Sukovataya, I.E., Tyulkova, N.A., 2001. Kinetic analysis of bacterial bioluminescence in water organic media. Luminescence 16, 271–273.

Tamburini, C., Garel, M., Ali, B.A., Mèrigot, B., Kriwy, P., Charrièl, B., Budillon, G., 2008. Distribution and activity of Bacteria and Archaea in the different water masses of the Tyrrhenian Sea. Deep Sea Research II, this issue [doi:10.1016/j.dsr2.2008.07.021].

Wimpee, C.F., Nadeau, T., Nealson, K.H., 1991. Development of species-specific hybridization probes for marine luminous bacteria by using in vitro DNA amplification. Applied an Environmental Microbiology 57 (5), 1319–1324.

Deep-Sea Research II 56 (2009) 768–773

Contents lists available at ScienceDirect

Deep-Sea Research II

journal homepage: www.elsevier.com/locate/dsr2

Cultivation-independent assessment of the bathypelagic archaeal diversity of Tyrrhenian Sea: Comparative study of rDNA and rRNA-derived libraries and influence of sample decompression

Violetta La Cono [a], Christian Tamburini [b], Lucrezia Genovese [a], Gina La Spada [a], Renata Denaro [a], Michail M. Yakimov [a,*]

[a] Institute for Coastal Marine Environment (IAMC), CNR, Molecular Microbiology and Ecology, Spianata S. Raineri 86, 98122 Messina, Italy
[b] Laboratoire Microbiologie, Géochimie et Ecologie Marines, Université de la Méditerranée, Centre d'Océanologie de Marseille, 13288 Marseille, France

ARTICLE INFO

Article history:
Accepted 8 July 2008
Available online 5 November 2008

Keywords:
Phylogeny
Deep Tyrrhenian Sea
16S rRNA
Crenarchaeota Marine Group I
Euryarchaeota Marine Group II

ABSTRACT

Two samples of the same bathypelagic bacterioplankton community (Tyrrhenian Sea at the depth of 3000 m) were collected during single cast by both traditional sampling with Niskin bottle and using a high pressure-maintaining HPSS sampler. Total RNA was isolated, reverse transcribed, amplified with *Archaea*-specific primers and cloned. Riboclones were sequenced, 117 riboclones from decompressed library and 104 rRNA-based riboclones retrieved from HPSS sampler. Both RNA libraries were additionally compared with 115 riboclones based on DNA obtained from the decompressed sample (16S rRNA genes). In terms of repetitive riboclones, obtained in all three libraries, the bathypelagic community was dominated by *Crenarchaeota* Marine Group I (52–64%). The combined analysis led to a characterization of sampling-specific phylotypes otherwise uncharacterized if only one type of library had been analyzed alone. Of the DNA riboclones, 22% were found only in this library and no close relatives of *Euryarchaeota* Marine Group II were detected in both RNA-based libraries, suggesting the dormant state of these organisms in deep-sea environment. For clones from the RNA libraries, one *Crenarchaeota* MG I phylotype did not indicate close relatives in the DNA library. In general, among 10 archaeal phylotypes recovered in total, 8, 7 and 6 of them were faced in DNA, RNA_HPSS and RNA decompressed libraries, respectively. Based on comparisons between all three libraries, our data indicate that (i) the short-term decompression of seawater samples during cast recovery and following treatments caused only slight changes in the total rRNA diversity and (ii) rRNA-based analysis is likely affected the characterization of phylotypes, present in deep-sea environment as the dormant cells, detected only on the DNA level.

1. Introduction

The deep ocean is one of the most important and less understood microbial-driven ecosystem on Earth. The largest fraction of the ocean is at depths >200 m and this physically uniform (low temperature, high hydrostatic pressure and the absence of solar radiation) environment is believed to account for 55% of all the prokaryotes found in aquatic habitats (Whitman et al., 1998; Karner et al., 2001). This piezophilic microbiota [term introduced by Yayanos (1995) from the greek verb *piezo*, to press], evolutionary adapted to the life under elevated hydrostatic pressure, is characterized by a high diversity but low abundance of organisms (Fuhrman et al., 1992; Sogin et al., 2006). Piezophilic microorganisms have been isolated from many regions of the world, displaying pressure optima for growth that span the entire range of pressures existing in the ocean biosphere (for a brief review see Simonato et al., 2006). Recently, the comparative analysis of the first genomes of psychro- and piezophilic (cold- and pressure-loving) bacterial isolates with those of phylogentically closely related surface-water species/strains revealed the identification of depth-specific ecotypes, defined as a population of a species genetically adapted to a certain depth in the water column (Lauro and Bartlett, 2008). Deep-sea bacteria have been shown to possess piezo-specific adaptations in terms of many essential cellular processes including enzymatic activity, protein–protein, protein–DNA interactions, un-saturation of phospholipids and cell division (Bianchi et al., 1999; Lauro and Bartlett, 2008). The piezo-specific adaptation likely also has affected the replication and translation processes: 16S ribosomal RNA comparisons between strains from different depths has identified

* Corresponding author. Tel.: +39090669003; fax: +39090669007.
E-mail address: michail.yakimov@iamc.cnr.it (M.M. Yakimov).

0967-0645/$ - see front matter © 2008 Elsevier Ltd. All rights reserved.
doi:10.1016/j.dsr2.2008.07.025

structures that appear to be specific to the piezophiles (Lauro et al., 2007), suggesting functional constraints for ribosomal function in the deep sea.

When delving into the ecology of any environment, the first question that comes to mind is invariably "who is there". The phylogenetic analysis of 16S rRNA gene sequences is well established in microbial ecology (Olsen et al., 1986) and has been also applied to deep-ocean samples (DeLong et al., 2006; Zaballos et al., 2006; Sogin et al., 2006; Lauro and Bartlett, 2008 for the further references). These investigations provided not only the first clues to the extreme complexity of deep-sea microbial communities, but also raised the problem of discrepancy between the results obtained by different sampling strategies and molecular approaches applied (Acinas et al., 1999; DeLong et al., 1993, 2006; Sogin et al., 2006). As discussed elsewhere (Nogales et al., 1999; Mills et al., 2005; Moeseneder et al., 2005; Gentile et al., 2006), 16S rRNA gene (DNA-based) quantitative assessments of microbial communities are inherently skewed by differences in copy number of ribosomal operons among different phyla. Another complicating factor in the DNA-based studies of deep-sea samples is the problem of discriminating against surface-derived bacteria. Many microbes will become attached to sinking particles, making their way to sediments and waters of the deep-sea where they can survive in a metabolically inactive state for indefinite periods of time (Lauro and Bartlett, 2008).

One solution to the problem of distinguishing between autochthonous and allochthonous members of the community is to analyze an environmental rRNA as an indicator of metabolically active microbial populations (Mills et al., 2004, 2005; Poulsen et al., 1993; Wawer et al., 1997). Although, the analysis of bulk rRNA has also some limitations, such as high instability of these type of nucleic acids and the complex secondary structure of rRNA molecules, which prevents their efficient transcription in vitro, the generally higher quantity of ribosomes, present in actively living microbial cells, provides a more accurate platform to analyze the active autochthonous fraction of microbial community (Felske et al., 1997; Miskin et al., 1999).

In this paper we report the contemporary construction of DNA- and RNA-based libraries to phylogenetically characterize the total and active archaeal assemblages extant in bathypelagic realm of Tyrrhenian Sea at the depth of 3000 m. Taking into consideration that both cast recovery and sample processing have taken several hours, the effect of decompression on the instable bulk of rRNA was studied by the application of high-pressure-maintaining device HPSS mounted on the same rosette with Niskin bottles.

2. Methods

2.1. Sampling

One liter of seawater from 10 L Niskin bottle were sampled during the CIESM-SUB1 cruise (21–30 July 2005, RV *Universitatis*) from the depth of 3000 m at Station 4 (VECTOR), located in the Southern Tyrrhenian Sea area at Lat. 39°32.050′N and 13°22.280′E. Contemporary, the same volume of seawater at the same depth was collected by means of the high-pressure serial sampler (HPSS) (Bianchi et al., 1999), to maintain deep-sea samples at the *in situ* conditions (pressure, temperature). The temperature of the seawater samples collected by Niskin and HPSS bottles was 13.49 °C. Niskin bottle sample was filtered through a 47-mm diameter, 0.2-μm pore-size Nuclepore filters (Millipore). The recovery and handling samples filtration was at least 90 min. To minimize the effect of decompression, small aliquots (100 mL) of seawater from HPSS were taken and step-wisely filtered through the same a 47-mm diameter, 0.2-μm pore-size Nuclepore filters (Millipore). Before each following filtration, filter was immersed in RNAlater® solution (Ambion) for 2 min to preserve RNA and block RNAse activity. Collected material was re-suspended in 100 μL of TE buffer (pH 8.0) containing lysozyme (5 mg/mL), lysed by addition of 300 μL of lysis buffer QRL1 (Qiagen, Milan, Italy) and stored at −20 °C until processing.

2.2. DNA, RNA extraction and 16S rRNA RT-PCR

Total genomic DNA and RNA were extracted from filters using Qiagen RNA/DNA Mini Kit (Qiagen). The extraction was carried out as according to the manufacture's instructions. RNA was treated with "DNA-free" kit (Ambion). The quality of the RNA sample was examined by agarose electrophoresis and concentrations were determined using the NanoDrop® ND-1000 Spectrophotometer (Celbio). crDNA synthesis with 16S rRNA as template was performed using SuperScript II Reverse Transcriptase (Invitrogen). Mixture (final volume 20 μL) for each reaction contained 4 μL of 5X First-Strand Buffer, 3 μL of template RNA, 1 μL (10 μM) of reverse primer 958R (Hallam et al., 2003), dNTP (10 mM each) and 1 μl of SuperScript II RT (200 units). The reaction was carried out in a MasterCycler 5331 Gradient (Eppendorf). The cDNA synthesis was at 42 °C for 50 min. The reaction was stopped by heating at 70 °C for 15 min. The crDNA was used as the template for a further PCR amplification. Possible DNA contamination of RNA templates was routinely monitored by PCR amplification of RNA aliquots that were not reverse transcribed. No contaminating DNA was detected in any of these reactions.

2.3. 16S rRNA gene amplification, cloning and sequencing

Total DNA and the crDNA were used for the amplification of 16S rDNA/rRNA. The Archea-specific primers set was used to amplify 16S rDNA genes the primers used were A20F (5′-TTCCGGTTGATCCYGCCRG) and A958-R (5′-YCCGGCGTTGAMT-CCAATT) (Hallam et al., 2003). The reaction was carried out in a MasterCycler 5331 Gradient (Eppendorf) as follows: initial denaturation at 94 °C for 5 min, 35 cycles of 1 min at 94 °C, 1 min at 50 °C, and 2 min at 72 °C; final extension step of 10 min at 72 °C. RT-PCR products and genomic DNA were visualized on an 1% agarose gel, specific bands were cut out and purified using QIAquick gel extraction kit (Qiagen). The purified PCR products were ligated into pGEM-T Easy® plasmid vector (Promega) and transformed by electroporation into the *Escherichia coli* DH10B cells (Invitrogen). Transformants were selected on LB containing 100 mg/mL of ampicillin under blue-white selection. The clone libraries were screened by direct colony PCR amplification. The amplification conditions are described above. Before sequencing, QIAquick 96 PCR Purification Kit (Qiagen) was used for the purification of PCR products.

Sequencing reactions were performed using the ABI Prism Big Dye 3.1 Terminator Cycle sequencing kit and an ABI Prism 3100 Avant (Applied Biosystems), DyeEx 96 Kit (Qiagen) was used for removal of unincorporated dye terminators from the products.

2.4. Sequencing and phylogenetic analysis

Sequence analysis was performed as previously described (Hallsworth et al., 2007; Yakimov et al., 2007). Briefly, all sequences were edited with MacVector Software version 7.2.2 (Rajagopal, 2000) (Accelrys, San Diego, CA) and compared with DNA sequences in the public domain through the Basic Local Alignment Search Tool (BLAST) (Altschul et al., 1997). Phylogenetic trees were constructed using the neighbor-joining method and Jukes–Cantor distance matrix; 1000 bootstrap re-samplings were

performed to estimate the reproducibility of the tree. Random order input of sequences, single jumbling, and the global rearrangement option were used.

2.5. Coverage of the clone libraries and cluster analysis

Coverage values were calculated to determine how efficient our clone libraries described the complexity of a theoretical community of infinitive size, i.e. the original community. The coverage (C) was derived from the equation $C = 1-(n/N)$, where n is the number of clones that occurred only once, and N is the total number of clones examined (Good, 1953). For phylotype definition, we assumed the clones with a sequence similarity of $\geqslant$97% to be of an identical phylotype. Moreover, we have assumed the clones with a sequence similarity of $\geqslant$99% are identical (Stackebrandt and Goebel, 1994; Rossello-Mora and Amann, 2001). The significance of the 16*S rRNA* gene in HPSS and Niskin clones libraries were statistically compared using the LIBSHUFF software (Singleton et al., 2001).

2.6. Nucleotide sequence accession numbers

Twenty-seven sequences from 336 clones sequenced through this study (at least one for each of the 10 archaeal phylotypes retrieved) have been assigned in the GenBank database under AM937080–AM937106.

3. Results and discussion

3.1. Distribution of rDNA and rRNA clones and representation of archaeal divisions

Analysis of deep-sea archaeal community extant in bathypelagic realm of Tyrrhenian Sea has been carried out by creation of 16S rDNA and two 16S rRNA clone libraries (compressed and decompressed), designated as NB_DNAA, HP_RNAA and NB_RNAAR libraries, respectively. All sequences with similarity $\geqslant$97% were considered to represent one phylogenetic group or phylotype. The phylogenetic analysis of 336 partial sequences (average length of 450 bp) obtained from three clone libraries revealed their distribution within 10 major taxonomical groups of *Eury-* and *Crenarchaeota*: 8 for NB_DNAA, 7 for HP_RNAA and 6 for NB_RNAAR libraries, respectively (Fig. 1). Clone library coverage at $\geqslant$97% level was estimated at 98.26% for NB_DNAA library, 100% for HP_RNAA library and 97.12% for NB_RNAA library. Four phylotypes were common in all three libraries encountered for 70–91% of all clones, unambiguously indicating that these abundant phylotypes represent the active members of the complex deep-sea archaeal community (Table 1).

The sequences that grouped within the Marine Group I *Crenarchaea* formed four clades, which were supported by high bootstrap values: the *Nitrosopumilus* group (single distant riboclone from DNA-based library), and three phylotypes closely related to the fosmid clones of an environmental libraries sampled from 3000 m-deep seawater of Ionian Sea (South-Eastern Mediterranean basin) (Martin-Cuadrado et al., 2007) and meso-pelagic water column (500 and 770 m depth) of North Pacific Subtropical Gyre at HOT station ALOHA (DeLong et al., 2006). Phylotype 8 does not contain any sequence from DNA-based library and the members of this cluster were visualized only by rRNA approach. Two remaining clusters featured sequences from all the three clone libraries with comparable high abundance: 61%, 75% and 79% of all clones sequenced from NB_DNAA, NB_RNAA and HP_RNAA libraries, respectively (Table 1). This finding corroborates the recent evidences that the absolute dominance of planktonic *Crenarchaea* in the active microbial communities of sub-euphotic zone of all oceans is not a simple accumulation of these organisms from the shallow zones of the water column (Karner et al., 2001; DeLong et al., 2006; Gillan and Danis, 2007; Mincer et al., 2007).

Seven deep Tyrrhenian sequences of Marine Benthic Group *Crenarchaea* (Kendall et al., 2007) found in all three libraries were almost identical to each other and grouped with clone Papm3A65 (AB213105) recovered from hydrothermal fluid at the southern slope of Mariana Trough. No relative to this group sequences was retrieved from either Ionian Sea or ALOHA Station. The affiliation of residual *Crenarchaea* phylotypes to pSL12 clade was unanticipated, because until recently (Zaballos et al., 2006; Mincer et al., 2007), its members have only been rarely encountered in the marine environments such as deep-ocean sediments (Vetriani et al., 1999) and deep-sea brine salterns (van der Wielen et al., 2005). pSL12-related sequence was recently obtained in fosmid library of 3000 m-deep Ionian Sea seawater (Martin-Cuadrado et al., 2007), confirming the ubiquitous distribution of these organisms in bathypelagic realm of Mediterranean Sea.

The members of two *Euryarchaea* groups (Marine Group II and Unaffiliated Group) encountered 22.6% of all DNA-derived sequenced clones, whereas only one riboclone affiliated with deep-sea hydrothermal vent Ma-NAO2 (AB193961) was recovered in HP_RNAA library, and no *Euryarchaea* sequences were obtained in decompressed RNA-based library (Fig. 1 and Table 1). Although the sequences of two clones, TS_HP_RNAA_16 and TS_NB_DNAA_112, along with Ma-NAO2 possessed all the signature nucleotides of the *Euryarchaea* (Vetriani et al., 1999), they were not included in any of the previously defined clusters (Gillan and Danis, 2007; Kendall et al., 2007) and might represent a novel *Euryarchaea* lineage whose closest relatives are Marine Group II (DeLong, 1992). The present results are in accordance with the recent statement that marine *Euryarchaea* are more abundant and active in superficial, euphotic zone where light- and surface-derived nutrients critical in their ecophysiology are present (Frigaard et al., 2006; Mincer et al., 2007). Absence of marine *Euryarchaea* in corresponding rRNA libraries confirmed that their metabolic activity is significantly decreased in deep seawater and their presence in total bathypelagic microbial community is likely due to simple settlement from the superficial euphotic layer.

3.2. Influence of decompression on rRNA diversity

In order to determine the significance between 16S rRNA diversity in decompressed and *in situ* pressure-maintained archaeal populations, LIBSHUFF method was applied to compare the corresponding libraries. The analysis of two coverage curves indicated that the composition of HP_RNAA and NB_RNAA libraries was not significantly different between each other when the HPSS library was compared to the Niskin library ($P = 0.348$). This finding indicates that short-term decompression probably did not create significant changes in the diversity patterns of deep-sea archaeal community at 16S rRNA level, although the variations in mRNA profiling caused by decompression effect cannot be excluded. Concerning the evolutionary distance $\geqslant$0.05, all the diversity of RNA libraries is contained in the DNA library, although a considerable difference between the two coverage curves ($P = 0.001$) describes the loss of an important phylogenetic group close to 0.03 of evolutionary distance (data not shown).

The observations we report here add to a picture of archaeal distribution in bathypelagic environment of Mediterranean Sea (Zaballos et al., 2006; Martin-Cuadrado et al., 2007), where members of the *Crenarchaeota*, including planktonic Marine Group

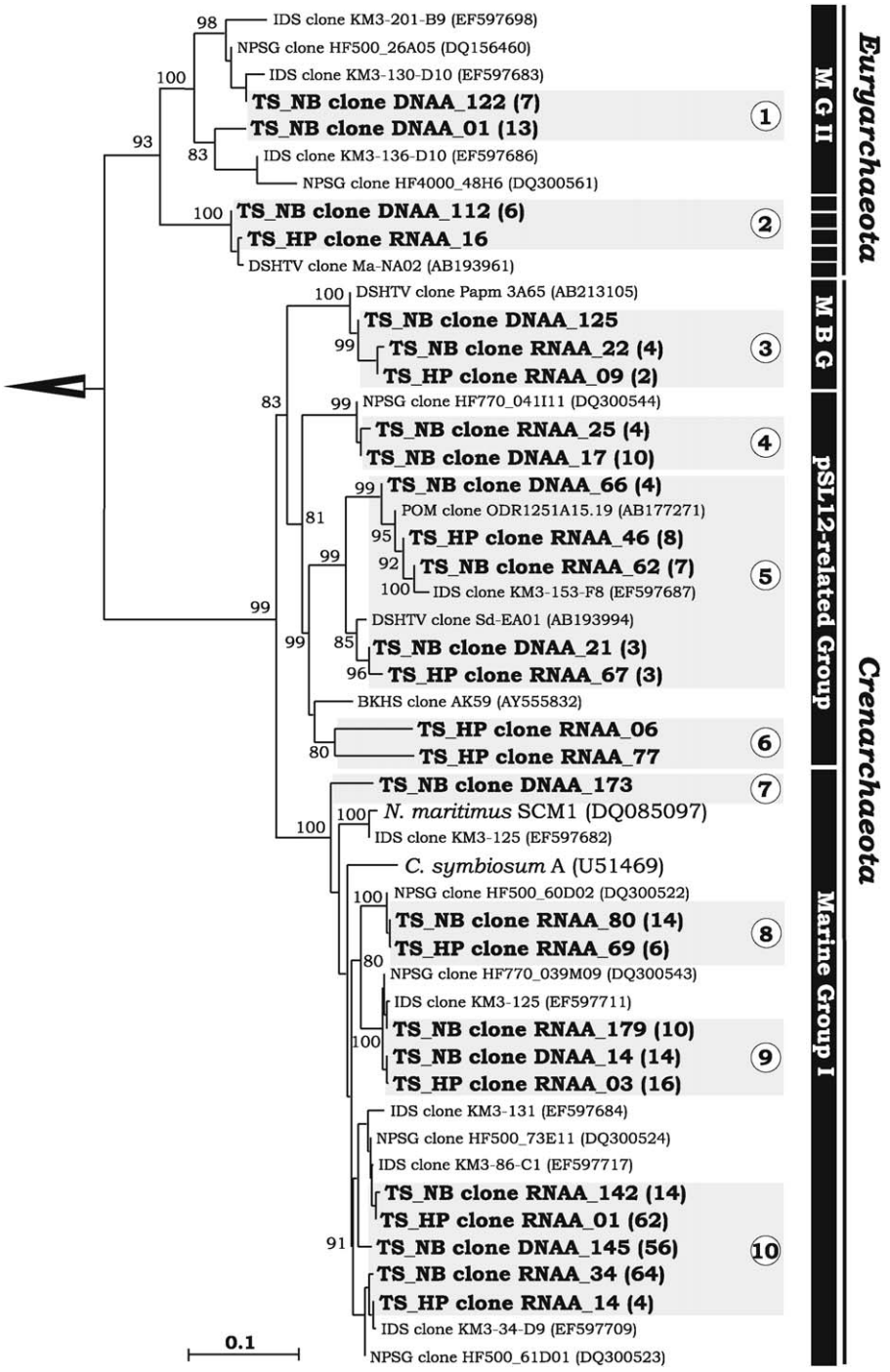

Fig. 1. Phylogenetic tree of the *Archaeota*-related 16S rRNA gene sequences retrieved from deep (3000 m) Tyrrhenian Sea. The tree was constructed by neighbor-joining analysis. The numbers at the branch nodes are bootstrap percentage values based on 1000 iterations and are shown for branches with more than 50% bootstrap support. Sequences from cultivated isolates are in italics, sequences from environmental gene clones are in plain font, and sequences from this study are in bold. Numbers of similar riboclones ($\geqslant$97% of identity) are in parentheses. The tree was rooted with 16S RNA gene sequence of *Marinobacter aquaeolei* (AY669169). Abbreviation used: BKHS, Bor Khlueng Hot Spring (Thailand); MG, Marine Group; MBG, Marine Benthic Group; DSHTV, Deep Sea Hydrothermal Vent; IDS, Ionian Deep Sea; POM, Pacific Ocean Margin; NPSG, North Pacific Subtropical Gyre. The scale bar represents the number of fixed mutations per nucleotide position.

I and the pSL12-related clade dominate the metabolically active archaeal community at the expenses of the *Euryarchaeota*. While the specific physiological properties of planktonic *Euryarchaea* are not well known, their higher abundance, observed in the superficial euphotic zone, coincides with the presence of proteorhodopsin-like genes in their genome (Frigaard et al., 2006). Based on this finding, it was recently proposed that planktonic *Euryarchaea* have an inverse tendency of distribution relative to planktonic *Crenarchaea* (Mincer et al., 2007).

Since RNA molecules have a much shorter lifetime compared to that of DNA, an environmental RNA (both rRNA and mRNA) can serve as an alternative indicator of metabolically active microbial populations (Mills et al., 2004, 2005; Poulsen et al., 1993; Wawer et al., 1997), and the mismatch between DNA and

Table 1
Phylotypes abundance, dominance (D), Shannon diversity indexes (H) and diversity coverages (DC) of marine *Archaea* retrieved from three clone libraries.

Phylotype groups	TS_NB_DNAA%	TS_NB_RNAA%	TS_HP_RNAA%
1	17.4	–	–
2	5.2	–	0.9
3	0.9	3.5	1.9
4	8.7	3.5	–
5	6.1	6	10.6
6	–	–	2
7	0.8	–	–
8	–	12	5.8
9	12.2	8.4	15.4
10	48.7	66.6	63.4
D	0.2963	0.472	0.4418
H	1.53	1.134	1.175
DC (%)	98.26	100	97.12

RNA libraries, observed in our study, likely reflects the dormant state of planktonic *Euryarchaeota* at 3000 m depth. Additionally, the short-term decompression of the deep-seawater samples, during cast recovery and following treatment, seems do not affect significantly the pool of rRNA molecules, while the same behavior of more unstable mRNA molecules is not expected and has to be verified specifically. Although we have analyzed the archaeal community from only one deep compartment of Tyrrhenian Sea, the combination of 16S rDNA and 16S rRNA gene sequencing, applied to microbial ecology, permits obtaining a more reliable vision on the total microbial community and on its potentially active fraction thriving in different habitats.

Acknowledgments

This study was supported by the CIESM under CIESM-SUB activity and as a part of the European Science Foundation EUROCORES Programme EURODEEP under MIDDLE (06-EuroDEEP-FP-004 MIDDLE) project. We thank the captain and the crew of RV *Universitatis* for their expert handling of our casts and equipment in the Tyrrhenian Sea and for highly productive oceanographic cruise CIESM-SUB1.

References

Acinas, S.G., Antón, J., Rodríguez-Valera, F., 1999. Diversity of free-living and attached bacteria in offshore Western Mediterranean waters as depicted by analysis of genes encoding 16S rRNA. Applied and Environmental Microbiology 65, 514–522.

Altschul, S.F., Madden, T.L., Schaffer, A.A., Zhang, J., Zhang, Z., Miller, W., Lipman, D.J., 1997. Gapped BLAST and PSI-BLAST: A new generation of protein database search programs. Nucleic Acids Research 25, 3389–3402.

Bianchi, A., Garcin, J., Tholosan, O., 1999. Effects of hydrostatic pressure on microbial activity through a 2000 m deep water column in the NW Mediterranean Sea. Marine Ecology Progress Series 183, 49–57.

DeLong, E.F., 1992. Archaea in coastal marine environments. In: Proceedings of the National Academy of Sciences of the United States of America, Vol. 89, pp. 5685–5689.

DeLong, E.F., Franks, D.G., Alldredge, A.L., 1993. Phylogenetic diversity of aggregate-attached vs. free-living marine bacteria assemblages. Limnology and Oceanography 38, 924–934.

DeLong, E.F., Preston, C.M., Mincer, T., Rich, V., Hallam, S.J., Frigaard, N.U., Martinez, A., Sullivan, M.B., Edwards, R., Brito, B.R., Chisholm, S.W., Karl, D.M., 2006. Community genomics among stratified microbial assemblages in the ocean's interior. Science 311, 496–503.

Felske, A., Rheims, H., Wolterin, k.A., Stackebrandt, E., Akkermans, A.D., 1997. Ribosome analysis reveals prominent activity of an uncultured member of the class Actinobacteria in grassland soils. Microbiology 143, 2983–2989.

Frigaard, N.U., Martinez, A., Mincer, T.J., DeLong, E.F., 2006. Proteorhodopsin lateral gene transfer between marine planktonic *Bacteria* and *Archaea*. Nature 439, 847–850.

Fuhrman, J.A., Mccallum, K., Davis, A.A., 1992. Novel major archaebacterial group from marine plankton. Nature 356, 148–149.

Gentile, G., Giuliano, L., D'Auria, G., Smedile, F., Azzaro, M., De Domenico, M., Yakimov, M.M., 2006. Study of bacterial communities in Antarctic coastal waters by a combination of 16S rRNA and 16S rDNA sequencing. Environmental Microbiology 8, 2150–2161.

Gillan, D., Danis, B., 2007. The archaebacterial communities in Antarctic bathypelagic sediments. Deep-Sea Research II 54, 1682–1690.

Good, I.J., 1953. The population frequencies of species and the estimation of the population parameters. Biometrika 40, 237–264.

Hallam, S.J., Girguis, P.R., Preston, C.M., Richardson, P.M., DeLong, E.F., 2003. Identification of methyl coenzyme M reductase A (mcrA) genes associated with methane-oxidizing archaea. Applied Environmental Microbiology 69, 5483–5491.

Hallsworth, J.E., Yakimov, M.M., Golyshin, P.N., Gillion, J.L., D'Auria, G., de Lima, A.F., La Cono, V., Genovese, M., McKew, B., Hayes, S.L., Harris, G., Giuliano, L., Timmis, K.N., McGenity, T.J., 2007. Limits of life in MgCl2-containing environments: Chaotropicity defines the window. Environmental Microbiology 9, 801–813.

Karner, M.B., DeLong, E.F., Karl, D.M., 2001. Archaeal dominance in the mesopelagic zone of the Pacific Ocean. Nature 409, 507–510.

Kendall, M.M., Wardlaw, G.D., Tang, C.F., Bonin, A.S., Liu, Y., Valentine, D.L., 2007. Diversity of Archaea in marine sediments from Skan Bay, Alaska, including cultivated methanogens, and description of *Methanogenium boonei* sp. nov. Applied and Environmental Microbiology 73, 407–414.

Lauro, F.M., Bartlett, D.H., 2008. Prokaryotic lifestyles in deep sea habitats. Extremophiles 12, 15–25.

Lauro, F.M., Chastain, R.A., Blankenship, L.E., Yayanos, A.A., Bartlett, D.H., 2007. The unique 16S rRNA genes of piezophiles reflect both phylogeny and adaptation. Applied and Environmental Microbiology 73, 838–845.

Martin-Cuadrado, A.-B., Lòpez-Garcia, P., Alba, J.-C., Moreira, D., Monticelli, L., Srittmatter, A., Gottschalk, G., Rodriguez-Valera, F., 2007. Metagenomics of the deep Mediterranean, a warm bathypelagic habitat. Public Library of Science One 9, e914.

Mills, H.J., Martinez, R.M., Story, S., Sobecky, P., 2004. Identification of members of the metabolically active microbial populations associated with Beggiatoa species mat communities from Gulf of Mexico cold-seep sediments. Applied and Environmental Microbiology 70, 5447–5458.

Mills, H.J., Martinez, R.J., Story, S., Sobecky, P.A., 2005. Characterization of microbial community structure in Gulf of Mexico gas hydrates: Comparative analysis of DNA- and RNA-derived clone libraries. Applied and Environmental Microbiology 71, 3235–3247.

Mincer, T.J., Church, M.J., Taylor, L.T., Preston, C., Karl, D.M., DeLong, E.F., 2007. Quantitative distribution of presumptive archaeal and bacterial nitrifiers in Monterey Bay and the North Pacific Subtropical Gyre. Environmental Microbiology 9, 116–1175.

Miskin, I.P., Farrimond, P., Head, I.M., 1999. Identification of novel bacterial lineages as active members of microbial populations in a freshwater sediment using a rapid RNA extraction procedure and RT-PCR. Microbiology 145, 1977–1987.

Moeseneder, M.M., Arrieta, J.M., Herndl, G.J., 2005. A comparison of DNA- and RNA-based clone libraries from the same marine bacterioplankton community. FEMS Microbiology Ecology 51, 341–352.

Nogales, B., Moore, E.R., Abraham, W.R., Timmis, K.N., 1999. Identification of the metabolically active members of a bacterial community in a polychlorinated biphenyl-polluted moorland soil. Environmental Microbiology 1, 199–212.

Olsen, G.J., Lane, D.J., Giovannoni, S.J., Pace, N.R., Stahl, D.A., 1986. Microbial ecology and evolution: A ribosomal RNA approach. Annual Reviews in Microbiology 40, 337–365.

Poulsen, L.K., Ballard, G., Stahl, D.A., 1993. Use of rRNA fluorescence in situ hybridization for measuring the activity of single cells in young and established biofilms. Applied and Environmental Microbiology 59, 1354–1360.

Rajagopal, I., 2000. SOFTWARE: Genomics made easy. Science 290, 474.

Rossello-Mora, R., Amann, R., 2001. The species concept for prokaryotes. FEMS Microbiology Review 25, 39–67.

Simonato, F., Campanaro, S., Lauro, F.M., Vezzi, A., D'Angelo, M., Vitulo, N., Valle, G., Bartlett, D.H., 2006. Piezophilic adaptation: a genomic point of view. Journal of Biotechnology 126, 11–25.

Singleton, D.R., Furlong, M.A., Rathbun, S.L., Whitman, W.B., 2001. Quantitative comparisons of 16S rDNA sequence libraries from environmental samples. Applied and Environmental Microbiology 67, 4373–4376.

Sogin, M.L., Morrison, H.G., Huber, J.A., Welch, D.M., Huse, S.M., Neal, P.R., Arrieta, J.M., Herndl, G.J., 2006. Microbial diversity in the deep sea and the underexplored "rare biosphere". In: Proceeding of National Academy of Science USA, vol. 103, pp. 12115–12120.

Stackebrandt, E., Goebel, B.M., 1994. Taxonomic note: A place for DNA–DNA reassociation and 16S rRNA sequence analysis in the present species definition in Bacteriology. International Journal of Systematic and Evolutionary Microbiology 44, 846–849.

van der Wielen, P.W., Bolhuis, H., Borin, S., Daffonchio, D., Corselli, C., Giuliano, L., D'Auria, G., de Lange, G.J., Huebner, A., Varnavas, S.P., Thomson, J., Tamburini, C., Marty, D., McGenity, T.J., Timmis, K.N., BioDeep Scientific Party, 2005. The

enigma of prokaryotic life in deep hypersaline anoxic basins. Sciente 307, 121–123.
Vetriani, C., Jannasch, H.W., MacGregor, B.J., Stahl, D.A., Reysenbach, A.L., 1999. Population structure and phylogenetic characterization of marine benthic *Archaea* in deep-sea sediments. Applied and Environmental Microbiology 65, 4375–4384.
Wawer, C., Jetten, M.S., Muyzer, G., 1997. Genetic diversity and expression of the [NiFe] hydrogenase large-subunit gene of Desulfovibrio spp. In environmental samples. Applied and Environmental Microbiology 63, 4360–4369.
Whitman, W.B., Coleman, D.C., Wiebe, W.J., 1998. Prokaryotes: the unseen majority. In: Proceeding of National Academy of Science USA 95, pp. 6578–6583.
Yakimov, M.M., La Cono, V., Denaro, R., D'Auria, G., Decembrini, F., Timmis, K.N., Golyshin, P.N., Giuliano, L., 2007. Primary producing prokaryotic communities of brine, interface and seawater above the halocline of deep anoxic lake L'Atalante, Eastern Mediterranean Sea. The ISME Journal 1, 743–755.
Yayanos, A.A., 1995. Microbiology to 10,500 m in the deep-sea. Annual Reviews in Microbiology 49, 777–805.
Zaballos, M., Lopez-Lopez, A., Ovreas, L., Bartual, S.G., D'Auria, G., Alba, J.C., Legault, B., Pushker, R., Daae, F.L., Rodriguez-Valera, F., 2006. Comparison of prokaryotic diversity at offshore oceanic locations reveals a different microbiota in the Mediterranean Sea. FEMS Microbial Ecology 56, 389–405.